
Interference analysis of and dynamic channel assignment algorithms in TD-CDMA/TDD systems

Harald Haas



A thesis submitted for the degree of Doctor of Philosophy.
The University of Edinburgh.
November 2000

Abstract

The radio frequency spectrum for commercial wireless communications has become an expensive commodity. Consequently, radio access techniques are required which enable the efficient exploitation of these resources. This, however, is a difficult task due to an increasing diversity of wireless services. Hence, in order to achieve acceptable spectrum efficiency a flexible air-interface is required.

It has been demonstrated that code division multiple access (CDMA) provides flexibility by enabling efficient multi user access in a cellular environment. In addition, time division duplex (TDD) as compared to frequency division duplex (FDD) represents an appropriate method to cater for the asymmetric use of a duplex channel. However, the TDD technique is subject to additional interference mechanisms in particular if neighbouring cells require different rates of asymmetry. If TDD is combined with an interference limited multiple access technique such as CDMA, the additional interference mechanism represents an important issue. This issue poses the question of whether a CDMA/TDD air-interface can be used in a cellular environment. The problems are eased if a hybrid TDMA (time division multiple access) / CDMA interface (TD-CDMA) is used. The reason for this is that the TDMA component adds another degree of freedom which can be utilised to avoid interference. This, however, requires special channel assignment techniques.

This thesis analyses cellular CDMA/TDD systems used in indoor environments. A key parameter investigated is the interference in such systems. In the interference analysis a special focus is placed on adjacent channel interference since the jamming entity and victim entity can be in close proximity. The interference analysis shows that co-location of BS's using adjacent channels is not feasible for an adjacent channel protection factor that is less than 40 dB and frame synchronisation errors of more than 10%. Furthermore, it is demonstrated that ideal frame synchronisation does not necessarily yield the highest capacity. As a consequence, a new technique termed 'TS-opposing' is introduced. This method is intended to enable a cellular TD-CDMA/TDD system to apply cell independent channel asymmetry. For this purpose, a centralised DCA is developed. It is found that this algorithm indeed enables neighbouring cells to adopt different rates of asymmetry without a significant capacity loss.

Moreover, a decentralised DCA algorithm based on the TS-opposing principle is developed. In this context, a novel TS assignment concept is proposed which reduces the complexity associated with the TS-opposing technique. In addition, the TS assignment plan allows for full spatial coverage. It is shown that the capacity of a TD-CDMA/TDD interface can be greater than the capacity of an equivalent FDD interface. The performance of the decentralised DCA algorithm is limited by the interference in the uplink. Therefore, additional methods which assist in reducing the interference in the uplink are envisaged to further improve the performance of the decentralised DCA algorithm.

The exploitation of the TS-opposing technique in two different ways demonstrates that this method can be used to improve the performance of a TD-CDMA/TDD system significantly.

Declaration of originality

I hereby declare that the research recorded in this thesis and the thesis itself was composed and originated entirely by myself in the Department of Electronics and Electrical Engineering at The University of Edinburgh.

Harald Haas

Acknowledgements

First and foremost, I wish to thank my supervisor Dr. Stephen McLaughlin whose continuous guidance as well as his timely advice contributed greatly to the completion of this dissertation. I would also like to thank Dr. Gordon Povey for his support during the first 22 months of my PhD.

Moreover, I owe thanks to the Faculty of Science and Engineering at Edinburgh University for providing the initial financial support without which I would not have been in the position to commence this PhD project. Furthermore, I owe gratitude to the Department of Electronics & Electrical Engineering for appointing me as a Research Associate during this PhD project. Moreover, I would like to thank Nokia Networks Oy in Oulu/Finland for their financial support. In this context, I particularly wish to thank Dr. Harri Posti, Kalle Passoja and Dr. Kari Rikkinen for many fruitful discussions.

Special thanks are due to my colleagues in the Signals & Systems group and the engineers in the computing department who always provided help and advice throughout my entire PhD project. In particular I wish to thank Ian Band, Iain Mann, John Thompson and Trina Dinnis for proof reading parts of my PhD thesis and for their valuable comments regarding technical matters as well as the 'nitty-gritty' bits of the English language. In this context, I will not forget, the 'word-of-the-day' project which gave me a useful insight into the sophisticated elements of the English vocabulary; but I doubt that anybody would ever use what I learnt there.

I would also like to thank Prof. Peter Grant for his final comments and support.

Last but not least, I wish to thank my family for their continuous support. Most importantly, I wish to thank my wife, Sibylle, without whose true love, support and patience this thesis would not have been possible.

Contents

Declaration of originality	iii
Acknowledgements	iv
Contents	v
List of figures	vii
List of tables	xi
Acronyms and abbreviations	xii
List of principal symbols	xv
1 Introduction	1
1.1 Introduction	1
1.2 The multi user access	2
1.3 The cellular concept	4
1.4 Modes of channel operation	6
1.5 Aims of this work	8
1.6 Thesis structure	9
2 Wireless telecommunications using CDMA and TDD techniques	11
2.1 Introduction	11
2.2 Multiple access methods in wireless communications	12
2.2.1 Cellular FDMA systems	13
2.2.2 Cellular TDMA systems	14
2.2.3 Cellular SDMA systems	15
2.2.4 Cellular CDMA systems	16
2.3 TDD inherent properties	25
2.3.1 Channel reciprocity	26
2.3.2 Round trip delays	28
2.3.3 Synchronisation and channel asymmetry	29
2.3.4 The TDD underlay concept	30
2.4 The TDD air interface of UMTS	36
2.5 Radio resource allocation techniques	37
2.5.1 Fixed channel assignment techniques	37
2.5.2 Dynamic channel assignment techniques	39
2.5.3 Random channel assignment techniques	42
2.6 Summary	43
3 Interference & capacity analyses	45
3.1 Introduction	45
3.2 Capacity definition	46
3.2.1 Capacity assuming ideal power control	46
3.2.2 Capacity assuming non-ideal power control	49
3.3 Adjacent channel interference in a CDMA-TDD system	52
3.3.1 Characterisation of adjacent channel interference	52

3.3.2	Single interfering cell	56
3.3.3	Multiple interfering cells	70
3.4	Co-channel interference in a CDMA-TDD system	80
3.4.1	Simulation platform	80
3.4.2	Methodology of analysis	80
3.4.3	Results	82
3.5	Conclusions	83
4	Centralised DCA algorithm using the TS-opposing idea	86
4.1	Introduction	86
4.2	TS-opposing technique applied to a single cell	86
4.2.1	System model	88
4.2.2	A simple DCA algorithm	92
4.2.3	Simulation environment	93
4.2.4	Results	93
4.3	TS-opposing technique in a multiple cell environment	96
4.3.1	System model	96
4.3.2	DCA algorithm	103
4.3.3	Simulation platform	108
4.3.4	Results	111
4.4	Conclusions	126
5	Distributed DCA algorithm utilising the TS-opposing idea	128
5.1	Introduction	128
5.2	Problem formulation	129
5.3	TS assignment plan	131
5.4	TS-opposing algorithm	136
5.5	System model	138
5.5.1	Uplink	139
5.5.2	Downlink	140
5.5.3	Capacity and Blocking Definitions	141
5.6	Results	143
5.7	Conclusions	148
6	Conclusions	150
6.1	Summary	150
6.2	Conclusions	153
6.3	Limitations and Future work	154
A	Derivation of CDMA capacity by Viterbi	157
B	Publications & Patents	159
B.1	Published papers	159
B.2	Submissions to advisory bodies	160
B.3	Patents	161
	References	192

List of figures

1.1	The principles of multi user access.	3
1.2	A cellular wireless system.	4
1.3	The cellular concept.	5
1.4	Modes of channel operation.	6
1.5	The principles of TDD as compared with FDD.	7
2.1	Frequency re-use distance in cellular FDMA and TDMA systems.	13
2.2	Theoretical capacity limits of a DS-CDMA multiple cell system with and without interference cancellation.	23
2.3	The Pre-RAKE concept.	26
2.4	The round trip delay in TDD.	28
2.5	Interference scenarios in cellular TDD systems with cell independent channel asymmetry.	29
2.6	The TDD underlay concept.	31
2.7	Frequency use in a dual interface system in which the TDD underlay is applied in order to achieve greater flexibility.	32
2.8	The additional numbers of MS's in the pico cell are indicated by red curves. Whereas, the capacity reduction in the FDD uplink is shown by the blue curves. Different lognormal shadowing scenarios are depicted in each plot. Moreover the effects of different BS separations are shown in plot a)-d): (a) $d_0=200\text{m}$, b) $d_0=300\text{m}$, c) $d_0=400\text{m}$ and d) $d_0=500\text{m}$	34
2.9	The area defined by \mathcal{D} serves as a measure for the flexibility of the TDD Underlay. Within the area specified by \mathcal{D} the FDD uplink radio resources can be exchanged between the macro cell and pico cell.	35
2.10	Probability of channel assignment failures for varying re-use cluster sizes and a constant number of totally available channels.	39
2.11	Classification of dynamic channel assignment algorithms.	40
3.1	Probability of outage as a function of simultaneously active MS's with: $pg=16$, $\mu_\epsilon^u=3.5$ dB and σ_ϵ^u as a parameter.	51
3.2	Adjacent TDD carriers can belong to independent operators (operator A and operator B) with the consequence that cells can overlap randomly. The potential interference links with respect to the UL direction are shown.	52
3.3	Interference in a TDD system dependent on frame synchronisation.	54
3.4	A single cell causing ACI at a cell which is located at a distance d_0 from the cell of interest (COI).	56
3.5	The correlation of the desired and the interference signal is dependent on the location of the transmitter relative to the first and second receiver.	57
3.6	Simulation model to derive the pdf of interference at the BS of a neighbouring cell.	60
3.7	A comparison of the cdf's and pdf's obtained by the analytical approach in (3.48) with the results of Monte Carlo simulations.	65

3.8	ACI power assuming four active interfering users.	67
3.9	Cell capacity with four interfering MS's. The capacity is shown for different cell load factors and different ACIR factors.	68
3.10	Cell capacity with six interfering MS's. The cell load factor, χ , is 0.75.	70
3.11	Multiple cells causing ACI at a cell located on top of the interfering cell cluster.	71
3.12	Handover model: within the grey shaded areas a MS's is located to the best serving BS.	73
3.13	The MS is assigned to BS ₀ . The handover threshold, δ , is used to model situations where a MS is not necessarily allocated to the BS which offers the lowest path loss (BS ₂ in this case).	74
3.14	Minimum coupling losses assuming different handover thresholds.	75
3.15	ACI distribution assuming 4 simultaneously active MS's in each interfering cell. Ideal power control in the UL and a DL power control algorithm given in (3.30) is assumed. The dotted lines represent the cdf of ACI for the case that handovers are not considered. The solid graphs depict the probability of ACI considering handover with a threshold of 5 dB. The ACIR, κ_I , is 35 dB.	76
3.16	ACI distribution assuming 4 simultaneously active MS's in each interfering cell, C/I -based power control algorithms in the UL and DL, non-ideal power control and handovers (solid graphs). For comparison the dotted curves show the results for ideal power control, a simple DL power control algorithm and handovers (the same as the dotted curves in Figure 3.15)	76
3.17	Relative cell capacity with four interfering MS's. The capacity is shown for different ACIR factors. The frame synchronisation α is used as a parameter. The cell load factor is $\chi=0.75$ and the tolerable outage, P_{out} , is 5 %. The graphs with solid lines depict the results of scenario (A) whereas the dotted curves show the results of scenario (B). All results implicitly assume handovers.	78
3.18	Cell model used to calculate interference in the COI	81
3.19	3d plots of the probabilities that I_b is greater than I_m within and around the COI.	83
3.20	Contour plots of the probabilities that I_b is greater than I_m within and around the COI.	84
4.1	A cell arrangement with each cell using two successive time slots where the first begins at the same time in each cell is shown. The direction of transmission is arranged so that the cell of interest (COI) and cell 2 receive in TS 0 and transmit in TS 1. In contrast, the BS of cell 3 first transmits and then receives.	87
4.2	Relative capacity of a TDD cell when using the TS-opposing algorithm compared with an equivalent FDD cell.	94
4.3	BS to BS interference, and MS to BS interference respectively, normalised by the total own-cell interference power (I_{own}) as a function of the number of active users per cell. The results assume the use of the TS-opposing algorithm.	95
4.4	A cell arrangement with each cell using two successive time slots where the first begins at the same time in each cell is shown. The direction of transmission is arranged so that the cell of interest (cell 1) and cell 2 receive in TS 0 and transmit in TS 1. In contrast, the BS of cell 3 first transmits and then receives.	104
4.5	The dependencies of α	105
4.6	The centralised DCA algorithm exploiting the TS-opposing idea.	107

4.7	The user distribution and user assignment based on the minimum path loss is shown for a random scenario. A wrap around technique is applied to prevent cell boundary effects.	108
4.8	Wrap around technique applied.	109
4.9	Deployment scenario.	110
4.10	Dynamic uplink power control: The transmission power of the mobile is successively adjusted.	110
4.11	The initial TS assignment for scenario 1.	112
4.12	Results of scenario 1. The rate of asymmetry, UL:DL, in cell 1 is 3:1 and 1:1 in all other-cells. The graphs show: for a) the capacity in each cell in [kbps/TS] and b) the total capacity in [kbps/Cell/TS]. The results labelled with 'FCA' are obtained by the fixed channel assignment procedure and the results labelled with 'DCA' are these obtained from the novel centralised DCA algorithm.	113
4.13	Scenario 1: The expected values of the components of α as a result of the novel DCA algorithm are depicted for all 4 TS (In a) the results with respect to TS 1 are depicted, in b) the results with respect to TS 2, <i>etc.</i>).	115
4.14	This illustration shows the initial TX/RX configuration with respect to the BS's for scenario 1. The arrows highlight the TS's which changed most frequently and the associated maximum probabilities are shown.	116
4.15	The initial TS assignment for scenario 2. The modification with respect to the previous scenario is highlighted.	116
4.16	Results of scenario 2. The rate of asymmetry, UL:DL, in cell 1 is 3:1, in cell 2:0 and 1:1 in all other-cells (cell 3 and cell 4). The graphs show: for a) the capacity in each cell in [kbps/TS] and b) the total capacity in [kbps/Cell/TS]. The results labelled with 'FCA' are obtained by the fixed channel assignment procedure and the results labelled with 'DCA' are these obtained from the novel centralised DCA algorithm.	117
4.17	Scenario 2: The expected values of the components of α as a result of the novel DCA algorithm are depicted for all 4 TS (In a) the results with respect to TS 1 are depicted, in b) the results with respect to TS 2, <i>etc.</i>).	119
4.18	This illustration shows the initial TX/RX configuration with respect to the BS's for scenario 2. The arrows highlight the TS's which changed most frequently and the associated maximum probabilities are shown.	120
4.19	The initial TS assignment for scenario 3. The modification with respect to the previous scenario is highlighted.	120
4.20	Results of scenario 3. The rate of asymmetry, UL:DL, in cell 1 is 2:2 and 1:1 in all other cells. The graphs show: for a) the capacity in each cell in [kbps/TS] and b) the total capacity in [kbps/Cell/TS]. The results labelled with 'FCA' are obtained by the fixed channel assignment procedure and the results labelled with 'DCA' are these obtained from the novel centralised DCA algorithm.	121
4.21	Scenario 3: The expected values of the components of α as a result of the novel DCA algorithm are depicted for all 4 TS (In a) the results with respect to TS 1 are depicted, in b) the results with respect to TS 2, <i>etc.</i>).	122
4.22	The initial TS assignment for scenario 4. The modification with respect to the previous scenario is highlighted.	123

4.23	Results of scenario 4. The rate of asymmetry, UL:DL, in cell 1 is 1:3 and 1:1 in all other-cells. The graphs show: for a) the capacity in each cell in [kbps/TS] and b) the total capacity in [kbps/Cell/TS]. The results labelled with 'FCA' are obtained by the fixed channel assignment procedure and the results labelled with 'DCA' are these obtained from the novel centralised DCA algorithm. . . .	124
4.24	Scenario 4: The expected values of the components of α as a result of the novel DCA algorithm are depicted for all 4 TS (In a) the results with respect to TS 1 are depicted, in b) the results with respect to TS 2, <i>etc.</i>).	125
4.25	This illustration shows the initial TX/RX configuration with respect to the BS's for scenario 4. The arrows highlight the TS's which changed most frequently and the associated maximum probabilities are shown.	126
5.1	TS assignment plan. The 'X' indicates that the respective TS pair is opposed. . .	132
5.2	The mechanism of measuring the interference from BS's and MS's at the opposed channels.	133
5.3	TS configuration in a 7-cell cluster.	134
5.4	Decentralised DCA algorithm exploiting the TS-opposing technique.	136
5.5	Interference vectors for an arbitrary location within cell 0. It is assumed that a channel consists of at least two TS's, one for the uplink and one for the downlink.	137
5.6	Simulation environment: The DCA algorithm is operated at the cell of interest (COI). The first tier of cells is equally populated and handover regions (grey shaded area) are considered so that MS's can be allocated to the best serving BS.	139
5.7	Blocking and maximum cell load criterion.	141
5.8	Average capacity results of the decentralised DCA algorithm.	144
5.9	Blocking results of the decentralised TS-opposing algorithm.	146

List of tables

3.1	The theoretical upper capacity limit M_{max} (assuming less than 5 % outage) using the following parameters: $pg=16, \mu_{\varepsilon}^u=3.5$ dB.	51
3.2	Simulation parameters used in the verification of the analytically derived pdf of ACI with results obtained by Monte Carlo simulations.	63
3.3	Comparison of mean and standard deviation of \hat{I}_{ad} for $d_0 = R$	63
3.4	Comparison of mean and standard deviation of \hat{I}_{ad} for $d_0 = 2R$	64
3.5	Simulation parameters for ACI analysis.	66
4.1	Parameters used for the simulation of the simple DCA algorithm.	93
4.2	Simulated scenarios: The ratio of UL (uplink) versus DL (downlink) usage is shown. The first figure corresponds to the number of TS's used for the UL and the second figure shows the number of TS's used for the DL.	111
4.3	Parameters used for the simulation of the centralised DCA algorithm.	112
5.1	Simulation parameters used to assessing the performance of the combination of the novel TS assignment plan and the decentralised DCA algorithm.	142
5.2	Average capacity for the case of 2 users per cell/TS each with a data rate of 64 kbps.	147
5.3	Average number of users blocked for the case of 2 users per cell/TS each with a data rate of 64 kbps.	147

Acronyms and abbreviations

AAD	Angle-of-arrival difference.
ACI	Adjacent channel interference.
ACIR	Adjacent channel interference ratio.
ACLR	Adjacent channel leakage ratio.
ACS	Adjacent channel selectivity.
AWGN	Additive white Gaussian noise.
BS	Base station.
BS's	Base stations.
CB	Citizen band.
CCI	Co-channel interference.
cdf	Cumulative density function.
CDMA	Code division multiple access.
COI	Cell of interest.
COST	European CO-operation in the field of Science and Technical research.
CT	Cordless telephony.
DCA	Dynamic channel assignment.
DCS	Dynamic channel selection.
DECT	Digitally enhanced cordless telecommunications.
DL	Downlink.
DS	Direct sequence.
ETSI	European telecommunications standards institute.
FCA	Fixed channel assignment.
FDD	Frequency division duplex.
FDMA	Frequency division multiple access.
FH	Frequency hopping.
FM	Frequency modulation.
FRAMES	Future radio wideband multiple access system.
GSM	Global system for mobile communications.
HIPERLAN	High performance radio local area network.

IMT–2000	International mobile telephony, 3rd generation networks are referred as IMT–2000 within ITU.
IS–95	Interim standard–95.
ITU	International telecommunications union.
kbps	kilo bit per second.
LAN	Local area network.
MAI	Multiple access interference.
Mcps	Mega chips per second.
MCL	Minimum coupling loss.
MoU	Memorandum of understanding.
MS	Mobile station.
MS's	Mobile stations.
MP	Maximum packing.
ODMA	Opportunity driven multiple access.
OVSF	Orthogonal variable spreading factor.
pdf	Probability density function.
PHS	Personal handyphone system.
PN	Pseudo noise.
PSTN	Public switched telephone network.
QoS	Quality of service.
RCA	Random channel assignment.
RF	Radio frequency.
RNC	Radio network controller.
RRM	Radio resource management.
RU	Resource unit.
RV	Random variable.
RX	Reception.
SDMA	Space division multiple access .
SF	Spreading factor.
TD–CDMA	Time division CDMA (hybrid TDMA–CDMA interface).
TDD	Time division duplex.
TDMA	Time division multiple access.
TS	Time slot.

TX	Transmission.
UMTS	Universal mobile telecommunications system.
UTRA	UMTS terrestrial radio access (ETSI).
UTRA	Universal terrestrial radio access (3GPP).
UDD	Unconstrained delay data.
UL	Uplink.
VCE	Virtual centre of excellence in mobile & personal communications.
W-CDMA	Wideband CDMA.
3G	Third generation.
3GPP	Third generation partnership project.
4G	Fourth generation.

List of principal symbols

α	synchronisation matrix with each element either being 1 or 0.
$\tilde{\alpha}$	complementary matrix of α .
$\alpha_{i,j}$	frame synchronisation factor between cell i and cell j : $\alpha_{i,j} = t_{\text{off}_{i,j}}/t_{\text{slot}}$.
β	constant: $\beta = \log_{10}(10)/10$.
γ^u	carrier to interference ratio: $\gamma = \varepsilon^u \frac{W}{B} = \frac{\varepsilon^u}{pg}$ at the BS receiver.
γ^d	carrier to interference ratio: $\gamma = \varepsilon^d \frac{W}{B} = \frac{\varepsilon^d}{pg}$ at the MS receiver.
γ	vector of carrier to interference ratios.
δ	handover margin.
ε^u	ratio of signal energy per bit to spectral interference density power at the BS.
ε^d	ratio of signal energy per bit to spectral interference density power at the MS.
$\zeta_{i,j}$	total other-cell interference from cell i to own-cell interference in cell j in a TDD system.
η	ratio of thermal noise to total interference at the receiver: $\eta = \frac{N}{N+I_o+I_{\text{own}}}$.
κ_L	adjacent channel leakage ratio (ACLR).
κ_S	adjacent channel selectivity (ACS).
κ_I	adjacent channel interference ratio (ACIR).
λ	mean of a Poisson distribution reflecting the number of instantaneously active users in a cell.
μ	mean of a Normal distribution.
ν	interference margin.
ξ	RV of lognormal shadowing.
ρ_i	random variable modelling voice/data activity.
σ	standard deviation of a Normal distribution.
τ	orthogonality factor in the downlink.
v	uncorrelated random component between desired and any interference path.
v_i	correlated random component between desired and the interference path i .
ϕ	angle between two entities, <i>i.e.</i> MS's, BS's or between both.
φ	path loss exponent.

χ	cell load factor: $\chi = \frac{M_0}{M_{max}}$.
ψ	user specific fraction of the total carrier power in the downlink.
$\Psi(x, y)$	Metric to calculate the probability: $Pr(I_b > I_m)$ at the location (x, y) .
ω	relative traffic load: $\omega = \frac{\lambda}{M}$.
$a_{i,j}$	path loss in between entities i and j .
A	ratio of: distance between MS and target BS to distance between MS and victim BS in logarithmic units.
B	signal bandwidth.
\mathcal{B}	set of BS's.
\mathbf{B}	auxiliary matrix.
B_c	channel bandwidth.
b_i	BS number i .
\overline{Bl}	average number of blocked MS's.
\mathbf{BB}	path gain matrix between BS's.
\mathbf{BM}_{c_i, c_j}	path gain matrix between the BS in cell i and the MS's in cell j .
B_t	total available bandwidth.
C	total carrier power.
C_i	carrier power of user i .
\mathcal{C}	set of cells.
\overline{C}	average capacity in [kbps].
c_i	cell number i .
d	transmitter–receiver separation distance.
D	minimum frequency re–use distance.
\mathcal{D}	operation area of the TDD underlay defined as: $\mathcal{D} = \mathcal{E} \cap \mathcal{F}$.
\mathcal{E}	operation area of additional pico cell capacity.
E_b	signal energy per bit.
\mathcal{F}	operation area of additional of FDD uplink capacity.
$f_{i,j}$	ratio of interference from the MS's in the neighbouring cell i to own–cell interference in cell j : $f_{i,j} = I_{mb_{j,i}}/I_{own_j}$.
$g_{i,j}$	ratio of interference from the BS in cells i to own–cell interference in cell j : $g_{i,j} = I_{bb_{j,i}}/I_{own_j}$.
G	ratio of the number of users with interference cancellation to

		the number of users without interference cancellation.
I		total interference power.
\mathbf{I}		identity Matrix.
$I_{ad}(x, y)$		adjacent channel interference power at the location specified by the Cartesian coordinates (x, y) .
I_b		substitution for: $I_o^u + N$.
\mathbf{Ib}		interference vector at the BS's.
I_b		interference at location (x, y) caused by BS's.
$I_{bb_{i,j}}$		interference power from the BS in cell i to the BS in cell j .
$I_{bm_{i,j}}$		interference power from the BS in cell i to the MS number j .
I_o^u		total other cell interference power at the BS.
I_o^d		total other cell interference power at the MS.
$I_{bb_{i,j}}$		interference power from the BS number i to the BS number j .
I_m		substitution for: $I_o^d + N$.
\mathbf{Im}		interference vector at the MS's.
$I_m(x, y)$		interference at location (x, y) caused by MS's.
$I_{mb_{i,j}}$		interference power from MS's in cell i to the BS in cell j .
$I_{mm_{i,j}}$		interference power from MS's in cell i to the MS number j .
I_{own}		own-cell interference as a consequence of the multiple access on a radio channel.
I_0		spectral interference density power.
\mathbf{J}		vector which each element set to one.
K		cluster size.
L		total number of cells.
M		number of simultaneously active users assuming non-ideal multiple access interference cancellation.
\tilde{M}		number of simultaneously active users assuming ideal multiple access interference cancellation.
\mathcal{M}_i		set of MS's assigned to BS i .
M_c		Poisson distributed number of simultaneously active MS's.
m_i		MS number i .
M_j		total number of simultaneously active MS's in cell j .
\mathbf{MB}_{c_i, c_j}		path gain matrix between MS's in cell i and BS's in cell j .

M_{FDD}	number of users in an equivalent CDMA–FDD system.
$\mathbf{M}\mathbf{M}_{c_i,c_j}$	path gain matrix between MS's in cell i and MS's in cell j .
M_{max}	theoretical capacity maximum of a single user detector (pole capacity).
M_{out}	total number of MS's which experience outage.
M_{TDD}	number of users in a CDMA–TDD system.
M_{tot}	total number of distributed MS's.
M_0	maximum number of users that are permitted by the admission control.
M/M_0	relative remaining capacity as a consequence of other–cell interference.
N	background noise power: $N = N_0 B$.
N_0	background noise density power.
p	number of floors in an indoor propagation environment.
\mathcal{P}	circuit in a cellular network with the BS's being the vertices.
Pc_j^d	transmitted carrier power of the BS in cell j .
$\tilde{P}c_i^d$	code power to user i transmitted by the BS.
$\mathbf{P}\mathbf{c}^d$	vector of transmitted slot powers at the downlink.
$\tilde{\mathbf{P}}\mathbf{c}_i^d$	vector of transmitted downlink code powers in the i th cell.
$Pc_{i,j}^u$	transmitted code power of the i th MS in cell j .
$\mathbf{P}\mathbf{c}^u$	vector of transmitted code powers at the uplink.
pg	processing gain: $pg = B/W$.
P_{out}	probability of outage.
P_{pilot}	pilot signal power.
$P_{u_i}^d$	required signal power of user i at the BS receiver.
P_{users}	accumulated code powers in the downlink.
q_s	co–channel interference reduction factor.
r	total correlation coefficient between the desired and interfering path.
r_1	coefficient of the correlated part between desired and interfering path.
r_2	coefficient of the uncorrelated part between desired and interfering path.
R	cell radius.
$t_{off\ i,j}$	time offset between frame in cell i and frame in cell j .
t_{slot}	time duration for one TS.
U_{c_i}	substitution for: $\left(\frac{\mathbf{V}}{1-\mathbf{J}\mathbf{V}}\right) \odot \mathbf{M}\mathbf{B}_{c_i,c_i}$.

v	ratio of: distance between MS and BS to distance between BS and BS.
V	substitution for: $\left(\frac{\gamma_1^u}{1+\gamma_1^u}, \dots, \frac{\gamma_{ \mathcal{M}_i }^u}{1+\gamma_{ \mathcal{M}_i }^u} \right)^T$.
w	auxiliary function: $f(\xi) = \xi$.
W_i	data rate of an individual user i .
X	threshold of propagation model at which the correlation coefficient reaches a minimum.
y	auxiliary function: $f(\phi) = \phi$.
$Z(x, y)$	Probability that at location (x, y) the interference from BS's is greater than the interference from MS's.
$\stackrel{\text{def}}{=}$	by definition.
$E(\cdot)$	expected value of a probability distribution function.
$(\cdot)^T$	matrix/vector transpose.
\odot	Hadamard product.
$\text{diag}(\cdot)$	diagonal matrix.
$\log_2(\cdot)$	logarithm to base 2.
$\log_{10}(\cdot)$	logarithm to base 10.
$f(\cdot)$	function of (\cdot) .
$\exp(\cdot)$	natural exponential function.
$\cos(\cdot)$	cosine function.
$p(\cdot)$	probability density function.
$\widehat{(\cdot)}$	variable in logarithmic scale: $10 \log_{10}(\cdot)$.
$\partial(\cdot)$	operator for partial differentiation.
$J(\cdot)$	Jacobian.
$ \cdot $	Cardinality.
\emptyset	The empty set.

Chapter 1

Introduction

1.1 Introduction

The last decade of the 20th century was characterised by the “digital revolution”. The fact that personal computers have emerged as a mass product has represented an ideal ground for the tremendous growth of the Internet. By the end of the second quarter of 2000 already 280 million Internet users exist worldwide [1]. The Internet represents an enormous source of information and is evolving to a virtual store. The fact that companies sell their products through the Internet rather than with outlets throughout the country leads to considerable cost savings. Furthermore, the e-mail service is a good example of how material streams (transport of letters, documents, *etc.*) can be replaced by information streams. Another sign of a fundamental change is that some people do not need to travel to work as they can work at home (teleworking). Already, about 2 million Europeans practice teleworking [2]. This shows that the Internet has already become a significant pillar in modern societies.

A further significant step in the “digital revolution” is the huge success of digital mobile telephony. In Europe, in particular, the foundation had been laid when 13 countries agreed to adopt a single digital standard for cellular mobile communications (The Memorandum of Understanding (MoU) signed on 7 September 1987 in Copenhagen) [3]. The development of the Global System for Mobile Communications (GSM) followed with about 175 million subscribers in Europe by mid 2000 [1]. Worldwide there are 550 million mobile subscribers [1] the majority of which use the GSM system. It is forecast that by the year 2005 the number of mobile users will exceed the number of fixed line subscribers [4].

The future challenge is to merge the data oriented services prevalent on the Internet and wireless communication so as to fulfil the vision of: *anyone, anytime and anywhere* [5]. The first step into a new area of wireless data applications has been taken by the standardisation of the Universal Mobile Telecommunication System (UMTS)¹ in Europe and the equivalent

¹Sometimes also referred to as: Universal Mobile Telecommunications Services [6].

W-CDMA (wideband code division multiple access) system in Japan. These systems aim to provide 144 kbps in vehicular environments, 384 kbps in outdoor to indoor environments and 2 Mbps in indoor or picocell environments (low mobility populations) [5]. Although UMTS is not yet in operation, requirements with respect to the fourth generation wireless communication systems already appear in literature and are the focus of Mobile VCE Core 2 research 4G (4th generation). For example, in [7] high speed data (approx. 10 Mbps) for vehicular environments and full spatial coverage is a target for future systems that would begin operation after 2007.

The radio frequency spectrum has become an expensive commodity. In the UK, for example, a sum equivalent to US\$ 154 per citizen has been paid for 2x15 MHz radio frequency spectrum for UMTS [8]. In order to use the radio frequency spectrum efficiently and at the same time meet the requirements of future wireless communication systems, a high degree of flexibility is required [9]. As a result, a single radio channel access interface which is tailored to the needs of a specific service will not fulfil the extended requirements efficiently. Therefore, new radio interface concepts have to be investigated.

1.2 The multi user access

The basic mechanism of the communication system which will be considered throughout this thesis is that a set of entities (users) access a common medium which, in this case, is the radio channel. This concept is depicted schematically in Figure 1.1. The frequency spectrum or bandwidth that is allocated to a certain system is a limited resource indicated by the rectangular frame. In general, there are many co-existing wireless systems. In order to avoid interference to and from other systems a certain level of protection is required. This is indicated by the shaded frame. The aim is to accommodate as many simultaneous users as possible (capacity) within the limited resource. In the example, 4 users are considered each of whom requires an equivalent fraction of the total radio resource (illustrated by a circle). In a digital context, this corresponds to services which require the same information bit-rate. In the picture, the size of the circles and hence the required radio capacity are constant. In real systems the size may be time variant (resulting in breathing circles in Figure 1.1). Consider, for example, a speech service and periods when a speaker is silent, there is no requirement to transmit data and thus the size of the circle would shrink to merely a single point in the space. An ideal multiple access technique supports the time variant request of radio capacity because this means that, at any given time, only those resources are allocated which are actually required. Consequently,

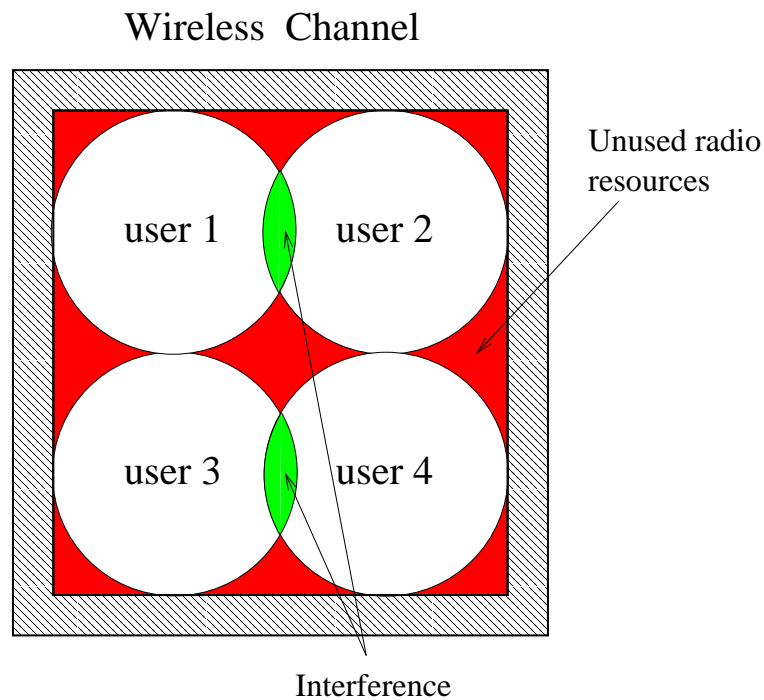


Figure 1.1: *The principles of multi user access.*

situations are avoided where more capacity is allocated than would actually be required.

If the system is not designed carefully, users or mobile stations (MS's) will *interfere* with each other (green areas). Therefore each user needs some protection which is equivalent to moving users apart. This measure, however, results in *unused radio resources* which, considering the immense costs for the radio frequency spectrum, is inefficient. Therefore, the aim is to accommodate as many users as possible (minimising the red coloured areas) while keeping the interference at a tolerable level. The separation of users can be done in any dimensions as long as it fulfils the interference requirements. In practice the following dimensions are used:

- Frequency \rightsquigarrow frequency division multiple access (FDMA)
- Time \rightsquigarrow time division multiple access (TDMA)
- Space \rightsquigarrow space division multiple access (SDMA)
- Code \rightsquigarrow code division multiple access (CDMA)

The space dimension is of particular significance as it allows the use of the same radio resource at the same time, frequency and with the same code at another physical location which is

spatially separated in distance or angle. The magnitude of spatial separation depends on the required level of interference protection. This circumstance leads to the cellular concept which, in theory, enables a wireless system to completely cover an infinite area with a limited radio resource.

1.3 The cellular concept

For certain types of services the aim is to achieve full spatial coverage. In conventional wireless systems a mobile entity is linked to a base station (BS). BS's are connected to a radio network controller which uses additional interfaces that cater for the access to the public switched telephone network (PSTN). The principle structure of a cellular wireless system is shown in Figure 1.2. The signals on the air–interface experience a distance dependent attenuation. Since

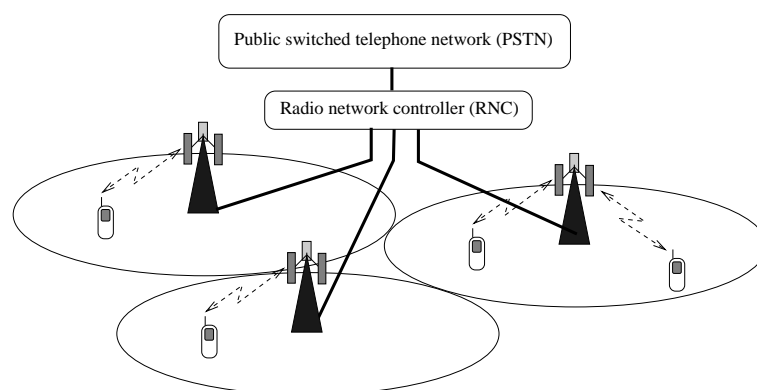


Figure 1.2: A cellular wireless system.

the transmit powers are limited, the coverage area of a BS is limited, as well. Due to the radial signal propagation, in theory, a single BS covers a circular area. The area which is covered by a BS is also referred to as a cell². When modelling cellular systems, cells are approximated by hexagons as they can be used to cover a plane without overlap (tessellation) and represent a good approximation of circles.

Since the total available radio resource is limited, the spatial dimension is used to allow wide area coverage. This is achieved by splitting the radio resource into groups. These groups are then assigned to different contiguous cells. This pattern is repeated as often as necessary until the entire area is covered. A single pattern is equivalent to a cluster. Therefore, a radio

²Cordless systems are usually composed of a single cell.

resource which is split into i groups directly corresponds to a cell cluster of size i . In this way it is ensured that the same radio resource is only used in cells that are separated by a defined minimum distance. This mechanism is depicted in Figure 1.3 (A group of radio resource units is indicated by a certain colour.). As a consequence the separation distance grows if the

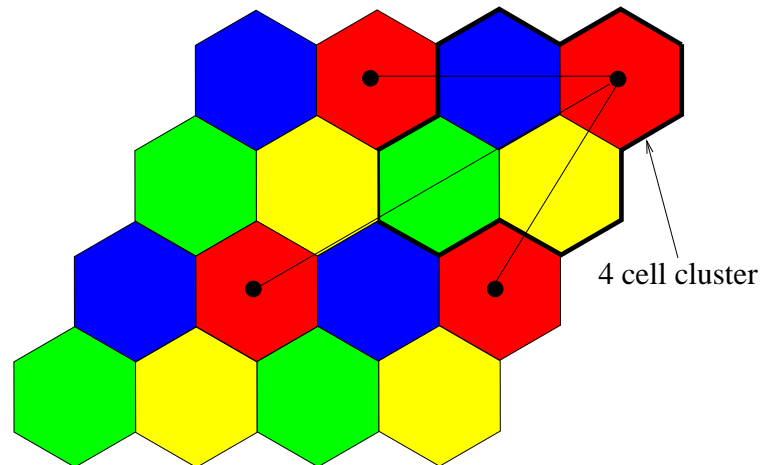


Figure 1.3: *The cellular concept.*

cluster size increases. Hence, increasing the cluster size acts in favour of low interference. However, an increased cluster size means that the same radio resource is used less often within a given area. As a result, fewer users per unit area can be served. Therefore, there is a trade-off between cluster size and capacity. In an ideal scenario the total available radio resource would be used in every cell whilst the interference was kept at a tolerable level. Herein lies a particular advantage of CDMA over all other multiple access modes since the same frequency carrier can be re-used in every cell [10]. It is clear that this results in increased co-channel interference (CCI) which gradually reduces cell capacity, but the magnitude of the resulting reduction of spectral efficiency is usually less than would be obtained if a fixed frequency re-use distance was applied [11, Chapter 8]. The cell capacity, finally, is dependent on many system functions such as power control, handover, *etc.* which is why capacity in a CDMA system is described as soft-capacity. However, the fact that in a CDMA system frequency planning can be avoided may not only result in capacity gains, but it eventually makes CDMA a more flexible air interface.

1.4 Modes of channel operation

There are three basic modes for operating a communication channel, namely: simplex, half duplex and full duplex. The basic mechanisms are depicted in Figure 1.4. In the case of a

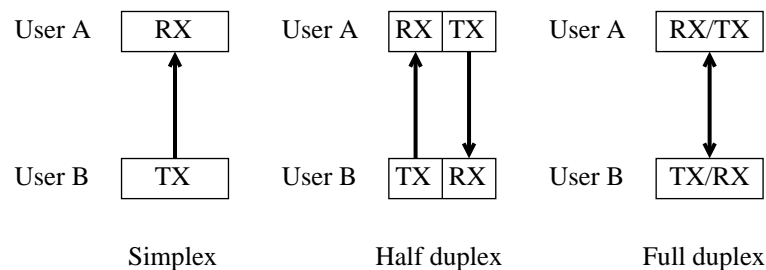


Figure 1.4: *Modes of channel operation.*

simplex communication the information is passed from one entity to another without permitting any acknowledgement (one way communication). Notable examples are television and radio broadcasting.

A half duplex channel can send and receive, but not at the same time. This means one entity transmits at a time while the other entity listens, and vice versa. A user A indicates when he wishes to terminate transmission giving the counterpart, user B in this case, the chance to talk. This leads to a 'ping-pong' type of communication. This technique is used in talk-back radio and CB (Citizen Band) radio where only one person can talk at a time. Note that access to the Internet merely requires a half duplex channel: consider user A sending a download request — in principle, no further information needs to be transmitted and, thus, user A can go into the receive mode until all the required information is downloaded³.

Information that travels in both directions simultaneously is referred to as a full duplex channel. Two entities can receive and transmit at the same time. Telephony is an eminent example from this category.

In wireless communication systems two methods are used to achieve a full duplex channel — time division duplex (TDD) and frequency division duplex (FDD). If the receive and transmit slots of a half duplex channel are repeated periodically in short intervals, a full duplex channel can be emulated by a half duplex channel. This is exactly the mechanism used in TDD. In contrast, an FDD system separates both directions in the frequency domain so as to eliminate

³In reality the protocols involved are more complex, but the basic principle remains the same.

cross-talk. This means the full duplex channel is accomplished by two independent simplex channels. The basic mechanism of TDD and FDD are shown in Figure 1.5. In cellular com-

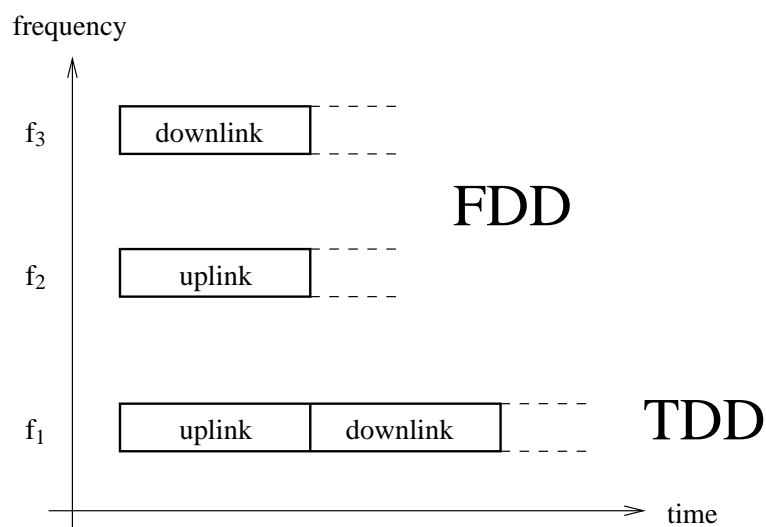


Figure 1.5: *The principles of TDD as compared with FDD.*

munication, the direction from the BS to the MS is referred to as the downlink⁴. Similarly, the direction from the MS to the BS is the uplink.

The advantage of FDD is that it represents a true full duplex channel which does not need any coordination between uplink and downlink transmission. The disadvantage is that two separated channels have to be maintained. Given that many new services do not require a full duplex channel (predominately data applications as illustrated by an Internet session), FDD offers more performance than would be required. In the case of a file download, for instance, the uplink channel is underused or even unused which results in the waste of expensive radio resources. In comparison, the TDD technique does not represent a true full duplex channel. It requires co-ordination (synchronisation), but due to its nature, it ideally supports services which basically only require a asymmetric half duplex channel. Given that future wireless communication is evolving towards the wireless Internet, the significance of TDD will grow.

⁴The terms ‘downlink’ and ‘forward link’ are synonymous. The terms ‘forward link’ is used primarily in the American literature. A similar dualism can be observed between ‘uplink’ and ‘reverse link’ and ‘handover’ and ‘hand-off’, respectively.

1.5 Aims of this work

The key objective of this thesis is the investigation of interference in a cellular CDMA–TDD system with a focus on indoor environments. The simulation parameters are primarily taken from the ETSI (European Telecommunications Standards Institute) proposal for the 3rd generation mobile communication system submitted to the ITU (International Telecommunications Union) [12].

In this context, special emphasis is placed on the calculation of adjacent channel interference (ACI) for different cell layouts, power control algorithms, handover schemes and time slot (TS) synchronisations. In order to quantify the effect of ACI it is aimed to derive a new capacity equation which relates the capacity in the presence of ACI to capacity of a single, non–interfered cell.

As TS synchronisation is generally assumed to be critical to interference particularly in a TDD system, the investigation of its impact on ACI is of utmost importance. This is because TS misalignments between neighbouring cells create additional interference mechanisms in a TDD system.

If it can be demonstrated that in some cases opposed transmission and reception between neighbouring cells achieve greater capacity than synchronous transmission and reception this may be further exploited. For example, methods may be developed which enable TDD cells to offset the negative effects of cell–independent asymmetry in TDD. In this context, in order to provide further insights into interference related issues an additional co–channel interference (CCI) analysis is conducted to highlight the impact of opposed transmission and reception.

The findings of the interference analyses outlined above are then applied to the hybrid TDMA–CDMA/TDD air–interface (TD–CDMA/TDD) of UMTS. It is an ultimate goal of this research to exploit the findings of the interference investigations to develop dynamic channel assignment (DCA) algorithms. In particular, for the commonly accepted issue that cell independent channel asymmetry in a TD–CDMA/TDD network may cause a significant capacity reduction [6, p. 301] solutions shall be provided by this research.

As part of the interference analysis, the TDD underlay concept [13] is further examined. In this study a new method is developed which allows the assessment of the performance of the TDD underlay. In addition, the TDD underlay is used to exploit guard times in a TDD system [14].

In order to ensure the clear focus of this thesis the decision was made to include only a brief outline of this research in chapter 2. The interested reader may, however, refer to [15–17] for more detailed information.

Moreover, in the context of the ACI investigation, a comprehensive interference analysis at the frequency boundary of 1920 MHz in UMTS is carried out ⁵. For the same reason as described above the results of this investigation are not included in this thesis. The interested reader may refer to [18, 19].

1.6 Thesis structure

This chapter is a brief introduction into the principles of wireless communication. It highlights why the combination of CDMA and TDD was chosen as the subject to be investigated in this PhD project.

Chapter 2 discusses the CDMA system in more detail by comparing it with alternative multiple access methods. It also shows the problems arising when using the total available bandwidth in every cell. The impact of two basic interference sources (inter-cell and intra-cell) on capacity are discussed. In addition, the properties of the TDD mode are presented where the focus is on the interference mechanisms in a cellular TDD system. The final part of chapter 2 categorises DCA algorithms. The reason for this is that DCA algorithms are an appropriate means to avoid interference and thereby increase the capacity of a TD-CDMA/TDD air interface.

Chapter 3 presents an in-depth interference analysis of a CDMA-TDD system. The analysis is carried out at the system level. Monte Carlo techniques, verified by an analytical approach, are used to calculate interference. This investigation reveals the interesting property that opposed transmission and reception may not necessarily yield capacity reductions in TDD systems. This property enables the use of TDD in achieving cell independent asymmetry in a cellular network without a significant capacity reduction. The resulting, novel concept, termed 'TS-opposing technique' is exploited extensively in the subsequent chapters which address DCA algorithms in a cellular TD-CDMA/TDD network.

Chapter 4 is dedicated to investigating a novel centralised DCA algorithm using the TS-opposing

⁵1920 MHz is the frequency at which the TDD and FDD mode have adjacent carriers in UMTS. This special case is chosen because both modes are affected differently from ACI in this particular spectrum assignment.

technique. The results corroborate the fact that TDD can be used to achieve cell independent asymmetry without a significant capacity loss.

Chapter 5 applies the TS-opposing technique to a decentralised DCA algorithm using a novel time slot assignment plan. The results reveal that the capacity of a cellular TDD system can be greater than an equivalent FDD system.

The objective of the last chapter is threefold: It summarises and concludes the work presented, highlights the limitations and points towards potential future work.

Chapter 2

Wireless telecommunications using CDMA and TDD techniques

2.1 Introduction

The capacity of cellular systems which use code division multiple access (CDMA) combined with frequency division duplex (FDD) were studied by many researchers [20–24] after the pioneering papers of Gilhousen, *et al.*, [25] and Viterbi [26, 27] had appeared. Gilhousen and Viterbi applied spread spectrum techniques, which, until then, had primarily been used in military applications, to commercial wireless communication systems — the foundation for which was laid by Shannon’s communication theory in [28]. Due to its flexibility CDMA had been considered as a strong candidate for the air–interface of the 3rd generation mobile communication system. During the European FRAMES (future radio wideband multiple access system) project different air–interface proposals were investigated including a hybrid TD–CDMA/FDD system (delta concept), results of which are reported in [29–31].

The time division duplex (TDD) technique has been applied successfully to frequency division multiple access (FDMA) systems and time division multiple access (TDMA) systems [32, 33]. Notable examples are the second generation cordless telephony (CT) system CT2 [34], the Digitally Enhanced Cordless Telecommunications (DECT) system and the personal handyphone system (PHS) [35]. A more recent representative of wireless systems which employ the TDD technique is the wireless local area network (LAN) standard HIPERLAN/2 (HIgh PERformance Radio Local Area Network) [36]. These short range wireless communications standards are primarily designed for high data rate applications (up to 54 Mbps), but require low mobility populations. Another TDD representative which falls into the same category is ‘Bluetooth’ which is used for cordless data communication between electronic devices [37]. Moreover, in January 1998 ETSI (European Telecommunications Standards Institute) decided to specify two air interfaces for the European candidate of the 3rd generation mobile telecommunications systems: UMTS (universal mobile telecommunications system). The UMTS terrestrial radio access (UTRA) is divided into a FDD and a TDD mode [38]. The UTRA–TDD mode employs a

hybrid form of CDMA and TDMA [39] which is referred to as TD-CDMA [40]. The UTRA-TDD interface is closely related to the 'delta concept', but uses TDD instead of FDD. This modification has a significant impact on the capacity which has not been investigated widely.

UMTS belongs to the IMT-2000¹ family and is designed to be capable of offering new services including multimedia and access to the Internet with a maximum data rate of 2 Mbps for a single user [41]. A common property of these packet-data oriented services is that they often result in an unbalanced load in the uplink and downlink direction [5]. This requires the support of an asymmetrical use of a communication channel. The TDD mode can easily arrange channel asymmetry, but is subject to more interference mechanisms if it is used in a cellular environment [42]. A further unique property of TDD is that it enables the use of the opportunity driven multiple access (ODMA) technique which is based on intelligent relaying [43]. ODMA is part of a new system concept which is based on localised cellular structures (Ad hoc and self organising networks) which are starting to attract the researchers' interest [43, 44] — in particular with respect to future mobile communications standards. Consequently, this thesis presents in-depth interference and capacity investigations with the emphasis on a cellular TD-CDMA/TDD system.

This chapter sets out the background of TDD and CDMA techniques. It contains a brief description of different multiple access modes in section 2.2 where a particular emphasis is put on CDMA techniques. An overview of the properties inherent to the TDD method can be found in section 2.3. In section 2.4 the basic radio interface properties of UTRA-TDD are described. In section 2.5 channel assignment issues are discussed. The chapter is summarised in section 2.6.

2.2 Multiple access methods in wireless communications

The basic problem in connection with multiple access in wireless communications is to divide a finite radio resource in such a way that portions of this resource can be assigned to a number of independent users without creating significant mutual interference. This requires a set of orthonormal functions [45]. Orthonormality can be arranged in four basic dimensions: a) frequency dimension, b) time dimension, c) space dimension and d) code (power) dimension which correspond to a) FDMA, b) TDMA, c) space division multiple access (SDMA) and d)

¹International mobile telephony (IMT), 3rd generation networks are referred to as IMT-2000 within ITU (International Telecommunications Union).

CDMA. In the following, these multiple access methods are discussed in brief.

2.2.1 Cellular FDMA systems

In FDMA systems the radio frequency spectrum is divided into several frequency bands separated by a certain guard band. Each frequency band can be used simultaneously. The guard band is required to reduce interference resulting from adjacent channel power leakage due to receiver and transmitter imperfections (cross-talk or adjacent channel interference (ACI)). Each frequency band is regarded as a physical channel assigned to a single user. When ACI is neglected and only a single cell is considered, all users are separated in an orthogonal fashion. However, in the case of a cellular FDMA system, the same frequency is re-used in some other cell separated by a certain minimum distance D^2 . This mechanism is illustrated in Figure 2.1. The spatial separation of cells which use the same frequency (f_1 in the example) reduces co-

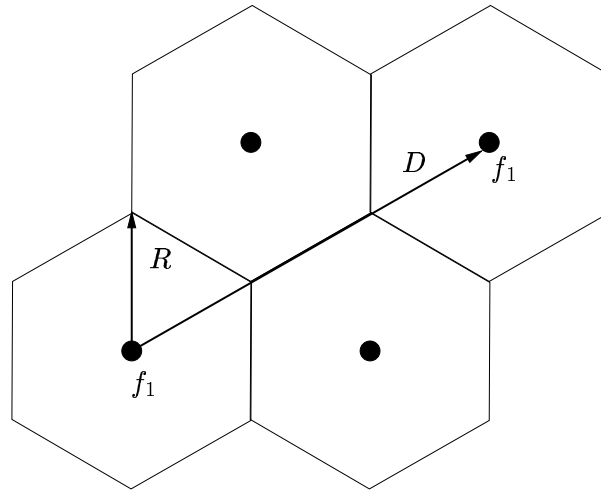


Figure 2.1: Frequency re-use distance in cellular FDMA and TDMA systems.

channel interference (CCI) but diminishes the spectral efficiency [46]. The factor: $q_s = \frac{D}{R}$ is defined as the CCI reduction factor [47], where R represents the cell radius. The relationship between the number of cells in a frequency re-use pattern (cluster size), K , and q_s is found in [48, page 516] and yields:

$$q_s = \sqrt{3K} . \tag{2.1}$$

²Since in FDMA systems a single frequency represents a channel, in this context D is described as the frequency re-use distance. This concept can also be applied to other multiple access techniques which is why D can be generalised as channel re-use distance

Moreover, in [47] the relationship between the required carrier to interference ratio, γ^u , at the BS (indicated by the superscript 'u' for uplink³) and q_s is found for the scenario of 6 interfering cells at distance D where the MS's of the interfering cells are located at the centre whereas the MS in the desired cell is located at the cell boundary. This results in:

$$q_s = \frac{D}{R} = 6 (\gamma^u)^\varphi , \quad (2.2)$$

where φ is the path loss exponent.

The number of channels per cell is

$$M = \frac{B_t}{B_c K} , \quad (2.3)$$

where B_t is the available bandwidth and B_c is the channel bandwidth. Substituting (2.1) and (2.2) into (2.3) and assuming that the propagation power loss increases according to the fourth power of the distance, *i.e.* $\varphi = 4$, then the "radio capacity by Lee" [47] can be denoted as follows:

$$M = \frac{B_t}{B_c \sqrt{\frac{2}{3}} (\gamma^u)} \quad \text{number of channels / cell} . \quad (2.4)$$

Given that the theoretical maximum number of channels in a single cell environment is: $M = B_t/B_c$, it can be seen from (2.4) that the capacity of a cellular system is reduced by a factor of $\sqrt{\frac{2}{3}} (\gamma^u)$ as a consequence of the frequency re-use. Note that the capacity reduction decreases as γ^u diminishes.

2.2.2 Cellular TDMA systems

In TDMA systems the entire bandwidth is used by each MS. The orthogonality between users is achieved in the time domain by dividing the time scale into time slots (TS's) which are periodically allocated to each MS for the duration of a call. Guard times between TS's are required in order to prevent symbol collisions. These collisions can occur due to signal propagation time differences. These guard times, as in guard bands, result in wasted radio resources.

³Note that symbols which are followed by the superscript 'u' are associated with the uplink channel; symbols which are followed by the superscript 'd' are associated with the downlink channel. This applies throughout this thesis.

A sequence of TS's forms a communication channel. The transmitter is silent between the consecutive TS's of a certain sequence. This results in a bursty transmission of data and a time compression of the information which is to be sent. The TDMA technique requires precise synchronisation between the communicating entities. Therefore it is more complex than the FDMA technique. It is found in [47] that the capacity of cellular TDMA and FDMA systems is the same. Therefore, (2.4) can also be applied to TDMA systems. The basic difference is that the transmitted powers in a TDMA system are greater than in an FDMA system. If a TDMA interface consists of n channels, then the transmitted powers are $10 \log n$ times higher than in an FDMA system [47]. The capacity of a TDMA systems is investigated in [49].

2.2.3 Cellular SDMA systems

In SDMA systems the multiple access is achieved by a spatial separation of the transmitted signals. Techniques such as antenna sectorisation, fixed beams or antenna beamforming can be applied. These techniques enable the transmitter to deliver the required signal power to the desired users and at the same time to reduce the interference from other links [50]. This means that SDMA exploits the spatial dimension [51, 52] rather than the time or frequency dimension⁴ in order to separate the users within a cell. As a consequence, spatially separated users transmit or receive at the same time and at the same frequency. Two basic beamforming techniques are differentiated [53]: a) *phased array antennas*: where the beamforming is achieved at the RF (radio frequency) level by controlling the amplitudes and phases of the feeding currents by means of attenuators and phase shifters, and b) *smart antennas*: where the beamforming is controlled at the baseband, *i.e.* the feeding currents of the sensor elements are directly proportional to the modulated baseband signal [54, 55]. As a counterpart to the beamforming algorithm at the transmitter a spatial filtering algorithm is required at the receiver in order to eliminate residual interference from other users. In particular, the spatial filtering requires knowledge of the spatial covariance matrix which contains essential spatial channel parameters. The following parameters, for example, form an essential input to the spatial filtering: a) number of dominant propagation paths, b) the direction of arrival of all dominant propagation paths and c) the attenuation of each path. The receiver, in turn, uses the information contained in the spatial covariance matrix for its beamforming. However, the spatial covariance matrix can only be used directly if the channel guarantees a certain grade of reciprocity, which normally is the case

⁴Note that the channel re-use in FDMA and TDMA systems is also an exploitation of the spatial dimension.

when using the TDD method. Therefore, TDD is the preferred duplex method in combination with SDMA⁵.

2.2.4 Cellular CDMA systems

The CDMA technique CDMA differs from TDMA and FDMA in that it permits multiple access at the same frequency carrier and at the same time. The user separation is achieved in the power or code domain because all co-existing users appear as noise by utilising spread spectrum techniques. These techniques build the foundation for CDMA. Therefore, a brief summary of spread spectrum communication is presented in the following.

For over half a century spread spectrum techniques had been used in military communication systems before they were considered for commercial wireless applications [56–60]. In a spread spectrum system, the frequency bandwidth is greater than the minimum bandwidth required to transmit the desired information. There are different methods as to how the spreading of the spectrum can be accomplished:

Direct sequence (DS) spread spectrum: A signal with a certain information bit rate is modulated on a frequency carrier with a much higher bandwidth than would be required to transmit the information signal. Each user is assigned a unique code sequence⁶ which has the property that the individual users information can be retrieved after despreading.

Frequency hopping (FH) spread spectrum: The available channel bandwidth is subdivided into a large number of contiguous frequency slots. The transmitted signal occupies one or more of the available frequency slots which are chosen according to a pseudo-random sequence.

Time hopping spread spectrum: A time interval which is much larger than the reciprocal of the information bit rate is subdivided into a large number of TS's. The information symbols are transmitted in a pseudo-randomly selected TS.

Chirp or pulse-FM modulation system: The frequency carrier is swept over a wide band during a given pulse interval.

⁵The FDD mode would require a frequency transformation of the spatial covariance matrix.

⁶In some literature code sequences are also referred to as 'signature waveforms'.

It is common in all spread spectrum techniques that the available bandwidth, B , is much greater than the bandwidth required to transmit a signal with an information data rate, W . The ratio B/W is the bandwidth spreading factor or processing gain, pg . The processing gain results in an interference suppression which makes spread spectrum systems highly resistant to interference or jamming. This property in particular makes spread spectrum techniques interesting for the application to wireless multiple access communication where a large number of uncoordinated users in the same geographical area access a radio frequency resource of limited bandwidth. Using the spread spectrum technique, the number of simultaneously active users permitted is proportional to the processing gain [61]. Since the early 1980s, this has led to the development of the CDMA technology which primarily utilises the pseudo noise (PN) DS spread spectrum technique [62–64]. Apart from the PN direct sequencing a second category of CDMA techniques exists. This is described as orthogonal DS–CDMA [65, Chapter 1]. The most significant differences between orthogonal DS–CDMA and PN DS–CDMA are highlighted below:

Orthogonal DS–CDMA systems Each data symbol is spread by an orthogonal code sequence.

Notable examples of orthogonal spreading codes are Walsh codes and OVVSF (orthogonal variable spreading factor) codes [66]. The number of users is upper bounded by the time–bandwidth product rather than by multiple access interference. This technique belongs to the same class of orthogonal systems as TDMA and FDMA systems. The disadvantage of the aforementioned orthogonal codes is that they do not fulfil the pseudo noise properties. Therefore, the performance of such a system is not robust against non–synchronous data transmissions and multipath propagation. In addition, synchronisation is often difficult to achieve because the size of the off–peak value relative to the peak value of the autocorrelation function is high.

PN DS–CDMA systems These systems use spreading codes which are not orthogonal, but have (almost) ideal properties with respect to the autocorrelation and the mutual cross–correlation functions [10, 56, 60]. The properties of the PN code sequences significantly determine the performance of the spread spectrum system. Therefore, several code families have been developed in recent years the most important of which are Gold codes, Kasami codes and random codes. The main advantages over orthogonal codes are;

- The users can be asynchronous. This means that the bit transmissions need not be aligned as, for example, in the uplink direction. Despite the asynchronous bit–overlaps the spread spectrum signals are still ‘quasi–orthogonal’.

- The number of users is no longer constrained by the time–bandwidth product of the code sequences (soft–capacity), but is primarily interference limited.
- The channel resources are shared dynamically. The reliability depends on the number of simultaneously active users rather than on the usually much larger number of potential users. This means that it is possible to trade off the quality of service (QoS) for an increased capacity. As a consequence, the calculation of the system capacity has become more complex.

In this thesis, PN DS–CDMA systems are considered because orthogonal CDMA systems would require an ideal channel. In addition, CDMA based standards use, at least, a PN code for the final scrambling of the transmitted data.

The wireless communication standards which utilise CDMA techniques, for example, IS–95 and UMTS use a combination of orthogonal codes and PN codes [6, 11], but this is merely aimed to increase the robustness of the system. However, in recent papers the concept of channel overloading is introduced. By using the channel overloading technique the overall system capacity [67, 68] is to be increased. In one application, for example, orthogonal DS–CDMA is overloaded with PN DS–CDMA techniques. It is reported in [68] that this method can increase the single cell capacity by about 40 %.

Since in this thesis PN DS–CDMA techniques are considered, henceforth the expression CDMA will be used to describe this particular multiple access method. As mentioned above, the capacity calculation of a CDMA system is more complex since it is interference limited. Each user contributes to the common noise floor which is usually assumed to be Gaussian [25]. Thus, interference is a most important parameter in a CDMA system and capacity analyses focus on calculating interference quantities [25]. Since interference is dependent on many factors, for example, power control, adjacent channel leakage and handover strategies to name only a few, the capacity figures can vary significantly (soft–capacity). The capacity in the uplink direction of CDMA systems has been investigated by many researchers [22, 25, 69–73]

CDMA is used in the 2nd generation mobile communication standard IS–95 [61] which gained special interest after it had been claimed that CDMA can achieve a greater spectral efficiency than conventional FDMA and TDMA methods [25]. In [74], for example, Viterbi claims that

the capacity of a CDMA system can be:

$$\text{Capacity (CDMA)} \approx 1 \text{ Bit/Sector/Hz/Cell ,}$$

assuming the voice activity of each user to be 50 % and the sectorisation gain to be 4 – 6 dB. This figure was compared to the capacity of GSM (Global system for mobile communications)

$$\text{Capacity (GSM)} \approx 1/10 \text{ Bit/Sector/Hz/Cell ,}$$

where a frequency re-use factor of 1/4, *i.e.* $q_s=3.46$, was assumed. Theoretically, when considering a single cell and an AWGN (additive white Gaussian noise) channel the multiple access schemes CDMA, FDMA and TDMA are equivalent with respect to spectral efficiency [45, 75]. Therefore, the greater spectral efficiency of CDMA systems primarily results from three basic principles:

1. The same channel is used in every cell (channel re-use factor of 1) [10],
2. Interruptions in transmission, *e.g.* quiet periods of a speaker, when assuming a voice service, are exploited [25].
3. Antenna sectorisation is used.

Apart from the above methods there are further techniques such as macro diversity [45] and soft handovers [76, 77] which are exploited in CDMA systems to enhance the spectral efficiency. However, it was demonstrated that the advantages of CDMA systems were slightly overestimated [20, 21, 78] due to two basic hypotheses which usually cannot be fulfilled in a realistic environment:

1. Perfect power control,
2. All MS's are allocated to the most favourable BS, *i.e.* the BS offering the lowest path loss,

In further analyses, it became obvious that the requirements on power control in CDMA systems is a critical issue [79–83] as otherwise the capacity can suffer significantly. Furthermore, in [20] it was demonstrated that the allocation of a MS to the nearest BS rather than the BS

offering the lowest path loss can increase interference by a factor of 4. This requires special handover techniques as otherwise capacity can suffer significantly.

2.2.4.1 The uplink in a CDMA system

Ideally, in a CDMA system all co-existing users appear as Gaussian noise. Therefore, the required carrier to interference ratio, γ^u , when assuming a multiple cell environment can be denoted as follows:

$$\gamma^u = \frac{P_{u_i}^u}{\underbrace{\sum_{i \neq j}^M \rho_j P_{u_j}^u}_{\text{own cell interference}} + \underbrace{I_o^u}_{\text{other cell interference}} + \underbrace{N}_{\text{noise power}}}, \quad (2.5)$$

where $P_{u_i}^u$ is the signal power of the desired user in the uplink; $P_{u_j}^u$ is the interference power received from a MS using the same channel in the same cell; ρ_j is the voice/data activity factor (usually modelled as independent Bernoulli random variables [23]) of the j th user; I_o^u is the interference power from other cells; N is thermal noise power and M is the number of MS's per cell. It can be seen that the interference is composed of three parts:

Own cell interference This is equivalent to multiple access interference (MAI) due to the cross correlation of the spread spectrum signals in a CDMA system. Intensive research on receiver structures is carried out to eliminate or reduce MAI by multi-user [65, 84–87] or joint-detectors [88, 89]. The problem of these receivers is that the complexity increases with the length of the spreading codes.

Other cell interference Other cell interference can be divided into CCI and ACI conveyed by neighbouring or co-existing cells in a cellular environment. In [27] the power ratio of co-channel interference to the desired signal power is calculated. The results of this paper show that co-channel interference can be $6.23 M$ times higher than the desired signal power if a MS is assigned to the closest BS. This figure varies considerably if the MS is allocated to a BS which offers the lowest path loss. If, for example, the MS can choose the best out of 3 closest BS's the inference ratio decreases to $0.74 M$. Since own-cell interference is also proportional to M , the ratio of other cell interference to own-cell interference is independent of

the number of users and varies between 6.23 and 0.74 for the observed case. Therefore, perfect own-cell interference cancellation may, in the worst case, only reduce the total interference by $\leq \frac{1}{6.23+1} = 13.8\%$ (equality applies if the thermal noise power is zero). For comparison the interference reduction due to perfect own-cell interference cancellation in the case of assigning the MS to the best BS (best out of 3 BS's) yields $\leq \frac{1}{0.75+1} = 57.1\%$. Given that the frequency re-use of a cellular CDMA system is generally considered to be one [10], it is obvious that other cell interference can significantly reduce the advantages obtained by multiuser detectors. This mechanism was put into a more general context using the Shannon capacity equation [48, 90]. Viterbi [90] compared the capacity of a multi cell system without interference cancellation with the capacity of a multiple cell system assuming perfect own-cell interference cancellation. In the latter case, the total carrier-to-noise ratio is:

$$\frac{C}{N_0} = \sum_{i=1}^M \frac{C_i}{N_0}, \quad (2.6)$$

where N_0 is the thermal noise density power and C_i is the carrier power of the i th user. The Shannon's channel capacity for the AWGN (additive white Gaussian noise) channel is:

$$W < B \log_2 \left(1 + \frac{C}{N_0 B} \right), \quad (2.7)$$

where B is the total channel bandwidth and W is the total bit-rate calculated as $W = \sum_{i=1}^M W_i$ with W_i being the bit-rate of a single user. If the bit-rate of each user is the same it holds that:

$$W = \tilde{M} W_i, \quad (2.8)$$

where \tilde{M} is the number of simultaneously active users when assuming ideal interference cancellation. Substituting (2.8) into (2.7) and re-arranging yields:

$$\frac{\tilde{M}}{pg} < \log_2 \left(1 + \frac{C}{N_0 B} \right), \quad (2.9)$$

where pg is the processing gain defined as $pg = \frac{B}{W_i}$. It is shown in [27] that in the case when all cells are equally loaded, and all BS's employ power control on their populations of MS's, the other cell interference is proportional to C . Furthermore, the assumption that the interference from other cells is Gaussian is justified by the Central Limit Theorem. Thus, the interference

power from the neighbouring cells can be written as follows:

$$I_o^u = N_0 B = f C , \quad (2.10)$$

where f is the proportionality factor described above. The relationship in (2.10) is substituted into (2.9) which yields:

$$\frac{\tilde{M}}{pg} < \log_2 \left(1 + \frac{1}{f} \right) . \quad (2.11)$$

In order to assess the impact of interference cancellation for a cellular CDMA system in the following the performance of ideally coded users without interference cancellation is considered. Perfect power control is assumed, *i.e.* the power received from each MS within a cell is the same ($P_u^u = P_{u_1}^u = P_{u_2}^u = \dots , P_{u_M}^u$). Hence, the own-cell interference can be expressed as follows:

$$I_{own} = (M - 1)P_u^u \approx M P_u^u = C , \quad (2.12)$$

where M is the number of simultaneously active MS's in the multi cell environment without interference cancellation. Using (2.10), (2.12) and assuming N to be negligible, (2.5) becomes:

$$\gamma^u = \frac{P_u^u}{M (I_{own} + I_o^u)} = \frac{1}{M (1 + f)} = \frac{E_b/N_0}{pg} , \quad (2.13)$$

The bit-energy to interference ratio is expressed by E_b/N_0 . From (2.13) the number of users in the multi cell environment can be found as follows:

$$M = \frac{pg}{(E_b/N_0)(1 + f)} . \quad (2.14)$$

In a AWGN channel E_b/N_0 has a lower bound [28] as follows:

$$E_b/N_0 > \ln 2 . \quad (2.15)$$

This bound equals Shannon capacity for a channel with infinitely wide bandwidth. Applying (2.15) to (2.14), the number of users in a multi cell environment divided by the processing gain

is upper bound by:

$$\frac{M}{pg} < \frac{1}{(1+f) \ln 2} . \quad (2.16)$$

Let G be the ratio of the capacity in the case of perfect interference cancellation, (2.11), to the capacity in the case in which no interference cancellation is used, (2.16),

$$G = \frac{\tilde{M}}{M} = (1+f) \ln \left(1 + \frac{1}{f} \right) . \quad (2.17)$$

The relative number of users with ideal interference cancellation, (2.11) and without interference cancellation, (2.16), and the respective capacity gain, (2.17), are depicted in Figure 2.2. From the results in Figure 2.2 two important conclusions of a DS-CDMA system can be de-

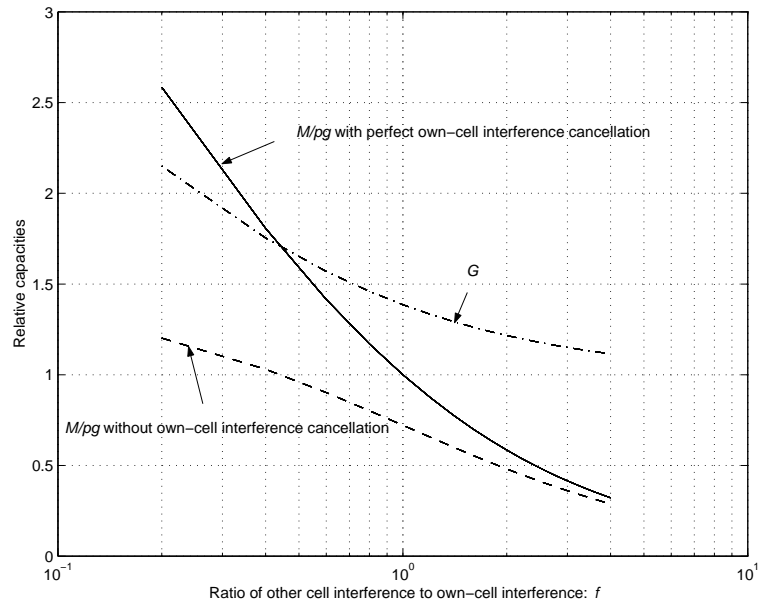


Figure 2.2: Theoretical capacity limits of a DS-CDMA multiple cell system with and without interference cancellation.

duced:

1. The capacity of a cellular CDMA system can be greater than the processing gain. In contrast, the capacity of a FDMA or TDMA system is always less than or equal to the processing gain which can be found from the “radio capacity equation by Lee”, (2.4).
2. As the other cell interference increases the total capacity diminishes and the gain due to multiuser detection decreases significantly. With a ratio of other cell interference to

own-cell interference of $f = 0.6$ the ideal interference cancellation merely increases the total capacity by less than 60 % — if $f = 4$ the capacity gain has decreased considerably to only about 13 %. Therefore, in order to achieve a high cellular capacity, the aim is to minimise other cell interference as only this enables the efficient use of techniques such as interference cancellation. For this reason, it becomes a main goal of this thesis to reduce other cell interference in a cellular TD-CDMA/TDD network.

2.2.4.2 The downlink in a CDMA system

The main differences between the uplink and downlink are: a) synchronous transmission can be applied in the downlink, whereas in the uplink asynchronous transmission must be assumed and b) each BS may transmit user specific signals and a common pilot signal for coherent demodulation (applied, for example, in IS-95). A consequence of a) is that if orthogonal codes are used (for example Walsh codes) to distinguish individual users, the orthogonality in the downlink can be maintained (no own-cell interference) assuming that multipath propagation does not violate the orthogonality at the mobile receiver [24, 91, 92]. Therefore an orthogonality factor, τ , is defined [91],

$$\tau = \frac{E_b}{I_0} \left(\frac{E_b}{N_0} \right)^{-1}, \quad (2.18)$$

where $\frac{E_b}{I_0}$ is the bit-energy to interference ratio when the orthogonality is not maintained and, thus, the signal is corrupted by own-cell interference. The ratio $\frac{E_b}{N_0}$ is the bit-energy to interference ratio for the case that orthogonality is entirely maintained. From the definition of τ it can be seen that the higher its value the more the signals are corrupted by multipath propagation. It is reported that τ may vary between 0.3 and 0.8 [91] with the greater value obtained in environments which are subject to severe multipath propagation.

When an additional pilot signal is used, the total carrier power yields (symbols with the superscript d are associated with the downlink):

$$P_C^d = P_{pilot} + \underbrace{\sum_{i=1}^M \tilde{P}c_i^d}_{P_{users}}, \quad (2.19)$$

where P_{pilot} is the pilot signal power and $\tilde{P}c_i^d$ is the code power for the i th user. A factor ψ is

used in [25] to model the user specific fraction of the total carrier power,

$$\psi = \frac{P_{users}}{P_C^d}. \quad (2.20)$$

In [25], $\psi = 0.8$ is used. With the approximation of $\sum_i^{M-1} \tilde{P}_{c_i}^d \approx \sum_i^M \tilde{P}_{c_i}^d$, the carrier-to-interference ratio at the MS, γ^d , can be modelled as follows:

$$\gamma^d = \frac{\frac{\tilde{P}_{c_i}^d}{a_i}}{\underbrace{\frac{\tau}{\psi a_i} \left(\sum_{i \neq j}^M \tilde{P}_{c_j}^d \right)}_{\text{own cell interference}} + \underbrace{I_o^d}_{\text{other cell interference}} + \underbrace{N}_{\text{noise power}}}, \quad (2.21)$$

where a_i is the path loss between the desired user i and the respective BS. In a severe multipath environment ($\tau = 0.8$) the advantages due to the synchronous transmission may be cancelled by a greater transmitted carrier power as a consequence of the pilot signal ($\psi = 0.8$). For this scenario ($\tau = \psi$), (2.21) yields:

$$\gamma_i^d = \frac{\frac{\tilde{P}_{c_i}^d}{a_i}}{\underbrace{\frac{1}{a_i} \left(\sum_{i \neq j}^M \tilde{P}_{c_j}^d \right)}_{\text{own cell interference}} + \underbrace{I_o^d}_{\text{other cell interference}} + \underbrace{N}_{\text{noise power}}}, \quad (2.22)$$

2.3 TDD inherent properties

This section addresses the properties inherent to TDD. The advantages and disadvantages of TDD are discussed. The basic mechanism of TDD is that both the uplink and downlink are carried out at the same radio frequency carrier. In contrast, the FDD technique requires a separate frequency carrier for each transmission direction (paired radio frequency spectrum). For new global wireless communications systems or in the case of spectrum re-farming it has often been shown to be difficult to allocate a paired radio frequency spectrum to the new system. The TDD mode, in contrast, only needs a single carrier to achieve duplex communication. This is one reason why the Universal Mobile Telecommunications System (UMTS) in Europe and the equivalent W-CDMA standard in Japan, in addition to the FDD mode, also include a TDD interface [39, 93].

2.3.1 Channel reciprocity

Since the uplink and the downlink use the same radio frequency channel, both directions experience the same propagation conditions (channel reciprocity), provided that the TDD frame length is shorter than the coherence time of the channel [94]. This assumption holds for slowly moving user populations. The reciprocity of the channel has several implications on the system design. These implications will be examined briefly in the following sections.

Pre-RAKE concept The reciprocity of the radio channel can be exploited in the design of receiver structures. A notable example is the Pre-RAKE architecture [42, 95–99] depicted in Figure 2.3. By using the Pre-RAKE technique it is possible to retain the advantages of the

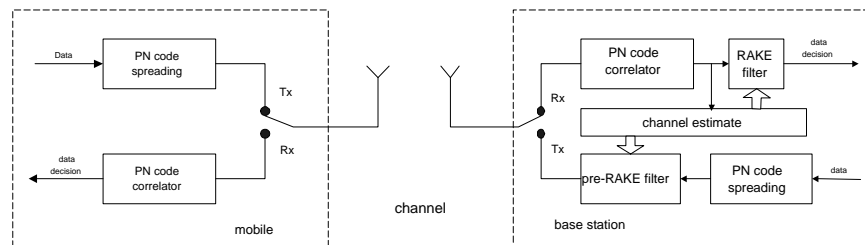


Figure 2.3: *The Pre-RAKE concept.*

RAKE combining and at the same time using a simple single path receiver at the mobile unit. The channel will only be estimated once, at the BS. With the knowledge of the impulse response of the channel, the BS performs the RAKE combining function *before* transmission (hence Pre-RAKE). Thus, the output signal of the Pre-RAKE combiner is the result of the convolution of the spread spectrum signal and the time-reversed channel impulse response. Since it is assumed that the channel does not vary between the reception and transmission period, a simple receiver structure can be applied at the mobile which ideally only consists of a matched filter. Therefore, the processing effort in the mobile is significantly reduced and, as a consequence, the power consumption can be kept low.

Space diversity Space diversity is also known as antenna diversity. In terrestrial wireless mobile communications, objects such as, for example, buildings, trees and mountains cause reflections of the transmitted signal. As a consequence, the signal may arrive via different paths.

Due to the accompanied phase shifts the signals may overlap constructively or destructively causing the so called 'fading' effect. This effect is usually modelled by a Rayleigh distribution [11]. Ideally, the fading statistics can be considered uncorrelated between antennas which are spatially separated by more than half the wavelength [100, p. 311]. In actual fact, the required spacing strongly depends on the disposition of the scatterers and the resulting angular spread of the signal. The antenna separation needs to be greater than half the wavelength in the case of a small angular spread. A small angular spread can be found at macro cell BS's with an antenna height of several meters above the ground. In these cases the antenna separation needs to be about 10–20 times the wavelength.

The little correlation of signals on spatially separated antennas can be exploited by antenna arrays which collect the (ideally) uncorrelated signals and combine them so as to improve the bit error performance. The reciprocity of the channel in TDD may be used to avoid antenna arrays at the MS, but still exploit space diversity on both links. This may be accomplished by an antenna array at the BS. The BS determines the antenna elements which receive the strongest signals and, in turn, transmit the highest power on these antennas (transmit diversity) while the reciprocal channel ensures that the MS receive a strong signal at a single antenna. It was demonstrated in [101, 102] that transmit diversity in TDD can significantly improve the bit error performance.

Open-loop power control In FDD the frequency separation of the uplink and the downlink causes both links to experience different fading conditions. This means that the power control unit cannot determine the required transmit power directly from the instantaneously received power level. In the downlink, for example, the received power level of a MS needs to be reported to the BS in order to enable the BS to determine the necessary power it has to transmit (closed loop-power control). This procedure can result in large delays and, in addition, requires extra capacity for signalling. In contrast, under the assumption of a reciprocal channel, a TDD system experiences correlated fading on both links. This means, for example, given that the path loss is known *a priori*, that a MS can directly determine the power it needs to transmit from the received power level (open-loop power control). This mechanism does not involve extra overhead for signalling. The benefits of open-loop power control are diminished if large delays occur between a transmit and receive TS at the same entity. Such delays may be induced when the TDD mode and the TDMA technique are combined. Several studies have been undertaken to examine the advantages of open-loop power control in TDD [103–105].

2.3.2 Round trip delays

Since the radio signals propagate with finite speed (speed of light), the transmitted signal arrives with a certain delay (access delay) at the target entity (BS or MS). Due to the TDD principle the same entity can only then start transmitting its information which arrives at its destination with the same access delay. Hence, during a time period of two times the access delay, which is equivalent to the round trip delay, no information can be sent. This mechanism is shown in Figure 2.4. The round trip delays require a certain guard time. It is easy to see that guard times

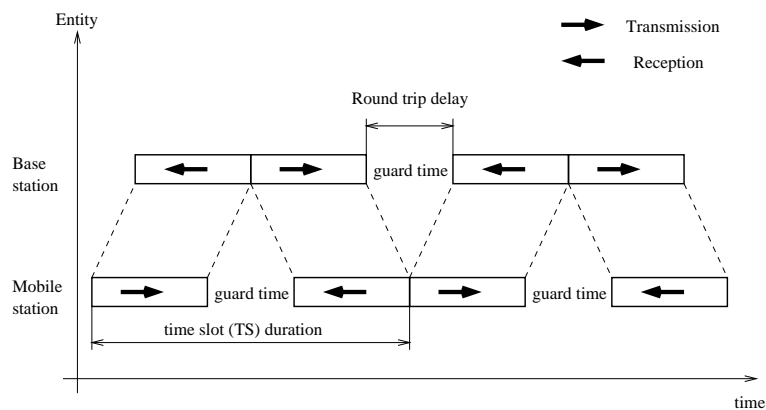


Figure 2.4: *The round trip delay in TDD.*

result in a reduction of the spectral efficiency. Round trip delays represent a major problem in TDD systems, as they increase with an increasing transmitter–receiver separation, TDD systems are primarily used for short range wireless communication (DECT, HIPERLAN, Bluetooth, to name only a few).

One possible measure to increase the ratio between guard times and TS duration is to increase the TS duration. This however can violate the channel reciprocity. Clearly, these conflicting requirements result in a trade–off between channel reciprocity and spectral efficiency which was investigated in [106].

Recently, relaying systems have attracted the interest of researchers [43]. The relaying technique implicitly reduces the problems resulting from round trip delays since there are now multiple hops from BS to MS, and vice versa. This increases the probability for shorter hops.

2.3.3 Synchronisation and channel asymmetry

A powerful advantage of TDD is to arrange channel asymmetry [42, 107] without on-the-fly filter reconfigurations (as would be required in FDD). This property becomes increasingly important as it is predicted that wireless data applications, *e.g.* wireless Internet, will demand up to 5 times more capacity in the downlink than in the uplink by the year 2005 — with the annual growth of mobile data traffic being anticipated to be 70 % over the next 5 years [5, 108]. However, if the TDD interface is used in a multiple cell environment severe interference problems can occur [42]. These problems arise primarily because TDD is exposed to additional interference mechanisms (in comparison with FDD). These mechanisms are illustrated with the aid of Figure 2.5. This Figure shows a simple cellular structure consisting of two adjacent cells.

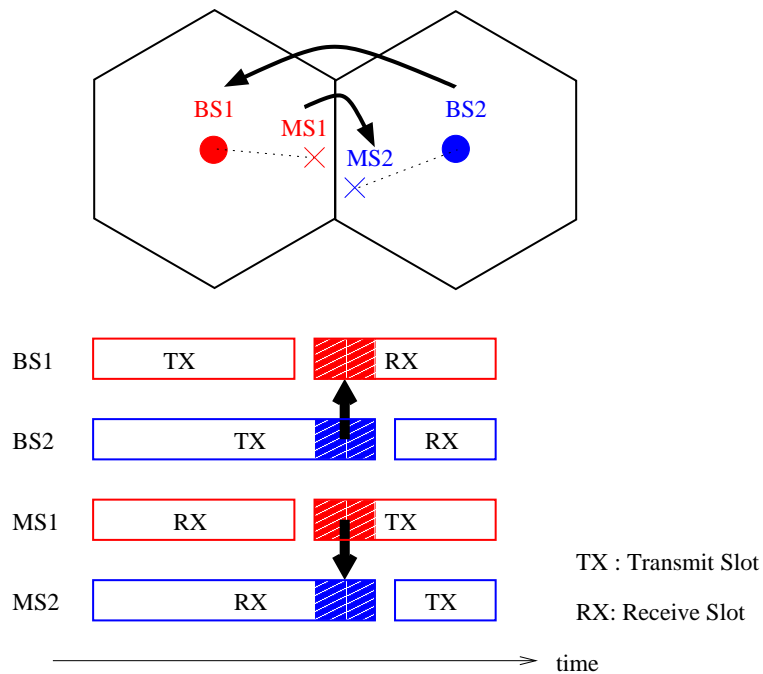


Figure 2.5: *Interference scenarios in cellular TDD systems with cell independent channel asymmetry.*

In each cell a different rate of asymmetry⁷ is used. This causes asynchronous TS overlaps (red and blue shaded areas) which has a significant impact on the total interference. In this context, the BS's not only interfere with the neighbouring MS's, and vice versa (FDD equivalent interference scenario), but also with other BS's. Similarly, MS's interfere with adjacent MS's. The latter interference scenarios are depicted in Figure 2.5 (BS→MS and MS→BS interference

⁷Note that symmetric traffic is only a special case of the set of achievable rates of asymmetry.

is left out for reasons of clarity). In particular, the interference between MS's can be severe given that the distance between two MS's at the cell boundary can be very low. However, in [109] BS \leftrightarrow BS interference was reported to be more significant than MS \leftrightarrow MS interference. It is important to note that downlink power control was not assumed in that investigation.

In order to avoid BS \leftrightarrow BS and MS \leftrightarrow MS interference the frames must be synchronised and both cells need to adopt the same rate of asymmetry. Clearly, this results in a significant limitation which may greatly affect the spectral efficiency and flexibility.

If the TDD mode is used in TDMA an additional degree of freedom (in the time domain) exists which can be used to resolve additional interference by using dynamic channel assignment (DCA) algorithms [110, 111]. The TDD mode of UMTS (UTRA-TDD) consists of a TD-CDMA interface which adds another dimension (code domain) that can be utilised to establish a connection [40]. The combination of a code, TS and frequency in UTRA-TDD is defined as a resource unit (RU) [112].

Chapter 3 is dedicated to characterising other cell interference in a hybrid TD-CDMA/TDD system assuming different rates of asymmetry in neighbouring cells. The results of the interference study will be used to develop DCA strategies, and it can be shown that asynchronous TS overlaps may be used constructively to permit cell independent asymmetries (chapter 4). It can also be shown that asynchronous TS overlaps can be utilised to enhance cell capacity (chapter 5).

2.3.4 The TDD underlay concept

Due to increasing asymmetric traffic on the air interface, one communication direction of an FDD interface will be underused provided that the carrier spacing is kept constant. The main idea behind the TDD underlay is to exploit this underused radio spectrum of a cellular CDMA-FDD system. A co-existing TDD interface, which only needs an unpaired frequency spectrum, utilises the underused FDD frequency band for additional connections. Technically a TDD interface can be used within either the FDD uplink or downlink frequency band.

A hierarchical system architecture [113, 114] consisting of TDD pico cells which exclusively use FDD resources of a macro cellular overlay is proposed [13, 115]. A DCA decides whether to use the FDD uplink or downlink frequency band. The TDD underlay concept is depicted in Figure 2.6. The red arrows indicated the interference paths when the TDD pico cell uses the

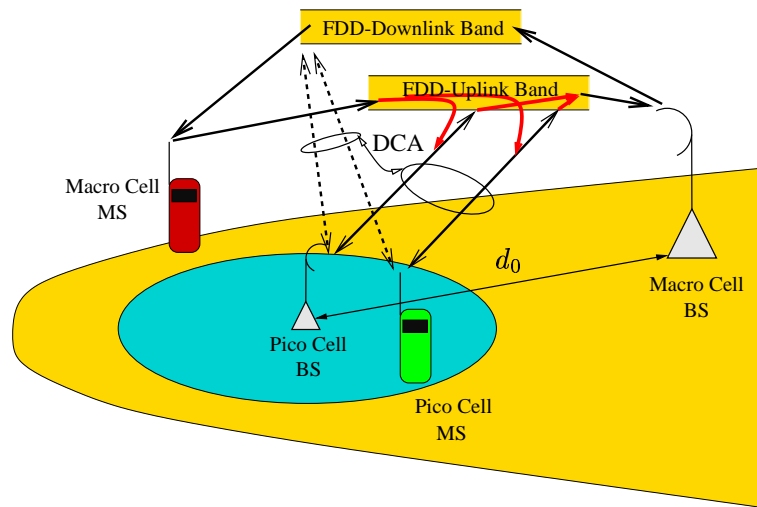


Figure 2.6: *The TDD underlay concept.*

FDD uplink frequency band. It can be seen that the macro cell MS interferes with the pico cell BS and MS. In turn, the pico cell entities interfere with the macro cell BS.

The proposed CDMA–TDD underlay in [13] uses a PN code sequence with a cell unique phase offset relative to the CDMA–FDD macro cellular overlay. The authors reported substantial capacity gains without a significant deterioration of the QoS. The pico cells are assumed to consist of a single indoor BS and a single indoor MS and are randomly distributed. Since, however, severe interference can be anticipated if macro and pico cells are in close proximity [116] a further investigation on the TDD underlay concept was carried out under this PhD project [15, 16] which led to a patent application transferred to Siemens AG [14]. In this investigation the TDD is only considered to be operated in the FDD uplink band due to an anticipated channel asymmetry in favour of the downlink.

In another investigation, the feasibility of the TDD underlay was confirmed [117, 118] provided that the BS separation distance is properly chosen. The frequency usage when operating the TDD underlay in a system with two air interfaces (FDD and TDD) and harmonised frame structures is shown in Figure 2.7. The components of the TDD pico cell or indoor cell are followed by the letter 'i' (BS_i, MS_i respectively) whilst the FDD macro cell or outdoor cell entities are marked with an additional 'o'.

Note, that the TDD underlay may be used to accomplish cell independent channel asymmetry in the TDD subsystem without asynchronous TS overlaps. Furthermore, the flexibility on the air interface is increased as, for example, uplink radio resources can be converted into downlink

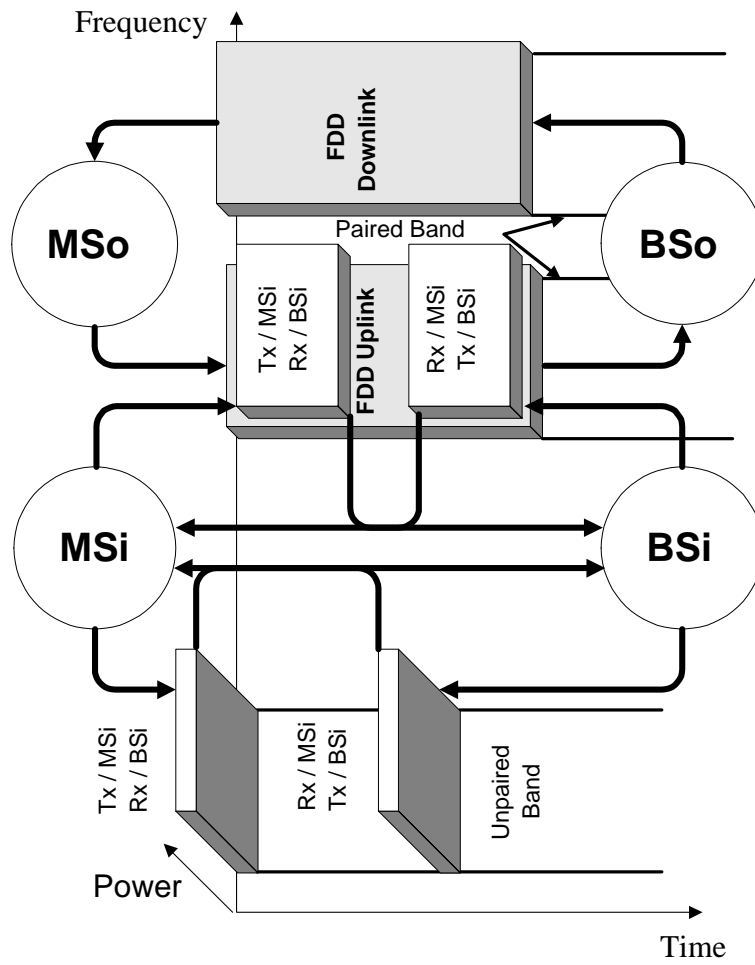


Figure 2.7: Frequency use in a dual interface system in which the TDD underlay is applied in order to achieve greater flexibility.

capacity. In [16] the system in Figure 2.7 is analysed under the following conditions:

- Carrier-to-interference threshold: $\gamma_{pico}^u = -8.5$ dB
- Carrier-to-interference threshold: $\gamma_{macro}^u = -19.0$ dB
- 10 dB wall attenuation around the indoor pico cell
- Symmetrical speech 8 kbps speech service
- Spatially uniform user distribution
- Tolerable outage of 5 %
- Pico cell radius of 50 m
- Macro cell radius of 1000 m
- Path loss exponent of 3.8

The capacity (number of simultaneous active MS's) is calculated with the standard deviation of lognormal shadowing (σ) and the BS separation distance (d_0) as a parameter. The results are depicted in Figure 2.8.

It is obvious that the smaller d_0 the more the FDD uplink capacity is required for an additional TDD link due to the high interference from the underlay. In turn, the greater d_0 the smaller the likelihood that spare capacity in the FDD uplink can be exploited by the TDD underlay. The reason is that the macro cell mobiles cause high interference since the distance between a MS_o and the BS_i can be very small. In Figure 2.8 the blue curves show the remaining capacity in the FDD uplink dependent on the number of MS_i's. In contrast, the red curves show the additional TDD capacity dependent on the number of MS_o's. In both cases the arrows indicate the functional relationship ($x \rightarrow f(x)$). It can be seen that the higher the BS separation the more the basic FDD uplink capacity is preserved. On the other hand, the higher the BS separation the less capacity can be found in additional pico cells due to the greater transmission powers of the macro cell mobiles at outer regions. This trade-off leads to an optimum for the BS separation.

The aim is to accommodate as many mobiles as possible within the joint layers (pico and macro cell) instantaneously. There is no real gain in flexibility if there is, for example, additional pico

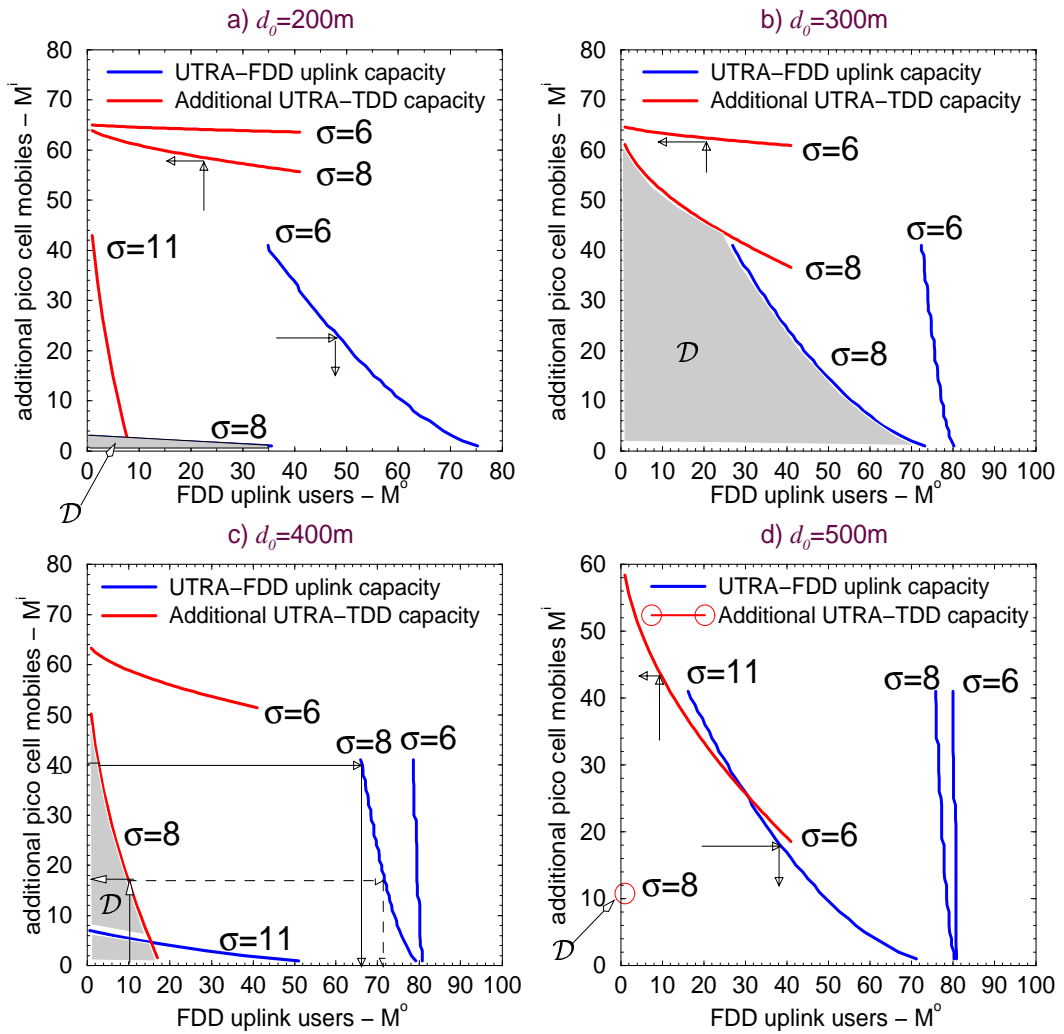


Figure 2.8: The additional numbers of MS's in the pico cell are indicated by red curves. Whereas, the capacity reduction in the FDD uplink is shown by the blue curves. Different lognormal shadowing scenarios are depicted in each plot. Moreover the effects of different BS separations are shown in plot a)–d): (a) $d_0=200m$, b) $d_0=300m$, c) $d_0=400m$ and d) $d_0=500m$.

cell capacity but the FDD uplink is occupied by a single user. One exception is when there is only downlink capacity required in the FDD cell and the FDD uplink is mainly unused (only a negligible amount of control traffic). Such a scenario is depicted in Figure 2.8(a) ($d_0=200\text{m}$). It can be seen that for $\sigma = 11$ dB there is only additional pico cell capacity, but any pico cell mobile will on average occupy the whole FDD uplink capacity due to the close location. This effect is explained more precisely with the aid of Figure 2.8(c) and with the following example. Initially 10 macro cell mobiles are assumed which leads to approximately 17 additional links in the pico cell. In turn, 17 pico cell users will accommodate up to about 72 macro cell mobiles. Here the effects of mutual interference become apparent because 72 macro cell mobiles would generate too much interference to permit an additional TDD link. Hence, the flexible exchange of radio resources between the FDD and the TDD mode is limited. It is desirable to define a measure for the flexibility of the pico cellular underlay. This is derived with the aid of Figure 2.9. The set \mathcal{E} is defined as the operation area of the additional pico cell capacity and \mathcal{F}

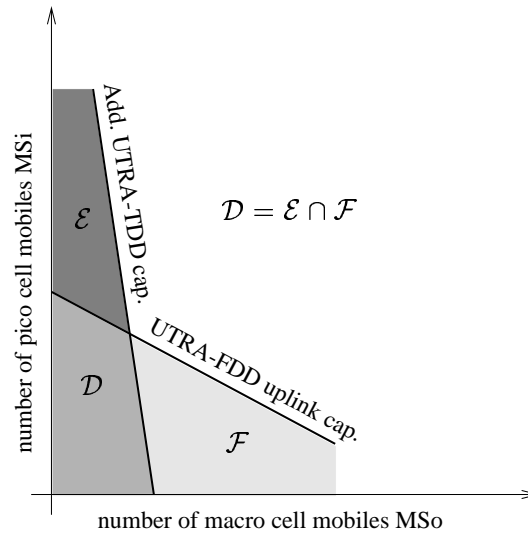


Figure 2.9: The area defined by \mathcal{D} serves as a measure for the flexibility of the TDD Underlay. Within the area specified by \mathcal{D} the FDD uplink radio resources can be exchanged between the macro cell and pico cell.

is defined as the operation area of the FDD uplink capacity. Let $\mathcal{D} = \mathcal{E} \cap \mathcal{F}$ then it can be stated that the flexibility increases with \mathcal{D} . This can be applied to the results in Figure 2.8(a)–(d). Set \mathcal{D} for $\sigma = 8$ dB is highlighted for $d_0=200\text{m}$ to $d_0=500\text{m}$. It can be seen that the maximum is reached for $d_0=300\text{m}$ whereas for $d_0=500\text{m}$ it shrinks to just one point. Furthermore, for small BS separations \mathcal{D} is determined by the intensive use of FDD uplink capacity. In contrast for high BS separations only the reduced additional TDD capacity limits \mathcal{D} .

The approximate maximum of capacity of one CDMA–TDD carrier is 64 (8 users per slot and in total 8 slots per frame) assuming equal data rates, symmetrical services and no multi–user detection. This maximum for the CDMA–FDD uplink is about 81 users with an overall spreading factor (SF) of 256. These figures can be compared with the cumulative maximum in Figure 2.8(b) with $\sigma = 8$ dB which is about 70 users (e.g. 40 pico cell users and 30 macro cell mobiles simultaneously). Thus, there is no significant increase in spectral efficiency.

Lognormal shadowing with $\sigma = 11$ dB results in no advantage to the TDD underlay, i.e. $\mathcal{D} = \emptyset$ for all d_0 . Furthermore, lognormal shadowing with $\sigma = 6$ dB yields the best results for $d_0=300$ m. In this case even the spectral efficiency can be increased because in total more than 81 users can be accommodated within the UTRA–FDD uplink (as an example, with 40 MSOs about 60 MSIs can be served in the FDD uplink resulting in an increased spectral efficiency of about 25 %).

Slow fading (shadowing), usually modelled as a lognormal random variable with zero mean, has a significant impact on the performance of the TDD underlay concept. The reason for this strong dependency is that the interference path and the desired path cannot be assumed to be strongly correlated since co–location is not feasible. As a consequence the interference signal can be significantly higher than the received signal at the desired BS. Furthermore, the extra capacity in the FDD uplink cannot be guaranteed at any time; it is scenario dependent. However, channel asymmetry is primarily required by packet–oriented data services which may not require a real time channel. Therefore, the characteristics of the additional capacity gained from the TDD underlay and the requirements of packet–data services are not contradictory.

2.4 The TDD air interface of UMTS

The air–interface of UMTS is known as: UMTS terrestrial radio access (UTRA) where the TDD and FDD mode are referred to as UTRA–TDD, and UTRA–FDD respectively. The UTRA–TDD mode is composed of a TDMA and a CDMA component. This hybrid multiple access technique is described as TD–CDMA. The basic radio interface parameters such as chip rate, bandwidth and modulation are harmonised between the UTRA–TDD and UTRA–FDD systems. A good overview of the UTRA–TDD interface can be found in [40].

The channel spacing is 5 MHz with the channel raster being 200 kHz [119] which means that the carrier frequency must be a multiple of 200 kHz. The frame duration is 10ms. One 10 ms

frame corresponds to one power control period. A frame is divided into 15 time slots (TS) and one TS consists of 2560 chips resulting in a chip rate of 3.84 Mcps. In addition, UTRA–TDD also supports a low chip rate option (1.28 Mcps) in order to facilitate future system extensions. Each TS can be allocated to either the uplink or downlink. This provides the basic mechanism to easily enable the asymmetric use of the channel. In any configuration at least one TS has to be allocated to the downlink and at least one TS has to be allocated to the uplink.

OVSF codes with a maximum SF of 16 are used for channelisation. The short spreading factor permits the use of joint detection [88]. In the downlink either a SF of 16 or 1 is applied. Parallel physical channels can be used to support higher data rates above the basic rate of 16 kbps. In the uplink the SF is variable and ranges from 1 to 16 [120].

Due to the TDMA component an effective interference avoidance mechanism exists, because interference between neighbouring MS's can be eliminated by using different TS's provided that the frames are synchronised. This however requires the use of certain channel allocation strategies [111, 121], in particular if different channel asymmetries between neighbouring cells should be supported.

2.5 Radio resource allocation techniques

In a cellular network certain radio resources allocation methods are required to mitigate the detrimental impact of interference (CCI and ACI). Three basic concepts of radio resource allocation can be distinguished [122, 123]:

- static or fixed channel assignment (FCA) techniques
- dynamic channel assignment (DCA) techniques
- random channel assignment (RCA) techniques

The principles of these methods are described in the following section.

2.5.1 Fixed channel assignment techniques

An FCA method allocates a fixed fraction of all available channels to an individual cell of a cellular environment. The same group of channels is only used in cells that are separated by a

minimum distance D . The channel re-use distance D ensures that CCI does not deteriorate the system performance greatly. The cluster size basically determines the system capacity since it specifies the maximum number of simultaneously active connections that can be supported at any given time. The group size which equals the number of channels per cell, M , can be found from (2.3). It can be seen that M is increasing with a decreasing cluster size K , but this also means that the interference is higher which, in turn, reduces the capacity or QoS.

The impact of the cluster size K on capacity can be studied with the following model: let the number of users who request a channel, M_c , be Poisson distributed with mean $E(M_c) = \lambda$, then the assignment failure probability can be defined as follows:

$$p(\lambda) = \frac{E[\max(0, M_c - M)]}{E(M_c)} = \sum_{i=M}^{\infty} (i - M) \frac{\lambda^{i-1}}{i!} \exp(-\lambda). \quad (2.23)$$

The relative traffic load can be expressed as:

$$\omega = \frac{\lambda}{M}. \quad (2.24)$$

Substituting (2.24) into (2.23) yields the final assignment failure probability,

$$p(\omega) = \sum_{i=M}^{\infty} (i - M) \frac{(M\omega)^{i-1}}{i!} \exp[-(M\omega)]. \quad (2.25)$$

Note, that equation (2.25) is merely based on traffic theory and assignment failures due to high CCI are therefore not considered. The results of (2.25) for a different number of available channels per cell is plotted in Figure 2.10. It is obvious that the assignment failure rate increases as the relative load, ω , grows. The interesting result is that for the same relative load the failure rate increases with a decreasing number of channels per cell, M . This means that a system with a greater number of channels per cell is more efficient than a system with only a few channels. This effect is well known as the trunking gain. Consequently, fixed channel assignment techniques result in poor spectral efficiency. Given that CCI varies with the cell load, there might be traffic scenarios where a lower channel re-use distance can be tolerated in favour of a temporarily higher number of channels available in a single cell (or cluster of cells). This would require methods which dynamically monitor interference and load situations throughout the network and which carry out channel re-configurations accordingly. In contrast to DCA strategies, FCA techniques are not designed to achieve this flexibility.

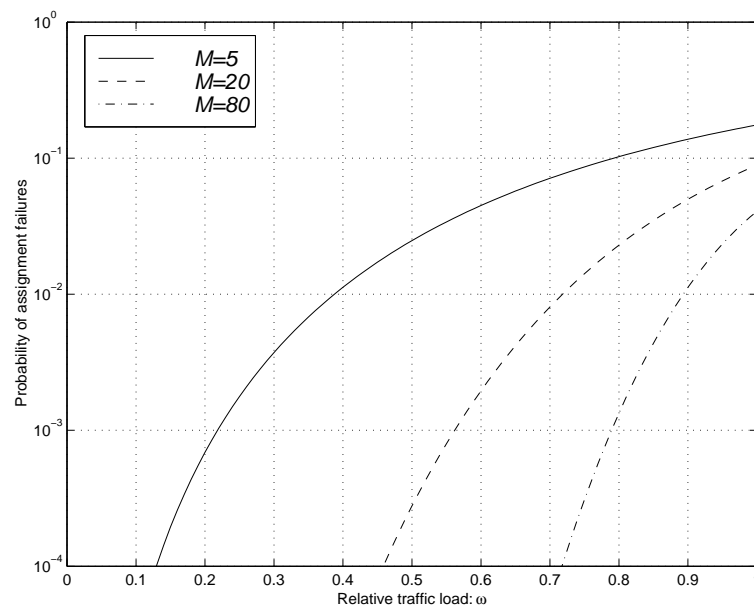


Figure 2.10: Probability of channel assignment failures for varying re-use cluster sizes and a constant number of totally available channels.

CDMA systems such as the UTRA-FDD interface of UMTS re-use the same channel in every cell which, in theory, makes FCA or DCA techniques superfluous [109], but requires special handover techniques (soft-handover). In contrast, the TDD mode of UMTS, UTRA-TDD, requires certain methods of intelligent channel assignment [40] due to the hybrid TD-CDMA interface and the additional interference mechanisms induced by TDD (see section 2.3.3).

2.5.2 Dynamic channel assignment techniques

DCA techniques enable a cellular system to adapt flexibly to different load situations thereby increasing the throughput and decreasing the call blocking. In addition, the efforts for frequency planning can be reduced or eliminated. An important issue, however, is to ensure that the DCA algorithm does not lead to the instability of the system [124]. In this context, it is reported that under high load conditions DCA algorithms can perform worse than FCA techniques due to continuous channel re-assignments [125]. Consequently, systems are investigated where FCA and DCA techniques are combined [126, 127]. As a result, for example, a subset of channels is assigned in a fixed way and the remaining channels are allocated to a common pool. A DCA algorithm uses the common pool from which it 'borrows' channels in order to allocate them to cells where heavy traffic occurs. In this way, the number of channels of a cell can be increased dynamically, but there is still a fixed number of channels which ensure a certain

QoS in situations where the entire network is heavily loaded. In addition, DCA and handover techniques are investigated for narrowband TDMA systems in a multi-layer (micro, pico and macro cell layer) environment [128–131].

A classification of different DCA approaches was made in [122, 125] which is repeated here for convenience (Figure 2.11). In the illustration 2.11 different DCA strategies are represented

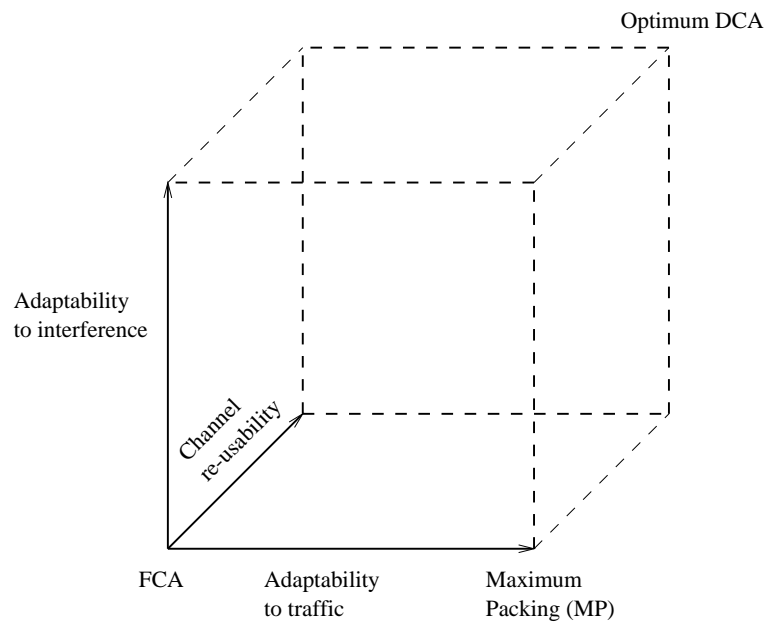


Figure 2.11: Classification of dynamic channel assignment algorithms.

by points in the space, except the origin which represents the FCA scheme. The three axis represent different optimisation criteria. One criterion is the knowledge about the load in every cell of the network. A DCA algorithm can be designed to optimise the number of active MS's in every cell (adaptability to traffic) — resulting in maximum packing (MP). A second criterion is the adaptability to interference variations which is particularly important for interference limited systems such as CDMA. This requires the DCA to have information of the instantaneous interference situation. A third criterion is to optimise the channel re-use distance which would eventually mean that each channel can be used in every cell. An ideal DCA algorithm tries to optimise each of the three parameters which would yield the optimum solution at the far upper corner of the cube. The ideal DCA algorithm would require information beyond the scope of a single cell. From this requirement it inherently follows that the respective DCA algorithm would ideally be operated at a central site. Consequently, two basic DCA schemes are distinguished [132]:

- Centralised DCA schemes
- Decentralised DCA schemes

A centralised DCA algorithm collects the required information for channel assignment decisions from the associated BS's and MS's. This type of DCA algorithm is located at a higher hierarchical level of the mobile network architecture. A centralised DCA algorithm can, for example, be located at the radio network controller (RNC) [112] which connects several BS's. The basic disadvantage is that a great amount of signalling is necessary to supply the vital information about the load, interference and channel status.

In a decentralised DCA algorithm the channel assignment decision is made by a local instance [133–136]. Thus, only local information is available. Hence, the complexity is reduced considerably when this type of DCA algorithm is used. The DECT standard, for example, uses a decentralised DCA algorithm [110]. Given that a decentralised DCA only has a limited knowledge about the system state, a global optimum is very difficult to achieve.

As a result of the DCA characterisation in Figure 2.10, three types of strategies can be formulated:

Traffic-adaptive channel allocation Instead of splitting the available radio resource into sets of channels which subsequently are then assigned to cells, the traffic-adaptive channel allocation techniques try to dynamically assign the required number of channels to cells [137]. In order to avoid the use of the same channel in the neighbouring cell, compatibility matrices are established. Since the interference level from neighbouring cells can vary significantly the compatibility matrices have to be designed in a way which also ensures a reliable connection under severe interference conditions. This results in capacity losses when static compatibility matrices are assumed since in low interference situations more channels per unit can be accommodated. The complexity of traffic-adaptive channel allocation algorithms increases exponentially with the number of cells, $(MK)^L$, where L is the total number of cells. Due to this complexity, graph theory is often used to solve these issues [137]. The optimum traffic-adaptive DCA algorithms result in the MP solution. This requires intra-cell handovers (channel re-assignments). As a consequence, users may be re-shuffled (although the QoS is still fulfilled) in order to optimise the total number of users. Hence, the complexity of MP strategies is further increased, which makes this type of DCA algorithm difficult to analyse. In [138] the cell

group decoupling method is proposed in order to calculate upper bounds on blocking performance. However, the MP problem is easier to solve if the cells are placed along a line. In this scenario, the complexity only increases linearly with L . The optimum solution is found using the Greedy algorithm [122]. In [135, 139–141] a different approach was taken to achieve the dynamic adaptation to traffic variations: channels were 'borrowed' from a common pool and assigned to cells which experience heavy traffic. This technique resembles the previously described combination of DCA and FCA methods.

Re-use Partitioning The entire set of channels is divided into subsets, similar to the FCA strategy. But, in the case of re-use partitioning, every group of frequencies is associated with a different re-use distance, D [142]. If the re-use distance is small it is more likely that severe interference is the reason why a channel cannot be assigned. However, due to the user mobility the interference level may be in favour of allocating a channel with a small re-use distance thereby increasing the total capacity. Hence, the respective DCA algorithm always tries to use a channel with the lowest re-use distance. It is reported that re-use partition algorithms can double the capacity compared to FCA schemes [143].

Interference-based DCA schemes Channels are assigned based purely on the interference power observed (no use of compatibility matrices). If the signal-to-noise ratio drops below a certain threshold a new channel is acquired. This requires steady and reliable measurements of the interference power and power control to minimise interference. Due to its simplicity (easy to implement as distributed DCA algorithm) this type of DCA is widely used. A notable example is the DCA algorithm of the DECT standard. Furthermore, since CDMA are interference limited systems interference based DCA algorithms play an important role in such systems [144]. In [145] a C/I -based DCA algorithm is compared with an FCA algorithm assuming non-uniform traffic. It was found that the DCA techniques increase the throughput by up to 16 % at the cost of higher average transmitted powers. Due to the sensitivity of CDMA to interference, the combination of DCA techniques and power control techniques also represents an interesting approach [146].

2.5.3 Random channel assignment techniques

In the case of narrowband FDMA systems, the RCA methods are closely related to slow FH techniques. The basic idea is to change the channels randomly in order to mitigate poor channel conditions (deep fade) of a static channel. Thereby the interference condition in each hop are

considered to be independent. It is anticipated that by changing the channels continuously the average signal-to-noise ratio is sufficiently high in order to enable error-correcting codes and interleaving techniques to achieve the required QoS.

2.6 Summary

Compared with other techniques discussed in this chapter, CDMA offers a high degree of flexibility since it is merely interference limited. The cost associated with the flexibility is that CDMA is very sensitive to system functions that have a vital impact on interference (handover, power control, channel assignment, *etc.*). An important consequence is that the actual system capacity significantly depends on these functions (soft-capacity).

The capacity enhancement of CDMA over FDMA and TDMA systems is primarily due to the fact that the same frequency can be used in every cell. This however requires a careful system design. In particular, power control and inter-cell handover are important functions as otherwise interference can rise considerably which can cause a significant capacity reduction. In the past, CDMA systems were almost exclusively considered in combination with FDD. Only recently, CDMA has been associated with TDD. A notable example is the UTRA-TDD interface of UMTS which is a hybrid TD-CDMA/TDD system.

There are distinct advantages of using the TDD mode which are primarily due to the reciprocity of the channel and the property that channel asymmetry can easily be adopted. In addition, a CDMA-TDD system can be used to increase the flexibility in a co-existing CDMA-FDD interface (TDD underlay concept). Furthermore, TDD enables the efficient use of enhanced technologies such as SDMA and ODMA. The main disadvantage of TDD is that additional interference scenarios can exist. These additional interference mechanisms occur if the network is not synchronised or the neighbouring cells apply different channel asymmetries. Furthermore, handover techniques such as soft-handover are of limited use in TDD systems such as, for example, UTRA-TDD.

Since CDMA is sensitive to interference, the capacity of a CDMA-TDD system can suffer significantly due to the additional interference mechanisms of TDD. If this problem can be resolved or eased, the CDMA-TDD system architecture represents a very flexible air-interface tailored to the needs of future applications such as wireless Internet. Therefore, new mechanisms have to be developed to exploit the TDD inherent advantages whilst minimising the

disadvantages. DCA techniques seem to be an appropriate means of achieving this requirement. In particular, interference based DCA algorithms are the most promising candidates as they inherently support the requirement of low interference. In order to find the best DCA strategy it is critical that as a first step the interference in such a system is characterised quantitatively. Since little is known about the interference properties of CDMA–TDD systems, a major part of this PhD project is dedicated to investigating this topic further (chapter 3). The results of these studies provide a valuable input to the investigation of interference based DCA algorithms. These investigations have led to a number of patents.

Chapter 3

Interference & capacity analyses

3.1 Introduction

The general aim of this work is to develop methods which enable a system operator to use the TDD technique in a cellular network efficiently. Therefore, it is a necessary prerequisite to first characterise interference, which is carried out in this chapter. A special property of the TDD mode is that not only the mobile stations (MS's) can interfere with base stations (BS's), but also MS's may interfere with each other. The same holds for BS's which can interfere with MS's and other BS's. This property of a TDD interface creates complex interference situations. The resulting interference has a significant impact on capacity due to the use of the interference limited code division multiple access (CDMA) technique. In this chapter, other cell interference including adjacent channel interference (ACI) and co-channel interference (CCI) are examined. The emphasis, though, will be on ACI since CCI in a CDMA-TDD system has already been addressed in a previous paper [109], but little is known about ACI in such systems. In this context, multi-operator scenarios are considered since in UMTS (Universal Mobile Telecommunications System), for instance, any one operator may only obtain a single TDD carrier ¹.

In order to assess the impact of interference on capacity (number of users which can be served simultaneously), in section 3.2 a new equation is derived to calculate the system capacity relative to the non-interfered state (single, isolated cell). In addition, the pole capacity (theoretical upper bound of capacity) is calculated for the case of ideal power control and non-ideal power control.

In section 3.3, ACI is studied in a single cell and multiple cell environment. The probability density function (pdf) of interference in the single cell environment is derived analytically in order to validate the simulation platform. In the multiple cell environment the effects of handover and power control on interference, and capacity respectively, are examined.

¹See, for example, the current set up in the UK

In section 3.4, CCI is analysed with a special focus on distribution of interference with respect to the basic interference sources: MS's and BS's. The reason for this is to use the information obtained to develop dynamic channel assignment techniques in the subsequent chapters.

3.2 Capacity definition

In communication systems where many MS's are connected to a single BS, the characteristics of the uplink (UL) and downlink (DL) are different. Since in CDMA systems all users share a common radio resource the different characteristics of the UL and the DL have a significant impact on these systems as will be explained in the following: The UL is a multi point-to-single point transmission (\leadsto the signals arrive asynchronously) whereas the DL is a single point-to-multi point transmission (\leadsto the signals arrive synchronously). Since the signal power of all MS's but the desired MS appears as noise, a close-by MS transmitting high powers can affect the quality of all other connections. This is the well known near-far effect which requires tight power control in the UL. This means, ideally the received signal powers of all MS's must be the same. Due to the near-far effect, the UL is often considered as the capacity limiting direction [21, 26]. In the subsequent section capacity is analysed assuming ideal power control in the UL, and in section 3.2.2 non-perfect power control is considered.

3.2.1 Capacity assuming ideal power control

In order to demonstrate the sensitivity of capacity on interference, a mathematical model for the relative capacity is established in this section. This means that the capacity relative to the state without any other cell interference (single, isolated cell) is calculated. In addition, it is assumed that dynamic power control in such a system is used. This requires the system to modify the power level of the desired signal in order to maintain the target carrier to interference ratio in the presence of other cell interference. The maximum desired signal power level is however limited as otherwise the cell coverage would be affected. Therefore, some form of admission control is necessary to prevent the reduction of the cell coverage area, or to prevent the deterioration of the quality of service of the existing connections. In general, the model follows closely the definitions used in papers by Gilhausen and Viterbi [25, 27]. For reasons of simplicity, in these papers ideal power control in the UL is assumed, *i.e.* the received signal power of each MS's is the same. As a consequence, the effects of the near-far effect are eliminated. With

the assumption of ideal power control and the same bit–rate for each user, the bit–energy to interference ratio at the BS, as given in [25], can be denoted as follows.

$$\varepsilon^u = \frac{P_u^u pg}{\underbrace{P_u^u (M - 1)}_{I_{own}} + I_o^u + N} , \quad (3.1)$$

where P_u^u is the received, power–controlled signal power from the desired user at the BS, M is the number of simultaneously active users of equal bit–rate. The interference power is represented by I_o^u , N is thermal noise power and pg is the processing gain. The term: $[P_u^u (M - 1)]$ represents own–cell interference. Note that symbols which are followed by the superscript 'u' are associated with the uplink channel; symbols which are followed by the superscript 'd' are associated with the downlink channel.

The target is to calculate the capacity relative to the single cell capacity. To start with, (3.1) is solved for P_u^u .

$$P_u^u = \frac{I_o^u + N}{\frac{pg}{\varepsilon^u} + 1 - M} . \quad (3.2)$$

Since the denominator in (3.2) must be positive and greater than zero, an upper bound for the cell load can be determined which yields M_{max} . This upper limit is also referred to as the pole capacity [6, Chapter 8]

$$M_{max} = \frac{pg}{\varepsilon^u} + 1 . \quad (3.3)$$

The admission control of a CDMA system ensures that the number of users is below this threshold. Hence, in this thesis a maximum cell load factor is defined as follows:

$$\chi = \frac{M_0}{M_{max}} \quad 0 \leq \chi \leq 1 , \quad (3.4)$$

where M_0 is the maximum number of simultaneously active users which can be permitted when assuming no other cell interference. The maximum cell load factor is assumed to be a fixed parameter set in the admission control. The actual value depends, for example, on the cell radius. For smaller cells a higher value of χ can be tolerated than for larger cells because the target receive power P_u^u can be greater due to lower path losses. The number of users, M_0 , however must always be less than the pole capacity which ensures that the desired signal P_u^u does not approach infinity (singularity in (3.2)) or becomes negative. Since a certain cell load

also corresponds to a certain power P_u^u , χ can be interpreted so as to define the upper bound for the dynamic power control. Thus, substituting (3.3) into (3.2) yields:

$$P_u^u = \frac{I_o^u + N}{M_{max} - M} = \frac{I_o^u + N}{M \left(\frac{1}{\chi} - 1 \right)}. \quad (3.5)$$

A single cell is modelled by setting $I_o = 0$. For this case (3.5) becomes

$$P_{u_0}^u = \frac{N}{M_{max} - M_0}. \quad (3.6)$$

Hence, (3.6) is the desired receive power level for the ideal case (single cell case) where no other cell interference is present. Subsequently, (3.5) is solved for M which yields

$$M = M_{max} - \frac{I_o^u + N}{P_u^u}. \quad (3.7)$$

Since it is aimed to obtain the capacity relative to the non-interfered state, (3.6) is substituted into (3.7). Hence, M represents the capacity assuming that the received signal power is the same as for the single cell case which also ensures that the cell radius is maintained.

$$M = M_{max} - \frac{(I_o^u + N)(M_{max} - M_0)}{N}, \quad (3.8)$$

The equation (3.8) can be simplified which yields:

$$M = M_0 - \frac{I_o^u}{N}(M_{max} - M_0). \quad (3.9)$$

If other cell interference equals zero, it can be seen that $M = M_0$. Finally, the relative remaining capacity as a consequence of I_o^u can be found by dividing (3.9) by M_0 :

$$M/M_0 = 1 - \frac{I_o^u}{N} \left(\frac{1}{\chi} - 1 \right). \quad (3.10)$$

The relative capacity in (3.10) has to be interpreted as follows: It is a measure of the capacity reduction due to other cell interference assuming ideal power control (the received signal of each user is the same). Furthermore, it is inherently assumed that the desired receive power is constant regardless of the cell load. The actual value of the target receive power is equivalent to a single cell scenario with an associated number of supported users of M_0 , and thus determined from the maximum cell load factor χ . This ensures that the cell coverage is maintained.

From (3.10) it can be seen that a higher value of χ results in less vulnerability to interference. From this the important conclusion can be drawn that with a given power budget of the MS's, smaller cells are more resistant to interference.

For reasons of simplicity, ideal power control was assumed in this section. In order to consider a more realistic scenario in the following section the pole capacity is calculated assuming non-ideal power control.

3.2.2 Capacity assuming non-ideal power control

In the remainder of this chapter the transformation:

$$\widehat{(\cdot)} = 10 \log_{10}(\cdot) , \quad (3.11)$$

is used frequently. Therefore, the hat $\widehat{(\cdot)}$ symbol describes the corresponding variable in the logarithmic scale according to the transformation given in (3.11).

In order to account for the near-far effect it is required that the useful signal power from each user arrives at the same level [25] at the BS. However, this would require ideal power control. In real systems power control inaccuracy cannot be avoided. This and excessive multi path conditions are responsible for a varying bit-energy to interference ratio, ε^u , at the BS receiver.

It is demonstrated in [26] that in order to maintain a certain frame error rate the resulting ε^u varies and the statistics can be approximated by a lognormal probability density function (pdf). Therefore, for an arbitrary user i , the bit-energy to interference ratio as, for example, used in [26] may be denoted as follows:

$$\varepsilon_i^u = \frac{pg P_{u_i}^u}{\sum_{j:j \neq i}^M P_{u_j}^u + I_o^u + N} , \quad (3.12)$$

where $P_{u_i}^u$ is the received signal power from the desired user i . Analogously, $P_{u_j}^u$ is the signal power received from the other user j .

The interest is on a service independent capacity. Therefore, it is part of the assumptions leading to (3.12) that the entire set of users (defined as the capacity) are permanently active. Furthermore, it is also clear that in the case of a speech service, for example, each user will not be active all the time and, therefore, a voice activity factor is introduced [26]. The voice

activity factor results in a specific capacity calculation (for speech) since at any given moment more users can be tolerated given that on average some of these mobiles are not active. This will not alter the basic interference characteristics. The reason for this is that despite the averaging the maximum number of simultaneously active users, permitted by the system, must not be exceeded. Therefore, it is considered to be sufficient to define the capacity such that M is deterministic.

In an interference limited system such as a cellular CDMA network, the power level of the useful signal $P_{u_i}^u$ at the receiver can be utilised to optimise capacity. This can be seen from (3.12). In a similar fashion interference has an impact on system capacity which was intensively investigated by several researchers [21, 25]. Since capacity is dependent on $P_{u_i}^u$ the target power level at the BS can be used to enhance capacity provided that the increased power does not result in a significant increase of interference in the other cells. It has been demonstrated by Veeravalli [23] that $P_{u_i}^u$ can be derived from (3.12) and becomes,

$$P_{u_i}^u = \frac{N + I_o^u}{\left(\frac{pg}{\varepsilon_i^u} + 1\right) \left(1 - \underbrace{\sum_{j=1}^M \frac{\varepsilon_j^u}{pg + \varepsilon_j^u}}_U\right)}. \quad (3.13)$$

From (3.13) it can be seen that a feasible solution for $P_{u_i}^u$ only exists if

$$U = \sum_{j=1}^M \frac{\varepsilon_j^u}{pg + \varepsilon_j^u} < 1. \quad (3.14)$$

This equation can be used to deduce the theoretical capacity maximum M_{max} . It was demonstrated previously that ε_i^u can be approximated by a random variable (RV) which follows a lognormal distribution which means that $\widehat{\varepsilon}_i^u$ is Gaussian distributed. The mean of $\widehat{\varepsilon}_i^u$ (μ_ε^u) is primarily dependent on the receiver architecture and the forward error correcting (FEC) coding scheme. The standard deviation of $\widehat{\varepsilon}_i^u$, (σ_ε^u) is dependent on the power control performance and the severity of the multi path fading. In [26] it is reported that σ_ε^u for the American IS-95 (Interim Standard-95) CDMA system is nominally 2.5 dB. Without loss of generality the M RV's, $\varepsilon_{1,\dots,M}^u$, can be assumed to be independent and identically distributed (i.i.d.). It is straightforward to calculate the pdf of $\frac{\varepsilon_i^u}{pg + \varepsilon_i^u}$ which was done in [23], but the sum of these RV's, U , as given in (3.14) involves numerical convolution.

σ_ϵ^u [dB]	M_{max}
0.1	8
0.5	8
1.0	7
1.5	6
2.0	6
2.5	5
3.0	5

Table 3.1: The theoretical upper capacity limit M_{max} (assuming less than 5 % outage) using the following parameters: $pg=16$, $\mu_\epsilon^u=3.5$ dB.

Outage is defined as the probability: $Pr(U \geq 1)$. The results are shown in Figure 3.1. In addition, the maximum number of users for less than 5 % outage are summarised in Table 3.1. As expected, power control imperfections increase outage considerably. For instance, when

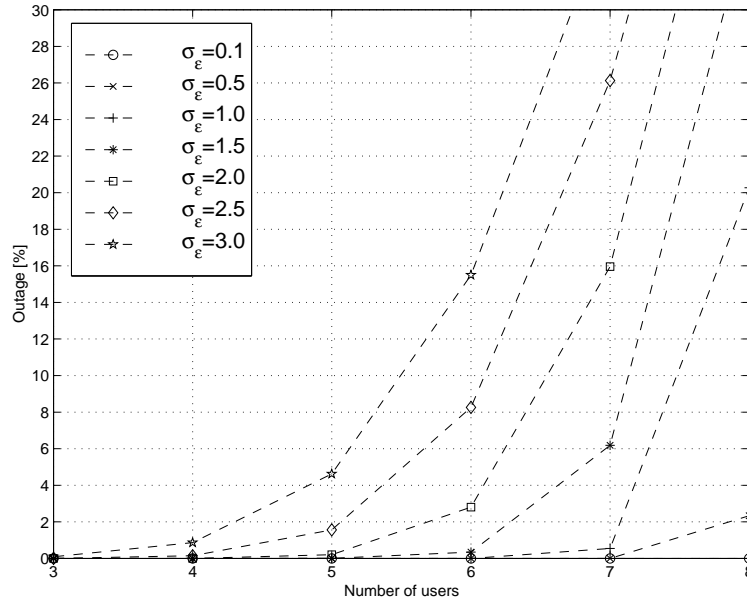


Figure 3.1: Probability of outage as a function of simultaneously active MS's with: $pg=16$, $\mu_\epsilon^u=3.5$ dB and σ_ϵ^u as a parameter.

increasing σ_ϵ^u from 0.1 dB to 3.0 dB and initially assuming 6 simultaneously active MS's the outage rises from approximately 0 % to 15.5 %. In contrast, in the case of only 4 active MS's outage increases from about 0 % to 1 % for the same variations of σ_ϵ^u .

When assuming non-ideal power control, the pole capacity is not deterministic as it was in the case of ideal power control (see (3.3)). However, it is interesting to note that for both cases the pole capacity, M_{max} , is independent of thermal noise and interference.

3.3 Adjacent channel interference in a CDMA–TDD system

In this section the effects of ACI on system capacity are investigated. A general description of ACI considering TDD properties is carried out in section 3.3.1. ACI is then investigated for two TDD deployment scenarios: In section 3.3.2 ACI is calculated assuming a single interfering cell. This model is chosen to account for the fact that the TDD mode is ideally suitable to cover traffic 'hot spots' [6, Chapter 12]. The location and load of the interfering cell, the frame synchronisation and the adjacent channel protection factor are varied. Initially, a simple model for the correlation of the desired signal power and the interference signal power, taken from [76], is assumed .

In section 3.3.3 a multiple–cell environment is applied. The interfering network consists of a cluster of seven hexagonal cells. With this scenario in particular the impact of power control and handover margins are investigated. A model for the correlation of signal paths reported by Klingenbrunn [147] is applied.

3.3.1 Characterisation of adjacent channel interference

In Figure 3.2, a possible multi–operator interference scenario is depicted. A scenario of two ad-

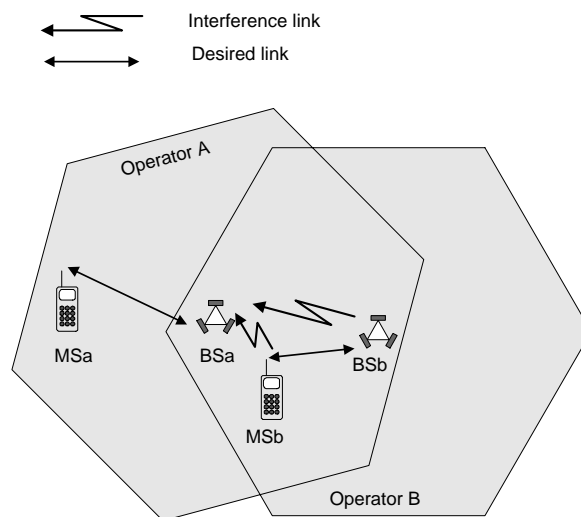


Figure 3.2: *Adjacent TDD carriers can belong to independent operators (operator A and operator B) with the consequence that cells can overlap randomly. The potential interference links with respect to the UL direction are shown.*

acent carriers belonging to different operators is considered. Since network planning between

independent operators can not be assumed cells can overlap randomly. Therefore, a transmitting entity and a receiving entity can be located in close proximity. The interference protection merely depends on the adjacent channel protection factor. In the case of CCI, in contrast to ACI, neighbouring cells are ideally separated such that cells do not overlap. Hence, interference protection in the case of CCI is achieved by a spatial separation of the transmitter and the victim receiver. In addition, handover techniques can be used to circumvent high CCI [27]. Since the mechanisms which create CCI and ACI are different it seems obvious that the quantitative characteristics of both interference types are different, too. Clearly, the focus in this section is to investigate adjacent channel interference applying to a CDMA/TDD interface.

The mutual interference mechanisms in an FDD system are that MS's interfere with the neighbouring BS's, and vice versa. In this system the UL and the DL are separated in the frequency domain. Therefore, cross-talk between UL and DL is negligible. However, when considering the TDD system the complexity in terms of interference is increased since both the UL and DL are time multiplexed on the same carrier frequency. If the frames and time slots (TS's) of two cells are not synchronised additional interference scenarios occur. As compared to an FDD mode, in the TDD mode the MS's can interfere with each other and so can the BS's. Either interference link (MS \leftrightarrow MS or BS \leftrightarrow BS) can be characterised as interference between the same types of entity (MS or BS). Therefore, these interference paths inherent to a TDD system are henceforth called 'same-entity interference'. Analogously, the interference scenarios: (MS \leftrightarrow BS or BS \leftrightarrow MS) are specified as 'other-entity interference'. Frame synchronisation in the TDD system has an impact on the quantity of same-entity interference and other-entity interference as can be found with the aid of Figure 3.3. This figure shows a possible TS's arrangement of the scenario in Figure 3.2. The model is composed of four entities: BSa, MSa, BSb and MSb, where BSa and MSa, BSb and MSb respectively, form a communication link. Therefore, if BSa transmits MSa receives and vice versa. Since each cell may belong to a different operator the frames or TS's are unlikely to be aligned in time. This is modelled by an arbitrary time offset, t_{off} . This time offset is normalised by the time slot (TS) duration t_{slot} yielding the synchronisation factor,

$$\alpha = \frac{t_{off}}{t_{slot}}. \quad (3.15)$$

Due to the frame misalignment, BSa and BSb interfere with each other and thereby create I_{bb} . In the same way as there is interference between the BS's, MSa and MSb interfere with each

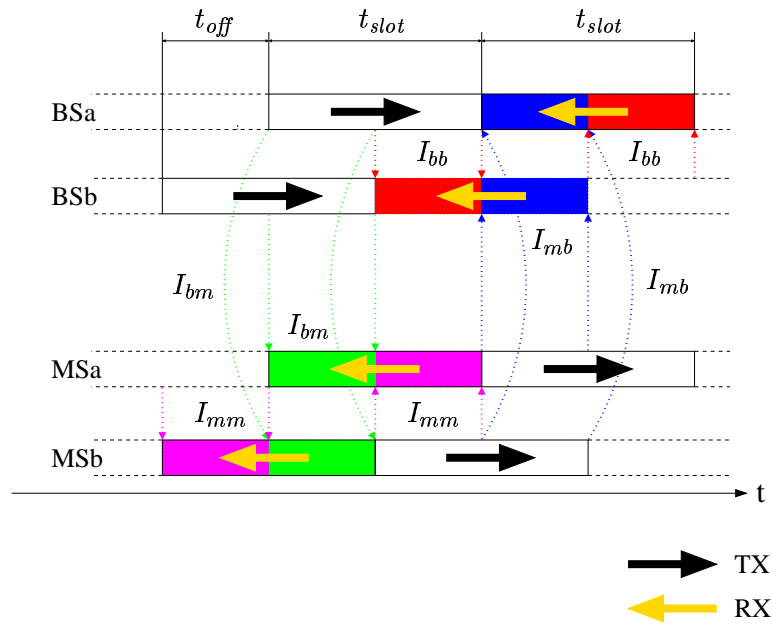


Figure 3.3: Interference in a TDD system dependent on frame synchronisation.

other and generate I_{mm} . Both types of interference are previously categorised as same-entity interference. It can be found that same entity interference is proportional to α . Similar properties can be found for other-entity interference except that it is proportional to $(1 - \alpha)$. Hence, as the synchronisation factor α increases other-entity interference diminishes, but same-entity interference increases, and vice versa. This leads to two special cases: If $\alpha = 1$ only same entity interference exists and similarly, if $\alpha = 0$ only other entity interference exists which emulates an equivalent FDD interface. The consequence is that during the entire receive period interference is present. Since other-entity and same-entity interference can be considered as independent (due to different interference sources) the magnitude of each type of interference can vary greatly. Therefore, it seems to be interesting whether it is possible to exploit the fact that same-entity interference and other-entity interference are different in order to minimise interference by altering frame synchronisation. This question is explored in depth in the following sections.

Using the synchronisation mechanism introduced above, ACI in a TDD system at an arbitrary location specified by its x and y coordinates, can be expressed as follows:

$$I_{ad}(x, y) = \frac{1}{\kappa_I} \sum_{j=1}^L \sum_{i=1}^{M_j} \alpha_j \frac{Pc_{i,j}^u}{a_i(x, y)} + (1 - \alpha_j) \frac{Pc_j^d}{a_j(x, y)}, \quad (3.16)$$

where L is the number of neighbouring cells taken into consideration, M_j is the total number of active users in the neighbouring cell j , $Pc_{i,j}^u$ is the transmitted carrier power of user i in cell j , Pc_j^d describes the total carrier power transmitted by BS j and $a_i(x, y)$ represents the path loss between the interfering user i and the location of interest (x, y) . Similarly, $a_j(x, y)$ is the path loss between the location of interest and the BS of cell j . The synchronisation between cell j and the point of interest (x, y) is expressed by α_j . The adjacent channel protection factor, κ_I , or adjacent channel interference ratio (ACIR) [148] is determined by two factors: a) one related to the transmitter filter and referred to as: Adjacent Channel Leakage Ratio (ACLR) b) one related to the receiver filter and described as Adjacent Channel Selectivity (ACS). The relationship between ACIR, ACLR and ACS was investigated in [148] and found to be:

$$\kappa_I = \frac{1}{\frac{1}{\kappa_L} + \frac{1}{\kappa_S}}, \quad (3.17)$$

where κ_L is the ACLR and κ_S is the ACS.

The transmitted powers $Pc_{i,j}^u$ and Pc_j^d are random variables which are determined by several factors, the most important of which are the location of MS's, the path loss, the severity of lognormal shadowing, the handover algorithm, the power control algorithm and the receiver architecture. Additionally, the path losses between the interferer and victim receiver, $a_i(x, y)$ and $a_j(x, y)$, are random variables, as well. Moreover, in the case of ACI the sink of interference and the desired receiver may be in close proximity so that the path loss on the desired link and interference link cannot be assumed to be uncorrelated. Frame synchronisation between different operators may also vary randomly, i.e. $0 \leq \alpha_j \leq 1$. Due to its complexity the ACI power as described in (3.16) is calculated using Monte Carlo techniques. However, in order to verify the Monte Carlo model the pdf of the interference power is calculated analytically for simplified scenarios and the results are compared with those obtained by the Monte Carlo approach. If the pdf of interference at the BS location is known, it is possible to analyse the impact of interference on capacity using (3.10). The TDD mode is generally considered to be used in low mobility environments and to cover 'hot spot' traffic areas [6, Chapter 12]. Therefore, in the following, a two-cell scenario (one cell per operator) is used to study the effects of ACI. This is in contrast to a multi-cell environment where handover techniques can be used to reduce interference significantly [27, 76] MS's are assigned to the single BS regardless of the path loss. It will be shown that this scenario is not necessarily the 'best' case scenario with respect to interference.

3.3.2 Single interfering cell

In the case of a single interfering cell, the cell topology as shown in Figure 3.4 is applied. The MS's are distributed uniformly within the cell area of the interfering cell. The pdf of ACI is calculated using the equation given in (3.16). The approach is twofold: Firstly, Monte Carlo simulations are carried out. Secondly, a closed-form solution of the pdf is derived in order to validate the simulation platform as well as the analysis.

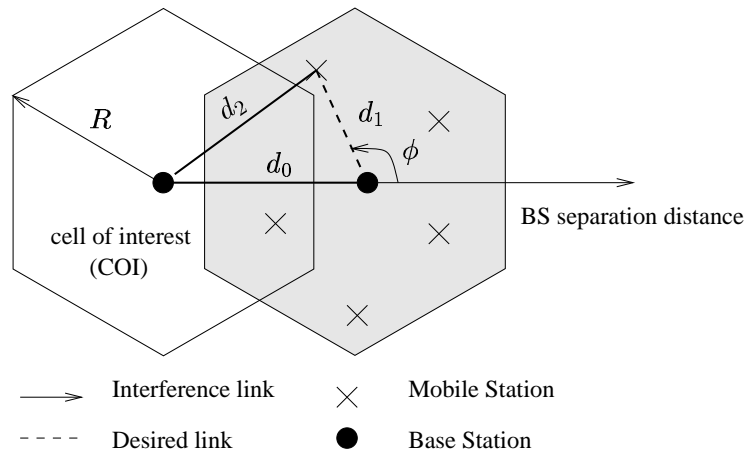


Figure 3.4: A single cell causing ACI at a cell which is located at a distance d_0 from the cell of interest (COI).

3.3.2.1 Propagation model

The path loss is modelled according to the indoor propagation environment with no wall or floor losses, as can be found in [149].

$$a = 37 + \varphi 10 \log (d) + \xi \text{ [dB]} , \quad (3.18)$$

where φ is the path loss exponent and d the distance between transmitter and receiver. Lognormal shadowing is modelled by ξ with the standard deviation σ and zero mean.

The BS's of the two cells with adjacent carrier frequencies can be in close proximity. This situation can easily happen if the cells belong to different operators. In such a case, the desired signal and the interference signal propagate through similar conditions and can therefore not be considered as uncorrelated. This mechanism is illustrated in Figure 3.5.

In a paper by Viterbi [27] a simple model of the signal correlation was introduced. In Viterbi's

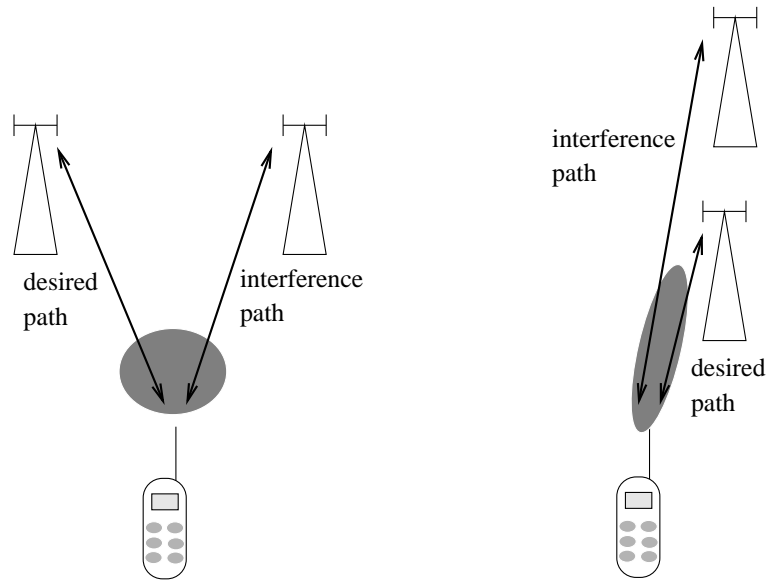


Figure 3.5: The correlation of the desired and the interference signal is dependent on the location of the transmitter relative to the first and second receiver.

paper a joint Gaussian probability density for losses to two or more more base stations is assumed. The random component as a consequence of shadowing is considered to be composed of two components: a) a component which is common to all BS's, and b) a component which pertains solely to the receiving BS and is independent from one BS to another. The common component described in a) is schematically depicted in Figure 3.5 by the grey shaded areas on the signal path. Thus, the lognormal shadowing on the propagation path to the i th BS is given as follows:

$$\xi_i = r_1 v + r_2 v_i, \quad \text{where} \quad r_1^2 + r_2^2 \stackrel{\text{def}}{=} 1, \quad (3.19)$$

and v is the random component common to the desired and the interference path and v_i is the uncorrelated random component on each path. Furthermore it is defined that:

$$E(\xi_i) = E(v) = E(v_i) = 0, \quad (3.20)$$

$$\text{Var}(\xi_i) = \text{Var}(v) = \text{Var}(v_i) = \sigma \quad \text{for all } i, \quad (3.21)$$

$$E(v, v_j) = 0 \quad \text{for all } i, \quad (3.22)$$

$$E(v_i, v_j) = 0 \quad \text{for all } i \text{ and } j, i \neq j. \quad (3.23)$$

Using the presuppositions (3.20)–(3.23), the correlation coefficient yields:

$$r = \frac{E(\xi_i, \xi_j)}{\sigma^2} = \frac{E[(\xi_i - \overbrace{E[\xi_i]}^{\text{def } 0})(\xi_j - \overbrace{E[\xi_j]}^{\text{def } 0})]}{\sigma^2}, \quad (3.24)$$

$$= \frac{r_1^2 E(v^2) + r_1 r_2 \overbrace{E(vv_j)}^{\text{def } 0} + r_1 r_2 \overbrace{E(vv_i)}^{\text{def } 0} + r_2^2 \overbrace{E(v_i, v_j)}^{\text{def } 0}}{\sigma^2}, \quad (3.25)$$

$$= \frac{r_1^2 \overbrace{\text{Var}(v)}^{\sigma^2}}{\sigma^2}, \quad (3.26)$$

$$= r_1^2 = 1 - r_2^2. \quad (3.27)$$

The joint pdf between the random component on the desired link ξ_i and the random component on the interference link, ξ_j , yields [150, Chapter 7]

$$p(\xi_i | \xi_j) = \frac{1}{\sigma \sqrt{2\pi(1-r)}} \exp\left(-\frac{(\xi_i - r\xi_j)^2}{2\sigma^2(1-r^2)}\right), \quad (3.28)$$

In [76] a constant value of $r_1 = 0.25$ is assumed. This is a reasonable assumption since in [76] merely co-channel interference is investigated, and therefore the cell topology is fixed. In the analysis here, the BS separation distances can vary from co-location to several times the cell radius. The following relationship between r_1 and the BS separation distance is introduced:

$$r_1 = \begin{cases} \sqrt{1 - \frac{d_0}{R}} & \text{if } d_0 \leq R, \\ 0 & \text{otherwise.} \end{cases} \quad (3.29)$$

where R is the cell radius and d_0 the BS separation distance (see Figure 3.4). From substituting (3.29) into (3.27) it can be seen that the correlation coefficient equals one if both cells are co-sited. This is obvious because the desired path and interference path are exactly the same. The signal are considered to be uncorrelated if the BS separation distance equals the cell radius. It is recognised that there is little experimental verification of this model, but it is a logical extension of reports on the correlation of shadow fading as for example given in [151]. In section 3.3.3 a correlation model reported by Klingenbrunn [147] is applied which also takes into account the angle of arrival difference of the signals. This model has been a subject of greater experimental verification. Monte Carlo simulations are carried out assuming a spatially uniform user distribution to obtain the pdf: $p(\hat{I}_{ad})$ at the BS of the cell of interest (COI). The

results of the Monte Carlo approach are verified against the analytical derivation of $p(\hat{I}_{ad})$. The derivation of $p(\hat{I}_{ad})$ is a novel approach and the equation can be used to study interference properties for various cell topologies and applications in which handover techniques are not applied. Therefore, this pdf is also used to investigate the feasibility of a TDD underlay which is described in chapter 2 and led to several papers [16, 17].

3.3.2.2 Power-control models

In the UL, ideal power control is assumed. In the DL a similar model as in [109] is used. First, the code power, $\tilde{P}_{c_j}^d$, of the MS j which experiences the greatest path loss is calculated. The same code power is then applied to each user within the same TS, $\tilde{P}_{c_i}^d = \tilde{P}_{c_j}^d$ with $i = 1, \dots, M$. This ensures that the required bit-energy to interference ratio is fulfilled for all M users as shown in the following: Let the maximum code power, $\tilde{P}_{c_j}^d$, be determined by the MS for which the maximum path loss, a_j , applies. The bit-energy to interference ratio, ε_j^d at the respective MS results in:

$$\varepsilon_j^d = \frac{\tilde{P}_{c_j}^d pg}{\tau (M - 1) \tilde{P}_{c_j}^d + a_j (I_{ad} + N)}, \quad (3.30)$$

where τ is the orthogonality factor. Since,

$$a_i < a_j \quad \text{for all} \quad i \neq j, \quad (3.31)$$

it follows that,

$$\varepsilon_i^d > \varepsilon_j^d \quad \text{for all} \quad i \neq j. \quad (3.32)$$

Hence, it is ensured that for each MS the required bit-energy to interference ratio, ε^d , is greater than a minimum threshold.

3.3.2.3 Analytical derivation of the pdf of ACI

The cell layout as depicted in Figure 3.4 is used to derive the pdf of the ACI at the BS of the COI. For reasons of simplicity, circular cells instead of hexagonal cells are assumed and the pdf is calculated assuming one uniformly distributed interfering user. In addition, the interference

is calculated for ideal synchronisation of TS's ($\alpha = 0$).

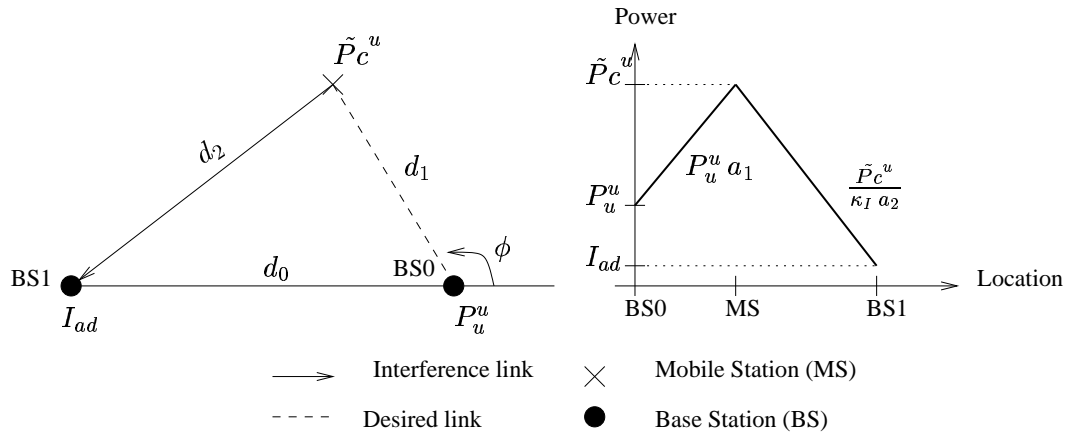


Figure 3.6: Simulation model to derive the pdf of interference at the BS of a neighbouring cell.

In Figure 3.6 the relationship between the transmitted code power (\tilde{P}_c^u), received power (P_u^u) and interference power (I_{ad}) are depicted qualitatively. Using (3.18) the interference power I_{ad} can be denoted as follows:

$$I_{ad} = P_u^u \left(\frac{d_1}{d_2} \right)^\varphi 10^{\frac{\xi_D - \xi_I - \kappa_I}{10}}, \quad (3.33)$$

where ξ_D is the random component due to shadowing on the desired link and similarly, ξ_I is shadowing component on the interference link, d_1 is the distance between the MS and the BS to which it is assigned and d_2 is the distance between the MS and the victim BS. The distance d_2 can be expressed as a function of the polar coordinates of the MS, d_1 and ϕ , and the BS separation distance d_0 :

$$d_2 = \sqrt{d_1^2 + d_0^2 + 2 d_1 d_0 \cos(\phi)}. \quad (3.34)$$

Substituting (3.34) into (3.33) and using the substitution: $\beta = \ln(10)/10$ yields:

$$I_{ad} = P_u^u \left[1 + \left(\frac{d_0}{d_1} \right)^2 + 2 \left(\frac{d_0}{d_1} \right) \cos(\phi) \right]^{-0.5\varphi} \exp[\beta (\xi_D - \xi_I - \kappa_I)]. \quad (3.35)$$

The distance d_0 is a constant. Therefore, the following substitution is introduced:

$$v = \frac{d_0}{d_1}. \quad (3.36)$$

The aim is to obtain the pdf of I_{ad} in logarithmic units. Therefore, (3.35) is transformed using (3.11),

$$\widehat{I}_{ad} = P_u^u + \underbrace{\xi_D - \xi_I}_{\xi} - \kappa_I - \frac{\varphi}{2\beta} (v^2 + 2v \cos(\phi) + 1) . \quad (3.37)$$

Due to the random location of the MS, v is a random variable. Since it is assumed that the MS is uniformly distributed the pdf: $p(d_1, \phi)$ can be derived by calculating and dividing appropriate cell areas,

$$p(d_1, \phi) = \frac{d_1}{R^2 \pi} . \quad (3.38)$$

As a consequence of the substitution used in (3.36), the pdf $p(v, \phi)$ has to be calculated. This is straightforward by using the random variable transformation method [150]:

$$p(v, \phi) = \frac{p(d_1, \phi)}{\left| \frac{d(v(d_1))}{d(d_1)} \right|} \Bigg|_{d_1=f^{-1}(v)} = \frac{d_0^2}{\pi R^2} v^{-3} \quad \frac{d_0}{R} \leq v \leq \infty . \quad (3.39)$$

In addition, ξ_D and ξ_I are random variables with normal pdf's each having zero mean and standard deviation σ . Therefore, the pdf of $\xi = \xi_D - \xi_I$ is a normal pdf with zero mean and standard deviation: $\sigma = \sqrt{2} \sigma$:

$$p(\xi) = \frac{1}{\sqrt{2} \pi \sigma} \exp - \left(\frac{\xi}{2\sigma} \right) . \quad (3.40)$$

In (3.37) the equation to calculate \widehat{I}_{ad} is given. It is found that this equation includes three random variables all of which are characterised by the respective pdf's, (3.39 and 3.40), where (3.39) is the joint pdf of the independent random variables ϕ and v . Hence, all functions which are necessary to calculate the final pdf of \widehat{I}_{ad} are determined. Since three random variables are involved, a random variable transformation system of third order has to be solved which is feasible by introducing two auxiliary functions [150, Chapter 6],

$$y = f(\phi) = \phi , \quad (3.41)$$

$$w = f(\xi) = \xi . \quad (3.42)$$

Using (3.41), (3.42) and (3.37) the Jacobian which is required to solve the random variable

transformation system can be established:

$$J(v, \xi, \phi) = \begin{vmatrix} \frac{\partial \widehat{I}_{ad}(v, \xi, \phi)}{\partial v} & \frac{\partial \widehat{I}_{ad}(v, \xi, \phi)}{\partial \xi} & \frac{\partial \widehat{I}_{ad}(v, \xi, \phi)}{\partial \phi} \\ \frac{\partial y(v, \xi, \phi)}{\partial v} & \frac{\partial y(v, \xi, \phi)}{\partial \xi} & \frac{\partial y(v, \xi, \phi)}{\partial \phi} \\ \frac{\partial w(v, \xi, \phi)}{\partial v} & \frac{\partial w(v, \xi, \phi)}{\partial \xi} & \frac{\partial w(v, \xi, \phi)}{\partial \phi} \end{vmatrix}, \quad (3.43)$$

which yields:

$$J(v, \xi, \phi) = \begin{vmatrix} \frac{\partial \widehat{I}_{ad}(v, \xi, \phi)}{\partial v} & \frac{\partial \widehat{I}_{ad}(v, \xi, \phi)}{\partial \xi} & \frac{\partial \widehat{I}_{ad}(v, \xi, \phi)}{\partial \phi} \\ 0 & 0 & 1 \\ 0 & 1 & 0 \end{vmatrix}, \quad (3.44)$$

and thus,

$$J(v, \xi, \phi) = \left| -\frac{\partial \widehat{I}_{ad}(v, \xi, \phi)}{\partial v} \right| = \left| \frac{2 P_u^u (v - \cos(\phi))}{v^2 + 2 v \cos(\phi) + 1} \right|. \quad (3.45)$$

The pdf of \widehat{I}_{ad} can be denoted as follows:

$$p(\widehat{I}_{ad}) = \int_0^{2\pi} \int_{-\infty}^{\infty} \sum_{i=1}^Q \frac{p(v_i, \phi) p(\xi)}{|J(v_i, \xi, \phi)|} \Big|_{v_i=f_i^{-1}(\widehat{I}_{ad}, \xi, \phi)} d\xi d\phi. \quad (3.46)$$

The inverse function of (3.37): $v_i = f_i^{-1}(\widehat{I}_{ad}, \xi, \phi)$ results in $i = 1, \dots, (Q = 2)$ solutions which are:

$$v_i(\widehat{I}_{ad}, \xi, \phi) = \begin{cases} \underbrace{-\cos(\phi) (-1)^i}_u \sqrt{\cos^2(\phi) + \exp\left[-\frac{2\beta}{\varphi} \left(\widehat{I}_{ad} - \xi - P_u^u + \kappa_I\right)\right] - 1} & \text{if } \sqrt{(\cdot)} \geq 0 \text{ and} \\ & \frac{d_0}{R} \leq u \sqrt{(\cdot)} \leq \infty \\ 0 & \text{otherwise} \end{cases} \quad i = 1, 2. \quad (3.47)$$

In the following, (3.39), (3.40) and (3.45) are substituted into (3.46):

$$p(\widehat{I}_{ad}) = \frac{2 \beta d_0^2}{\varphi R^2 \sigma \sqrt{8 \pi^3}} \int_0^{2\pi} \int_{-\infty}^{\infty} \left(\sum_{i=1}^2 \left| \frac{v_i^2 + 2 v_i \cos(\phi) + 1}{v_i^3 [v_i + \cos(\phi)]} \right| \right) \exp\left[-\frac{\xi^2}{2\sigma^2}\right] d\xi d\phi, \quad (3.48)$$

in which v_i can be substituted by (3.47) which then yields the final pdf $p(\hat{I}_{ad})$. This pdf can be used to examine many different interference problems in cellular communications. For example, it has been used by the author to investigate the feasibility of a TDD underlay [16] which was described in chapter 2.

The pdf, (3.48), is calculated numerically and the results are used to verify the pdf calculated using the Monte Carlo approach. The parameters used for the verification are summarised in Table 3.2.

Parameter	Value
BS separation distance, d_0	100 m
Cell radius, R	50 m
Path loss exponent, φ	3.0
ACIR, κ_I	30 dB
Desired signal power, P_u^u	-111 dBm
Monte Carlo runs	10,000

Table 3.2: Simulation parameters used in the verification of the analytically derived pdf of ACI with results obtained by Monte Carlo simulations.

3.3.2.4 Comparison of analysis approaches

The comparison is carried out for different parameters in order to obtain sufficient evidence as to whether both approaches lead to similar results. Firstly, the pdf, $p(\hat{I}_{ad})$, is calculated for two different BS separation distances, d_0 . Secondly, the standard deviation of lognormal shadowing, σ , is varied for each deployment scenario. The results for the mean and the standard deviation of $p(\hat{I}_{ad})$ for $d_0 = R$ are summarised in Table 3.3 and similarly, the results for $d_0 = 2R$ are shown in Table 3.4.

Standard deviation σ [dB]	Monte Carlo simulation		Analytical calculation	
	$E(\hat{I}_{ad})$	$\text{Var}(\hat{I}_{ad})$	$E(\hat{I}_{ad})$	$\text{Var}(\hat{I}_{ad})$
2	-147.47	9.96	-147.53	9.86
4	-147.45	10.60	-147.47	10.46
8	-147.32	12.72	-147.45	12.53
16	-147.47	18.47	-147.43	18.66

Table 3.3: Comparison of mean and standard deviation of \hat{I}_{ad} for $d_0 = R$.

Standard deviation σ [dB]	Monte Carlo simulation		Analytical calculation	
	$E(\hat{I}_{ad})$	$\text{Var}(\hat{I}_{ad})$	$E(\hat{I}_{ad})$	$\text{Var}(\hat{I}_{ad})$
2	-156.28	7.66	-156.44	7.33
4	-156.22	8.38	-156.44	8.11
8	-156.32	10.85	-156.40	10.63
16	-156.26	17.62	-156.44	17.46

Table 3.4: Comparison of mean and standard deviation of \hat{I}_{ad} for $d_0 = 2R$.

It is found that the results of both methods are extremely similar. The mean differs by maximal 0.1% and the standard deviation varies by about 1%. The variations tend to increase for a small σ which is obvious as in this case the pdf is dominated by the cell geometry rather than the lognormal shadowing, and thus a difference is inevitable due to the use of hexagonal cells for the Monte Carlo simulations and a circular cell in the analytical derivation.

The results also reveal some interesting properties. For example, the standard deviation for $\sigma = 2$ and $\sigma = 4$ does not differ greatly (between 5% – 10%). In this case the pdf's are primarily dominated by the cell geometry and the random user distribution. In contrast, for $\sigma = 8$ and $\sigma = 16$ the variance of $p(\hat{I}_{ad})$ changes significantly (between 50% – 65%) from which it can be inferred that shadowing is the dominating random factor in this case. Furthermore, the expected value is almost constant when varying σ . This is anticipated since the mean of lognormal shadowing is zero and independent of the cell geometry and the user distribution. It is interesting to note that the expected value increases by about 9 dB when the BS's are separated by twice the cell radius instead of only one time the cell radius. This means that ACI can increase about 8 times within the observed interval of BS separation distances which points towards potential problems which may be caused by the ACI since, as described previously, cell planning cannot be assumed.

In addition to the results in Table 3.3 and Table 3.4 the respective pdf's and cumulative distribution functions (cdf's) of $p(\hat{I}_{ad})$ are depicted in Figure 3.7. When comparing the pdf's in Figure 3.7(c) with the pdf's in Figure 3.7(d) it can be found that for $d_0 = R$, *i.e.* the BS of the interfering cell is located at the cell boundary of the victim cell, the pdf's are skewed towards greater values of \hat{I}_{ad} . This can be explained by the fact that the MS can be in close proximity to the victim BS. In this case, the high transmitted power (due to the location at the cell boundary) results in great ACI. In contrast, for $d_0 = 2R$ the opposite behaviour can be observed, *i.e.* the tails of the pdf's for greater values of \hat{I}_{ad} converge to zero more rapidly than for lower values

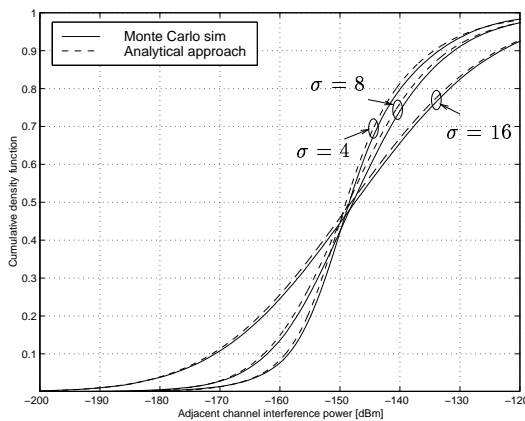
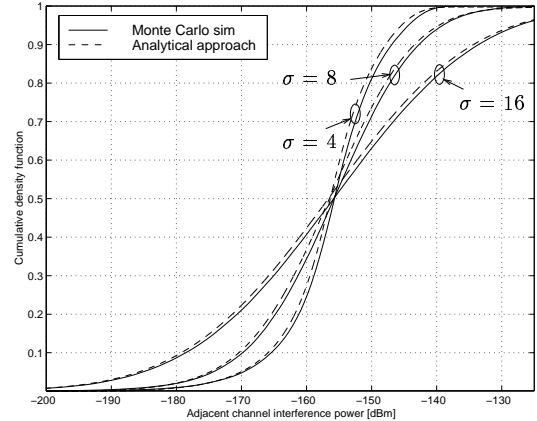
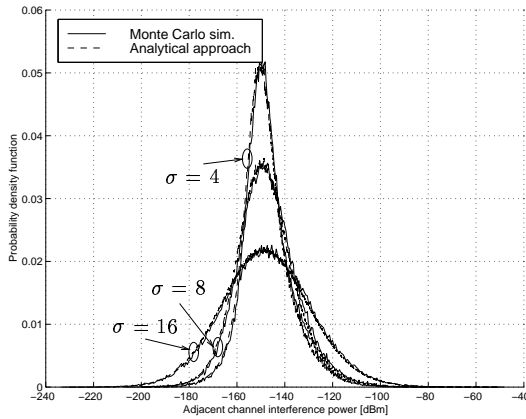
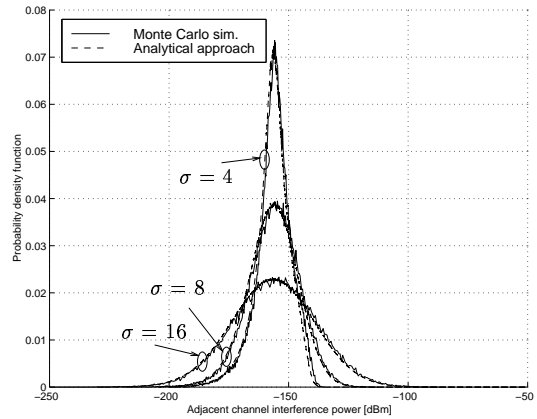

 (a) Cdf of \hat{I}_{ad} for $d_0 = R$.

 (b) Cdf of \hat{I}_{ad} for $d_0 = 2R$.

 (c) Pdf of \hat{I}_{ad} for $d_0 = R$.

 (d) Pdf of \hat{I}_{ad} for $d_0 = 2R$.

Figure 3.7: A comparison of the cdf's and pdf's obtained by the analytical approach in (3.48) with the results of Monte Carlo simulations.

of \hat{I}_{ad} . The reason for this is that the distance between the interfering MS and the victim BS is always more than the cell radius. This has a significant impact on interference. In the case of $d_0 = R$ and $\sigma = 8$, the probability that the interfering signal power is greater than, for example, -130 dBm is still about 10 %, whereas for $d_0 = 2R$, the probability that $\hat{I}_{ad} > -130$ dBm is only about 1 %.

3.3.2.5 Capacity results

It has been shown for a simplified scenario that the results of the Monte Carlo approach and the results of the analytical model do not differ significantly. This gives sufficient confidence to extend the Monte Carlo model to investigate the impact of different frame synchronisations on ACI.

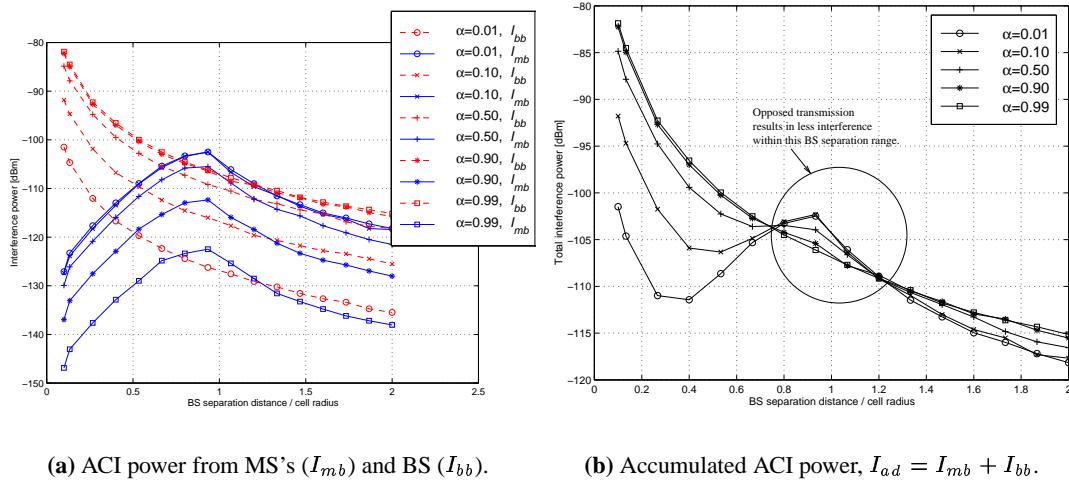
The cdf's of ACI caused by the transmitted code powers of the MS's and BS are calculated using the parameters in Table 3.5. The interference power derived from the cdf is chosen so that a

Parameter	Value
Cell radius, R	50 m
Bit rate	16 kbps
Chip rate	3.84 Mcps
Standard deviation of lognormal shadowing, σ	10 dB
Receiver noise figure	5 dB
Max. MS TX power	15 dBm
Max. BS TX power	24 dBm
Bit-energy to interference ratio, ε^u	3.5 dB
Tolerable outage, P_{out}	5 %

Table 3.5: Simulation parameters for ACI analysis.

maximum percentage of P_{out} users may experience outage. This means that in P_{out} percent of all investigated user distributions the interference is greater than the actual interference power used in the following analyses.

The interference results for a user population of four MS's are depicted in Figure 3.8. The interference caused by the BS is shown in red, whereas the interference resulting from the MS's are indicated by the blue curves. Note that when the interfering cells completely overlap, the MS→BS interference is lowest (due to power control and high cross-correlation of lognormal shadowing between the interference and desired path), but the BS→BS interference is highest. As the BS's are separated, the BS→BS interference is decreasing monotonically and at the same time the MS→BS interference is growing until the BS separation is about the cell radius. The reason for the peak of MS→BS interference is that the interference from MS's increases when the victim BS is moved towards the cell boundary due to the high transmission powers of the MS's at outer regions of the cell. The MS→BS interference however diminishes in a single cell scenario as the cells move further apart.


 (a) ACI power from MS's (I_{mb}) and BS (I_{bb}).

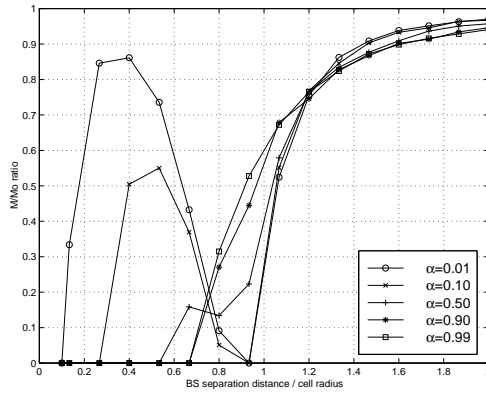
 (b) Accumulated ACI power, $I_{ad} = I_{mb} + I_{bb}$.

Figure 3.8: ACI power assuming four active interfering users.

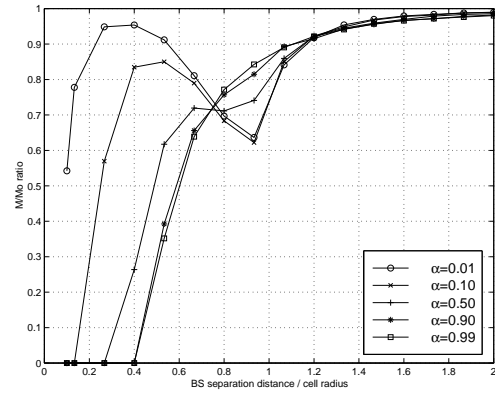
A highly synchronised transmission, $\alpha = 0.01$, compared to opposed transmission, $\alpha = 0.99$, results in greater MS \rightarrow BS interference, but in lower BS \rightarrow BS interference. However, despite the almost ideal synchronisation of $\alpha = 0.01$ (1 % synchronisation error) the interference power, I_{bb} for a BS separation distance of about 7 m is still -105 dBm – in comparison, the useful signal is -109 dBm. This means that the interference power from the close-by BS using the adjacent carrier is about 2.5 times greater than the useful signal power. Clearly, this renders the co-location of BS's difficult.

The most relevant discovery in this chapter is shown in Figure 3.8(b) where the total ACI power is depicted. Notice that for certain conditions it is advantageous to apply opposed synchronisation of TS's ($\alpha = 0.99$) rather than synchronous transmission and reception ($\alpha = 0.01$). This is highlighted by the circle in Figure 3.8(b). It will be shown that the same effect can also be observed when considering a multiple cell model as will be done in section 3.3.3. Therefore, this fundamental discovery is further exploited by the development by dynamic channel allocation (DCA) algorithms presented in chapter 4 and chapter 5 and has resulted in two patents [152, 153].

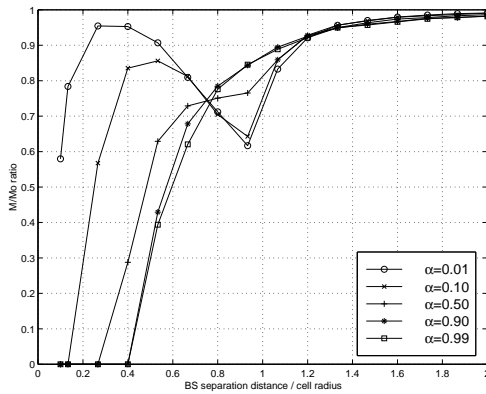
In Figure 3.9 the impact of ACI on capacity is shown. The capacity is calculated using (3.10) with other cell interference I_o^u being replaced by ACI, I_{ad} . When interpreting the capacity results, note that the outage threshold is 5 % which means that in 95 % of all user distribution scenarios the capacity is better than or equal to the actual figures presented. Therefore, if, for instance, the relative remaining capacity in the COI is 0 %, this means that there is a chance of



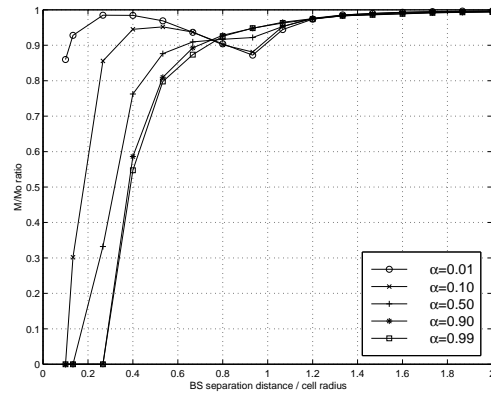
(a) Relative capacity with a cell load factor: $\chi=0.5$ and an ACIR: $\kappa_I=30$ dB



(b) Relative capacity with a cell load factor: $\chi=0.75$ and an ACIR: $\kappa_I=30$ dB



(c) Relative capacity with a cell load factor: $\chi=0.5$ and an ACIR: $\kappa_I=35$ dB



(d) Relative capacity with a cell load factor: $\chi=0.75$ and an ACIR: $\kappa_I=35$ dB

Figure 3.9: Cell capacity with four interfering MS's. The capacity is shown for different cell load factors and different ACIR factors.

95 % that the actual capacity is greater than 0 %.

The cell load factor in (3.10) determines the useful signal, P_u^u , at the BS in the COI. A linear increase of χ means that the useful signal P_u^u increases exponentially with a singularity at $\chi = 1$ which can be found by using (3.5). With the given parameters the pole capacity yields: $M_{max} = \frac{pq}{\varepsilon^u} + 1 = \frac{16}{10^{0.35}} + 1 \approx 8$. Therefore, the admission control of the system will restrict the maximum cell load to less than 8 users in order to prevent outage of users that are not able to achieve the increased P_u^u target at the BS receiver (usually MS's at outer regions of the cell). In Figure 3.9 the cell load is assumed to be 4 MS's which is equivalent to $\chi = 0.5$. If for the same actual user population, the cell load factor in (3.10) is increased, this has the equivalent effect of

a greater number of active MS's which inherently means an increased signal power P_u^u . Thus, by keeping the user population constant, but increasing χ , dynamic power control as a means to cope with ACI can be emulated. If, for example, in the case of four active MS's the cell load factor, χ , is increased from 0.5 to 0.75, the useful signal level is increased by a factor of three (4.77 dB) which is found using (3.5). The results (Figure 3.9(b) and Figure 3.9(c)) reveal that the increase of P_u^u by a factor of three has a similar effect as an increase of the ACIR, κ_I , by 5 dB. This is an expected result and thus helps to validate the entire model. As mentioned before, there is a potential disadvantage when increasing P_u^u which is that the coverage area can be affected. This yields the well known capacity–coverage trade off in CDMA systems [23]. An extended investigation was carried out in [154] assuming UTRA parameters, but the results are omitted in this thesis as the focus is merely on the relationship between interference and capacity.

Another interesting finding is that in all cases, the capacity for $\alpha = 0.01$ has a local maximum at a relative BS separation of about 0.2 – 0.5. This effect can be explained with the aid of the interference graphs which are depicted in Figure 3.8(b). The ACI power for $\alpha = 0.01$ is primarily determined by I_{mb} , but for small BS separations the interference contribution from the BS, I_{bb} , is significant which finally results in high interference for BS separations between 0 – 0.2 times the cell radius. The interference from the BS diminishes rapidly before I_{mb} starts increasing at a BS separation of between 0.6 – 1.0. This effect of I_{bb} and I_{mb} having their maximum at a relative BS separation of 0 and 1.0 respectively, results in a local minimum of I_{ad} and consequently in a local maximum of the relative capacity M/M_0 . This mechanism is inherent to a TDD system since in a FDD system only I_{mb} has to be considered and therefore a similar local maximum does not exist in such a system.

Co-siting is only feasible for $\kappa_I=35$ dB and $\alpha = 0.01$ without a significant capacity loss. In this case the capacity is between 59% and 85% dependent on P_u^u adjustments. The power adjustments are most effective for relative BS separations between 0.6 – 1.4. For a relative BS separation of 0.95 and $\kappa_I=30$ dB the gain by increasing P_u^u by a factor of three is about 60 %, whereas the gain is only about 10 % for a relative BS separation of 0.4 in which case the capacity is increased from 85% to 95%.

In Figure 3.10 the results of the relative capacity for six interfering MS's are presented. In this case an ACIR of 30 dB and TS synchronisations of $\alpha > 0.1$ prohibits connections at the respective TS's in the victim cell. This situation is improved significantly if the ACIR is

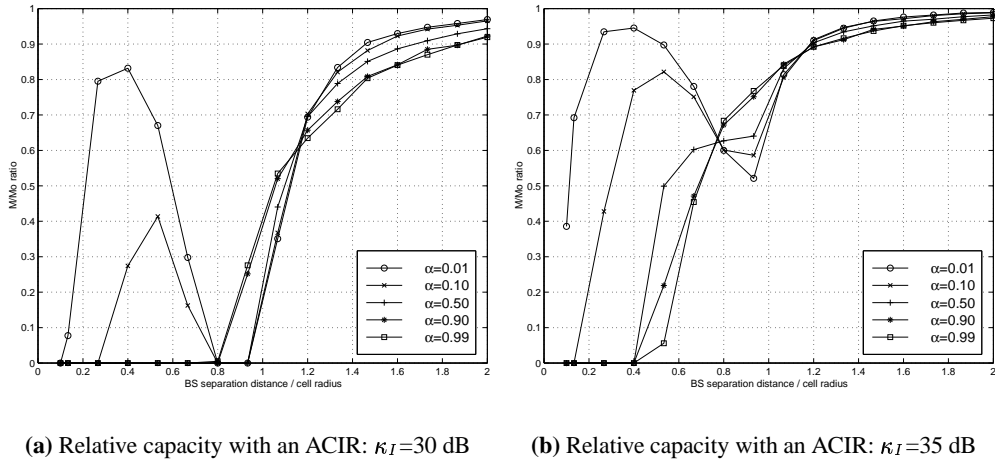


Figure 3.10: Cell capacity with six interfering MS's. The cell load factor, χ , is 0.75.

increased to 35 dB. In this case the capacity improvement is highest and about 50% for a BS separations range of 0.7 – 1.0 times the cell radius. If, however, the BS's separation is less than 0.4 times the cell radius and $\alpha > 0.1$ it is still not feasible to use the same TS's at the COI when assuming a tolerated outage of 5%. Despite an almost ideal synchronisation, $\alpha = 0.01$, an ACIR of 30 dB results in a significant capacity reduction within a relative BS separation range of 0 – 0.2 and 0.7 – 1.0. From these results and the results in Figure 3.9 it can be found that within the cell boundaries of the interfering cell, the best BS separation is at 30% – 50% of the cell radius provided that both cells transmit and receive synchronously, $\alpha < 0.01$. It is recognised that the condition of $\alpha < 0.01$ is difficult to satisfy, in particular, if the cells belong to two independent operators. Clearly, this case requires an ACIR greater than 35 dB, but there is obviously a trade-off between the costs associated when increasing the ACIR and the advantages obtained. In the following section the scope of investigation is extended in so far as a cluster of interfering cells rather than a single cells is considered.

3.3.3 Multiple interfering cells

One reason why a CDMA system has the potential to achieve greater flexibility than a TDMA or FDMA system is that in a cellular environment a frequency or TS re-use distance of one can be applied [10, 155]. Despite the greater interference and the accompanying effects on capacity, the system can be operated to allow high capacity and at the same time generate great flexibility. The disadvantage of CDMA systems is that power control and handover techniques have a vital

impact on interference [27, 76, 77]. This holds for CCI as well as ACI. Therefore, in this section, ACI in a cellular environment using different power control algorithms and handover margins is examined. Two different DL power assignment algorithms are applied: the power assignment method as described in section 3.3.2.2 and a C/I -based DL power control algorithm [156].

The cell topology as shown in Figure 3.11 is applied. The location of the COI is varied along

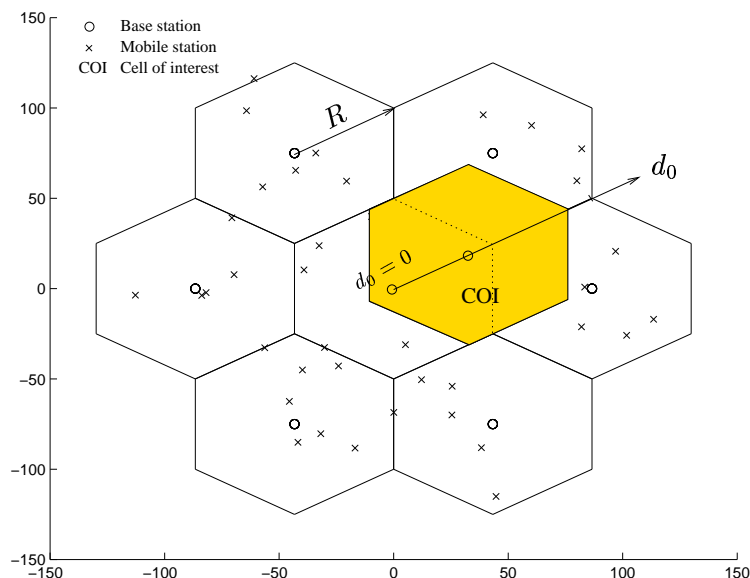


Figure 3.11: Multiple cells causing ACI at a cell located on top of the interfering cell cluster.

the d_0 -axis within the range: $5 \text{ m} \leq d_0 \leq R$.

3.3.3.1 Propagation model

The path loss model given in (3.18) is used. In the analyses of cellular networks it is usually assumed that lognormal shadowing on the propagation path is uncorrelated for different propagation paths. However measurements have shown that shadowing on the desired link and on the interference link can be highly correlated as illustrated in Figure 3.5. The correlation of lognormal shadowing is subject to many investigations by different researchers [147, 151, 157]

In the interference analysis conducted in this research a model reported by Klingenbrunn [147] is adopted. This paper reports that the correlation coefficient is primarily dependent on the relative distance difference of the receivers and the angle-of-arrival difference (AAD). It was found in [147] that the AAD dependency has the largest impact on the correlation coefficient of two signal paths. The correlation coefficient is computed as follows: firstly, the relative

difference between desired path, d_1 , and interference path, d_2 , is calculated as follows:

$$A = \left| 10 \log_{10} \left(\frac{d_1}{d_2} \right) \right| \text{ [dB]}. \quad (3.49)$$

A threshold, X , is introduced which determines the location when the distance dependency of the correlation coefficient reaches its minimum,

$$f(X, A) = \begin{cases} 1 - \frac{A}{X} & \text{if } A \leq X, \\ 0 & \text{otherwise.} \end{cases} \quad (3.50)$$

and finally, the correlation coefficient is obtained as:

$$r(\phi, A) = \begin{cases} f(X, A) \left(0.6 - \frac{|\phi|}{150} \right) + 0.4 & \text{if } |\phi| \leq 60, \\ 0 & \text{otherwise,} \end{cases} \quad (3.51)$$

Note, the minimum correlation coefficient is non-zero so as to account for local scattering around the receiver. It is reported in [147] that the threshold X is in the range of 6–20 dB. It is set to 6 dB in this evaluation because the correlation model is used in an indoor environment with a rapid change of the propagation conditions due to walls, doors and interior.

3.3.3.2 User distribution and handover

The total ACI power is dependent on the transmitted powers on the adjacent carrier. Therefore, methods such as handover in the interfering network reduce ACI. The significance of handovers are demonstrated by Chebaro [20] and later Viterbi [27]. In these papers it was shown that the allocation of a mobile to the closest BS rather than to the BS that offers the smallest signal attenuation can create up to 4–20 times higher interference. Note, that these results were obtained for an FDD system in which only the MS's contributed to interference at the BS and a cell re-use distance of one was assumed. In a TDD system this effect can be more significant since the UL and DL use the same radio frequency carrier. The severity of this problem in TDD with respect to ACI is investigated by considering handover regions as depicted in Figure 3.12. In the case that handovers are assumed, a MS which is located within the grey shaded areas chooses the best out of three BS's. The handover areas are determined by a circle with radius d_{1max} . The most significant criterion of the selection process is the lowest path loss. However, in order to avoid ping-pong effects handover algorithms such as, for example, the IS-95A algorithm [6]

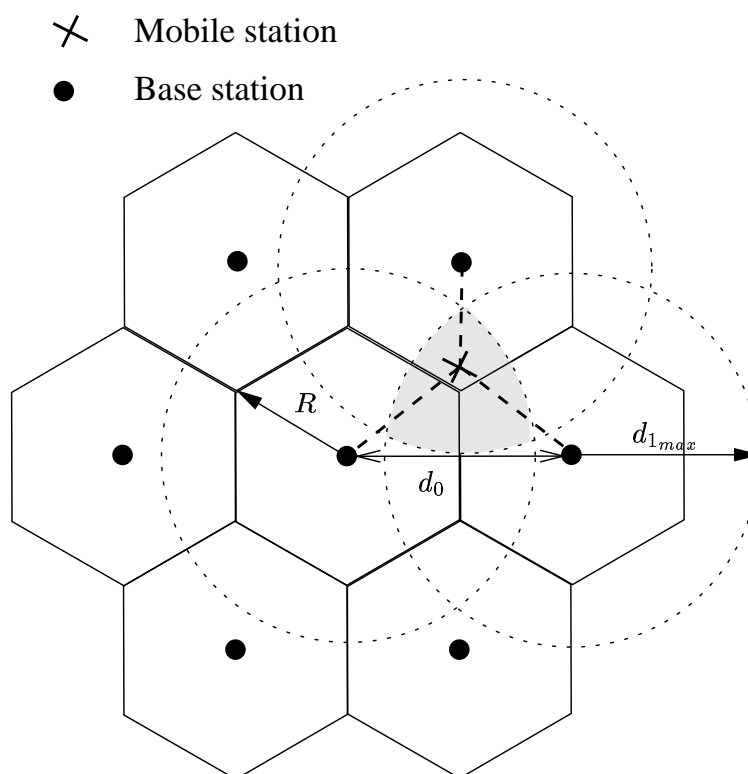


Figure 3.12: Handover model: within the grey shaded areas a MS's is located to the best serving BS.

incorporate a fixed handover threshold. The basic mechanism of a handover threshold may be explained with the aid of Figure 3.13. The path loss from an arbitrarily located MS to a set of its closest BS's (BS_0, BS_1, \dots, BS_n) is shown. It is assumed that the MS is located within the cell 0. Then the MS is served by the BS_0 if, and only if $a_0 \leq a_i + \delta$ for all $i = 0, 1, \dots, n$. The handover margin, δ , represents the additional path loss which can be tolerated until a handover process is executed to the cell offering the lower path loss. The effects of the handover mechanism can be examined by calculating the minimum coupling loss (MCL) between the BS and MS. The results of the MCL assuming a uniform user distribution and the path loss as given in (3.18) are presented in Figure 3.14. The handover mechanism reduces the probability of high coupling losses significantly. For example, the probability that the coupling losses are less than 70 dB is about 8 % if handovers are not used and about 17 % when implementing handovers with a 5 dB handover margin. This results in a difference of 9 %. For comparison, the difference for 90 dB MCL is 30 %. This shows how that the probability of great coupling losses are reduced considerably.

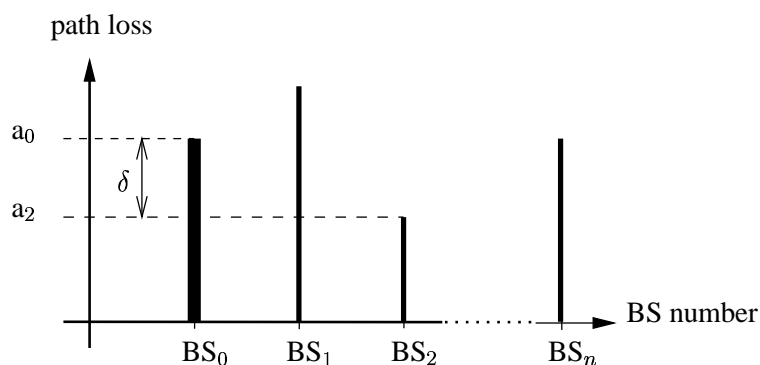


Figure 3.13: The MS is assigned to BS_0 . The handover threshold, δ , is used to model situations where a MS is not necessarily allocated to the BS which offers the lowest path loss (BS_2 in this case).

3.3.3.3 Interference results

Simulations are conducted using the parameters given in Table 3.5. For reasons of comparison the results in Figure 3.15 show the probability of ACI when handovers are used (solid curves) and when handovers are not used (dotted curves). As can be seen, handovers decrease the probability of ACI significantly. In the case of BS interference and $d_0=10$ m, the probability that I_{bb} is less than the thermal noise power (about -102 dBm) reduces from 15% to 3%. For the same cell configuration the probability of ACI from the MS's, I_{mb} , when permitting handovers resemble the distribution of ACI when disallowing handovers (Figure 3.15(b)). This effect is anticipated since the location of the victim cell is very close to an interfering BS. Since all MS's are power controlled to their respective BS the signal power of each MS is about the same at the BS receiver. Therefore, if a victim receiver is located close to a BS, the signal powers from the MS's do not vary greatly and are independent of the actual transmitted power of the MS. Hence, the reduction in the transmitted power due to handovers do not affect the ACI interference from MS's greatly. Therefore, it becomes clear that the total interference from the MS's is minimal for co-siting of both BS's. However, the total interference from BS's is highest for co-siting and reduces as the BS's are moved apart. These mechanisms are documented in Figure 3.15. If the victim BS is located at a cell corner at $d_0=50$ m the interference from the MS's is maximal – the probability that I_{mb} is greater than the thermal noise power when considering handovers is only about 1% and increases marginally to about 2% when handovers are omitted.

Given that two independent networks using an adjacent carrier are not synchronised such that cells receive and transmit at the same time, interference between BS's cannot be avoided. When comparing the worst case probabilities of I_{mb} and I_{bb} being less than the thermal noise power

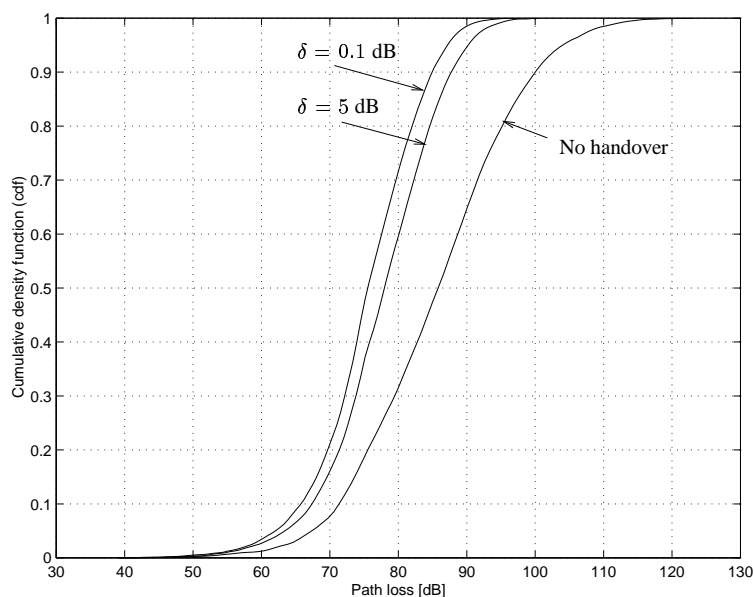
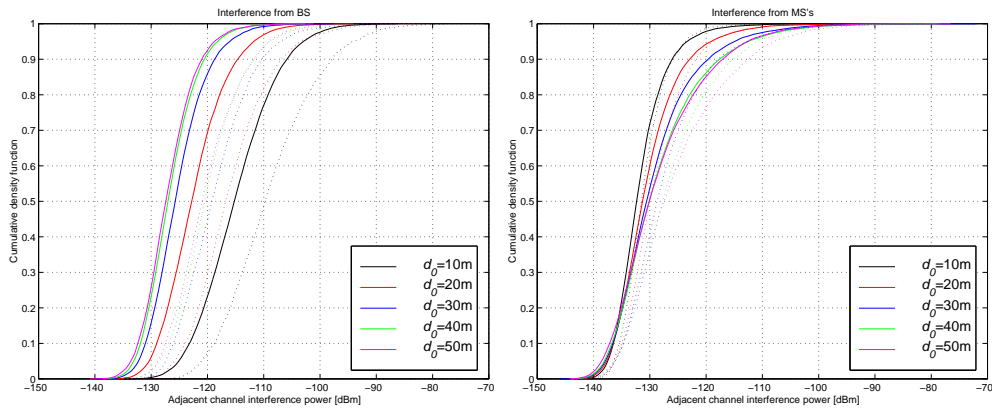


Figure 3.14: Minimum coupling losses assuming different handover thresholds.

an important statement can be made: It is more advantageous to locate BS's at the cell corners of the co-existing network rather than at the same site. This finding is significant as it says that the freedom in cell planning of a TDD network is strongly limited by co-existing networks which makes use of an adjacent carrier. In particular, the cost-effective option of using the same location for the BS's is the worst option if the ACIR at the BS and the MS is equal.

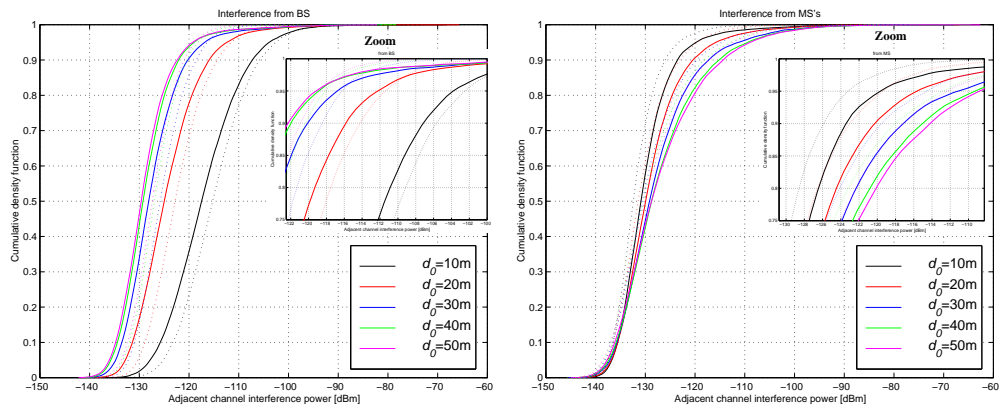
A further significant finding is that the interference from the BS's, I_{bb} , (Figure 3.15(a)) is affected by handovers to a greater extent than the interference from the MS's, I_{mb} , (Figure 3.15(b)). As an example, let d_0 be 30 m, then ACI from the MS's is in 90 % of all cases less than -120 dBm assuming handovers. This threshold increases to about -118 dBm for the case that handovers are not considered. The situation for I_{bb} and the same cell topology is that in 90 % of all cases the interference is less than -119 dBm with handovers carried out, but -110 dBm where there are no handovers. The effect that I_{bb} decreases by 9 dB whereas I_{mb} only reduces by 2 dB if handovers are used highlights the significance of handovers in such a TDD system.

However, so far the same DL power control algorithm as used in the single cell model and given in (3.30) is applied. This algorithm does not minimise the required code power for each MS. In a multiple cell environment the actual DL powers can considerably affect the performance in the neighbouring cells [80]. Therefore, C/I -based power control algorithms are used [156] in such


 (a) Probability of ACI from BS's ($\alpha = 1$)

 (b) Probability of ACI from MS's ($\alpha = 0$)

Figure 3.15: ACI distribution assuming 4 simultaneously active MS's in each interfering cell. Ideal power control in the UL and a DL power control algorithm given in (3.30) is assumed. The dotted lines represent the cdf of ACI for the case that handovers are not considered. The solid graphs depict the probability of ACI considering handover with a threshold of 5 dB. The ACIR, κ_I , is 35 dB.


 (a) Probability of ACI from BS's ($\alpha = 1$)

 (b) Probability of ACI from MS's ($\alpha = 0$)

Figure 3.16: ACI distribution assuming 4 simultaneously active MS's in each interfering cell, C/I -based power control algorithms in the UL and DL, non-ideal power control and handovers (solid graphs). For comparison the dotted curves show the results for ideal power control, a simple DL power control algorithm and handovers (the same as the dotted curves in Figure 3.15)

environments. On the one hand, it is anticipated that I_{bb} can be reduced using a more precise DL power control algorithm. On the other hand, the assumption of ideal power control in the UL and DL (all signals arrive at the same level) is not completely realistic as demonstrated in [26]. Therefore, simulations are conducted assuming a C/I -based power control algorithm and non-ideal power control in both direction. The standard deviation of the lognormally distributed bit-energy to interference ratios, σ_ε^u , and σ_ε^d respectively, are assumed to be 2.5 dB which is taken from [26]. For convenience the two cases which are compared are numbered as follows:

- (A) This is the case of ideal power control with handovers being considered (with an handover threshold of 5 dB) and the same DL power control algorithm as in the single cell scenario.
- (B) This is the case of non-ideal power control with a standard deviation $\sigma_\varepsilon^u = \sigma_\varepsilon^d = 2.5$ dB and C/I -based power control algorithms and considering handovers with a threshold of 5 dB.

The results in Figure 3.16 underline the trade-off described previously. This trade-off is most obvious in the following: In (B) (solid curves) the interference from the MS's is greater than in (A) (dotted curves), but this effect is reversed for the case of interference from the BS's. Therefore, from the latter it can be concluded that for the parameters used the impact of the C/I -based power control algorithm out-weights the effect of power control imperfections. In the case of interference from the MS's, of course, the C/I -based power control algorithm does not have an impact and thus the interference situation in (B) is worse than in (A). This can be expressed quantitatively as follows: assuming an interference threshold with the property that, for example, in 90% of cases the interference shall be less than the given threshold, the interference from MS's in (B) increases by about 3 dB for all BS locations observed. For the same scenario the interference from BS's decreases by about 1 dB. Thus, the capacity results assuming (A) underestimate I_{mb} and overestimate I_{bb} with respect to (B).

Capacity results In Figure 3.17 the relative remaining capacities in the COI are presented using (3.10) which assumes ideal power control within the COI. The scenarios described in (A) and (B) are investigated. The following properties become apparent:

- An ACIR of 25 dB can lead to significant capacity reductions.

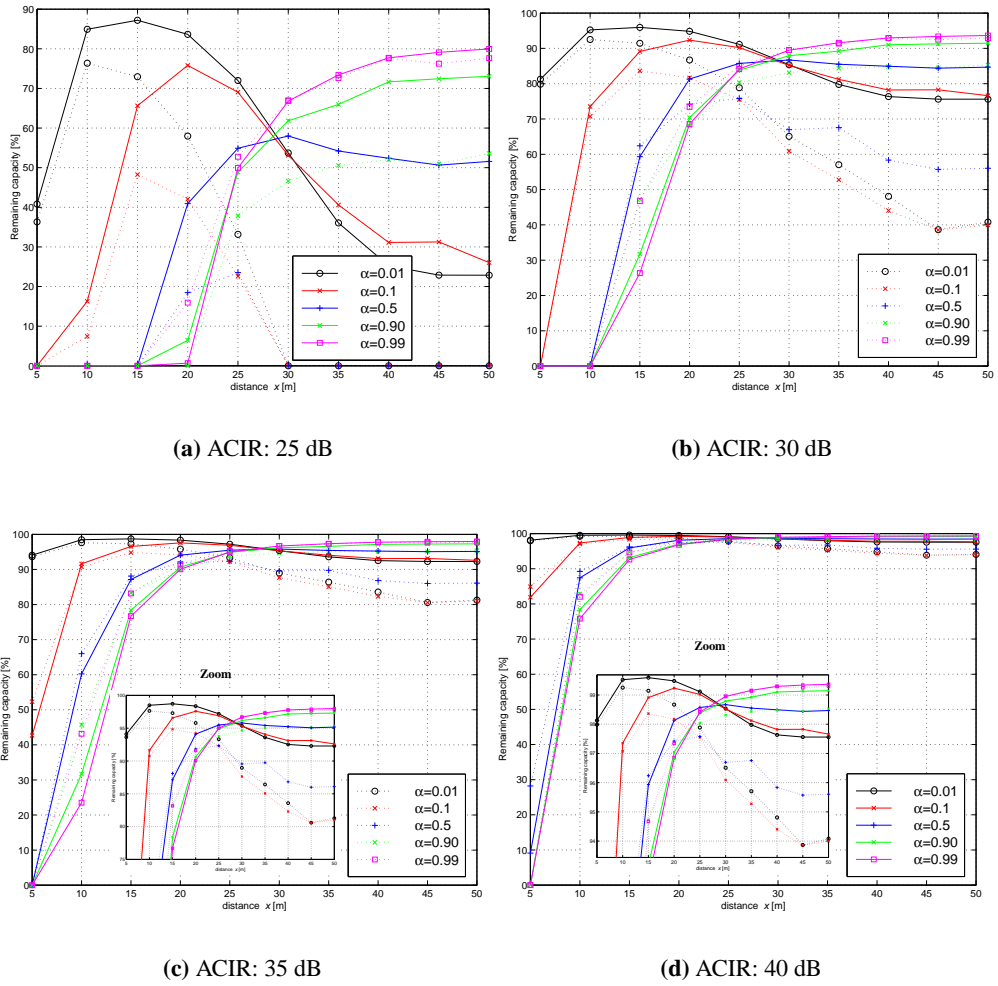


Figure 3.17: Relative cell capacity with four interfering MS's. The capacity is shown for different ACIR factors. The frame synchronisation α is used as a parameter. The cell load factor is $\chi=0.75$ and the tolerable outage, P_{out} , is 5%. The graphs with solid lines depict the results of scenario (A) whereas the dotted curves show the results of scenario (B). All results implicitly assume handovers.

- The effects of non-ideal power control (scenario **(B)**) on capacity are most significant for ACIR values less than or equal to 30 dB.
- The greater interference contribution from MS's in **(B)** mostly affects the capacity for BS locations of $x > 30$ m and synchronisations with $\alpha \leq 0.5$. This, in turn, means that the detrimental effects of greater interference from MS's at locations of $x > 30$ m can be avoided by changing the synchronisation so that $\alpha > 0.5$. Thus, the fundamental finding in section 3.3.2 is also valid for a multiple cell scenario. The basic finding is that opposed synchronisation ($\alpha = 0.99$) is sometimes more advantageous than synchronous transmissions ($\alpha = 0.01$). Thus, this mechanism inherent to a TDD system may be exploited to minimise severe interference scenarios resulting, for example, from non-ideal power control. This mechanism discovered by this analysis is termed TS-opposing technique [152, 153].
- For BS separations between $22.5 \text{ m} \leq x \leq 27.5 \text{ m}$ the capacity is least sensitive to variations in the frame synchronisation factor α . Alternatively to the TS-opposing technique, the fact that the interference for BS separation in the range between $22.5 \text{ m} \leq x \leq 27.5 \text{ m}$ is almost independent of TS synchronisation may be exploited to maintain a constant capacity in the COI regardless of the synchronisation to the interfering network. This may be important if the victim cell belongs to a different operator which does not synchronise to the co-existing network.
- An ACIR of 40 dB and $\alpha=0.01$ merely yields a capacity reduction between 0.1 % and 6 %.
- Location of the victim BS at $x < 10$ m results in a significant capacity drop due to the great interference from the close-by BS unless the TS's are synchronised with an error of less than or equal to 1 %.
- When comparing the results of the single cell scenario with an ACIR of 35 dB (Figure 3.9(d)) with the similar results obtained from the multiple cell scenario in Figure 3.17(c) (solid curves), it can be found that there are situations where the single interfering cell creates greater capacity losses in the victim cell than if an interfering network with handovers is considered. This finding is counter intuitive, but can be explained by the significant interference reduction due to handovers.

3.4 Co-channel interference in a CDMA-TDD system

In the previous sections various scenarios are considered to study the effects of ACI in a CDMA-TDD system. The parameters used in these investigations are closely related to the UTRA interface. The results reveal a significant property of such a system which is that synchronous transmissions between victim and interfering cells does not yield the lowest interference under all circumstances. The characteristics of CCI are different because cells usually do not overlap, but the same carrier is used in every cell. The interference protection results from the spatial separation and methods such as, for example, antenna sectorisation and handover.

If it can be shown that the novel, counter intuitive finding also holds in the case of CCI, DCA algorithms may exploit this mechanism to permit cell independent channel asymmetries between neighbouring cells using the same frequency carrier. Therefore, in this section the properties of CCI are investigated, given that synchronous as well as asynchronous transmission can occur in a CDMA-TDD system (if neighbouring cells adopt different traffic loads in the UL and DL by TS pooling, asynchronous transmissions occur inevitably.).

3.4.1 Simulation platform

The cell structure as depicted in Figure 3.18 is used to carry out the CCI analysis, *i.e.* a cell re-use distance of 1 is applied.

Interference is evaluated in the COI for different user populations within the first tier of cells. The propagation model and handover model are the same as described in section 3.3.3. CCI is calculated assuming non-ideal power control with $\sigma_{\epsilon}^u = \sigma_{\epsilon}^d = 2.5$ dB and C/I -based power control algorithms in the UL and DL. The simulations are conducted using the parameters given in Table 3.5.

3.4.2 Methodology of analysis

The six neighbouring cells of the COI are equally and uniformly populated. The power transmitting entities (MS's and BS's) of these neighbouring cells cause interference at the COI. For this purpose a quadratic mesh is placed on top of the cell of interest in Figure 3.18 and for each grid point, (x, y) , an interference vector is calculated with one component being the

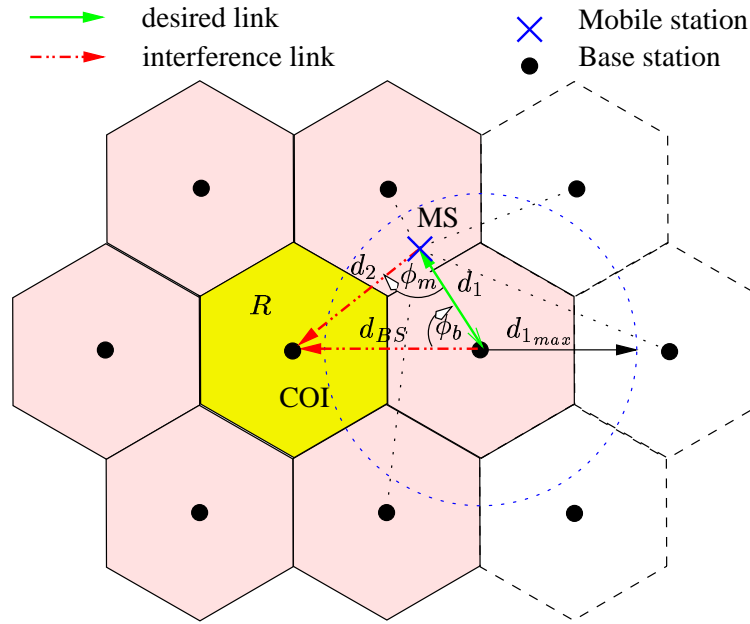


Figure 3.18: Cell model used to calculate interference in the COI

interference resulting from the neighbouring BS's,

$$I_b(x, y) = \sum_{j=1}^L \frac{Pc_j^d}{a_j(x, y)}, \quad (3.52)$$

and with a second component being the interference resulting from the MS's:

$$I_m(x, y) = \sum_{j=1}^L \sum_{i=1}^{M_j} \frac{Pc_{i,j}^u}{a_{i,j}(x, y)}, \quad (3.53)$$

where L is the number of adjacent cells (in the interference analysis here, L is confined to the first tier of cells), Pc_j^d is the transmitted carrier power [158] of BS j . Furthermore, $a_j(x, y)$ is the path loss between the grid point specified by the x and y coordinates and BS j , $a_{i,j}(x, y)$ is the path loss between the user i in cell j and the grid point in the COI specified by (x, y) . $Pc_{i,j}^u$ is the transmit power of mobile i in cell j .

At each grid point a binary decision is made whether I_b is greater than I_m ,

$$\tilde{\Psi}(x, y) = \begin{cases} -1 & \text{if } I_b < I_m, \\ 1 & \text{otherwise,} \end{cases} \quad (3.54)$$

Then Q Monte Carlo runs were carried out and for each grid point a weighting factor calculated

as follows:

$$\Psi(x, y) = \sum_i^Q b_i(x, y) . \quad (3.55)$$

Using $\Psi(x, y)$ it is possible to calculate the probabilities,

$$Z(x, y) = Pr [I_m(x, y) < I_b(x, y)] = 0.5 \left(1 + \frac{\Psi(x, y)}{Q} \right) . \quad (3.56)$$

3.4.3 Results

The probabilities, $Z(x, y)$, within the COI were calculated. The location of the BS of the COI is at $x = y = 0$. The radius which defines the handover regions (Figure 3.12), d_{1max} , equals: $d_{1max} = \frac{3\sqrt{3}R}{4} \approx 65$ m which is set to 75 % of the distance between two BS's . The results as 3d plots are depicted in Figure 3.19 whereas the same results as contour plots are shown in Figure 3.20. It is found that I_b dominates over I_m ($Z(x, y) \gg 50$ %) throughout the COI, but not as significantly as reported in [109]. The reason for this is primarily because a C/I -based DL power control algorithm is used whereas in [109] the DL is constant and determined by the maximum distance from the BS. Note, that the probability of the absolute interference cannot be inferred from $Z(x, y)$. The maximum probability of I_b being greater than I_m is obtained at the centre of the COI where $Z(x, y)$ is between 58.5 % – 75 % (assuming 3 to 6 interfering MS's). This is of particular interest since the UL performance for all connections is determined at this location. From the contour plots it can be seen that the probability that I_b is greater than I_m at the cell corners varies between 56 % – 66 %. At these locations $Z(x, y)$ is lowest because the MS's transmit highest powers at the cell corners.

The results in Figure 3.20 can also be used to find an upper limit for outage caused by MS \leftrightarrow MS interference at any given point within the COI. When assuming an ideal synchronised network, I_b and I_m are mutually exclusive. This means either I_b or I_m represents co-channel interference. It merely depends on the TS configuration between neighbouring cells as to which component needs to be considered. It is found that the maximum probability of I_m being greater than I_b is only about 44 % for a worst case location at any of the 6 cell corners. As a consequence, only in 44 % of the cases will outage be caused by another mobile. Hence, for the scenario investigated, an upper bound of outage as a consequence of MS \leftrightarrow MS interference is given by evaluating $1 - Z(x, y)$. This means, if a MS at the location (x, y) experiences outage,

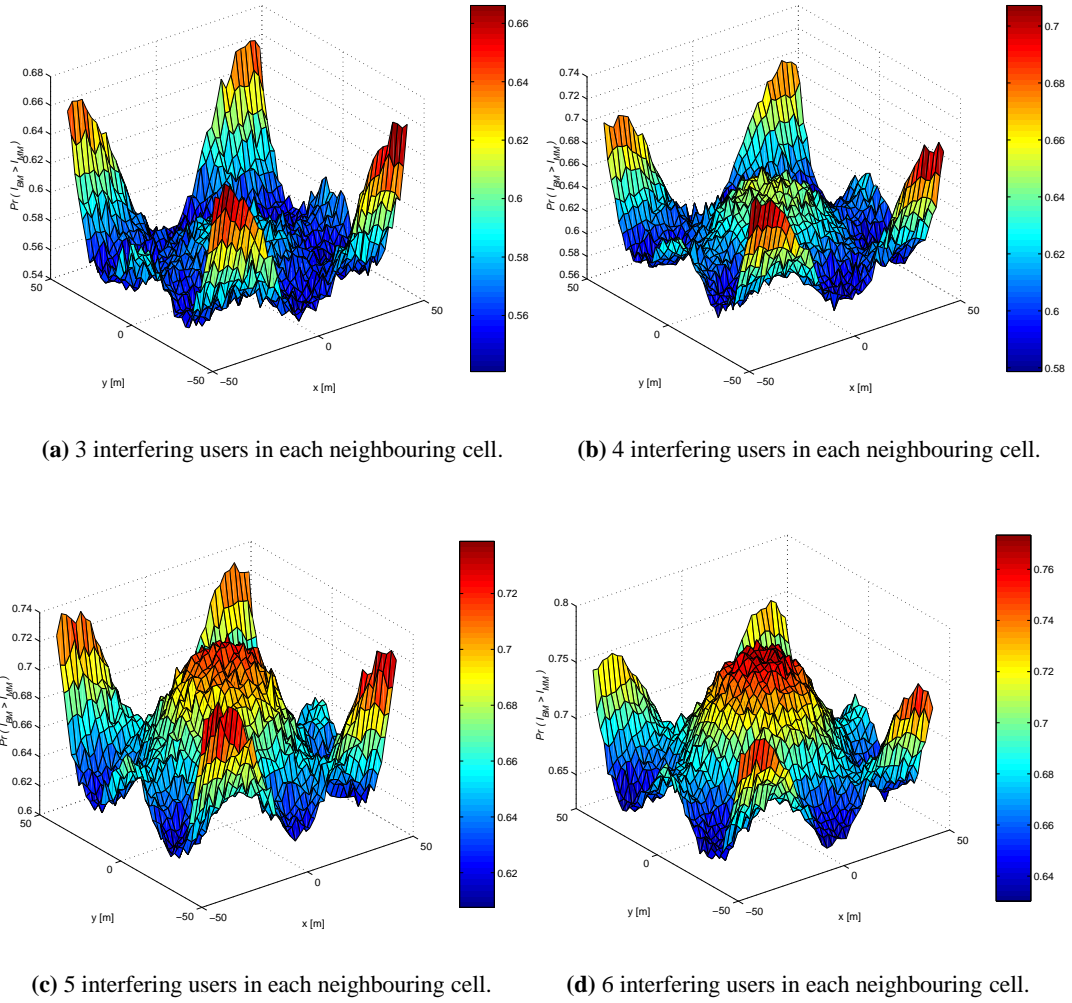
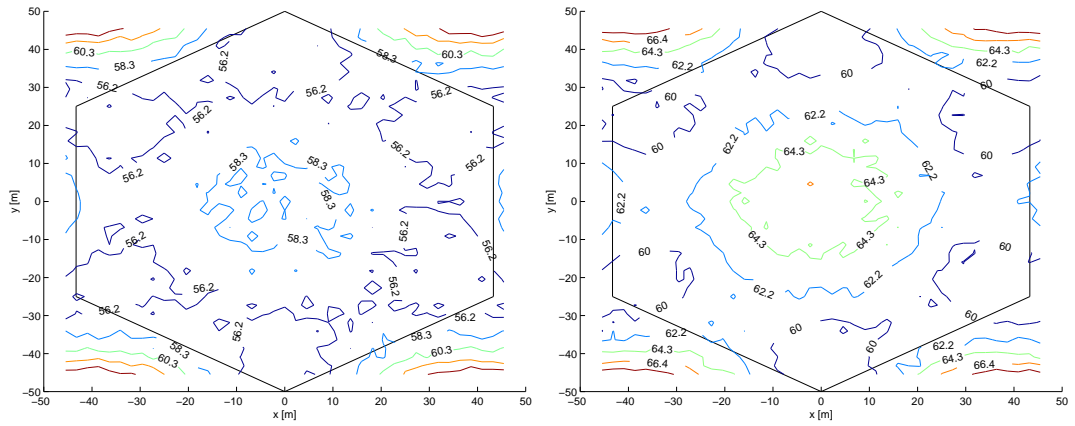


Figure 3.19: 3d plots of the probabilities that I_b is greater than I_m within and around the COI.

the maximum probability that this is caused by MS \leftrightarrow MS interference is $1 - Z(x, y)$.

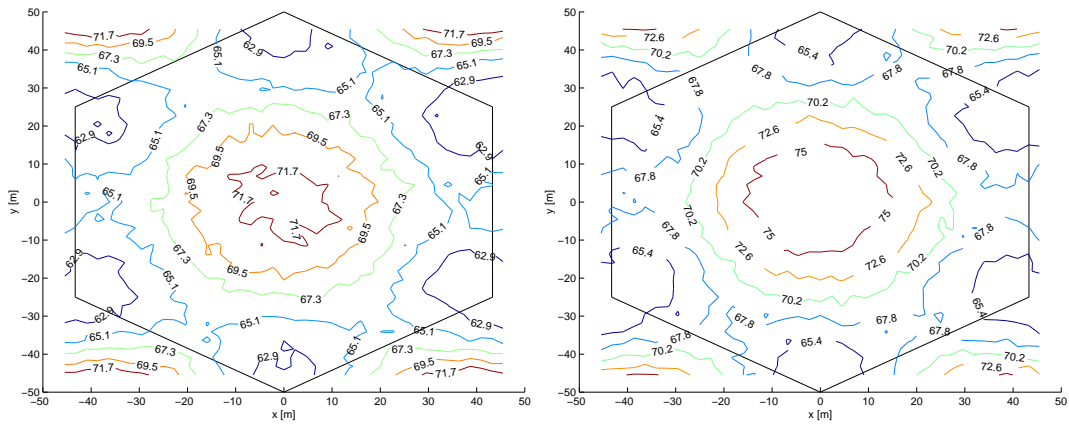
3.5 Conclusions

This chapter considered interference issues inherent to a CDMA/TDD air interface. The analysis of ACI showed that interference resulting from BS's can cause a significant capacity loss if BS's are located in close proximity and if both cells do not receive and transmit synchronously. This limits the freedom in planning such a network if the ACIR is not increased beyond 40 dB for such BS locations. It was found that the ACI resulting from an isolated cell can be greater than ACI from an underlying network in which handovers are used. This finding



(a) 3 interfering users in each neighbouring cell.

(b) 4 interfering users in each neighbouring cell.



(c) 5 interfering users in each neighbouring cell.

(d) 6 interfering users in each neighbouring cell.

Figure 3.20: Contour plots of the probabilities that I_b is greater than I_m within and around the COI.

supports the use of the TDD mode to build a cellular network. This is further supported by a new discovery which is that opposed synchronisation of TS's can yield higher capacity than synchronous transmissions regardless of whether an adjacent carrier or the same carrier is used in any close-by cell. In the case of ACI, cells may not be able to synchronise to cells belonging to another operator. The study on ACI revealed that for BS locations at about half the cell radius the interference power is least varying with different TS synchronisations. It was further found that a TDD system can suffer significantly if the transmitted powers in the DL are not reduced to a minimum required power determined by the C/I ratio at each MS individually. Hence, tight DL power control is required.

A co-channel interference investigation was carried out. In particular, the TDD inherent property that at any given point in the network interference may result from MS's or BS's were studied. It was found that at the centre of the COI, in up to 75 % of cases the interference power from the BS's of the other cells, I_b , is greater than the interference power from all MS's in the neighbouring cells, I_m . An upper bound on outage due to MS \leftrightarrow MS interference was found which yields 44 %. The investigation on CCI confirmed the novel finding of the ACI analysis: in 25% – 41.7% of all investigated user distributions it is more advantageous to apply opposed synchronisation in a TDD system. These figures are obtained of a load between 3 – 6 simultaneously active MS's in each of the six interfering cells. If this new finding is exploited systematically, cell independent channel asymmetries between neighbouring cells using a TD-CDMA/TDD interface, such as UTRA-TDD, can be enabled whereby capacity can be gained. This finding is counter intuitive since it is commonly assumed that cell independent channel asymmetries in such a system yield a significant capacity drop as, for example, can be found in [6, Chapter 10]: "Cell-independent asymmetric capacity allocation between UL and DL is not feasible for each cell in the coverage area". In chapter 4 and chapter 5 of this thesis DCA algorithms are developed which exploit the novel finding and prove that cell independent asymmetries between neighbouring cells can be feasible.

In these analyses cell sectorisation and antenna array techniques were not considered, but may be used to reduce ACI as well as CCI. Therefore, further investigation may address the problems of ACI and CCI in this context.

Chapter 4

Centralised DCA algorithm using the TS-opposing idea

4.1 Introduction

This chapter aims to exploit the key finding of chapter 3 and to apply it to the TDD air-interface of UMTS (UTRA-TDD). The significant finding of the previous chapter is that ideal synchronisation is not necessarily a prerequisite to obtaining the maximum capacity in a TD-CDMA/TDD network. This has led the author to develop a novel technique which is termed: *time slot (TS)-opposing* method [152, 153]. In this chapter this method is used to develop a centralised dynamic channel assignment (DCA) algorithm [152].

The approach in this chapter is as follows: Firstly, in section 4.2 a simple centralised DCA algorithm used in a single cell is studied. This investigation aims to find an upper bound of the network performance when combining the TS-opposing technique with a DCA algorithm. Secondly, in section 4.3 the TS-opposing algorithm is investigated in a cellular TD-CDMA/TDD network. For this approach it is assumed that a group of BS's (following the so called bunch concept [112]) is connected to a radio network controller (RNC).

4.2 TS-opposing technique applied to a single cell

In this investigation an idealised deployment scenario is assumed to investigate the new TS-opposing mechanism. This means that a TS-opposing algorithm is employed with the aim of improving the capacity only with respect to a single cell. The capacity obtained thereby is then compared with the capacity of an equivalent FDD interface.

A cluster of seven hexagonal cells is assumed with the cell of interest (COI) in the centre. The effects of the TS-opposing technique on the interfering cells is neglected in order to find the maximum capacity gain. In section 4.2.1 the TS-opposing technique is described mathematically. In section 4.2.2 a simple DCA algorithm is presented and applied to the simulation

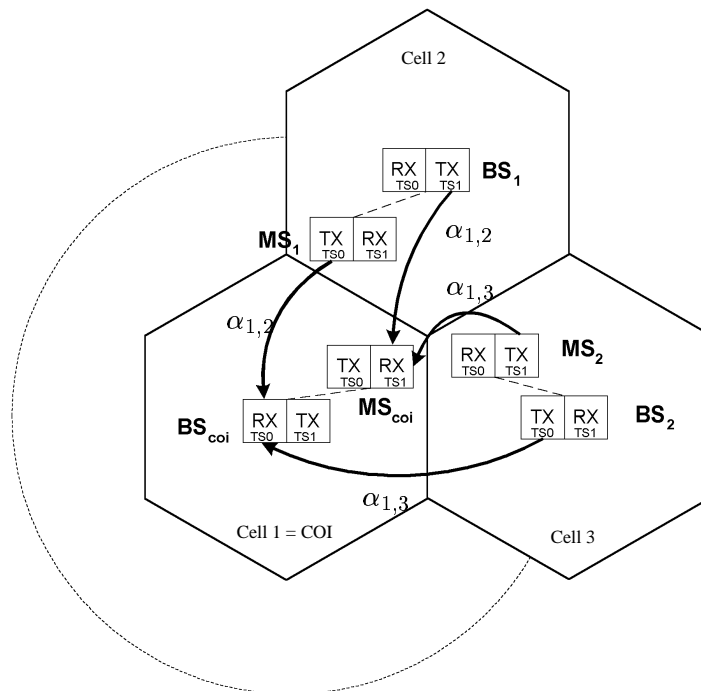


Figure 4.1: A cell arrangement with each cell using two successive time slots where the first begins at the same time in each cell is shown. The direction of transmission is arranged so that the cell of interest (COI) and cell 2 receive in TS 0 and transmit in TS 1. In contrast, the BS of cell 3 first transmits and then receives.

environment described in section 4.2.3. The performance of the DCA is compared with the capacity of an equivalent FDD interface with the results being discussed in section 4.2.4.

4.2.1 System model

It is demonstrated in chapter 3 that the received, power-controlled signal power from the desired user (3.2) can be found as:

$$P_u^u = \frac{I_o^u + N}{\frac{pg}{\varepsilon^u} + 1 - M_{FDD}}, \quad (4.1)$$

where M_{FDD} is the number of simultaneously active users in an FDD system, I_o^u the total other-cell interference power, N the thermal noise power, ε^u the bit-energy to interference ratio and pg the processing gain. Note that symbols which are followed by the superscript 'u' are associated with the uplink channel; symbols which are followed by the superscript 'd' are associated with the downlink channel.

It can be seen that P_u^u is a function of the number of simultaneously active users, M . Therefore, a factor can be defined as to how the required signal power at the receiver has to be increased as the cell load increases. This factor is commonly known as the interference margin [144]:

$$\nu = \frac{P_u^u(M)}{P_u^u(M=0)} = \frac{1}{1 - \underbrace{\frac{(M_{FDD} - 1) \varepsilon^u}{pg}}_q}. \quad (4.2)$$

Using (4.2) the desired signal power in (4.1) can be re-written as:

$$P_u^u = \frac{\nu N \varepsilon^u}{pg}. \quad (4.3)$$

This allows study of the dependency of the desired signal power, P_u^u , on the number of active mobiles in the cell. Since the term $q = \frac{(M_{FDD}-1)\varepsilon^u}{pg}$ in (4.2) has to fulfill $|q| < 1$, ν can be interpreted as the value to which the infinite geometric series converges:

$$\nu = 1 + q + \dots + q^{n-1} \quad n \rightarrow \infty \quad (4.4)$$

Hence, it can be seen that P_u^u increases non-linearly with an increasing cell load.

It is well known that CDMA is an interference limited multiple access technique. This means

that in a system with a single user detector, the capacity is primarily limited by the multiple access interference (MAI) power, which, in this thesis, is equivalent to the own-cell interference power. With the aid of (3.1) given as follows:

$$\varepsilon^u = \frac{P_u^u pg}{\underbrace{P_u^u (M - 1)}_{I_{own}} + I_o^u + N} , \quad (4.5)$$

the own-cell interference power yields:

$$I_{own} = P_u^u (M_{FDD} - 1), \quad (4.6)$$

Since P_u^u increases non-linearly with the number of active users in a cell, it directly follows from (4.6) that own-cell interference, too, increases non-linearly. Moreover, (4.1) contains a singularity at $M_{FDD} = \frac{pg}{\varepsilon^u} + 1$ which defines the theoretical maximum of users that can be served. The capacity maximum is also referred to as the pole capacity [6, 23]. At the pole capacity the desired signal and own-cell interference approaches infinity. This relationship will be useful in explaining our later results.

It is illustrated in the Appendix A that (4.1) can be transformed into an equation used in a paper by Viterbi [26]. In this paper, it was demonstrated that the maximum number of users which can have access to a FDD-CDMA system using a single-user detector can be expressed as:

$$M_{FDD} \leq \frac{pg (1 - \eta)}{\varepsilon^u (1 + f)} , \quad (4.7)$$

where $\eta = N/I_{tot}$ with I_{tot} being the maximal total acceptable interference power and f the ratio of other-cell interference to own-cell interference at the COI.

In the assumptions leading to (4.7) only other-entity interference, as defined in the previous chapter, is included because it describes the capacity of an FDD system. It is demonstrated in chapter 3 that when using the TDD mode also BS \leftrightarrow BS and MS \leftrightarrow MS interference, characterised as same-entity interference, can exist. With the aid of Figure 4.1, equation (4.7) will be modified to also include same entity interference. Figure 4.1 shows a cell arrangement with each cell using two successive time slots (TS 0 and TS 1) — with TS 0 synchronised in all cells. The direction of transmission is arranged such that the BS in the COI (cell 1) and the BS in cell 2 receive in TS 0 and transmit in TS 1. In contrast, the BS in cell 3 first transmits

and then receives resulting in an asynchronous TS overlap¹ at TS 0 and TS 1 between the COI and cell 3, and between cell 2 and cell 3 respectively. At the COI, when comparing interference from cell 2 with interference from cell 3, two entirely different interference scenarios exist. The interference between the COI and cell 2 only consists of other entity interference. This is the same as for an FDD system. When investigating interference between the COI and cell 3, it can be found that other entity interference does not exist, but instead, same entity interference can be observed. Assuming a network with ideally aligned TS's these are the two different interference scenarios which can occur in a TDD system. A factor, α , is introduced to account for the different interference scenarios shown in Figure 4.1. Since all TS's are assumed to be aligned α can only take values of 0 or 1. Thus, interference from the first tier of adjacent cells can be written as

$$I_o^u = \sum_{i=2}^7 [(1 - \alpha_{i,1}) I_{mb_{i,1}} + \alpha_{i,1} I_{bb_{i,1}}] \quad \alpha_{i,1} \in \{0, 1\}, \quad (4.8)$$

where $I_{mb_{i,1}}$ is the interference power at the BS of cell 1 resulting from all mobiles in the adjacent cell, i . Similarly, $I_{bb_{i,1}}$ is the interference power at the BS of cell 1 caused by the BS in the neighbouring cell, i , and

$$\alpha_{i,1} = \begin{cases} 1 & \text{if opposed transmission (TX) and reception (RX),} \\ 0 & \text{otherwise.} \end{cases} \quad (4.9)$$

Substituting (4.8) into (4.7) yields,

$$M_{TDD} \leq \frac{pg(1 - \eta)}{\varepsilon^u \left(1 + \sum_{i=2}^7 [f_{i,1} + \alpha_{i,1} (g_{i,1} - f_{i,1})]\right)}, \quad (4.10)$$

where $g_{i,1}$ is the ratio of other-cell interference conveyed by the BS i to own-cell interference in the COI. Similarly, $f_{i,1}$ is the ratio of the total MS interference of cell i to own-cell interference.

It holds that:

$$f = \sum_{i=2}^7 f_{i,1}, \quad (4.11)$$

¹The expression 'asynchronous TS overlap' is used to express the state in a TDD system when the same type of entity (BS or MS) in two adjacent cells does not transmit and receive synchronously at any time. This state is automatically created if two adjacent cells adopt a different rate of channel asymmetry.

and

$$g = \sum_{i=2}^7 g_{i,1} . \quad (4.12)$$

The value obtained by (4.11) is the same as observed in an FDD system and the result of (4.12) is inherent to a TDD system.

Eqn. (4.10) shows an interesting property of a CDMA/TDD system in that the capacity can, in principle, be higher than in an equivalent FDD system if the RX/TX direction of two neighbouring cells are chosen as follows: If, for example, $g_{i,1}$ is smaller than $f_{i,1}$ and $\alpha_{i,1}$ is chosen such that TS's of the respective cells overlap asynchronously (BS_i is transmitting while the BS of the COI is receiving ($\alpha_{i,1} = 1$), the total other-cell interference is smaller than $f_{i,1}$ and thus smaller than in an equivalent FDD system. Moreover, the implications of these findings are counter intuitive, *i.e.* one would expect neighbouring cells in a TDD system adopting different rates of asymmetry (with the consequence that TS's will overlap asynchronously) to cause a significant capacity loss. However, the results in section 3.4 reveal that in 25%–41.7% of all uniform users distributions it would be more advantageous if same-entity interference was effective. Since this scenario inevitably occurs in the case of asynchronous TS overlaps, the strategy is to exploit the previous finding by a DCA algorithm which reduces interference in the occurrence of asynchronous TS overlaps. This eventually enables neighbouring cells to apply different rates of channel asymmetry. Therefore, a DCA algorithm is presented which adapts $\alpha_{i,1}$ for each neighbouring cell so as to minimise interference. The DCA algorithm is assumed only to minimise interference in the COI. This optimisation process, however, has mutual effects on the interference in each of the 6 neighbouring cells. These effects are that the interference in the neighbouring cells may not necessarily be diminished or may even be increased. In addition, the simple DCA algorithm merely minimises the interference at the BS. Although it was found that MS \leftrightarrow MS interference is not a critical issue [109], the situation may arise where severe MS \leftrightarrow MS interference needs to be arbitrated. Hence, interference minimisation with respect to the BS of a single cell results in an idealised scenario which however provides a valuable bound on network performance.

The aim of this analysis is to directly compare the capacity results of an equivalent FDD interface obtained using (4.7) with the capacity of a TDD system which uses a TS-opposing algorithm as described in (4.10). Note, (4.10) can be reduced to (4.7) by setting $\alpha \equiv 0$ for all

user scenarios. Thus, the relative capacity can be expressed as:

$$M_{TDD}/M_{FDD} = 1 - \frac{\sum_{i=1}^6 \zeta_{i,1}}{1 + \sum_{i=1}^6 (f_{i,1} + \zeta_{i,1})}, \quad (4.13)$$

with $\zeta_{i,1} = \alpha_{i,1} (g_{i,1} - f_{i,1})$.

4.2.2 A simple DCA algorithm

From (4.10) it follows that the best strategy is to minimise $\zeta_{i,1}$ with respect to $\alpha_{i,1}$ which can be achieved by:

$$\alpha_{i,1} = \begin{cases} 1 & \text{if } g_{i,1} < f_{i,1}, \\ 0 & \text{otherwise.} \end{cases} \quad (4.14)$$

An interpretation of (4.14) is that, whenever the BS interference contribution from adjacent cell i is smaller than the total MS interference power from cell i , the algorithm forces an asynchronous overlap to occur at the respective TS's. The consequence is that the uplink and downlink between two cells are in opposed direction. Using the strategy as described in (4.14), $\zeta_{i,1}$ in (4.13) becomes:

$$\zeta_{i,1} = \begin{cases} 0 & \text{if } g_{i,1} \geq f_{i,1}, \\ g_{i,1} - f_{i,1} & \text{if } g_{i,1} < f_{i,1}. \end{cases} \quad (4.15)$$

As a consequence, and quite important to note, it holds that

$$\zeta = \sum_{i=2}^7 \zeta_{i,1} \leq 0. \quad (4.16)$$

Combining this property with (4.13), it can be found that

$$M_{TDD} / M_{FDD} \geq 1. \quad (4.17)$$

This means that by using the proposed TS-opposing algorithm the uplink capacity of a single cell is always greater than or equal to the capacity of an equivalent FDD cell for the scenario investigated. Monte Carlo techniques are used to calculate the expected value, $E(M_{TDD}/M_{FDD})$.

4.2.3 Simulation environment

A 7-cell cluster of hexagonal cells with the COI in the centre, as shown in Figure 4.1, is applied. The interfering mobiles are distributed uniformly and allocated to the BS which offers the least signal attenuation [20]. However, a handover margin, δ , is considered such that it holds:

$$a_i < a_j + \delta \quad \text{for all } j \neq i, \quad (4.18)$$

where a_i is the path loss from a MS to its serving BS and a_j is the path loss from the same MS to the neighbouring cell j . The path loss is calculated using the static COST-231 indoor path loss model with no wall or floor losses [149],

$$a = 37 + 30 \log_{10}(d) + \xi \quad [dB], \quad (4.19)$$

where d is the transmitter-receiver separation distance in metres and ξ is a lognormal random variable modelling shadowing effects. The model of correlated propagation paths as given in section 3.3.2.1 is used. In addition, a simple downlink power control algorithm as described in section 3.3.2.2 is applied. The simulations are conducted using the parameters as listed in Table 4.1.

Parameter	Value
Information bit rate	16 kbps
Chip rate	3.84 Mcps
Standard deviation of lognormal shadowing	10 dB
Receiver noise figure	5 dB
Max. MS TX power	10 dBm
Max. BS TX power	24 dBm
bit energy to interference ratio, ε^u	3.5 dB
Handover margin δ	5 dB
Cell radius R	50 m

Table 4.1: Parameters used for the simulation of the simple DCA algorithm.

4.2.4 Results

Monte Carlo techniques are used to calculate the expected value $E(M_{TDD}/M_{FDD})$ of (4.13). The investigation is restricted to a single pair of TS's because this is sufficient to demonstrate the

mechanism of the TS-opposing algorithm. The results are depicted in Figure 4.2. The number

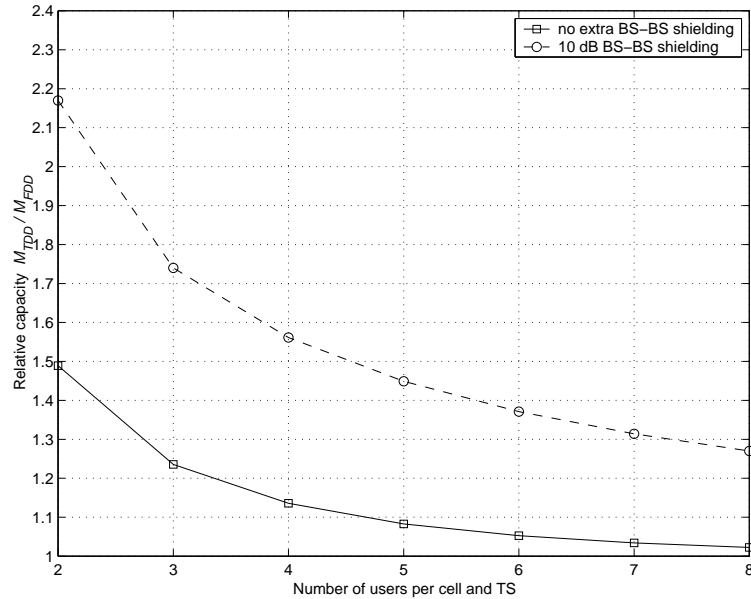


Figure 4.2: Relative capacity of a TDD cell when using the TS-opposing algorithm compared with an equivalent FDD cell.

of equally distributed users per cell and TS is varied and drawn on the abscissa. The interference analysis carried out in section 3.4 of the previous chapter has revealed that interference from neighbouring BS's is dominating over the interference resulting from MS's. Therefore, two cases are investigated: a) extra 10 dB signal attenuation is considered between the static BS \leftrightarrow BS interference path, b) no extra signal attenuation is assumed. The extra attenuation may be obtained by, for example, antenna beam-forming or additional BS isolation due to walls. It can be seen that the largest capacity increase for the case of no extra shielding is a factor of 1.48 for 2 users per cell. In contrast, if an extra 10 dB BS \leftrightarrow BS isolation is considered the capacity gain is a factor of about 2.18. It can be seen that the capacity gain decreases monotonically as the number of active MS's increases. This behaviour can be explained with the aid of Figure 4.3. In Figure 4.3 the expected values $E(f)$, (4.11), and $E(g)$, (4.12), as a function of the active number of users per cell is depicted. Two interesting properties can be found. Firstly, in the case of no extra shielding between BS's, the interference from the surrounding BS's is about 10 to 15 times greater than the interference resulting from all MS's. This is primarily due to the simple downlink power control algorithm used. However, as expected, $E(g)$ is reduced by a factor of 10 if 10 dB extra attenuation is considered. Secondly, $E(g)$ increases almost linearly whereas $E(f)$ decreases non-linearly as the number of users in the cells increase. These effects can be explained as follows. For a given number of distributed MS's the desired signal power,

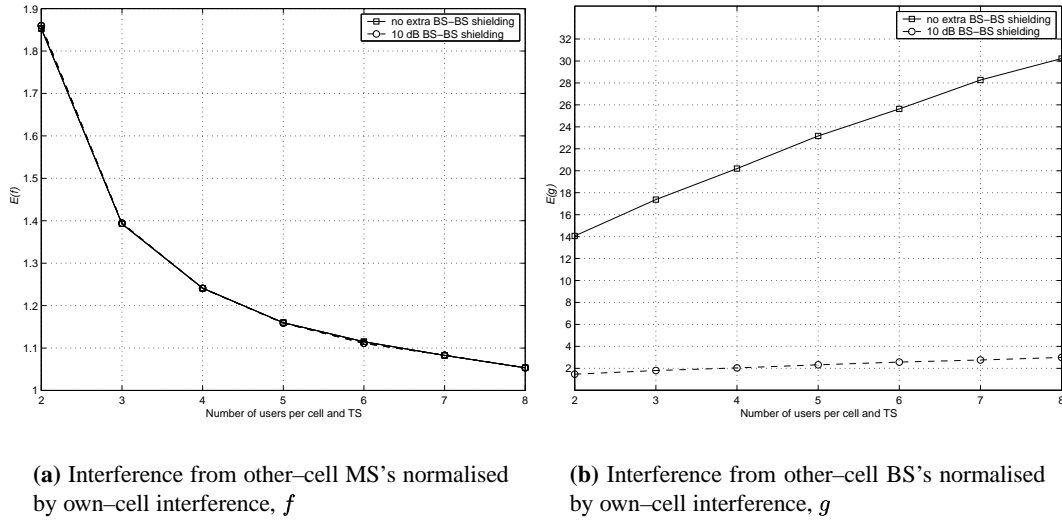


Figure 4.3: BS to BS interference, and MS to BS interference respectively, normalised by the total own-cell interference power (I_{own}) as a function of the number of active users per cell. The results assume the use of the TS-opposing algorithm.

P_u^u , can be calculated using (4.3). The power transmitted by a MS is found by multiplying the respective path loss between the MS and its BS by the signal power P_u^u required at the receiver. This transmitted power causes interference at the BS of the COI which can be modelled as a sum of independent lognormal random variables [80] where the mean of which does not increase linearly with P_u^u which can be found from [159] and the pdf calculated in (3.48). Given, however, that own-cell interference increases directly proportional to P_u^u , which can be found from (4.6), it follows that $E(f)$ decreases non-linearly. The situation is different for $E(g)$ since the transmitted code power for each user causes interference via the same path. This causes the steady increase of $E(g)$. As $E(g)$ increases and at the same time $E(f)$ decreases the cases that $g_{i,1}$ is smaller than $f_{i,1}$ are less likely and thus it is obvious that the capacity diminishes as depicted in Figure 4.2. Since FDD systems have been investigated intensively, the results for $E(f)$ can be compared with results of an investigation by Viterbi [27], in which an analysis of other-cell interference in an FDD system (only other entity interference applies) is carried out. The interference in the victim cell is related to the desired signal P_u^u instead of I_{own} as in our considerations. However, the results for two users can be compared since in this case own-cell interference is identical to the desired signal power, P_u^u , which can be seen from (4.6). $E(f)$ was found by Viterbi to be 1.32 [27], whereas 1.85 (Figure 4.2) is obtained in this investigation. The difference observed can primarily be attributed to the following: The path loss exponent in

our model is 3.0 compared to 4.0 used by Viterbi. This is verified by conducting the simulation with the parameters applied by Viterbi's approach. This results in: $E(f) = 1.306$ which provides the necessary evidence to support the model used and the results obtained. It is found that the capacity gains of a CDMA/TDD interface over an equivalent CDMA/FDD interface can be significant, but the assumed simplifications lead to a more detailed approach in the following section.

4.3 TS-opposing technique in a multiple cell environment

Based on the findings of the investigation in section 4.2, a new, centralised DCA algorithm applied to a multiple cell environment is developed. Once again, this algorithm exploits the discovery made in chapter 3 which is that it sometimes is advantageous to oppose TS's. In the following, a limited number of BS's connected to a RNC is assumed. The DCA algorithm considered henceforth is assumed to be operated at the RNC level. At this level considerably more system information is available than at the MS or BS level. For example, information about the state of interference in several cells is available simultaneously.

The group of cells which are connected to the RNC can be considered as a higher level cell. These assumptions are used to build a mathematical framework as described in section 4.3.1 followed by the description of the new DCA algorithm in section 4.3.2. The simulation platform is presented in section 4.3.3. In section 4.3.4 the results are discussed. As a consequence of the novel DCA algorithm, cell independent asymmetric capacity allocation between the uplink and downlink for each cell do not cause a significant capacity loss. In some cases, with different channel asymmetries in neighbouring cells a greater capacity can be obtained than if synchronous transmission and reception is applied.

4.3.1 System model

In the following, several definitions are made to describe the system and its mutual dependencies. The set of L cells connected to the RNC is defined as:

$$\mathcal{C} \stackrel{\text{def}}{=} \{c_1, c_2, \dots, c_L\}. \quad (4.20)$$

Each cell consists of one BS and as there are L cells the set of BS's yields:

$$\mathcal{B} \stackrel{\text{def}}{=} \{b_1, b_2, \dots, b_L\}. \quad (4.21)$$

Moreover, several MS's are allocated to one BS which results in L sets of MS's,

$$\mathcal{M}_i \stackrel{\text{def}}{=} \{m_1, m_2, \dots, m_{|\mathcal{M}_i|}\} \quad i = 1, \dots, L, \quad (4.22)$$

where $|\cdot|$ is the cardinality of the respective set. Note, in a practical scenario, each BS of \mathcal{B} serves a different number of MS's. Therefore, $|\mathcal{M}_i|$ may be different for each cell, i .

A single radio frequency carrier is assumed. Due to the TDMA component in UTRA-TDD a frame is divided into a maximum of N TS's which can asynchronously overlap with respect to the transmission direction, *i.e.* neighbouring cells may or may not simultaneously transmit and receive. Therefore, for each TS a symmetric synchronisation matrix can be defined by:

$$\boldsymbol{\alpha} = \begin{pmatrix} 0 & \alpha_{1,2} & \cdots & \alpha_{1,L} \\ \alpha_{2,1} & 0 & \cdots & \alpha_{2,L} \\ \vdots & \vdots & \ddots & \vdots \\ \alpha_{L,1} & \alpha_{L,2} & \cdots & 0 \end{pmatrix}, \quad (4.23)$$

where

$$\alpha_{i,j} = \begin{cases} 0 & \text{if } c_i \text{ and } c_j \text{ simultaneously transmit or receive at TS } n, \\ 1 & \text{if } c_i \text{ and } c_j \text{ adopt opposed transmission at TS } n. \end{cases} \quad (4.24)$$

As $\boldsymbol{\alpha}$ only consists of binary elements a complementary matrix $\tilde{\boldsymbol{\alpha}}$ can be defined so that:

$$\tilde{\boldsymbol{\alpha}} = \begin{pmatrix} 0 & 1 & \cdots & 1 \\ 1 & 0 & \cdots & 1 \\ \vdots & \vdots & \ddots & \vdots \\ 1 & 1 & \cdots & 0 \end{pmatrix} - \boldsymbol{\alpha}. \quad (4.25)$$

For each set of MS's, \mathcal{M}_i , and each TS, n , a vector of transmitted powers can be established,

$$\mathbf{P}c_i^u = (Pc_{1,1}^u, \dots, Pc_{|\mathcal{M}_i|,1}^u) \quad i = 1, \dots, L, \quad (4.26)$$

Given that L cells are connected to a RNC, (4.26) finally yields:

$$\mathbf{Pc}^u = (\mathbf{Pc}_1^u, \dots, \mathbf{Pc}_L^u) . \quad (4.27)$$

Similarly, the slot powers transmitted by the L BS's can be denoted as:

$$\mathbf{Pc}^d = (P_1^d, \dots, P_L^d) . \quad (4.28)$$

As demonstrated earlier, four interference scenarios can be ascertained in a TDD system (MS \leftrightarrow BS, BS \leftrightarrow MS, MS \leftrightarrow MS and BS \leftrightarrow BS). Therefore, in general, four path loss matrices between the respective entities can be established. It can be shown that it is convenient to use the reciprocal value of the path loss, also referred to as path gain. The path gain matrix for the MS \leftrightarrow MS case is a symmetric block matrix denoted as:

$$\mathbf{MM} = \begin{pmatrix} \mathbf{0} & \mathbf{MM}_{c_1, c_2} & \cdots & \mathbf{MM}_{c_1, c_L} \\ \mathbf{MM}_{c_2, c_1} & \mathbf{0} & \cdots & \mathbf{MM}_{c_2, c_L} \\ \vdots & \vdots & \ddots & \vdots \\ \mathbf{MM}_{c_L, c_1} & \mathbf{MM}_{c_L, c_2} & \cdots & \mathbf{0} \end{pmatrix}, \quad (4.29)$$

where \mathbf{MM}_{c_i, c_j} is a $|\mathcal{M}_i| \times |\mathcal{M}_j|$ matrix and represents the path gain between all MS's in c_i to all MS's in c_j ,

$$\mathbf{MM}_{c_i, c_j} = \begin{pmatrix} \frac{1}{a_{m_1, m_1}} & \cdots & \frac{1}{a_{m_1, m_{|\mathcal{M}_j|}}} \\ \vdots & \ddots & \vdots \\ \frac{1}{a_{m_{|\mathcal{M}_i|}, m_1}} & \cdots & \frac{1}{a_{m_{|\mathcal{M}_i|}, m_{|\mathcal{M}_j|}}} \end{pmatrix}. \quad (4.30)$$

For example, a_{m_1, m_1} , is the path loss between MS m_1 in cell c_i and MS m_1 in cell c_j . With (4.29) the path gain between any MS and all other MS's within the set \mathcal{C} is fully described and used to calculate MS \leftrightarrow MS interference.

The path gain matrix for the BB \leftrightarrow BB case is:

$$\mathbf{BB} = \begin{pmatrix} 0 & \frac{1}{a_{b_1, b_2}} & \cdots & \frac{1}{a_{b_1, b_L}} \\ \frac{1}{a_{b_2, b_1}} & 0 & \cdots & \frac{1}{a_{b_2, b_L}} \\ \vdots & \vdots & 0 & \vdots \\ \frac{1}{a_{b_L, b_1}} & \frac{1}{a_{b_L, b_2}} & \cdots & 0 \end{pmatrix}. \quad (4.31)$$

In a similar way the path gain matrix for the MS \leftrightarrow BS case is found as:

$$\mathbf{MB} = \begin{pmatrix} 0 & \mathbf{MB}_{c_1, c_2} & \cdots & \mathbf{MB}_{c_1, c_L} \\ \mathbf{MB}_{c_2, c_1} & 0 & \cdots & \mathbf{MB}_{c_2, c_L} \\ \vdots & \vdots & \ddots & \vdots \\ \mathbf{MB}_{c_L, c_1} & \mathbf{MB}_{c_L, c_2} & \cdots & 0 \end{pmatrix}, \quad (4.32)$$

where \mathbf{MB}_{c_i, c_j} is a vector defined as

$$\mathbf{MB}_{c_i, c_j} = \left(\frac{1}{a_{m_1, b_j}}, \cdots, \frac{1}{a_{m_{|\mathcal{M}_i|}, b_j}} \right)^T, \quad (4.33)$$

and T is the matrix transpose operator. a_{m_1, b_j} is the path loss between m_1 in cell i and the BS in cell j . For the reciprocal case that the BS in cell j interferes with the MS's in cell i the path gain matrix is:

$$\mathbf{BM} = \mathbf{MB}^T. \quad (4.34)$$

The interference experienced by the MS's can now be written as:

$$\mathbf{Im} = \underbrace{(\mathbf{Pc}^u) (\boldsymbol{\alpha} \odot \mathbf{MM})}_{\text{same entity interference}} + \underbrace{(\mathbf{Pc}^d) (\tilde{\boldsymbol{\alpha}} \odot \mathbf{BM})}_{\text{other entity interference}}. \quad (4.35)$$

Similarly, the BS's experience:

$$\mathbf{Ib} = \underbrace{(\mathbf{Pc}^d) (\boldsymbol{\alpha} \odot \mathbf{BB})}_{\text{same entity interference}} + \underbrace{(\mathbf{Pc}^u) (\tilde{\boldsymbol{\alpha}} \odot \mathbf{MB})}_{\text{other entity interference}}, \quad (4.36)$$

where \odot is the operator for the Hadamard Product [160]. The generalised equations, (4.35)

and (4.36), for other-cell interference in a TDD system highlight that the uplink and downlink cannot be treated independently unless α equals the null matrix, *i.e.* synchronous transmission and reception would result in an equivalent FDD system. If this is not the case the required uplink power of an arbitrary MS is not only dependent on the transmitted powers of the MS's in the other cells, but also on the powers transmitted by the BS's in the neighbouring cells, *i.e.* the power transmitted in the downlink. Note, that this has an impact on the requirements for the downlink power control algorithm.

In the following, the vectors of transmission powers \mathbf{Pc}^u , and \mathbf{Pc}^d respectively, in (4.35) and (4.36) are calculated. This can be achieved by writing (3.12) in matrix notations. Equation (3.12) is repeated here for convenience:

$$\varepsilon_i^u = \frac{pg P_{u_i}^u}{\sum_{j:j \neq i}^M P_{u_j}^u + \underbrace{I_o^u + N}_{Ib}}, \quad (4.37)$$

The transformation using matrix notations yields:

$$(\mathbf{I} + \text{diag}(\boldsymbol{\gamma}) - \boldsymbol{\gamma}\mathbf{J}) (\mathbf{Pc}_i^u)^T = (\boldsymbol{\gamma} I b_i) \odot \mathbf{M}\mathbf{B}_{c_i, c_i}, \quad (4.38)$$

where \mathbf{I} is the identity matrix; $\text{diag}(\cdot)$ is the diagonal matrix representation, $\boldsymbol{\gamma} = (\gamma_1^u, \dots, \gamma_{|\mathcal{M}_i|}^u)^T$ is the vector of the required carrier to interference ratios at the BS in cell i with dimension: $\dim(\boldsymbol{\gamma}) = |\mathcal{M}_i|$; \mathbf{J} is also a vector of dimension: $\dim(\mathbf{J}) = |\mathcal{M}_i|$ with each element set to one; $I b_i$ is the accumulated interference from other cells and thermal noise at the BS in the cell, c_i .

Making the substitution: $\mathbf{B} = \mathbf{I} + \text{diag}(\boldsymbol{\gamma})$, (4.38) yields:

$$(\mathbf{B} - \boldsymbol{\gamma}^T \mathbf{J}) (\mathbf{Pc}_i^u)^T = (\boldsymbol{\gamma}^T I b_i) \odot \mathbf{M}\mathbf{B}_{c_i, c_i}. \quad (4.39)$$

Using the Bartlett-Sherman-Morrison-Woodbury Formula [161, Chapter 2] and the property of \mathbf{B} being a diagonal matrix, (4.39) can be solved for \mathbf{Pc}_i^u which results in:

$$(\mathbf{B} - \boldsymbol{\gamma}^T \mathbf{J})^{-1} = \mathbf{B}^{-1} + \frac{\mathbf{B}^{-1} \boldsymbol{\gamma}^T \mathbf{J} \mathbf{B}^{-1}}{1 - \mathbf{J} \mathbf{B}^{-1} \boldsymbol{\gamma}^T}, \quad (4.40)$$

and thus

$$\mathbf{Pc}_i^u = \left(Ib_i \mathbf{B}^{-1} \boldsymbol{\gamma}^T + \frac{Ib_i \mathbf{B}^{-1} \boldsymbol{\gamma}^T \mathbf{J} \mathbf{B}^{-1} \boldsymbol{\gamma}^T}{1 - \mathbf{J} \mathbf{B}^{-1} \boldsymbol{\gamma}^T} \right) \odot \mathbf{M} \mathbf{B}_{c_i, c_i}. \quad (4.41)$$

The denominator in (4.41) is a scalar and a singularity is observed at the pole capacity. Thus, by re-arranging the two terms within the brackets of (4.41) using the lowest common denominator, equation (4.41) can be simplified yielding:

$$\mathbf{Pc}_i^u = \underbrace{\left(\frac{\mathbf{V}}{1 - \mathbf{J} \mathbf{V}} \right)}_{\mathbf{U}_{c_i}} \odot \mathbf{M} \mathbf{B}_{c_i, c_i} Ib_i, \quad (4.42)$$

where

$$\mathbf{V} = \left(\frac{\gamma_1^u}{1 + \gamma_1^u}, \dots, \frac{\gamma_{|\mathcal{M}_i|}^u}{1 + \gamma_{|\mathcal{M}_i|}^u} \right)^T. \quad (4.43)$$

From (4.42), given the Ib_i term, it can be seen that the transmission powers of the mobiles are linearly dependent on the interference received at the associated BS. The interference power at b_i , Ib_i , is a function of the transmitted powers of the MS's and BS's in the other cells which can be seen from (4.36). This describes a system of mutual dependencies, *i.e.* theoretically any change of a transmission power, regardless whether it is an MS or a BS, has an impact on the required transmission powers of all other entities.

The transmitted code powers of the MS's in a single cell i is described in (4.42). The scope of this equation can be extended to the entire network. Using the vector $\mathbf{U} = (U_{c_1}, \dots, U_{c_L})^T$ where U_{c_i} is given in (4.42), the general expression for \mathbf{Pc}^u can be found as

$$\mathbf{Pc}^u = \mathbf{U} \odot \mathbf{Ib}. \quad (4.44)$$

A similar equation can be derived for the the transmitted code powers in the downlink. It is assumed that C/I -based downlink power control is employed. The equation (2.22) which is repeated here for convenience,

$$\gamma_i^d = \frac{\frac{\tilde{P}c_i^d}{a_i}}{\frac{1}{a_i} \left(\sum_{i \neq j}^M \tilde{P}c_j^d \right) + \underbrace{I_o^d + N}_{I_m}}, \quad (4.45)$$

can be written in matrix notation. This yields:

$$\left[\underbrace{\text{diag} \left((\boldsymbol{\gamma} \odot \mathbf{M}\mathbf{B}_{c_i, c_i})^T \right) + \text{diag}(\mathbf{M}\mathbf{B}_{c_i, c_i})}_{\mathbf{B}} - \underbrace{(\boldsymbol{\gamma} \odot \mathbf{M}\mathbf{B}_{c_i, c_i})}_{\mathbf{e}} \mathbf{J} \right] (\tilde{\mathbf{P}}\mathbf{c}_i^d)^T = (\boldsymbol{\gamma} \odot \mathbf{I}\mathbf{m}_{c_i})^T, \quad (4.46)$$

where $\tilde{\mathbf{P}}\mathbf{c}_i^d$ are the transmitted code powers at one TS in the i th cell — in contrast to the slot power which is the sum of all code powers; $\mathbf{I}\mathbf{m}_{c_i}$ is the interference vector at the MS's in cell, c_i ; $\boldsymbol{\gamma} = \left(\gamma_1^d, \dots, \gamma_{|\mathcal{M}_i|}^d \right)^T$ is the vector of the required carrier to interference ratios at the MS in cell i with dimension: $\dim(\boldsymbol{\gamma}) = |\mathcal{M}_i|$.

Using the substitutions as indicated in (4.46) the matrix inverse of $(\mathbf{B} - \mathbf{e}\mathbf{J})$ yields:

$$(\mathbf{B} - \mathbf{e}\mathbf{J})^{-1} = \mathbf{B}^{-1} + \frac{\mathbf{B}^{-1}\mathbf{e}\mathbf{J}\mathbf{B}^{-1}}{1 - \mathbf{J}\mathbf{B}^{-1}\mathbf{e}}. \quad (4.47)$$

Applying (4.47) to (4.46) the required code powers at the BS in cell c_i , can be found as:

$$(\tilde{\mathbf{P}}\mathbf{c}_i^d)^T = \frac{\mathbf{B}^{-1} (\boldsymbol{\gamma} \odot \mathbf{I}\mathbf{m}_{c_i})^T + \mathbf{B}^{-1}\mathbf{e}\mathbf{J}\mathbf{B}^{-1} (\boldsymbol{\gamma} \odot \mathbf{I}\mathbf{m}_{c_i})^T - \mathbf{B}^{-1} (\boldsymbol{\gamma} \odot \mathbf{I}\mathbf{m}_{c_i})^T \mathbf{J}\mathbf{B}^{-1}\mathbf{e}}{1 - \mathbf{J}\mathbf{B}^{-1}\mathbf{e}}. \quad (4.48)$$

The pole capacity in the downlink is reached if: $\mathbf{J}\mathbf{B}^{-1}\mathbf{e} = 1$.

It is straightforward to calculate the slot power for cell c_i from (4.48) which results in:

$$\mathbf{P}\mathbf{c}_i^d = \mathbf{J}\tilde{\mathbf{P}}\mathbf{c}_i^d, \quad (4.49)$$

which gives the final vector of transmitted slot powers:

$$\mathbf{P}\mathbf{c}^d = \left(\mathbf{J}\tilde{\mathbf{P}}\mathbf{c}_1^d, \dots, \mathbf{J}\tilde{\mathbf{P}}\mathbf{c}_L^d \right). \quad (4.50)$$

From (4.48) it can be seen that the slot power in each cell, c_i , is a function of the interference powers at the served MS's, $\mathbf{I}\mathbf{m}_{c_i}$. Thus (4.50) may be more generally denoted as:

$$\mathbf{P}\mathbf{c}^d = f(\mathbf{I}\mathbf{m}). \quad (4.51)$$

Using (4.51) and (4.44) the system equations in (4.35) and (4.36) may be rewritten:

$$\begin{array}{l}
 \text{downlink: } \mathbf{I}_m = \mathbf{U} \odot \mathbf{I}_b (\boldsymbol{\alpha} \odot \mathbf{M}\mathbf{M}) + \mathbf{P}c^d(\mathbf{I}_m) (\bar{\boldsymbol{\alpha}} \odot \mathbf{B}\mathbf{M}), \\
 \text{uplink: } \mathbf{I}_b = \mathbf{P}c^d(\mathbf{I}_m) (\boldsymbol{\alpha} \odot \mathbf{B}\mathbf{B}) + \mathbf{U} \odot \mathbf{I}_b (\bar{\boldsymbol{\alpha}} \odot \mathbf{M}\mathbf{B}).
 \end{array}
 \tag{4.52}$$

The annotated system equations in (4.52) highlight the interference dependencies in a CDMA-TDD system. The self-jamming effect due to co-channel interference is inherent in a cellular system with frequency re-use. This effect also appears in an FDD interface and can be reduced by power control and manipulating the path gain matrix, $\mathbf{B}\mathbf{M}$, for example, by applying frequency re-use factors greater than 1. A notable example where this technique is employed is GSM — a second generation FDMA-TDMA/FDD system. When using TDD instead of FDD an additional cross-jamming effect can be ascertained. The magnitude of self-jamming and cross-jamming in a TDD system can be manipulated by the synchronisation matrix, $\boldsymbol{\alpha}$. If $\boldsymbol{\alpha}$ is the zero-matrix cross-jamming is eliminated, but self-jamming may be increased. In contrast, if each element of $\boldsymbol{\alpha}$ equals one, self-jamming does not exist, only cross-jamming. If, as in UTRA-TDD, the multiple access mode consists of a hybrid TD-CDMA interface an additional degree of freedom is added due to the TDMA mode. One TDMA frame is divided into N TS's where each TS can be used for either uplink or downlink traffic. Since the symmetric use of a channel can be considered as a special case of asymmetric usage, the more general term rate of asymmetry is introduced to characterise the load in the uplink and downlink more precisely. For a given rate of asymmetry several solutions for all $\boldsymbol{\alpha}^n$, where $n = (1, \dots, N)$, may exist. This particular degree of freedom is exploited by the centralised DCA algorithm which utilises the TS-opposing idea. Due to the complexity of the system equations in (4.52) the model is estimated by Monte Carlo simulations. The novel DCA algorithm which is applied to these equations is described in the following section.

4.3.2 DCA algorithm

A DCA algorithm is developed which minimises interference at the BS's by either applying opposed or synchronous transmission to the neighbouring cells. It has been demonstrated that

a cellular TDD system can be exposed to more interference scenarios than an FDD system. Since CDMA, as an interference limited technique, heavily relies on low interference, the performance of UTRA-TDD can be significantly poorer compared to an equivalent FDD system. However, it was demonstrated in section 4.2 that the additional interference mechanism and the resulting flexibility in a TDD system can be exploited constructively in order to minimise interference. In a system such as UTRA-TDD which uses CDMA a reduction of interference is equivalent to increasing capacity. Such a capacity improvement or an increase of the quality of service (QoS) is intended to be achieved by the new centralised DCA for a TD-CDMA/TDD air interface. The basic principle of how this DCA functions, can be explained with the aid of Figure 4.4. The DCA algorithm is executed for each BS of a cellular network. In the example

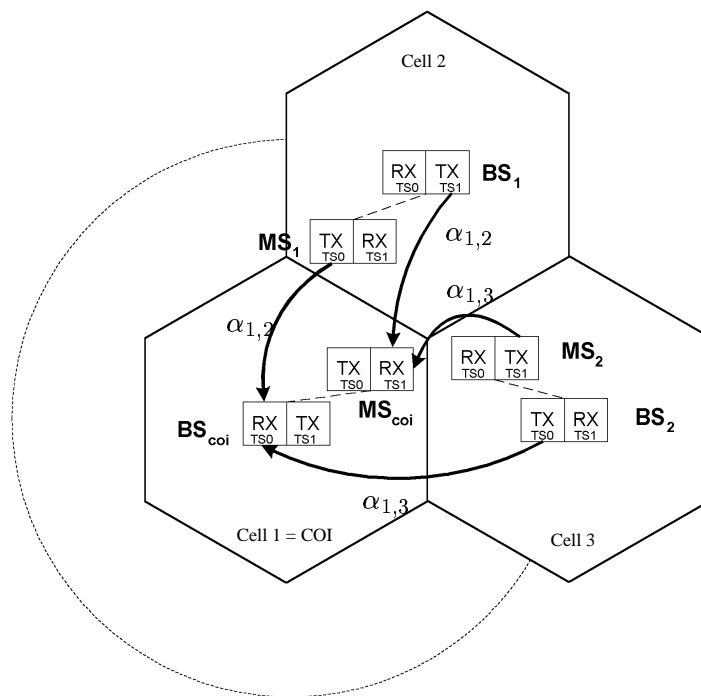


Figure 4.4: A cell arrangement with each cell using two successive time slots where the first begins at the same time in each cell is shown. The direction of transmission is arranged so that the cell of interest (cell 1) and cell 2 receive in TS 0 and transmit in TS 1. In contrast, the BS of cell 3 first transmits and then receives.

of Figure 4.4, the DCA algorithm is executed in cell one (COI). In order to reduce interference, in the example the DCA algorithm decides to use synchronous transmission with respect to cell 2 ($\alpha_{1,2} = 0$), but opposed transmission with respect to cell 3 ($\alpha_{1,3} = 1$). For each TS in Figure 4.4 a symmetric synchronisation matrix can be established. Since only two TS's are used and a symmetric service in each cell is implied the synchronisation matrices for both TS's

are equivalent and yield:

$$\boldsymbol{\alpha}^{\text{TS1}} = \boldsymbol{\alpha}^{\text{TS2}} = \begin{pmatrix} 0 & 0 & 1 \\ 0 & 0 & x \\ 1 & x & 0 \end{pmatrix}. \quad (4.53)$$

The x in (4.53) indicates the synchronisation factors $\alpha_{2,3}$, and $\alpha_{3,2}$ between cell 2 and cell 3 are not directly manipulated when the DCA is carried out at the BS of cell 1. It however indirectly follows from the settings of $\alpha_{1,2} = 0$ and $\alpha_{1,3} = 1$ that $\alpha_{2,3}$ must be 1 as shown in Figure 4.5. This can be explained using graph theory [162] and the Kirchhoff's laws because the state of

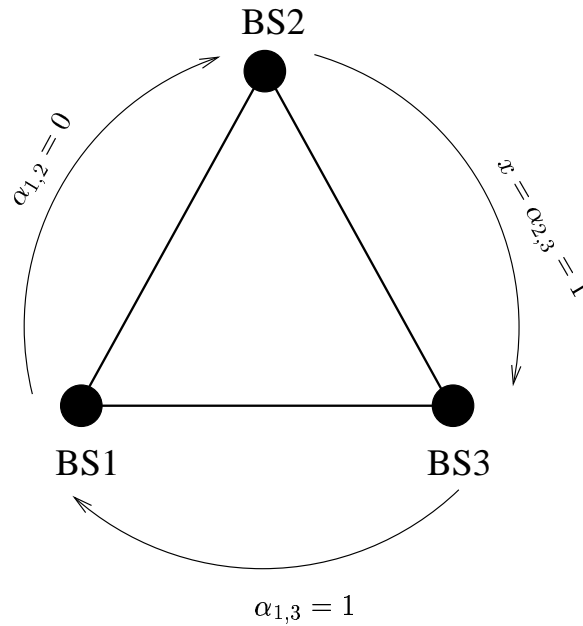


Figure 4.5: The dependencies of α .

opposed TS can be interpreted as a potential difference between two vertices (BS's). With the definition of $\boldsymbol{\alpha}$ in (4.23), for any circuit \mathcal{P} as, for example, $(\text{BS1} \rightarrow \text{BS2} \rightarrow \text{BS3} \rightarrow \text{BS1})$ it holds that:

$$\left(\sum_{\mathcal{P}} \alpha \right) \text{ mod } 2 \equiv 0, \quad (4.54)$$

where mod is the operator for modulo division. The dependency which results from (4.54) leads to: $x = \alpha_{2,3} = 1$. This effect may cause greater interference in cells for which the DCA is currently not executed (cell 2 and cell 3) and thus cancels out or diminishes the capacity gains in cell 1. However, situations can occur where cell 2 or cell 3 can tolerate higher interference, but

only little interference at the BS in cell 1 may be permitted. Hence, the algorithm effectively improves capacity in this case. The final algorithm is explained in pseudo-code depicted in Figure 4.6.

The algorithm starts when the mobile is requested to transmit with higher power than the maximum power permitted, *i.e.* the state at which outage or service degradation would occur. The algorithm steps in assuming that a MS uses at least two TS's for the communication to the BS ($\text{TS_in_Use} \geq 2$). It monitors the interference in all n TS's of all neighbouring cells. Two cases can then be distinguished:

1. If TS n in cell l is used for RX (from the BS point of view) the interference from this particular neighbouring TS is caused exclusively from its MS's since $\alpha = 0$ and ideal synchronisation is assumed. Furthermore, it is assumed that the MS's in the neighbouring cell are able to determine the path loss to their neighbouring BS's. This may be accomplished by a fixed transmission power on the pilot channel. The MS's report their transmission power and path loss measurements to the BS which makes it available to the RNC². Hence, the information about the path gain matrix of the mobiles in cell l to the BS in cell j , \mathbf{MB}_{c_l, c_j} , and the vector of transmission powers of the mobiles in cell l , \mathbf{Pc}_l^u , are assumed to be available to the DCA algorithm.
2. If TS n at the BS is used for transmission the interference contribution from cell l results only from the BS (same entity interference as $\alpha = 1$). The transmission powers at the BS's are known and can easily be reported to the RNC and so can the path loss to the neighbouring BS's, \mathbf{BB}_{c_l, c_j} .

A check is made to examine if there is one TS n in the neighbouring cell c_j which would cause less interference than the current TS k . If this is true **and** TS n is used for RX while TS k was used for TX, or vice versa, then the neighbouring cell, c_l , interchanges TS n with TS k . This results in TS-opposing time slots with respect to the c_j . Note, the algorithm is only carried out if the TX power of a MS tends to exceed a given TX power maximum.

²These measurements may already be required for handover decisions. Hence, the signalling traffic is not increased significantly

```

BEGIN
Request the measurement of the required TX power,  $Pc_i^u$ , of user  $i$  in time slot  $k$  of cell  $c_j$ 

if  $Pc_i^u > Pc_{\max}^u$ 

    for  $l = 1 : \max(\text{Neighbouring\_Cells})$ 
        for  $n = 1 : \max(\text{TS\_in\_Use})$  where  $n \in$  set of used TS's

            if  $\text{TS}_{c_l}^n == \text{RX time slot}$ 
                determine interference from mobiles:

                
$$Ib_l^n = (\mathbf{P}c_l^u)^n (\mathbf{M}\mathbf{B}_{c_l, c_j})^n$$

            else
                determine interference from BS:

                
$$Ib_l^n = (Pc_l^d)^n (\mathbf{B}\mathbf{B}_{c_l, c_j})^n$$

            end if

            if  $\left[ \begin{array}{l} (Ib_l^n < Ib_l^k) \ \& \\ (\text{direction}(\text{TS}_l^n) \neq \text{direction}(\text{TS}_l^k)) \end{array} \right]$ 
                exchange TS  $n$  for TS  $k$  in cell  $l$ 
            end if

        end for
    end for
else
    Assign channel
end if
Repeat this algorithm for each user in the RNC area if necessary
END

```

Figure 4.6: The centralised DCA algorithm exploiting the TS-opposing idea.

4.3.3 Simulation platform

A propagation environment with severe lognormal shadowing, a cell re-use factor of one and user assignments based on the minimum path loss results in a negligible impact on system performance for particular cell shapes. Of more importance is the maximum distance to the closest BS, usually at the furthest corner of the cell. In order to overcome cell boundary effects a cell wrap around technique is used. Square shaped cells as depicted in Figure 4.7 are applied. The reasons for this are: firstly, the cell wrap around technique is easy to apply and secondly, the square shaped cells represent a good approximation to an indoor environment. The wrap around

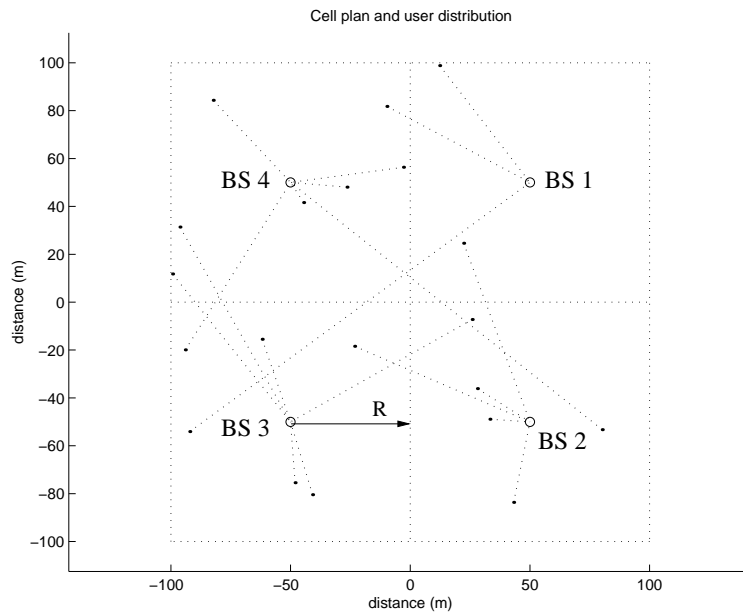


Figure 4.7: The user distribution and user assignment based on the minimum path loss is shown for a random scenario. A wrap around technique is applied to prevent cell boundary effects.

technique ensures that each cell is completely surrounded by a symmetric pattern composed of three different cells. The principle of this method is depicted in Figure 4.8. MS's are assigned to the BS offering the lowest path loss, but a handover margin as described in section 3.4.1 is considered. Ideal power control in the uplink is assumed.

The path loss model for indoor office test environment as described in [149] is used,

$$a = 37 + 30 \log_{10}(d) + 18.3 p^{\left(\frac{p+2}{p+1} - 0.46\right)} + \xi \text{ [dB]}, \quad (4.55)$$

where d is the transmitter–receiver separation in metres, p is the number of floors in the path

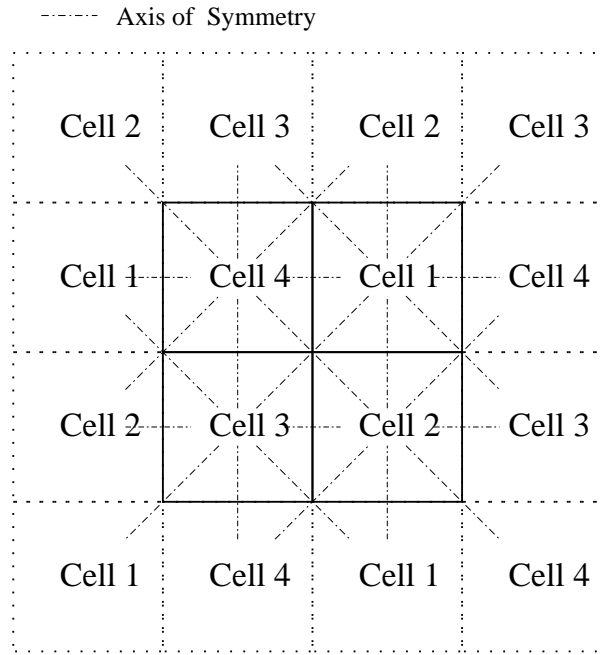


Figure 4.8: Wrap around technique applied.

and ξ is the lognormal variable modelling shadow fading.

In the simulation environment four consecutive TS's are considered. An example is presented in Figure 4.9. It is assumed that the MS's in cell 2 – cell 4 use two TS's whereas in cell 1 a MS occupies 4 consecutive TS's. This enables an asymmetric communication channel to be created in cell 1 with different loading in uplink and downlink. Channel asymmetry in cell 1, in turn, inevitably results in asynchronous TS overlaps to at least one of the neighbouring cells. After a predefined number of users have been distributed randomly and uniformly in space, the power control loops in the up- and downlink are initiated (equations (4.44) and (4.48)). In Figure 4.10, a power control snapshot of a mobile, which was randomly chosen, is shown. It can be seen that the transmission power rapidly increases, which leads to the conclusion that the total noise floor in the system is high, because of mutual interference effects in a CDMA system. However, a high noise floor means that some mobiles will not achieve the target C/I at the BS and so will experience outage. Removing extreme interferers in turn results in a reduction of the noise floor until the TX power converges to a stable level as can be seen in Figure 4.10. If the required code power of a MS exceeded the maximum power threshold the novel DCA algorithm described above would step in and try to reduce interference to maintain the required bit-energy to interference ratio, ε^u , for the MS. If this method fails, one or more MS's experience outage, M_{out} . Monte Carlo techniques are used to calculate the pdf of outage,

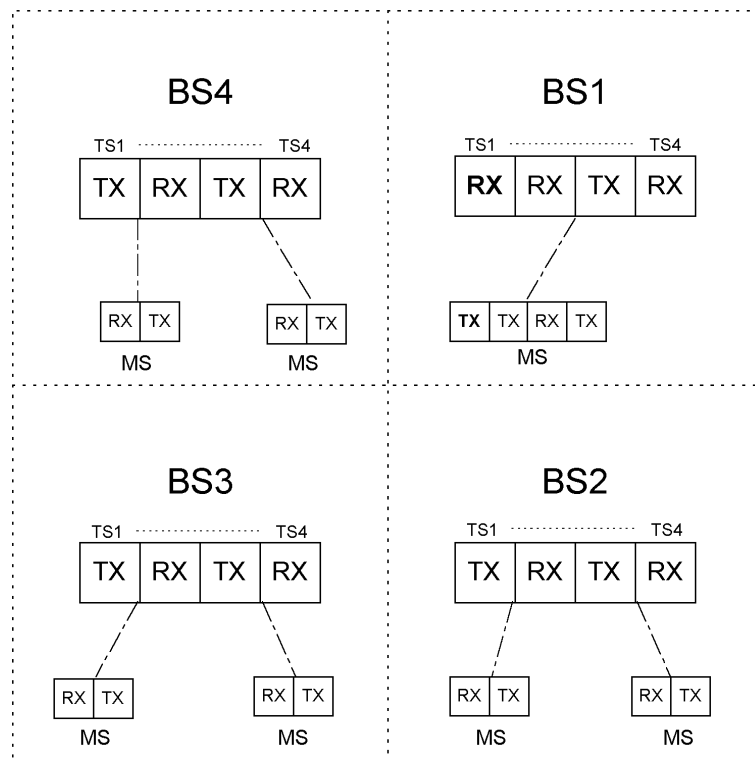


Figure 4.9: Deployment scenario.

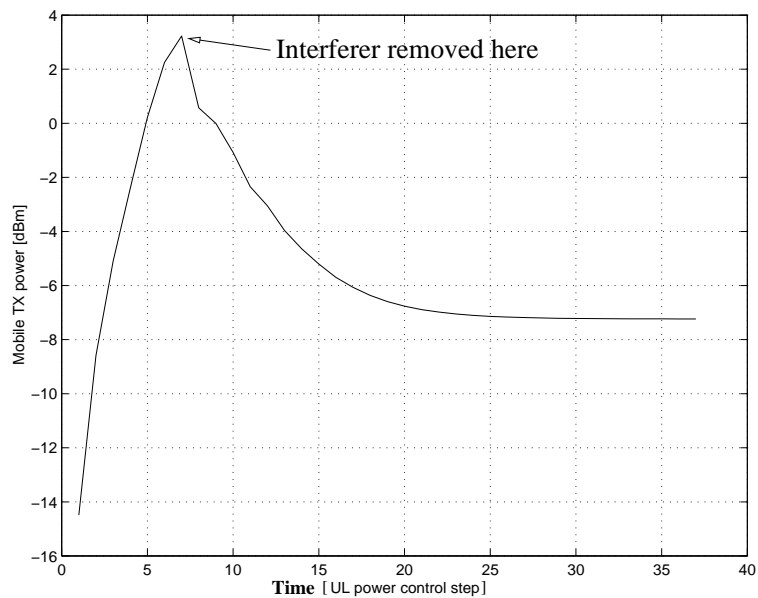


Figure 4.10: Dynamic uplink power control: The transmission power of the mobile is successively adjusted.

$p(M_{out})$. The expected value thereof, $E[M_{out}]$, is used to analyse the system performance of the centralised DCA algorithm. From $E[M_{out}]$ the capacity for cell: c_i is determined as follows:

$$\bar{C}_{c_i} = \frac{1}{4} (1 - E[M_{out}]) W M_{tot} \quad [\text{kbps/TS}] , \quad (4.56)$$

where W is the user data rate and M_{tot} is the total number of MS's which are distributed to the network. Since 4 TS's are assumed in the model, an averaging factor of $\frac{1}{4}$ is applied. The capacity per cell and TS can be calculated from (4.56):

$$\bar{C} = \frac{1}{4} \sum_i^4 \bar{C}_{c_i} \quad [\text{kbps/cell/TS}] . \quad (4.57)$$

Two channel assignment approaches are compared:

1. TX and RX transmission direction are chosen such that the number of asynchronous TS overlaps is minimum and the MS's are then allocated randomly. Hence, this method is equivalent to a fixed channel assignment (FCA) strategy.
2. The new centralised DCA algorithm developed in section 4.3.2 is applied which uses the new TS-opposing technique.

4.3.4 Results

Four scenarios with different rates of asymmetry are investigated: two which favour the uplink, one of symmetric TS arrangement and one which favours the downlink. These scenarios are summarised in Table 4.2.

TS _{RX} :TS _{TX}	cell 1	cell 2	cell 3	cell 4
Scenario 1	3:1	1:1 / 1:1	1:1 / 1:1	1:1 / 1:1
Scenario 2	3:1	2:0 / 1:1	1:1 / 1:1	1:1 / 1:1
Scenario 3	2:2	1:1 / 1:1	1:1 / 1:1	1:1 / 1:1
Scenario 4	1:3	1:1 / 1:1	1:1 / 1:1	1:1 / 1:1

Table 4.2: *Simulated scenarios: The ratio of UL (uplink) versus DL (downlink) usage is shown. The first figure corresponds to the number of TS's used for the UL and the second figure shows the number of TS's used for the DL.*

The parameters given in Table 4.3 are used for the simulations. MS's are distributed uniformly

Parameter	Value
Cell radius, R	50 m
Bit rate, W	16 kbps
Chip rate	3.84 Mcps
Standard deviation of lognormal shadowing	10 dB
Thermal noise density	169 dBm
Max. MS TX power	10 dBm
Max. BS TX power	24 dBm
Bit energy to interference ratio, ε^u	3.5 dB
Path loss	indoor test environment [148]
Handover margin γ	5 dB

Table 4.3: Parameters used for the simulation of the centralised DCA algorithm.

throughout the entire area covered by cell 1 – cell 4. The path loss and the handover margin determine to which cell a MS is allocated.

	TS1	TS2	TS3	TS4
cell 1	1	1	0	1
cell 2	0	1	0	1
cell 3	0	1	0	1
cell 4	0	1	0	1

1 := BS receives

0 := BS transmits

(a) Scenario 1

Figure 4.11: The initial TS assignment for scenario 1.

Results of scenario 1 The results of scenario 1 are depicted in Figures 4.12(a) and 4.12(b) which show the capacity versus the number of distributed MS's. Figure 4.12(a) shows the average capacity for each cell individually (using (4.56)), while Figure 4.12(b) depicts the accumulated average capacity (using (4.57)) over all cells. It can be found that for a distributed

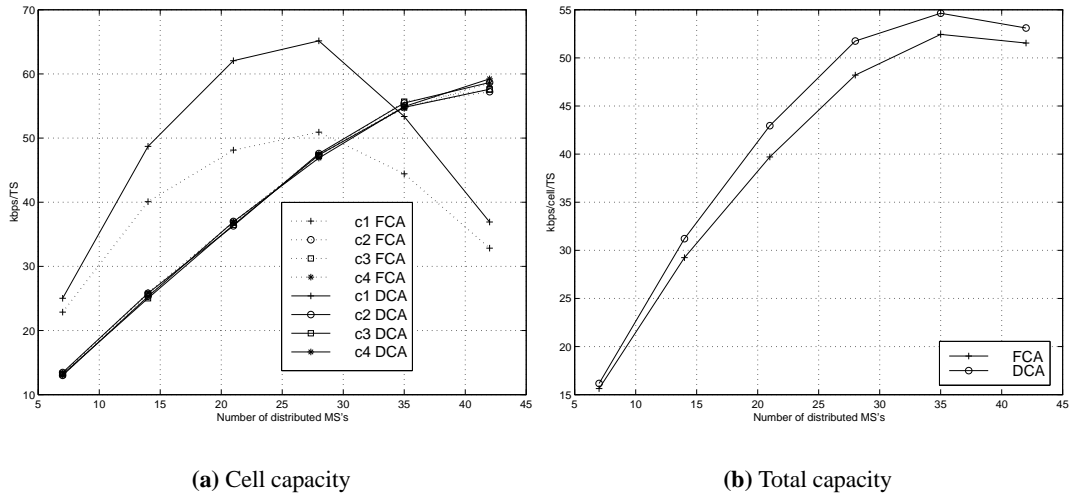


Figure 4.12: Results of scenario 1. The rate of asymmetry, $UL:DL$, in cell 1 is 3:1 and 1:1 in all other-cells. The graphs show: for a) the capacity in each cell in [kbps/TS] and b) the total capacity in [kbps/Cell/TS]. The results labelled with 'FCA' are obtained by the fixed channel assignment procedure and the results labelled with 'DCA' are these obtained from the novel centralised DCA algorithm.

load of less than 28 MS's the capacity in cell 1 is greater than in cell 2 – cell 4. The reason for this is that one MS in cell 1 occupies twice as many TS's as a MS in all other-cells (Figure 4.9). Furthermore, the capacity in cell 1 has a maximum for a total number of 28–32 distributed MS's. This can be explained with the aid of (3.3). With the parameters applied, it can be found that the pole capacity is reached when about 8 MS's are instantaneously active ($M = \frac{2q}{\epsilon^u} + 1 = \frac{16}{10^{0.35}} \approx 8$). This means that every additional MS (beyond the 8th user) experiences outage. This state is reached when a total number of about 28–32 users are distributed throughout the network due to the uniform user distribution. The situation is different in cell 2 – cell 4 because every MS in these cells only utilise 50% of the data rate that is used by a MS in cell 1. This means that approximately twice as many MS's can be accommodated in cell 2 – cell 4. As a consequence of an increasing number of users in cell 2 – cell 4, the interference in cell 1 is increasing accordingly which results in capacity losses in that cell. Therefore, a capacity maximum in cell 1 can be ascertained at about 28 MS's. Note, that the capacity maximum is strongly dependent on the required bit-energy to interference ratio ϵ^u at the BS receiver. Methods that enable the same bit-error performance at a reduced bit-energy to interference ratio have a vital impact on the pole capacity and hence on the overall system performance.

As expected, the capacity in cell 2 – cell 4 is almost the same due to symmetry. The centrally operated TS-opposing algorithm improves capacity in cell 1 considerably by about 20 % – 30 % in the range between 14 and 35 distributed users. The improvement in the other-cells is negligible which causes the total capacity improvement to be averaged to about 8 % (48 kbps/Cell/TS instead of 52 kbps/Cell/TS for 28 distributed users). As described earlier the TS-opposing algorithm re-adjusts the components of α in (4.52) dynamically in order to obtain the best capacity. For scenario 1, the expected values, $E(\alpha)$, resulting from this optimisation process are presented in Figure 4.13. In the case of using the FCA strategy all components of α are deterministic and its values are given in the sub-captions of Figure 4.13. From the results in Figure 4.13 two important properties with respect to scenario 1 can be derived:

1. The DCA algorithm does not change α significantly for TS 3 and TS 4, *i.e.* synchronous transmission and reception for all cells is applied. This is the same as for the FCA scheme. Furthermore, since each MS in cell 1 occupies all 4 TS's, and swapping TS's in cell 1 would involve TS 3 (because it is the only TS used for TX), it can be inferred that primarily TS 1 and TS 2 in cell 2 – cell 4 are re-arranged in this scenario. The results in Figure 4.13 are analysed and the probabilities of those TS's which change most frequently are depicted in Figure 4.14. The arrows indicate which TS's are re-arranged with the highest probability. Moreover, with the aid of Figure 4.13 it can also be found that:

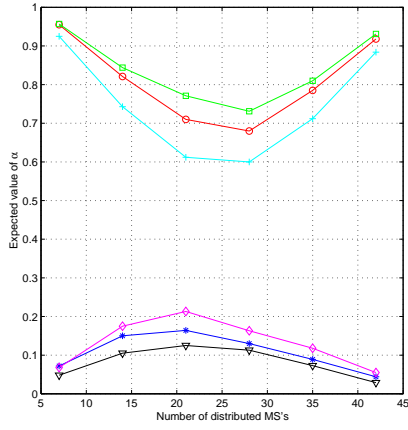
$$E^{\text{TS1}}(\alpha_{1,j}) \approx 1 - E^{\text{TS2}}(\alpha_{1,j}) \quad j = 2, \dots, 4 \quad (4.58)$$

$$E^{\text{TS1}}(\alpha_{i,j}) \approx E^{\text{TS2}}(\alpha_{i,j}) \quad i = 2, 3 \quad j = 3, 4 \quad \text{for all } i \neq j \quad (4.59)$$

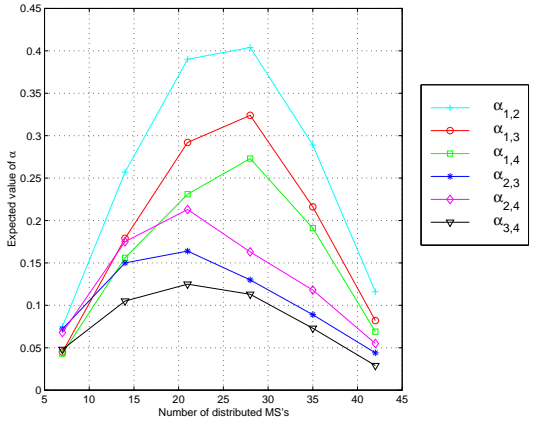
It can be summarised that for scenario 1 the DCA re-arranges TS's in cell 2 – cell 4 to improve the throughput in cell 1 without affecting the capacity in cell 2 – cell 4.

2. From Figures 4.13(a) and 4.13(b) it can be seen that the greatest changes with respect to the FCA strategy are for a load between 20 and 30 MS's which therefore can be considered as the optimal operation load for the centralised DCA.

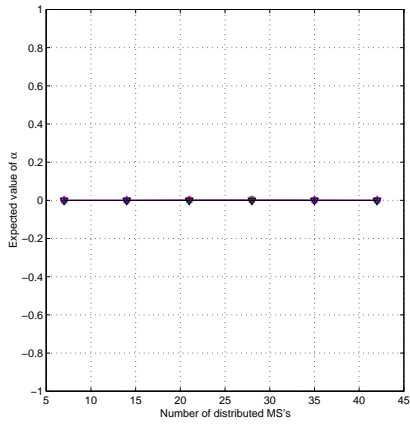
Results of scenario 2 In the second scenario, in addition to the asymmetric traffic in cell 1 (as discussed in scenario 1) the rate of asymmetry in cell 2 is different from 1:1. In this scenario cell 2 uses both TS 1 and TS 2 for reception inducing an additional asynchronous TS overlap



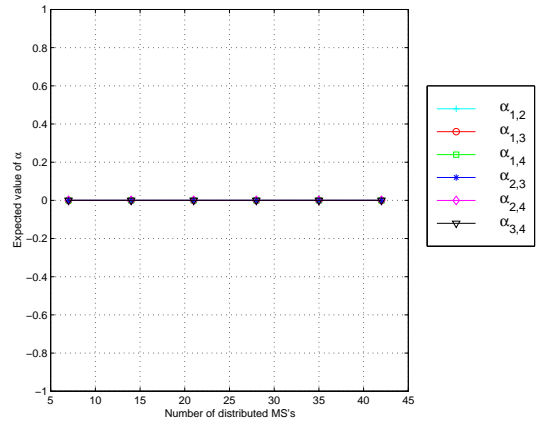
(a) Expected values of the components of α at TS 1. In the case of FCA: $\alpha_{1,2} = \alpha_{1,3} = \alpha_{1,4} = 1$ and $\alpha_{2,3} = \alpha_{2,4} = \alpha_{3,4} = 0$.



(b) Expected values of the components of α at TS 2. In the case of FCA: $\alpha_{1,2} = \alpha_{1,3} = \alpha_{1,4} = \alpha_{2,3} = \alpha_{2,4} = \alpha_{3,4} = 0$.



(c) Expected values of the components of α at TS 3. In the case of FCA: $\alpha_{1,2} = \alpha_{1,3} = \alpha_{1,4} = \alpha_{2,3} = \alpha_{2,4} = \alpha_{3,4} = 0$.



(d) Expected values of the components of α at TS 4. In the case of FCA: $\alpha_{1,2} = \alpha_{1,3} = \alpha_{1,4} = \alpha_{2,3} = \alpha_{2,4} = \alpha_{3,4} = 0$.

Figure 4.13: Scenario 1: The expected values of the components of α as a result of the novel DCA algorithm are depicted for all 4 TS (In a) the results with respect to TS 1 are depicted, in b) the results with respect to TS 2, etc.).

	TS1	TS2	TS3	TS4
Cell 1	1	1	0	1
Cell 2	0	1	0	1
Cell 3	0	1	0	1
Cell 4	0	1	0	1


$1 := \text{BS receives}$  $:= 27\% < p_{\max} < 40\%$
 $0 := \text{BS transmits}$

Figure 4.14: This illustration shows the initial TX/RX configuration with respect to the BS's for scenario 1. The arrows highlight the TS's which changed most frequently and the associated maximum probabilities are shown.

	TS1	TS2	TS3	TS4
cell 1	1	1	0	1
cell 2	1	1	0	1
cell 3	0	1	0	1
cell 4	0	1	0	1

$1 := \text{BS receives}$
 $0 := \text{BS transmits}$

(a) Scenario 2

Figure 4.15: The initial TS assignment for scenario 2. The modification with respect to the previous scenario is highlighted.

(see Figure 4.15(a)). In scenario 1 an asynchronous TS overlap between the following cells exists:

$$\begin{aligned} \text{Cell 2} &\rightarrow \text{Cell 1,} \\ \text{Cell 3} &\rightarrow \text{Cell 1,} \\ \text{Cell 4} &\rightarrow \text{Cell 1.} \end{aligned} \tag{4.60}$$

In scenario 2 the situation now is:

$$\begin{aligned} \text{Cell 3} &\rightarrow \text{Cell 1,} \\ \text{Cell 4} &\rightarrow \text{Cell 1,} \\ \text{Cell 3} &\rightarrow \text{Cell 2,} \\ \text{Cell 4} &\rightarrow \text{Cell 2.} \end{aligned} \tag{4.61}$$

It is obvious from (4.61) that the TS's between cell 1 and cell 2 can be arranged without generating an asynchronous overlap between these cells. Furthermore, compared to scenario 1, the minimum number of asynchronous TS overlaps experienced by cell 1 is reduced by one. The results in Figure 4.16 reveal that the capacity improvement in cell 1 is maintained and,

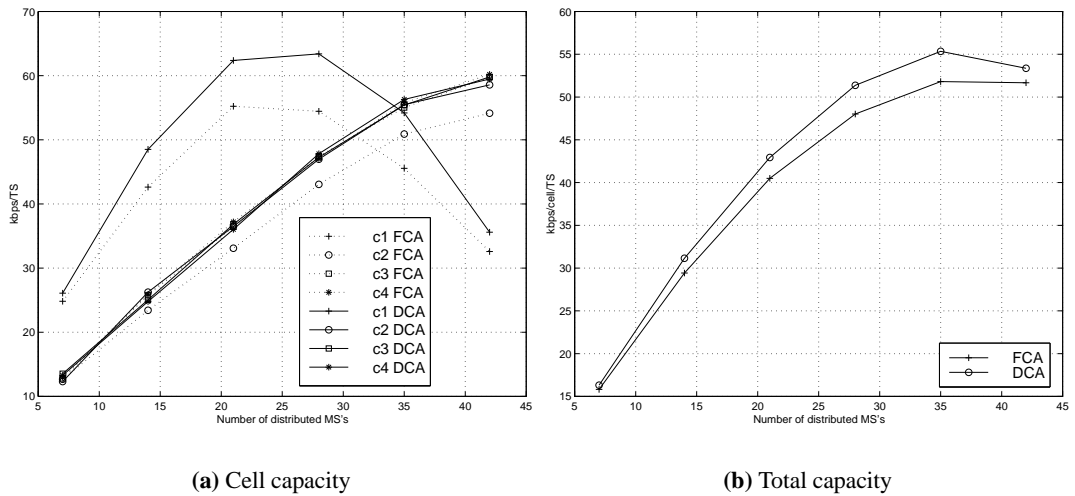


Figure 4.16: Results of scenario 2. The rate of asymmetry, $UL:DL$, in cell 1 is 3:1, in cell 2:0 and 1:1 in all other-cells (cell 3 and cell 4). The graphs show: for a) the capacity in each cell in [kbps/TS] and b) the total capacity in [kbps/Cell/TS]. The results labelled with 'FCA' are obtained by the fixed channel assignment procedure and the results labelled with 'DCA' are these obtained from the novel centralised DCA algorithm.

in addition, the capacity in cell 2 is improved over the FCA technique. Thus the improve-

ment in cell 2 is not at the expense of capacity in cell 1. It is important to note that since cell 1 only faces opposed transmission from two neighbouring cells, the capacity in cell 1 when applying the FCA method is greater than in scenario 1. However, since cell 2 suffers from asynchronous TS overlaps the capacity in cell 2 is reduced when using the FCA scheme. The gain over the FCA technique in both cells (cell 1 and cell 2) is between 10 % – 15 % resulting in a total maximum improvement of about 8 % (52 kbps/Cell/TS instead of 48 kbps/Cell/TS for 28 distributed users). It is interesting to note that the relative capacity improvement is similar to the one achieved in scenario 1. The results of the expected values of $\alpha_{i,j}$ are depicted in Figure 4.17. The following properties and upper bounds for $E^{TS_n}(\alpha_{i,j})$ can be observed:

$$0 \leq E^{TS1}(\alpha_{1,2}) \leq 0.014 \quad (4.62)$$

$$0 \leq E^{TS3}(\alpha_{1,2}) \approx E^{TS3}(\alpha_{1,3}) \approx E^{TS3}(\alpha_{1,4}) \leq 0.014 \quad (4.63)$$

$$0.63 \leq E^{TS1}(\alpha_{1,4}) \approx E^{TS1}(\alpha_{2,4}) \leq 0.93 \quad (4.64)$$

$$0.51 \leq E^{TS1}(\alpha_{1,3}) \approx E^{TS1}(\alpha_{2,3}) \leq 0.91 \quad (4.65)$$

$$0.05 \leq E^{TS2}(\alpha_{1,4}) \approx E^{TS2}(\alpha_{2,4}) \leq 0.37 \quad (4.66)$$

$$0.05 \leq E^{TS2}(\alpha_{1,3}) \approx E^{TS2}(\alpha_{2,3}) \leq 0.49 \quad (4.67)$$

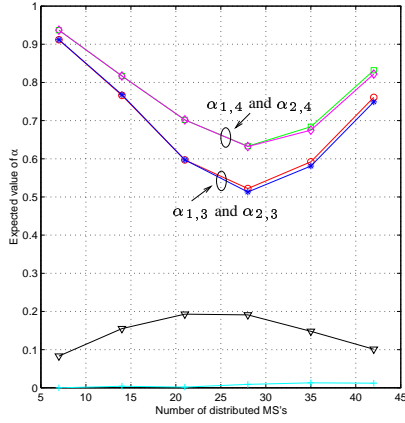
$$E^{TS1}(\alpha_{1,4}) \approx 1 - E^{TS2}(\alpha_{1,4}) \quad (4.68)$$

$$E^{TS1}(\alpha_{1,3}) \approx 1 - E^{TS2}(\alpha_{1,3}) \quad (4.69)$$

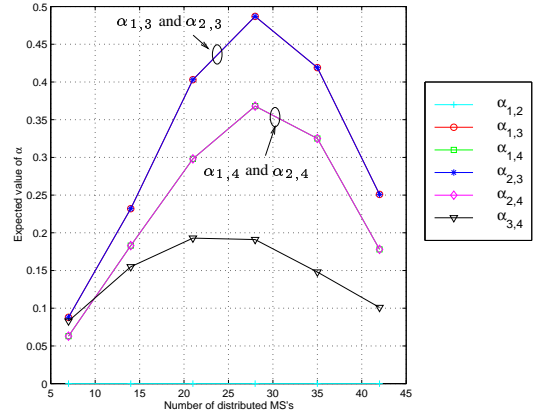
$$0.05 \leq E^{TS1}(\alpha_{3,4}) \approx E^{TS2}(\alpha_{3,4}) \leq 0.2 \quad (4.70)$$

Using properties (4.62) – (4.70) it can be concluded that the DCA algorithm primarily uses TS 1 and TS 2 in cell 3 and cell 4 to minimise interference. Only with a maximum probability of about 1.4 % is TS 3 in cell 1 exchanged with TS 1 in the same cell. These mechanisms are illustrated in Figure 4.18.

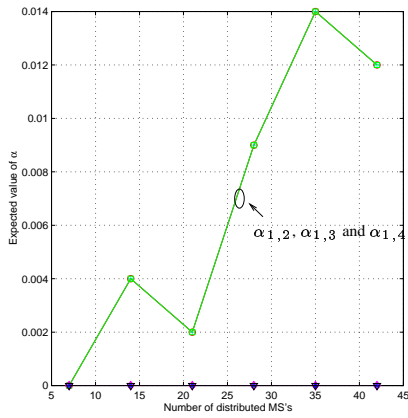
Results of scenario 3 In the third scenario it is investigated whether the TS-opposing algorithm can also achieve better results in the case when no asynchronous TS overlap exists, *i.e.* equal traffic in uplink and downlink applies. The results of the third scenario are depicted in Figure 4.20. Firstly, where the TS-opposing algorithm is not employed, the maximum capacity in cell 1, for example, is increased from 50 kbps to about 63 kbps compared to the first scenario. Note that in the case of symmetric traffic and no DCA algorithm the maximum capacity in cell 1 is greater than in the other cells. This is anticipated as the own-cell interference in



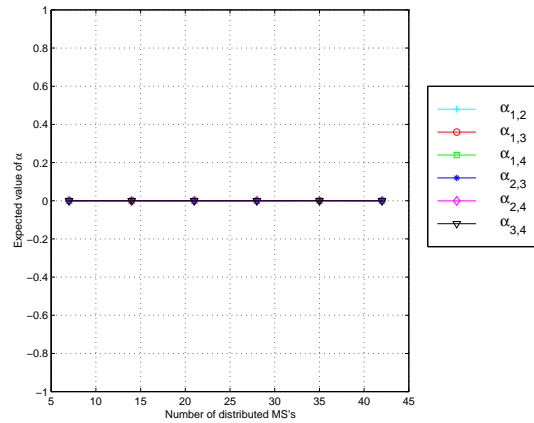
(a) Expected values of the components of α at TS 1. In the case of FCA: $\alpha_{1,3} = \alpha_{1,4} = \alpha_{2,3} = \alpha_{2,4} = 1$ and $\alpha_{1,2} = \alpha_{3,4} = 0$.



(b) Expected values of the components of α at TS 2. In the case of FCA: $\alpha_{1,2} = \alpha_{1,3} = \alpha_{1,4} = \alpha_{2,3} = \alpha_{2,4} = \alpha_{3,4} = 0$.



(c) Expected values of the components of α at TS 3. In the case of FCA: $\alpha_{1,2} = \alpha_{1,3} = \alpha_{1,4} = \alpha_{2,3} = \alpha_{2,4} = \alpha_{3,4} = 0$.



(d) Expected values of the components of α at TS 4. In the case of FCA: $\alpha_{1,2} = \alpha_{1,3} = \alpha_{1,4} = \alpha_{2,3} = \alpha_{2,4} = \alpha_{3,4} = 0$.

Figure 4.17: Scenario 2: The expected values of the components of α as a result of the novel DCA algorithm are depicted for all 4 TS (In a) the results with respect to TS 1 are depicted, in b) the results with respect to TS 2, etc.).

	TS1	TS2	TS3	TS4
Cell 1	1	1	0	1
Cell 2	1	1	0	1
Cell 3	0	1	0	1
Cell 4	0	1	0	1



$1 := \text{BS receives}$  $:= 37\% < p_{\max} < 49\%$
 $0 := \text{BS transmits}$  $:= p_{\max} \approx 1.4\%$

Figure 4.18: This illustration shows the initial TX/RX configuration with respect to the BS's for scenario 2. The arrows highlight the TS's which changed most frequently and the associated maximum probabilities are shown.

	TS1	TS2	TS3	TS4
cell 1	0	1	0	1
cell 2	0	1	0	1
cell 3	0	1	0	1
cell 4	0	1	0	1

$1 := \text{BS receives}$
 $0 := \text{BS transmits}$

(a) Scenario 3

Figure 4.19: The initial TS assignment for scenario 3. The modification with respect to the previous scenario is highlighted.

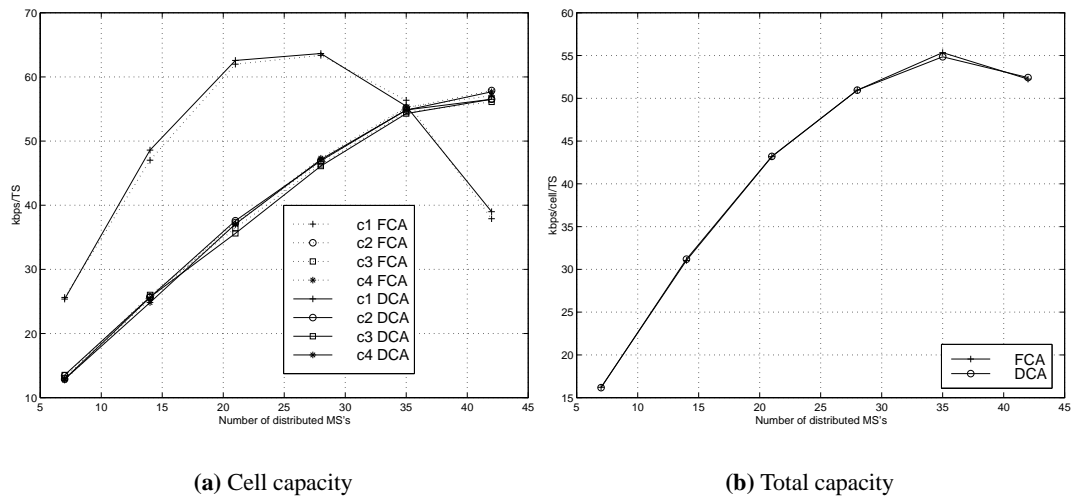


Figure 4.20: Results of scenario 3. The rate of asymmetry, $UL:DL$, in cell 1 is 2:2 and 1:1 in all other cells. The graphs show: for a) the capacity in each cell in [kbps/TS] and b) the total capacity in [kbps/Cell/TS]. The results labelled with 'FCA' are obtained by the fixed channel assignment procedure and the results labelled with 'DCA' are these obtained from the novel centralised DCA algorithm.

cell 1 is lower than in cell 2 – cell 4. The results reveal that the TS-opposing algorithm does not achieve a capacity improvement if the TS's can be arranged such that no asynchronous TS overlap exists. On the contrary, it was demonstrated previously in section 4.2 that synchronous transmission and reception is not the ideal case with respect to an isolated cell. However, it is anticipated that the capacity gains observed through the investigation in section 4.2 cannot be maintained when considering a cellular network. The reason for this is that TS-opposing with respect to a certain cell also has an impact on the neighbouring cells remaining. The impact on the remaining cells may be such that the interference in one cell, several cells or even all cells but one is increased. This, in turn, means that the capacity gain obtained for a particular cell is offset by higher interference in some other cells. If the higher interference in the neighbouring cells cannot be tolerated (usually the case when assuming uniformly distributed MS's) the TS-opposing does not increase the overall system performance.

Figure 4.21 demonstrates that in scenario 3 the DCA algorithm does not change the initial TS configuration which is not subject to an asynchronous TS overlap. The same configuration applies to the FCA scheme. Therefore, the capacity results of the FCA technique and the DCA algorithm are almost identical.

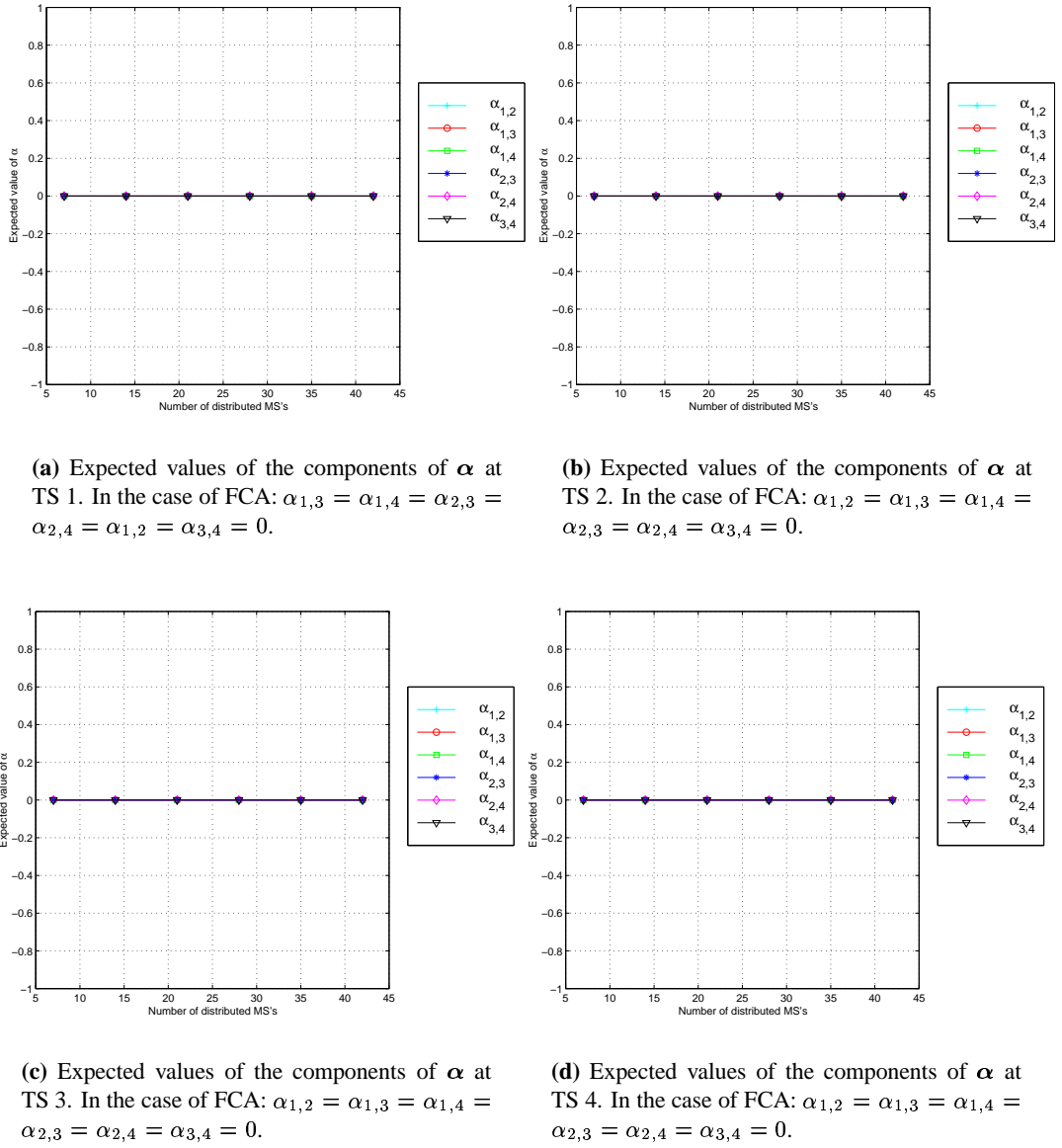


Figure 4.21: Scenario 3: The expected values of the components of α as a result of the novel DCA algorithm are depicted for all 4 TS (In a) the results with respect to TS 1 are depicted, in b) the results with respect to TS 2, etc.).

	TS1	TS2	TS3	TS4
cell 1	0	0	0	1
cell 2	0	1	0	1
cell 3	0	1	0	1
cell 4	0	1	0	1

1 := BS receives
0 := BS transmits

(a) Scenario 4

Figure 4.22: *The initial TS assignment for scenario 4. The modification with respect to the previous scenario is highlighted.*

Results of scenario 4 The first two scenarios are with channel asymmetry in favour of the uplink. In scenario 4 the performance of the TS-opposing algorithm for channel asymmetry in favour of the downlink is investigated. The results are depicted in Figure 4.23. In cell 1 the TS-opposing algorithm, since it is operated on the uplink, can minimise interference with respect to only one TS out of four available (TS 4). The TS's can be arranged such that no asynchronous TS overlap with respect to TS 4 exists. This is the reason why the capacity results in cell 1 do not differ greatly when using the DCA or FCA assignment strategies. The benefits due to the TS-opposing algorithm are now experienced by cell 2 – cell 4 as can be seen in Figure 4.23. The capacity in cell 2 for 35 initially distributed users increases from 50 kbps/Cell/TS to about 55 kbps/Cell/TS which results in a relative gain of about 10 %. Similar results can be obtained for cell 3 and cell 4.

Again, the results of the expected values of $\alpha_{i,j}$ are presented in Figure 4.24. It is useful to

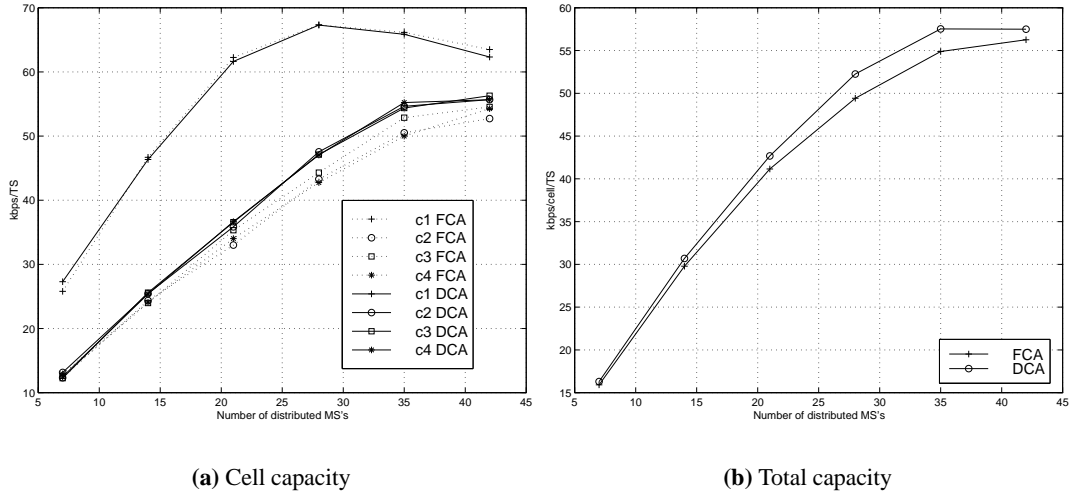


Figure 4.23: Results of scenario 4. The rate of asymmetry, $UL:DL$, in cell 1 is 1:3 and 1:1 in all other-cells. The graphs show: for a) the capacity in each cell in [kbps/TS] and b) the total capacity in [kbps/Cell/TS]. The results labelled with 'FCA' are obtained by the fixed channel assignment procedure and the results labelled with 'DCA' are these obtained from the novel centralised DCA algorithm.

highlight the following properties:

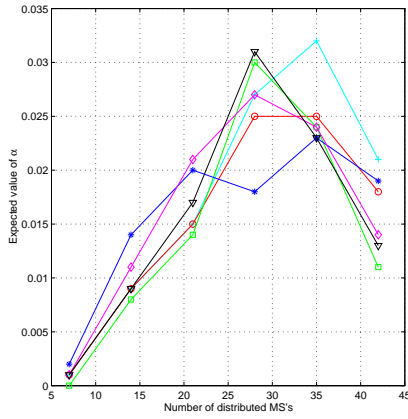
$$0 \leq E^{\text{TS1}}(\alpha_{i,j}) \quad i = 1, \dots, 3 \quad j = 2, \dots, 4 \quad \text{for all } i \neq j \quad \leq 0.033 \quad (4.71)$$

$$0.42 \leq E^{\text{TS2}}(\alpha_{1,2}) \approx E^{\text{TS2}}(\alpha_{1,3}) \approx E^{\text{TS2}}(\alpha_{1,4}) \quad \leq 0.93 \quad (4.72)$$

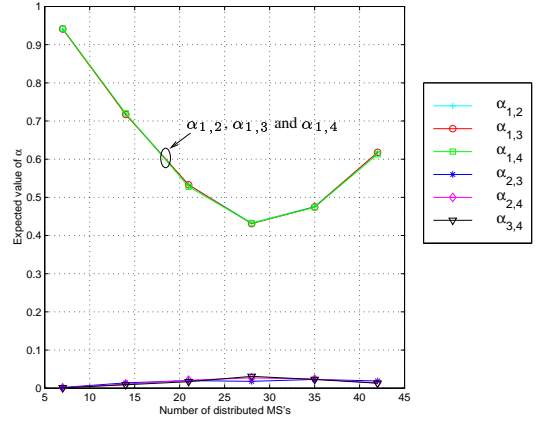
$$0.07 \leq E^{\text{TS4}}(\alpha_{1,2}) \approx E^{\text{TS4}}(\alpha_{1,3}) \approx E^{\text{TS4}}(\alpha_{1,4}) \quad \leq 0.59 \quad (4.73)$$

$$E^{\text{TS2}}(\alpha_{1,2}) \approx 1 - E^{\text{TS4}}(\alpha_{1,2}) \quad (4.74)$$

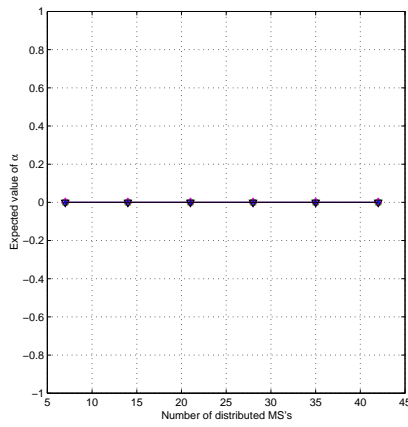
Using the properties (4.71) – (4.74) it can be inferred that the DCA algorithm uses TS 2 and TS 4 in cell 1 to a great extent to improve capacity in cell 2 – cell 4. Note that this mechanism is opposite to that used in scenario 1 and scenario 2. In scenario 1 and scenario 2 TS's in cells 2–4 are most frequently changed by the DCA algorithm to improve capacity in cell 1. In Figure 4.25 the basic mechanisms utilised by the new DCA algorithm with respect to scenario 4 are illustrated.



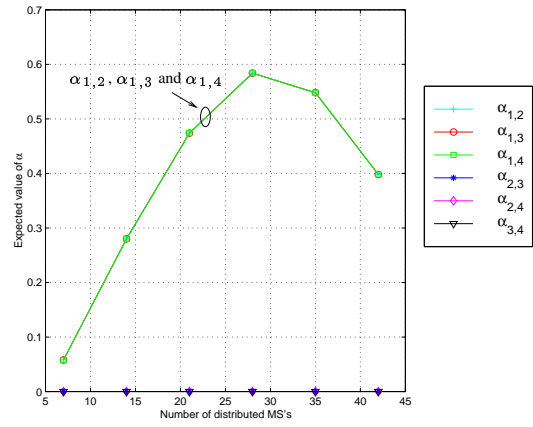
(a) Expected values of the components of α at TS 1. In the case of FCA: $\alpha_{1,3} = \alpha_{1,4} = \alpha_{2,3} = \alpha_{2,4} = \alpha_{1,2} = \alpha_{3,4} = 0$.



(b) Expected values of the components of α at TS 2. In the case of FCA: $\alpha_{1,2} = \alpha_{1,3} = \alpha_{1,4} = 1$ and $\alpha_{2,3} = \alpha_{2,4} = \alpha_{3,4} = 0$.



(c) Expected values of the components of α at TS 3. In the case of FCA: $\alpha_{1,2} = \alpha_{1,3} = \alpha_{1,4} = \alpha_{2,3} = \alpha_{2,4} = \alpha_{3,4} = 0$.



(d) Expected values of the components of α at TS 4. In the case of FCA: $\alpha_{1,2} = \alpha_{1,3} = \alpha_{1,4} = \alpha_{2,3} = \alpha_{2,4} = \alpha_{3,4} = 0$.

Figure 4.24: Scenario 4: The expected values of the components of α as a result of the novel DCA algorithm are depicted for all 4 TS (In a) the results with respect to TS 1 are depicted, in b) the results with respect to TS 2, etc.).

	TS1	TS2	TS3	TS4
Cell 1	0	0	0	1
Cell 2	0	1	0	1
Cell 3	0	1	0	1
Cell 4	0	1	0	1



$1 := \text{BS receives}$  $:= p_{\max} \approx 59\%$
 $0 := \text{BS transmits}$  $:= p_{\max} \approx 3.3\%$

Figure 4.25: This illustration shows the initial TX/RX configuration with respect to the BS's for scenario 4. The arrows highlight the TS's which changed most frequently and the associated maximum probabilities are shown.

4.4 Conclusions

For a single cell it was demonstrated that by using a TS-opposing technique in a TD-CDMA/TDD interface, capacity can be increased significantly compared with an equivalent FDD system. Assuming, for example, a population of 2 users per cell, with the same power levels, the capacity in the TDD cell is up to 48% greater than in an FDD cell.

The capacity gain was reduced as the population in the adjacent cells increased. This was due to: firstly, the BS↔BS interference being about 15–20 times greater than interference from other-cell mobiles, and secondly the non-linear increase of own-cell interference. BS↔BS interference might be reduced by static shielding between two BS's (location in different rooms which provide extra shielding or antenna beamforming) or by a more complex downlink power control algorithm. It was demonstrated that by decreasing the BS↔BS interference by a factor of 10, the gain due to the TS-opposing technique increased by a maximum of 118%.

The limitations of the approach used in this section were that outage due to high MS↔MS interference was not considered and that the optimisation was aimed at a single cell neglecting the mutual impacts on the adjacent cells. However, the results obtained provided an upper bound on capacity gains when using the TS-opposing technique. The simplifications applied

in the initial study were eliminated in a further, more complex investigation of a TS-opposing algorithm where the scope of operation was extended to a multiple cell environment.

In this context, a novel centralised DCA algorithm utilising the TS-opposing principle was operated at the RNC. This resulted in a strategy to avoid interference, with asynchronous overlaps being the prerequisite for capacity improvements. Thereby it could be demonstrated that the existence of asynchronous TS overlaps in a TD-CDMA/TDD system did not result in system degradations. The very important implication of this is that channel asymmetry between neighbouring cells in a TD-CDMA/TDD system did not cause a capacity reduction as a consequence of same entity interference ($MS \leftrightarrow MS$ and $BS \leftrightarrow BS$ interference). Since arranging channel asymmetry is one of the most significant advantages of TDD, the fact that the disadvantages of different rates of asymmetry within a TDD network were eliminated is an important result. Furthermore, it was found that the total maximum capacity for channel asymmetry in favour of the downlink is greater than the reverse or even synchronous case. This is equally important since it is predicted that future data applications such as Web browsing will require more downlink than uplink capacity [108].

The DCA algorithm applied to the model of a cellular network did not achieve greater spectral efficiency than an equivalent FDD interface. However, the main advantage was that different channel asymmetries in neighbouring cells did not result in a significant capacity loss regardless of the actual rate of asymmetry.

Furthermore, it can be concluded that $MS \leftrightarrow MS$ was not a severe problem with the system parameters used, but the uplink and downlink in TDD could be strongly coupled as demonstrated in (4.52).

Chapter 5

Distributed DCA algorithm utilising the TS-opposing idea

5.1 Introduction

In this chapter a novel distributed dynamic channel assignment (DCA) algorithm [153] applicable for the TDD mode of the UMTS terrestrial radio access (UTRA) is presented. It is closely related to the DCA used in the DECT (Digitally Enhanced Cordless Telecommunications) system [110]. Once again, the discovery made in chapter 3 is exploited; that is, that for certain scenarios opposed synchronisation of TS's between neighbouring cells is advantageous. The new distributed DCA algorithm is supported by the results of the investigation in section 4.2. In this section it was demonstrated that synchronous transmission and reception between neighbouring cells may not yield the greatest capacity that is attainable in a single cell. However, it was found that, when the centralised DCA algorithm developed in section 4.3 was applied to multiple cells, it was not feasible to fully exploit the potential gains revealed by the capacity analysis of a single cell.

In this chapter it is demonstrated that by applying the novel distributed DCA algorithm, which utilises the TS-opposing idea, greater capacity can result than would be obtained by synchronous transmissions. Most importantly, this is shown to be valid for a TDMA-CDMA/TDD (TD-CDMA/TDD) network which accounts for full spatial coverage. Channel asymmetry is assumed to be arranged by code pooling rather than TS pooling [163].

As a consequence of using the TS-opposing principle, a new method is required to separately measure the total interference from mobile stations (MS's) and the total interference from base stations (BS's). It is shown that this method can also be used to prevent cases of severe MS \leftrightarrow MS interference. This mechanism is incorporated into the new decentralised DCA algorithm presented here.

This chapter is structured as follows: in section 5.2 the problems are stated. In section 5.3 a novel TS assignment plan is presented, followed by a new decentralised DCA algorithm in

section 5.4. Subsequently in section 5.5 a brief description of the simulation model and the methodology for measuring the system performance is described. A discussion of the results follows in section 5.6 before conclusions are drawn in section 5.7.

5.2 Problem formulation

A channel in a TD-CDMA/TDD interface (used for UTRA-TDD) is characterised by a combination of a carrier frequency (FDMA component), time slot (TDMA component) and spreading code (CDMA component). Since only 4 carriers are available in the licensed UTRA-TDD frequency band, it is anticipated that any one operator will only be able to use one carrier which would reduce the channel characterisation to the combination of a time slot (TS) and spreading code. In this case the interfaces for DECT and UTRA-TDD are similar, the basic difference being that the FDMA component in DECT is replaced by the CDMA component in UTRA-TDD. In the DECT system a dynamic channel selection (DCS) procedure initiated by the MS is used. Due to the similarities between DECT and UTRA-TDD a distributed DCS incorporating the TS-opposing idea is investigated for the UTRA-TDD interface. This combined with the basic differences between UTRA-TDD and the DECT standard means that the following problems must be addressed:

1. The MS must be able to separately measure the interference contribution from other MS's (I_{mm}) and the interference component from neighbouring BS's (I_{bm}) in order to exploit the TS-opposing idea.
2. As the TS-opposing method is used, cases of severe MS \leftrightarrow MS may arise which need to be resolved by the DCA algorithm.
3. If a cellular TDD system is considered the same entity interference (BS \leftrightarrow BS and MS \leftrightarrow MS interference) may require a TS's re-use distances¹ greater than one. It is aimed to develop a decentralised DCA algorithm to avoid the necessity of cell re-use distances greater than one in order to maintain high spectral efficiency [10].

¹The terminology used here follows the terminology introduced for FDMA/FDD systems [164] where the re-use of channels separated in the frequency domain is described. The same logic can be applied to channels which are separated in the time domain.

In order to solve the problems mentioned above, the combination of a fixed TS plan and a TS-opposing algorithm is proposed. A fixed TS assignment means that TS's for uplink and downlink direction are pre-selected in a systematic manner. Thus, the target is to enable the MS to selectively and easily measure each interference component I_{bm} and I_{mm} . It could be argued that the pre-selection of the TS's reduces the flexibility to adjust the TDD mode to varying traffic loads in the up and downlink. However, in the UTRA-TDD mode a resource unit (RU) is specified by the combination of a TS, a code and a frequency carrier. Therefore, channel asymmetry can in principle be achieved in three dimensions: a) in the TS dimension by means of TS pooling (multislot operation) or b) in the code dimension by code pooling (multicode operation) c) in the frequency dimension, which is not realistic for UTRA-TDD due to the low number of carriers. In [163] this problem is taken into account. The finding is that code pooling is more advantageous using the 'unsatisfied users' criterion in [149] than TS pooling for UDD (unconstrained delay data) packet data. This supports the concept of pre-selected TS's. In addition, areas which are known for high traffic imbalances can be catered for by defining more downlink TS's than uplink TS's.

In the analysis carried out, for simplicity each user is assumed to be using the same service with one TS being allocated for uplink and downlink respectively. The total other-cell interference at any MS can be found as follows:

$$I_m = \sum_{j=1}^L \sum_{i=1}^{M_j} \alpha_{j,k} \underbrace{\frac{P_{c_{i,j}}^u}{a_{i,m}}}_{I_{mm_j}} + (1 - \alpha_{j,k}) \underbrace{\frac{P_{c_j}^d}{a_{j,m}}}_{I_{bm_j}}, \quad (5.1)$$

where L is the number of surrounding cells, M_j is the total number of active users in the neighbouring cell j , $a_{i,m}$ is the path loss between the user of interest, m , and the interfering user i . Similarly $a_{j,m}$ is the path loss between the user of interest, m , and the BS number j . The transmitted carrier power of user i in cell j is described by $P_{c_{i,j}}^u$ and $P_{c_j}^d$ is the total carrier power transmitted by the BS in cell j . The TS synchronisation factor between cell j and cell k to which user m is allocated is modelled by $\alpha_{j,k}$. Note that symbols which are followed by the superscript 'u' are associated with the uplink channel; symbols which are followed by a superscript 'd' are associated with the downlink channel.

The interference observed at any BS, b , can be calculated as follows:

$$I_b = \sum_{j=1}^L \sum_{i=1}^{M_j} (1 - \alpha_{j,k}) \underbrace{\frac{P_{c_{i,j}}^u}{a_{i,u}}}_{I_{mb_j}} + \alpha_{j,k} \underbrace{\frac{P_{c_j}^d}{a_{j,u}}}_{I_{bb_j}}. \quad (5.2)$$

From (5.1) it can be seen that the interference at any MS is composed of MS→MS interference multiplied by a synchronisation factor $\alpha_{j,k}$. Due to this synchronisation factor the MS→MS interference, I_{mm} , may only be a fraction of the maximum possible MS→MS interference. The second type of interference experienced at any MS is BS→MS interference (I_{bm}) for which a similar scaling applies as for (I_{mm}). Hence, the magnitude of each type of interference can be manipulated by varying $\alpha_{j,k}$, where $j = 1, 2, \dots, L$, with respect to cell k .

It is interesting to note that I_{bm_j} and I_{mb_j} , also described as other entity interference, are coupled through $\alpha_{j,k}$. The same holds for I_{mm_j} and I_{bb_j} which is categorised as same entity interference. This mechanism can be deduced from (5.1) and (5.2) which means that an interference reduction at the MS, for example, through adjusting $\alpha_{j,k}$ also has an impact on interference at the BS. In the worst case, the interference at the BS increases despite the interference reduction at the MS. Hence, the interference at the opposite end, for example at the BS, of a communication link may not be minimised automatically if the interference is minimised by manipulating $\alpha_{j,k}$ at one end, in this case the MS. This particular property is undesirable, but it is inherent in DCA algorithms [122, chapter 8].

In the following sections a novel decentralised DCA for UTRA-TDD is investigated, which is built on a TS assignment plan that enables a mobile to exploit the TS-opposing mechanism.

5.3 TS assignment plan

In the following a novel TS assignment scheme is presented which allows each TS to be used in each cell of a cellular TDD network with a frequency re-use distance of 1. However, in order to exploit the TS-opposing mechanism, fixed TS assignment patterns are introduced. In this way the TDD specific property of being able to use any TS for uplink or downlink traffic is exploited such that a TS-opposing algorithm can be operated locally.

In (5.1) it has been shown that any location within the network can be characterised by an interference vector with one component being the interference resulting from all MS's. The

second component describes the sum of the total interference caused by the BS's. If the frames are synchronised these components are mutually exclusive. It merely depends on $\alpha_{j,k} \in \{0, 1\}$ whether I_{bm_j} or I_{mm_j} becomes effective. Furthermore, if these interference components are known *a priori* a new mobile entering the cell² may be allocated to a channel with opposed TS's to all other cells if: $\sum_{j=1}^L I_{bm_j} > \sum_{j=1}^L I_{mm_j}$.

However, two notable problems result from the interference minimisation process described. Firstly, at the mobile receiver a composite interference signal from BS's and MS's is received. It is therefore difficult to measure the single interference components I_{mm_j} or I_{bm_j} since the MS and BS entities within the surrounding cells transmit at the same time. Secondly, adjusting $\alpha_{j,k}$ with respect to cell k will require the neighbouring cell j to alter the direction of transmission (uplink versus downlink, or vice versa). If the respective neighbouring cell j has L adjacent cells itself, this adjustment procedure might have undesirable implications for the interference in cell j and its $L - 1$ neighbouring cells.

The novel TS assignment plan depicted in Figure 5.1 is intended to mitigate these problems. It

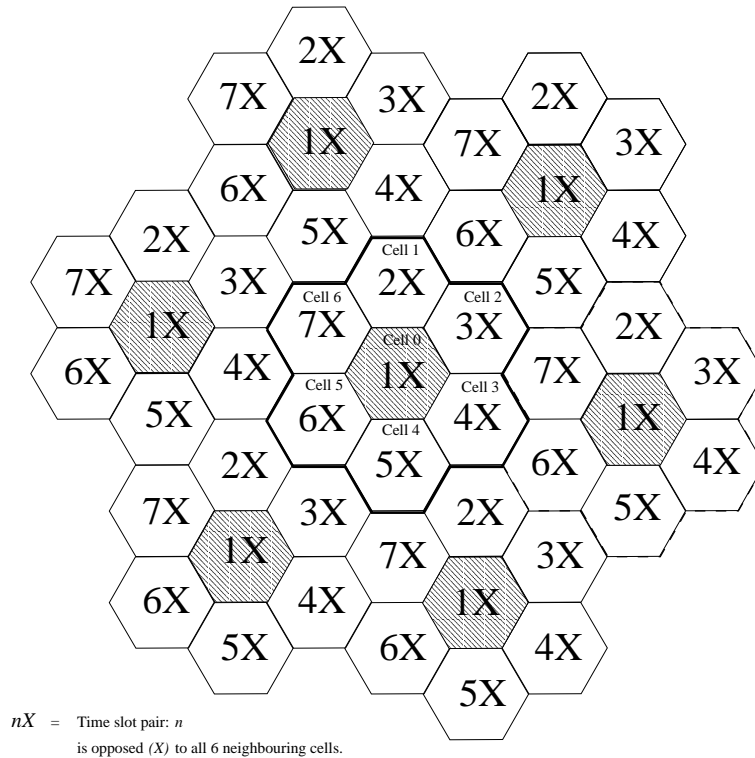


Figure 5.1: TS assignment plan. The 'X' indicates that the respective TS pair is opposed.

²This can be caused by a handover procedure or by a call establishment procedure

is assumed that one frame is composed of 7 symmetrical, full duplex channels³. It is designed so that at least one pair of TS's is opposed to all neighbouring cells permanently. The illustration in Figure 5.1 shows a multiple of 7-cell clusters. Each cell is supposed to occupy 7 subsequent pairs of TS's. In cell 0, for example, the first pair of TS's is opposed to all 6 neighbouring cells (cell 1 to cell 6), illustrated by the capital 'X'. Similarly, in cell 1, the second pair of TS's (TS 3 and TS 4) are opposed to all their neighbouring cells. This is repeated in cell 2, and so on. Since one pair of TS's per cell is opposed to the corresponding TS's in all its neighbouring

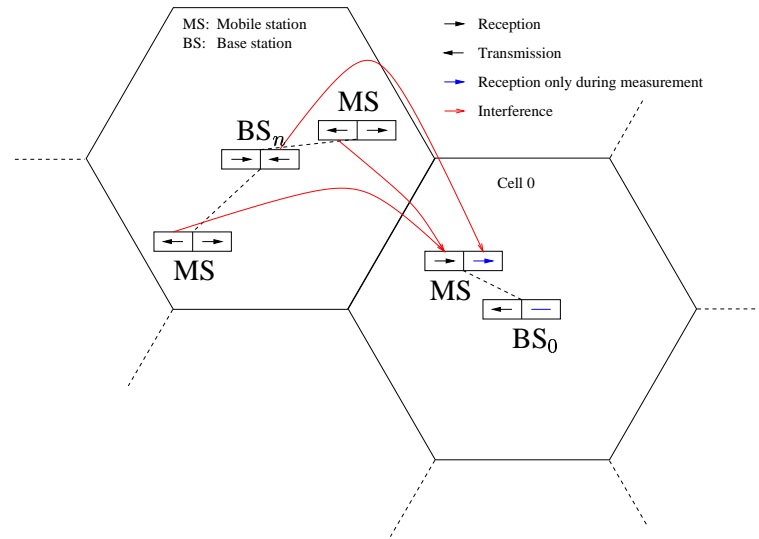


Figure 5.2: The mechanism of measuring the interference from BS's and MS's at the opposed channels.

cells, I_{mm} , can be measured easily as it can be found that:

$$\alpha_{j,k} = 1 \text{ for all } j \text{ and } k . \quad (5.3)$$

Hence, the interference measured at one of two TS's of the opposed full duplex channel merely results from other MS's since:

$$(1 - \alpha_{j,k}) I_{bm_j} = 0 \text{ for all } j \text{ and } k . \quad (5.4)$$

Similarly, the interference at the second TS of the opposed channel (which is only considered as a downlink channel during the measurement phase; during normal operation this is used for uplink traffic) results from the neighbouring BS's because when considering this TS as a

³Here the combination frequency/TS is referred to as a simplex channel. In UTRA-TDD each channel can be divided into subchannels by utilising the code domain

downlink TS it holds that:

$$\alpha_{j,k} = 0 \text{ for all } j \text{ and } k . \quad (5.5)$$

Consequently, the interference conveyed merely results from the surrounding BS's since:

$$(\alpha_{j,k}) I_{mm_j} = 0 \text{ for all } j \text{ and } k . \quad (5.6)$$

The basic mechanism of the measurement procedure described above is illustrated in Figure 5.2. In this figure the scenario is shown where cell 0 uses an opposed channel (with respect to all neighbouring cells) and measures the interference component from the MS's of the neighbouring cells, and BS's respectively.

In Figure 5.3 the actual TS assignment is depicted. This plan illustrates how the uplink and

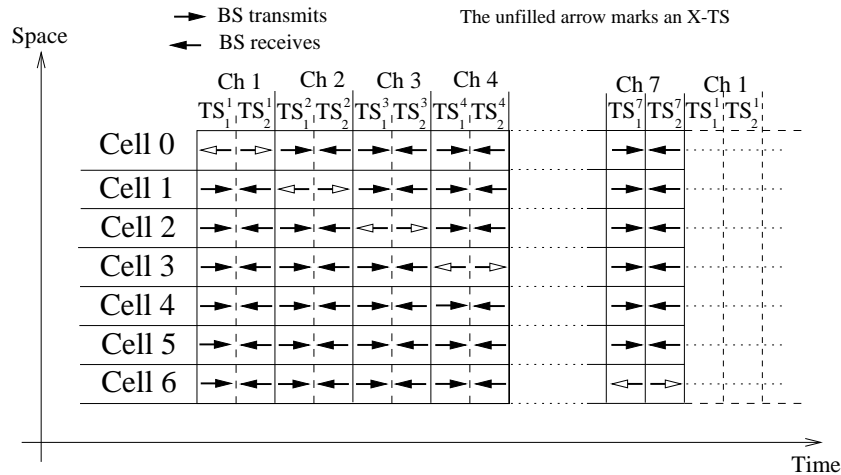


Figure 5.3: *TS configuration in a 7-cell cluster.*

downlink slots are distributed throughout a 7-cell cluster. This cluster can be repeated as often as required in order to achieve full spatial coverage. It can be seen that in cell 0, TS_1^1 (the superscript refers to the channel number whereas the subscript refers to the TS number of the respective channel) and TS_2^1 are opposed to all other adjacent cells. In cell 1 it is TS_1^2 and TS_2^2 , in cell 2 TS_1^3 and TS_2^3 , etc.

It can be found that the TS assignment plan illustrated in Figure 5.1 causes at least one pair of TS's to overlap asynchronously to one of its adjacent cells. Therefore, the term 'quasi-synchronous' channels is introduced. Once again, this can be illustrated with the aid of Figure 5.3. As an example, the TS's of channel 2 (Ch 2), TS_1^2 and TS_2^2 , in cell 0, are opposed to

cell 1, but synchronous to all other cells $j = 2, 3, \dots, 6$. The same mechanism can be found for all other channels in cell 0, except channel 1. Thus, in each cell there are 6 quasi synchronous channels and one channel with opposed synchronisation to all other cells.

The interference measured at any of the ‘quasi-synchronous’ channels can be found as:

$$I_{bm} = \sum_{i, i \neq n}^5 I_{bm_i} + I_{mm_n} \quad (5.7)$$

$$I_{mm} = I_{bm_n} + \sum_{i, i \neq n}^6 I_{mm_i} . \quad (5.8)$$

where n indicates the single, opposed duplex channel. In order to resolve severe MS \leftrightarrow MS interference it is necessary to determine I_{mm_n} and I_{bm_n} respectively. This can be achieved if an idle frame is introduced. This idle frame is also necessary to enable the opposed pair of TS’s to track the measurements of I_{mm} and I_{bm} after the resource units (RU’s) have been allocated. The duration of a multi-frame including one idle frame will depend on the maximum specified time for ‘service establishment’ and the maximum speed of a mobile in the TDD deployment environment. Let the maximum speed of a mobile be 3 km/h and assume that the shadowing will not change its characteristic within a range of about 1.5 m (obtained using the correlation model in [147] and assuming an average transmitter-receiver distance of 25 m and a correlation coefficient of $r = 0.95$), the time interval within which an idle frame is required will be 1.8 s. With a frame duration of 10 ms, the idle frame would need to occur every 180th frame. If not only an indoor scenario is considered, but also a higher mobility environment with, for example, a maximum speed of 50 km/h under the same propagation conditions, the idle frame would have to occur after every 20th frame. In the event of an idle frame in cell n which is the only cell with opposed synchronisation, (5.7) and (5.8) become,

$$I_{bm_{idle}} = \sum_{j, j \neq n}^5 I_{bm_j} \quad (5.9)$$

$$I_{mm_{idle}} = \sum_{j, j \neq n}^5 I_{mm_j} , \quad (5.10)$$

and subtracting (5.9) from (5.7) and (5.10) from (5.8) gives:

$$I_{mm_n} = I_{bm} - I_{bm_{idle}} \quad (5.11)$$

$$I_{bm_n} = I_{mm} - I_{mm_{idle}} , \quad (5.12)$$

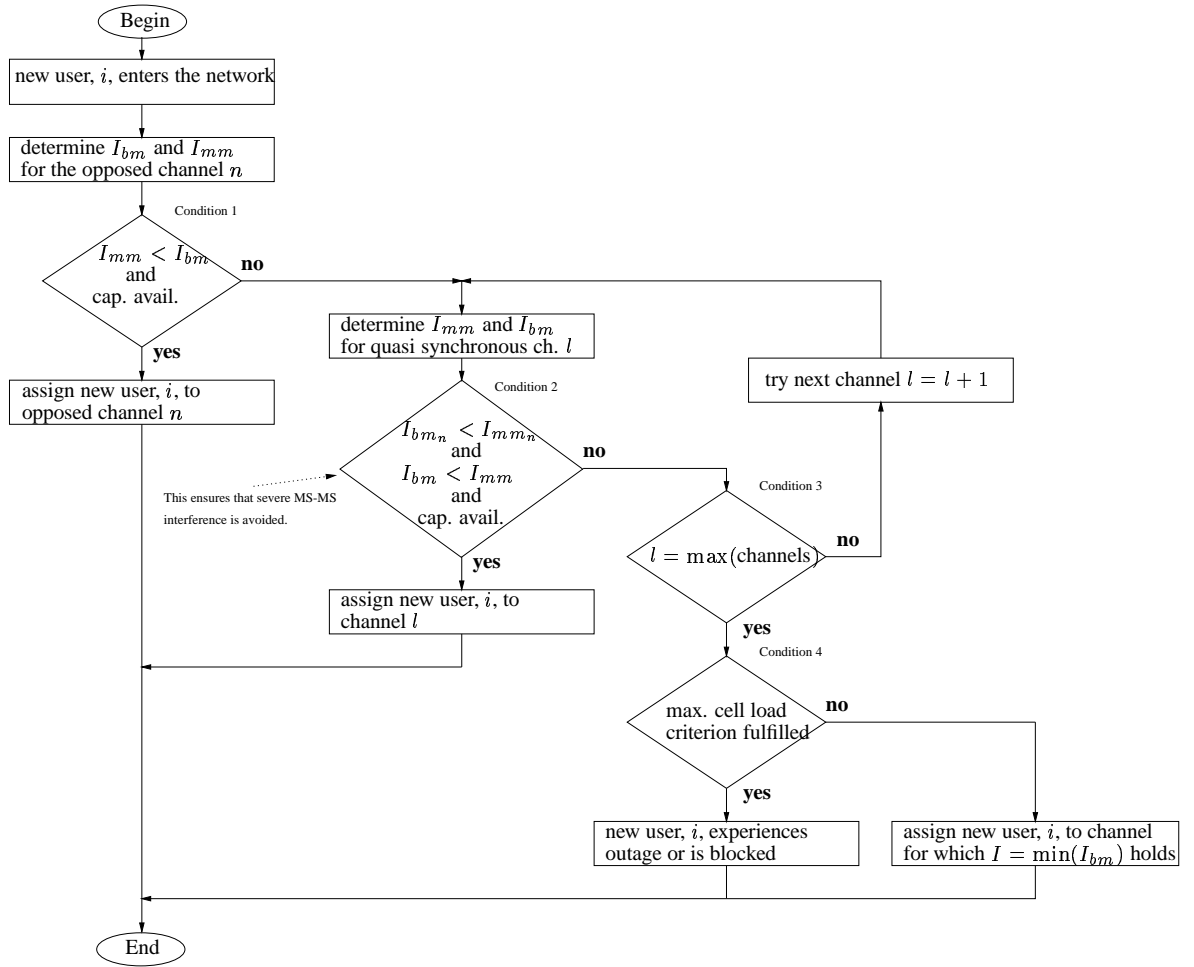


Figure 5.4: Decentralised DCA algorithm exploiting the TS-opposing technique.

and consequently,

$$I_{mm} = I_{mm_{idle}} + I_{mm_n} \quad (5.13)$$

$$I_{bm} = I_{bm_{idle}} + I_{bm_n} . \quad (5.14)$$

5.4 TS-opposing algorithm

The concept presented in the previous section represents the foundation for the decentralised DCA algorithm depicted in Figure 5.4. This DCA algorithm is operated as a fast DCA according to [163]. Due to the novel TS arrangements, the DCA algorithm is enabled to exploit an additional degree of freedom which is generated by the opposed TS's. This means that an

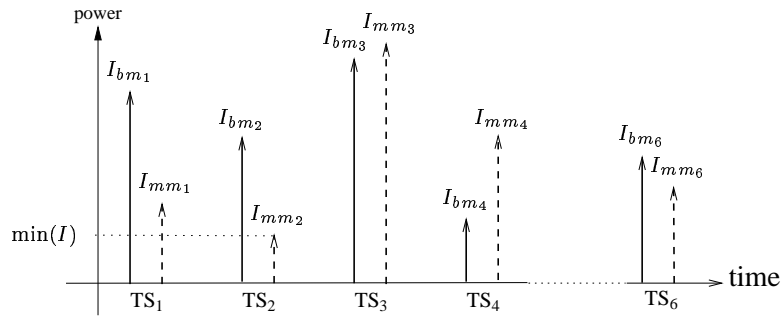


Figure 5.5: Interference vectors for an arbitrary location within cell 0. It is assumed that a channel consists of at least two TS's, one for the uplink and one for the downlink.

arbitrary location is characterised by an interference vector of two components as depicted in Figure 5.5. The property of each interference component is that the source of the interference (BS or MS) is the same. The DCA algorithm basically chooses a channel for which the lower interference component applies.

Moreover, the DCA algorithm (in particular the second condition) in Figure 5.4 ensures that MS→MS interference is always smaller than BS→MS interference. Hence the problem of MS↔MS interference inherent in a TDD system is eased so that its effects are less of an issue than BS→MS interference.

Each time a MS enters the network I_{bm} and I_{mm} are measured. First, it is calculated which of I_{mm} and I_{bm} is smallest, for the channel with opposed synchronisation. If I_{mm} is smallest, the MS requests to be allocated to the opposed channels provided that spare capacity is available. If however spare capacity is not available or I_{mm} is greater than I_{bm} , the MS assesses one of the ‘quasi synchronous’ channels. This means that exactly one neighbouring cell, n , transmits and receives opposed to the cell of interest (COI). The interference components conveyed by cell n , I_{mm_n} and I_{bm_n} , are calculated as described in section 5.3. If $I_{bm_n} < I_{mm_n}$ and $I_{bm} < I_{mm}$ the MS is allocated to the observed channel. In addition, this mechanism ensures that severe MS↔MS is prevented. If however the two conditions are not fulfilled, the same procedure is carried out for the next ‘quasi synchronous’ channel, $l + 1$, until the end is reached. If the two conditions above are still not fulfilled, the MS allocates itself to that ‘quasi synchronous’ channel for which $I = \min(I_{bm})$ holds.

5.5 System model

The simulation platform as described in section 3.4 is used to carry out Monte Carlo simulations of the DCA algorithm depicted in Figure 5.4. The cells will be populated under the following conditions:

- Non-optimal power control.
- Mobiles allocated to the best serving BS.
- Handover margin of 5 dB.
- Correlated shadowing according to a model by Klingenbrunn [147].
- Symmetrical speech service.
- 7-cell cluster with the COI in the centre.

In a CDMA system it is important that a MS is allocated to the best serving BS (in terms of received signal power) rather than the closest BS as otherwise the interference may increase by up to a factor of 20 as reported by Viterbi [27]. In this research, therefore, a simulation model is created where the MS's are allocated to a BS based on the minimum path loss criterion. In this context, however, in a real system a MS cannot always be assigned to the BS offering the lowest path loss due to handover imperfections. Thus, a handover margin as described in section 3.3.3 is considered. Furthermore, when assigning a MS to the best serving BS regardless of its location, situations may arise where a MS actually is located outside the cell from which it is served due to lognormal shadowing. This behaviour is accounted for by the introduction of a second cell radius, $d_{1_{max}}$, as depicted in Figure 5.6. With the radius $d_{1_{max}}$ the scope of a cell in terms of coverage can be expanded to cater for a more realistic scenario that MS's or BS's do not have knowledge about the actual cell boundaries. Instead, the path loss is the factor which determines which BS is to be used.

Again, as in chapter 4, the indoor office test environment described in [149] is used which gives the following relationship for the path loss, a , in terms of the transmitter-receiver separation distance, d , the number of floors, p , and the lognormal random variable (RV) ξ to model shadowing effects :

$$a = 37 + 30 \log_{10}(d) + 18.3 p^{\left(\frac{p+2}{p+1} - 0.46\right)} + \xi \text{ [dB]} . \quad (5.15)$$

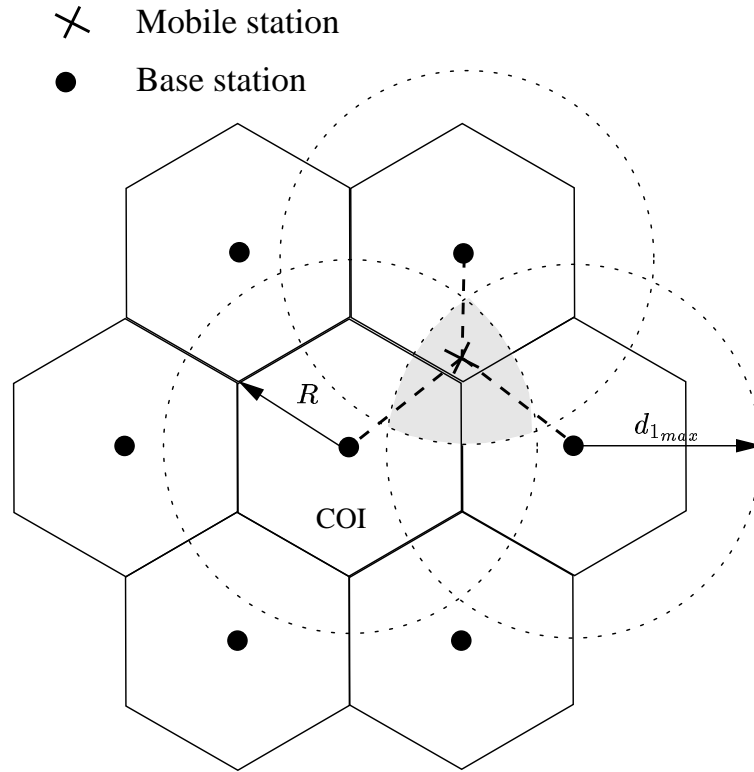


Figure 5.6: *Simulation environment: The DCA algorithm is operated at the cell of interest (COI). The first tier of cells is equally populated and handover regions (grey shaded area) are considered so that MS's can be allocated to the best serving BS.*

5.5.1 Uplink

For an arbitrary user i the bit-energy to interference ratio ε_i^u at the BS may be denoted as,

$$\varepsilon_i^u = \frac{\frac{P u_i^u}{R}}{\left(\sum_{j:j \neq i}^M \frac{P u_j^u}{W} \right) + I_o^u + N_0}, \quad (5.16)$$

where $P u_i^u$ is the received signal power from the desired user i , R is the information bit rate, W is the total bandwidth, I_o^u is the other-cell interference density and N_0 is the thermal noise density. It has been demonstrated in [26] that ε_i^u needs to be considered as a RV due to multipath propagation and power control imperfections. In addition, it was shown by Viterbi [26] that ε_i^u can be approximated by a lognormal RV with mean μ_ε^u and standard deviation σ_ε^u . Each time a new user enters the cell, the bit-energy to interference ratio of each user will be affected and some MS's may not be able to maintain the required threshold, and hence experience outage or a degradation in performance. Therefore, dynamic power control is assumed to maintain the required ε_i^u for each user i . Solving (5.16) for $P u_i^u$ and multiplying with the respective path

loss yields the carrier power for user i as follows:

$$Pc_i^u = a_i \varepsilon_i^u R \left(\sum_{j:j \neq i}^M \frac{Pu_j^u}{W} + I_o^u + N_0 \right). \quad (5.17)$$

From (5.17) it can be seen that any change in the desired power, (Pu_j^u) affects the transmitted power of all other MS's. With the substitutions of: $\gamma = \frac{R\varepsilon_i^d}{W}$, $I_b = W(I_o^u + N_0)$ and using matrix notations, (5.17) has been solved in section 4.3.1 resulting in (4.42).

5.5.2 Downlink

It has been demonstrated in [80, 91] that downlink power control in a cellular CDMA network is required in order to reduce interference, in particular for MS's located at outer regions of a cell. In addition, in [92] it has been reported that downlink power control is only effective if it is combined with some handover strategy.

For a TD-CDMA/TDD cellular network in general, and UTRA-TDD in particular, downlink power control seems to be required even more as BS's can interfere with each other and thereby affect the uplink performance (this is more precisely described in section 4.3.1 with (4.52)). In an investigation by Povey [109] it was found that BS \leftrightarrow BS interference is a severe problem in a TD-CDMA/TDD system. This, however, is primarily because only a simple downlink power control mechanism was assumed in that study.

In this analysis two different downlink power control algorithms are applied in order to assess their impact on system performance when using the new decentralised DCA:

- The first downlink power control approach is C/I based in which the code power for each mobile is adjusted so that: $\varepsilon_i^d \geq \varepsilon^d$ for all $i = 1, \dots, M$, where ε^d is the required bit-energy to interference ratio at the MS.
- The second downlink power control algorithm is related to the distance based algorithm as proposed in [80] and [164, Chapter 9]. Since distance based algorithms only function in low shadowing environments a modification is made to incorporate lognormal shadowing. Hence, the carrier power in the downlink is determined by that MS which experiences the highest path loss. The same code power is then applied to every other user. This algorithm is more precisely described in section 3.3.2.2.

```

BEGIN
Add new user,  $i$ , to the COI
if user  $i$  is blocked
    CellLoadMaxIdentifier++
    increment blocking counter,  $Bl$ :  $Bl = Bl + 1$ 
    if CellLoadMaxIdentifier == 10
        LoadStatus = MaxCapacityReached
         $Bl = Bl - 10$ 
    end if
else
    CellLoadMaxIdentifier=0
     $M = M + 1$ 
end if
END

```

Figure 5.7: Blocking and maximum cell load criterion.

5.5.3 Capacity and Blocking Definitions

The novel TS assignment as described in section 5.3 ensures that every cell has the same number of quasi-synchronous and opposed channels. Due to this symmetry, the performance of the DCA algorithm is evaluated for a single cell, the COI, whilst the neighbouring cells are being uniformly populated. The traffic load in the first tier of cells is varied. For a constant load in the neighbouring cells, the capacity (number of instantaneously active MS's) in the COI is determined by successively adding new users. The strategy as to how a new MS is allocated is such that an already established connection has higher priority than a new access attempt (resulting in user blocking in favour of outage). Therefore, if for any i , $i = 1, 2, \dots, M$ it is found that $Pc_i^u > Pc_{max}^u$ or $Pc_i^d > Pc_{max}^d$, the new MS cannot be assigned and is blocked for the respective TS's (function of the admission control). Due to the interference limited nature of CDMA a hard limitation of the number of users seems inappropriate. Therefore, in this analysis the 'maximum cell load criterion' (Figure 5.4) is defined as follows: the cell is considered to be fully loaded if a predefined number of consecutive blocking events have occurred. The number of permitted consecutive blocking events can be considered as a measure of the quality of service (QoS) and is set to 10. This parameter can be used to trade-off QoS and capacity. The mechanism to determine the maximum capacity and the resulting blocking is described with the algorithm in Figure 5.7.

From the total number of users obtained by the procedure described by the pseudo code above,

the average capacity in bit/(s·TS·cell) can be calculated. It is assumed that the data rate of each MS is the same. Then, the average capacity yields:

$$\overline{C} = \frac{R \sum_{i=1}^Q M_i}{Q}, \quad (5.18)$$

where Q is the number of Monte Carlo runs and M_i the maximum number of users for a single Monte Carlo run. Similarly, the average blocking is determined as:

$$\overline{Bl} = \frac{\sum_{i=1}^Q Bl_i}{Q}. \quad (5.19)$$

It must be stressed that blocking as defined above is dependent on the total maximum number of distributed MS's at the COI. The maximum number of distributed users at the COI is held constant, but it is varied in the first tier of cells.

The average capacity and blocking figures are used to compare the performance of the new DCA strategy with a system having a TS configuration such that all entities throughout the entire network transmit and receive at the same time. This means that only other entity interference is present and thus this configuration represents an equivalent FDD system. The parameters used for the simulation are based on [12], but modified as a consequence of the UTRA-TDD standardisation process. The principle parameters are summarised in Table 5.1.

Parameter	Value
TDD cell radius	50 m
Max MS TX power, $P_{c_{max}^u}$	15 dBm
Max BS TX power, $P_{c_{max}^d}$	21 dBm
Mean of ε , μ_ε^u	3.5 dB
Std. dev. of ε , σ_ε^u	2.5 dB
Std. dev. of lognormal shadowing, ξ	10 dB
Information bit rate, R	16 kbps
Bandwidth, W	4.68 MHz
Handover margin	5 dB
Total effective thermal noise density, N_0	169 dBm
Number of floors, p , in (5.15)	2

Table 5.1: *Simulation parameters used to assessing the performance of the combination of the novel TS assignment plan and the decentralised DCA algorithm.*

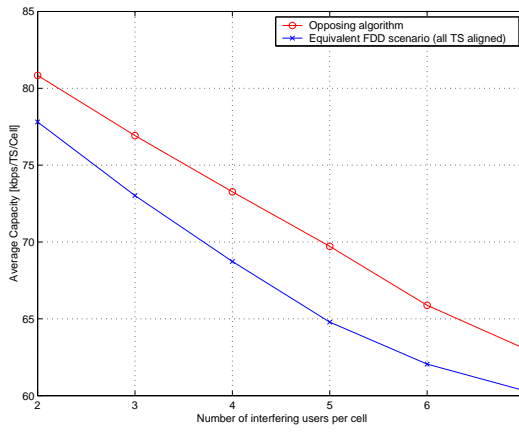
5.6 Results

When a new MS enters the network the aim is to assign it to the best serving BS. Due to handover imperfections and lognormal shadowing the best serving BS may not be located in the cell in which the MS resides. In order to account for this mechanism, two scenarios are investigated. The first scenario is where the MS allocated to a cell is bound within a circle specified by the radius $d1_{min}$ (Figure 5.6) which has an area approximately equal to that of the hexagon, *e.g.* a hexagon with radius of 50m corresponds to a circle with radius $d1_{min} \approx 45\text{m}$. The second, more realistic, scenario is that a MS can be located outside the respective cell, but still be served by the BS in the centre. This is arranged by setting $d1_{min}$ such that it exceeds the cell radius. Thus, in the second scenario $d1_{min}$ is set to 75 % of the distance between two BS's, which for a cell radius of 50m results in $d1_{min} \approx 65\text{m}$. The results of the DCA algorithm for these scenarios and two different DL (downlink) power control methods are depicted in Figure 5.8.

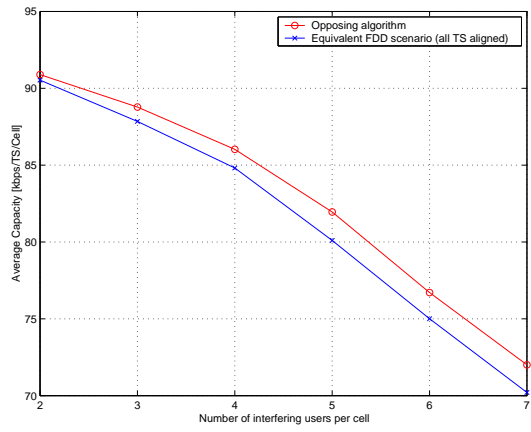
For all cases investigated the combination of the novel TS plan and the new distributed DCA algorithm performs better than an equivalent FDD scenario. This is a most important result. It was shown for a single cell scenario (section 4.2) that the capacity of a CDMA/TDD interface can, in principle, be greater than that of an equivalent CDMA/FDD interface. However, the disadvantage was that the DCA algorithm changed the uplink and downlink assignment of a TS which, in turn, effected the interference in the neighbouring cells. This disadvantage is eliminated here by the use of fixed TS assignment.

For the simple DL power control scheme the proposed method increases the capacity by up to 8 %. This is reduced to 5 % if the more sophisticated DL power control method is applied. Therefore, not only does the decentralised DCA algorithm achieve better capacity results, but it also can compensate for a poor DL power control algorithm.

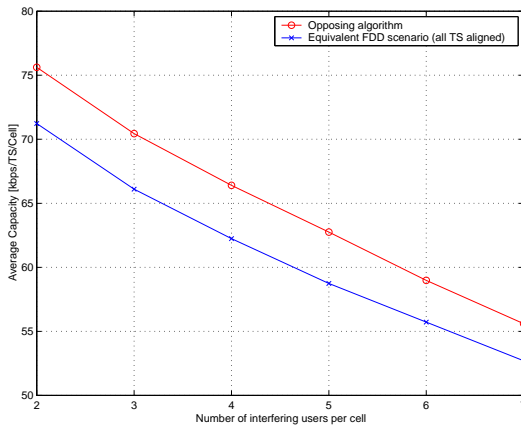
Note, as the DCA is operated in a decentralised manner, the decision of which TS's are to be used is made at a single end of the communication link ignoring the interference situation at the other end (at the BS). In addition, if the maximum path loss based DL power control method is applied, it can be derived from the results in section 3.3.3 that the BS \leftrightarrow BS interference at the opposed TS's will on average increase. This means that for the opposed pair of TS's the probability $Pr(I_{mm} < I_{bm})$ decreases. As a consequence the *relative* capacity improvement associated with the new DCA algorithm is expected to be less compared with the results of



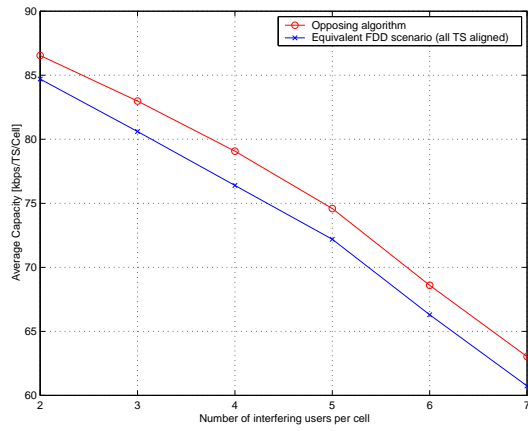
(a) Path loss based DL power control, $d1_{min} \approx 45m$



(b) C/I based DL power control, $d1_{min} \approx 45m$



(c) Path loss based DL power control, $d1_{min} \approx 65m$

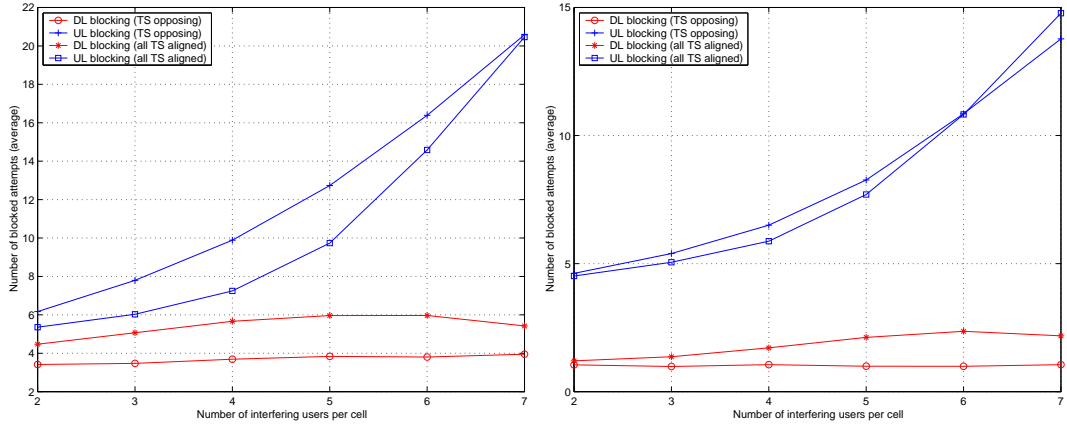


(d) C/I based DL power control, $d1_{min} \approx 65m$

Figure 5.8: Average capacity results of the decentralised DCA algorithm.

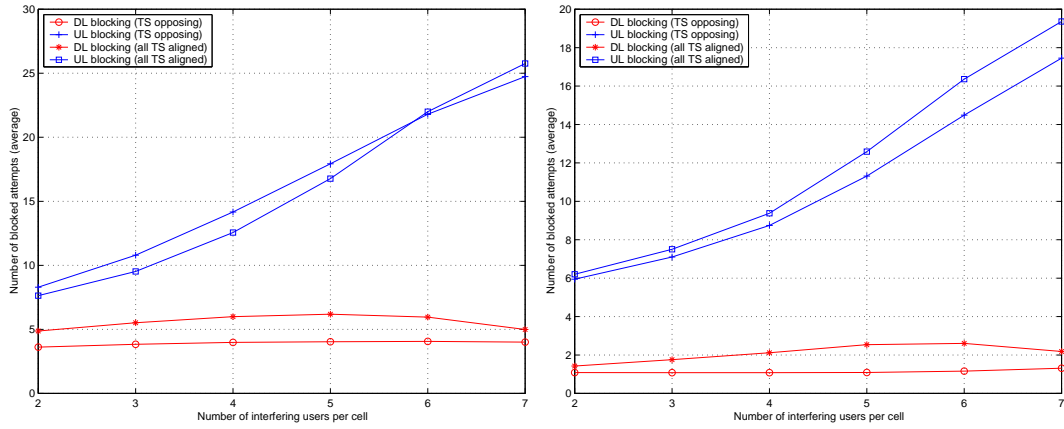
the C/I -based DL power control technique which minimises the transmitted power on the downlink. As the results reveal the opposite (8 % improvement for the simple DL power control compared with 5 % for the C/I -based DL power control algorithm), it can be concluded that the interference caused at the MS by a greater downlink power in the quasi-synchronous case is more detrimental than the greater BS \leftrightarrow BS interference at the opposed TS's. This is obvious because, with the cell topology applied, the distance between an interfering BS and any MS is always smaller than the BS-BS distance. Nevertheless, the *total* capacity improvement of the C/I -based DL power control algorithm, in all cases, is significantly greater than that of the simple path loss based DL power control technique. As an example, consider 4 interfering MS's using the decentralised DCA algorithm. The capacity as shown in Figure 5.8(a) and Figure 5.8(b) for the C/I -based DCA algorithm is about 18 % greater. This highlights the importance of a well designed DL power control algorithm as was also found in chapter 3. In the case that $d_{1_{max}}$ is increased from 45 m to 65 m, similar behaviour is found. In this case, however, the absolute capacity is reduced by about 5 – 10 % due to an increased interference. Although in this case the MS's are still assigned to the best serving BS (only limited by the handover margin) the probability of a greater path loss to the serving BS increases, resulting in a greater TX power and thus more interference. Note that in all scenarios investigated, the decentralised DCA algorithm performs better than an equivalent FDD system. This result is significant as a novel TS assignment plan enables the TDD system to account for full spatial coverage, too.

The blocking results are depicted in Figure 5.9. The noticeably high blocking is a consequence of the offered load being 7 simultaneously active users in the COI. In addition, the high blocking can be attributed to the use of the "blocking in favour of outage" strategy. It is interesting to note that uplink blocking in each scenario is higher than downlink blocking and that it increases with the load in the neighbouring cells, whereas downlink blocking is not a strong function of the number of distributed users. This is primarily due to the uplink being a multi-point to single-point transmission scheme and, in contrast, the downlink being a single-point to multi-point transmission scheme. Therefore, if the interference at the BS is at a high level all users are affected and this increases blocking as defined here. On the other hand, a single MS might require the BS to transmit high power, but the probability that this is the case for all randomly located MS is small and thus blocking is less likely than in the uplink direction. These results confirm the findings by other researchers that the uplink in a CDMA system limits the capacity [25, 26, 144]. However, the uplink and downlink cannot generally be treated as independent if



(a) Path loss based DL power control, $d_{1_{min}} \approx 45m$

(b) C/I -based DL power control, $d_{1_{min}} \approx 45m$



(c) Path loss based DL power control, $d_{1_{min}} \approx 65m$

(d) C/I -based DL power control, $d_{1_{min}} \approx 65m$

Figure 5.9: Blocking results of the decentralised TS-opposing algorithm.

TDD is employed. Since uplink and downlink are on the same frequency carrier both directions are coupled depending on synchronisation and asynchronous TS overlaps. This effect can be studied using the blocking results. If, for example, the results in Figure 5.9(a) and Figure 5.9(b) are compared it can be found that, although only the downlink power control algorithm is changed, the uplink blocking is greatly affected by the performance of DL power control. The reason for this is that the TS assignment plan used generates asynchronous TS overlaps which yield the strong coupling between uplink and downlink direction. However, it needs to be stressed that blocking and capacity are not independent, and as the capacity increases the probability of blocking is also affected. This is also why uplink blocking also decreases with a better DL power control algorithm in the case where all TS's are quasi-synchronous.

As expected, and demonstrated in Figure 5.9, the downlink blocking is significantly reduced by the decentralised DCA algorithm developed in this chapter. However, it also becomes clear that the total blocking is dominated by the uplink blocking which is about 4 – 10 times greater. Due to the nature of the decentralised DCA algorithm used, interference at the BS is not explicitly reduced. Therefore the uplink blocking is not improved. This proves to be a remaining problem.

In a further experiment it is assumed that each user requests a symmetric 64 kbps service. In this case a maximum of two users per cell and TS can be supported. The capacity results are summarised in Table 5.2 and blocking in Table 5.3.

$d1_{min} \approx 45m$ path loss based		$d1_{min} \approx 45m$ C/I-based		$d1_{min} \approx 65m$ path loss based		$d1_{min} \approx 65m$ C/I-based	
DCA	equiv. FDD	DCA	equiv. FDD	DCA	equiv. FDD	DCA	equiv. FDD
118.5	119.4	118.2	118.2	111.4	111.7	111.1	111.4

Table 5.2: Average capacity for the case of 2 users per cell/TS each with a data rate of 64 kbps.

The blocking in the uplink (UL) is presented in the first row of Table 5.3. Similarly, the row marked with DL presents the blocking in the downlink. As own-cell interference decreases

	$d1_{min} \approx 45m$ path loss based		$d1_{min} \approx 45m$ C/I-based		$d1_{min} \approx 65m$ path loss based		$d1_{min} \approx 65m$ C/I-based	
	DCA	equiv. FDD	DCA	equiv. FDD	DCA	equiv. FDD	DCA	equiv. FDD
UL	5.1	3.5	4.5	3.8	6.7	5.8	6.0	6.0
DL	0.1	0.7	0.4	0.7	0.2	1.0	0.3	1.1

Table 5.3: Average number of users blocked for the case of 2 users per cell/TS each with a data rate of 64 kbps.

with the number of users, the total capacity increases. Moreover, for the same reason, the effect of a tighter downlink power control algorithm is reduced. The gain of the proposed DCA algorithm with respect to capacity is diminished for the case of 2 high data rate users per cell. Once again, the reason that the DCA algorithm for a symmetric data rate of 64 kbps performs worse than for a symmetric rate of 16 kbps can predominantly be attributed to outage in the uplink due to a decreased processing gain.

Again from Table 5.3 it can be seen that uplink blocking is greater in the case of opposed TS's, but downlink blocking is significantly reduced.

5.7 Conclusions

A new distributed DCA algorithm exploiting the TS-opposing technique has been investigated. In addition, a fixed TS assignment was developed. Special emphasis was placed on ensuring ease of implementation. It was predominantly assumed that channel asymmetry is achieved by code pooling rather than TS pooling. The very important result is that this technique can result in higher capacity than an equivalent FDD system, even for a multiple cell environment. A further important result is that the DCA algorithm ensures that severe $MS \leftrightarrow MS$ is avoided.

The proposed DCA algorithm helps to abate a tight requirement on DL power control, but the relative capacity improvement obtained by using the DCA algorithm is less than the improvement which can be obtained by using a C/I -based DL power control algorithm instead of a path loss based DL power control method. Furthermore, the uplink and downlink direction are strongly coupled in a TD-CDMA/TDD interface if asynchronous TS overlaps occur. Therefore, an isolated treatment of either direction may produce unrealistic results.

A possible drawback is that the decentralised DCA algorithm does not minimise the interference at the BS. However, it has been demonstrated that the impact of interference at the BS can be more severe than at the MS's since several links are affected simultaneously. Hence, the uplink direction prevents to fully exploit the potential interference reduction capabilities of the decentralised DCA algorithm. This important finding may be used in further investigations of decentralised DCA techniques which make use of the novel TS-opposing principle. It may, for example, be interesting to study the effects of a combined decentralised and centralised DCA algorithm where the decentralised DCA algorithm is basically the same as presented in this chapter. When using the same algorithm at the MS and BS, conflicting decisions regarding the

best channel selection may arise which would need to be arbitrated by an additional algorithm.

If own-cell interference is reduced by, for example, joint-detection it is anticipated that the performance of the DCA concept presented in this chapter is further improved. This may be addressed in further research.

Chapter 6

Conclusions

The aim of this chapter is threefold: Firstly, a summary of the work that has been conducted in each of the previous chapters is presented. Secondly, the main conclusions that can be drawn from the novel findings and their exploitation are highlighted. Finally, the limitations of this work and further research options are outlined.

6.1 Summary

Chapter 1 described the key aim of cellular wireless communication systems which is to maximise the capacity per unit area of a limited radio resource. This has led to different multiple access methods with code division multiple access (CDMA) being the technique which fulfils the maximisation criterion best. In addition different channel modes were discussed (simplex, half duplex and full duplex). It was shown, that, although time division duplex (TDD) is a full duplex mode, it is based on the half duplex principle. Therefore, the TDD technique was deemed well suited to cater for asymmetric traffic of future data oriented services.

Chapter 2 discussed multiple access techniques focusing in particular on CDMA. It was shown that interference from other cells can offset the gains obtained by techniques that reduce multiple access interference (MAI). In addition, an overview of the TDD technique and its advantages and disadvantages was presented. In this context, results of an investigation of the TDD underlay concept carried out by the author were presented. These results confirmed the feasibility of the TDD underlay concept provided that certain constraints regarding the location of the base stations (BS's) are maintained. Another issue highlighted was how the ability of TDD to cater for channel asymmetry is compensated by additional interference mechanisms which create additional other cell interference in a cellular CDMA/TDD network. If CDMA is combined with the time division multiple access (TDMA) technique, dynamic channel assignment techniques may be used to avoid severe interference. A hybrid TDMA/CDMA-TDD interface, which is referred to as TD-CDMA/TDD, is used for the Universal Mobile Telecommunications

System (UMTS). This interface was described briefly. Finally, different DCA approaches were presented.

Chapter 3 addressed the interference issues of a CDMA–TDD air interface. In particular, adjacent channel interference (ACI) was investigated since this type of interference is considered to create a significant problem in a CDMA–TDD system if the same frequency is used in every cell (frequency re–use of one) and only a single carrier is available for any one operator. Furthermore, frame synchronisation to the cells of a co–operator could not be assumed. The pole capacity of such a system for ideal and non–ideal power control was calculated. Furthermore, a novel performance measure was introduced which is the capacity relative to a single, isolated and thus non–interfered cell. The relevant equations allowed for the study of the impact of power adjustments on capacity. An interference model for synchronisation errors in a TDD system was developed. Moreover, the probability density function (pdf) for interference from a neighbouring cell was derived assuming ideal power control and a propagation model that included lognormal shadowing. This pdf was used to verify a static Monte Carlo system simulation platform which was used to study two deployment scenarios: a) a hot spot scenario with only a single interfering cell and b) interference of a multi cell network. The effects of different base station (BS) separation distances and different frame synchronisations were investigated. It was found that the interference caused by the downlink renders co–location of BS’s difficult. In addition, this investigation led to the important discovery that ideal synchronisation is not always the ideal scenario in terms of interference powers. The same result was confirmed by the ACI study of a multiple interfering cell scenario. With the aid of the cellular network model, the impact of handover and downlink power control was investigated. It was found that these functions have a vital impact on system performance. In addition, it became clear that only the joint use of both techniques will eventually increase the capacity of the system investigated. Finally, co–channel interference for the system described was studied with the aim of confirming the validity of the finding that ideal synchronisation does not always yield the highest capacity. It was found that in 25%–41.7% of all cases it is more advantageous to apply opposed transmission with respect to the BS location. Furthermore, the results revealed that interference between mobile stations was not a significant issue. The remainder of this thesis was aimed at exploiting these key findings.

In chapter 4 the novel finding of chapter 3 which was that in 25%–41.7% of all scenarios it is more advantageous to apply opposed synchronisation, was exploited by developing centralised,

interference based DCA algorithms [152]. Since opposed synchronisation was to be exploited the new process was termed 'time slot (TS) opposing technique'. The approach was twofold: firstly, a TS opposing algorithm was applied to a single cell in order to identify upper bounds for the network performance. The results revealed that the capacity of a TDD network could be 48 % greater than that of an equivalent FDD network when using the TS opposing technique. If 10 dB static shielding between BS's could be achieved, the gain was even greater with a maximum of 118 %. These performance gains clearly represented an upper bound since the capacity maximisation was restricted to merely a single cell neglecting the mutual effects on the neighbouring cells. Secondly, the system model was refined so as to assess the network performance rather than the ideal performance of a single cell. The system investigated was first described mathematically which resulted in two novel system equations. The model revealed that uplink and downlink in a TDD system can be strongly coupled with the consequence that a poor downlink power control algorithm can have a severe impact on the uplink performance. Based on the system model which included all interference sources, a simulation environment consisting of 4 indoor cells was created. In addition, dynamic, C/I -based power control in the downlink was considered. A novel centralised DCA algorithm was developed and applied to the system model. The system performance was evaluated for four scenarios of different channel asymmetry between neighbouring cells. It was found that the novel centralised DCA algorithm prevented capacity losses as a consequence of different channel asymmetries in neighbouring cells. This result was significant since it had generally been assumed that in a cellular TD-CDMA/TDD network each cell needed to adopt the same rate of asymmetry in order to avoid severe interference. For instance, Holma [6, p. 301] writes: "Cell-independent asymmetric capacity allocation between uplink and downlink is not feasible for each cell in the coverage area".

Chapter 5 investigated the TS opposing technique when applied to a decentralised DCA algorithm. The aim was to simplify the measurement of the interference components from BS's and MS's by introducing idle slots. Cases of severe interference between MS's were arbitrated by the DCA algorithm. Furthermore, the complexity of the TS switching process was to be eliminated. The approach taken was to combine fixed channel assignment (FCA) with DCA where the direction of transmission (uplink and downlink) of TS's was pre-defined. Therefore, a new TS assignment scheme was developed. The aim was to fulfil three basic requirements: a) full spatial coverage, b) maintain a frequency (and TS) re-use of one and c) enable a DCA to exploit the TS opposing technique. The respected TS assignment plan consisted of 7 full duplex

channel utilising 14 TS's. The uplink and downlink directions were permanently assigned according to a novel TS assignment scheme [153]. This enabled the TS opposing technique to be used at the mobile entities. The disadvantage was the requirement of TS planning. A decentralised DCA algorithm was developed which was applied to the cellular network. Dynamic, C/I -based power control in the downlink was assumed. The key result was that the system performed better than an equivalent FDD system for low bit rate users — most importantly, this could be demonstrated for a cellular network. However, in the case of two MS's per TS where each required 64 kbps, the performance of the TDD system and an equivalent FDD system were found to be approximately the same. This could be attributed to the basic findings of the co-channel interference study of chapter 3. In this chapter, it was observed that the probability of interference from BS's being greater than interference from MS's, has a maximum at the centre of the cell which is the exact location of the BS. Since the decentralised DCA algorithm tries to minimise interference solely at the downlink direction, the uplink represents the capacity limiting direction (since there is no interference avoiding mechanism in this direction). This particularly holds in the case of high bit rate users where the processing gain is small.

6.2 Conclusions

The pdf of interference from the MS's in a neighbouring cell has been derived analytically. This function can be used to analyse many interference related issues of cellular networks. It provides an ideal means to study the effects of relevant system parameters such as, for example, the level of the desired signal power at the receiver or the impact of the path loss exponent.

In this thesis it has been shown that in a CDMA/TDD based system not only a tight power control algorithm in the uplink is required, but also a well performing power control algorithm in the downlink. This is primarily due to the potential coupling of uplink and downlink channels as both are at the same radio frequency carrier.

The investigation of ACI in a hybrid TD-CDMA/TDD interface using UMTS related parameters has revealed that a significant capacity reduction might be obtained for co-sited BS's. The capacity reduction has been found to be more than 20% if an adjacent channel protection factor of less than 40 dB and synchronisation errors of more than 10% are used. From this result it follows that adjacent channel protection factors greater than 40 dB or precise frame synchronisation are required if co-siting is to be used. However, in practice frame synchronisation

between adjacent carriers is considered to be difficult to achieve.

To the author's best knowledge it was shown for the first time that in a TD-CDMA/TDD network opposed synchronisation of TS's results in less interference for 25%–41.7% of all possible uniform user distributions. This finding has an important implication with respect to achieving cell independent asymmetry in a cellular TD-CDMA/TDD network. It was shown that cell independent asymmetry in a TD-CDMA/TDD system can be achieved without a significant capacity reduction. This enables such a cellular system to exploit this TDD inherent advantage without the accompanied potential disadvantage of greater interference.

The novel finding of systematically applying opposed synchronisation has been used to show that a TD-CDMA/TDD cell can achieve greater spectral efficiency than an equivalent FDD cell. It has also been demonstrated that the spectral efficiency of a cellular TD-CDMA/TDD system can be greater than that of an equivalent FDD system. This has been shown for symmetric channels.

The centralised DCA algorithm proved to be a powerful means to permit cell independent asymmetries without a significant capacity loss. The disadvantage is the operational complexity associated. The decentralised DCA algorithm proved to be a powerful compromise between fixed channel assignment (FCA) and DCA strategies. It was shown that TDD inherent properties (TS opposing) can still be exploited so as to avoid high other-cell interference. The advantage of this type of DCA is its simplicity with regard to the implementation. The results of two totally different DCA algorithms using the same principle (TS opposing technique) demonstrate that the use of this technique is not limited to a specific scenario. Furthermore, it is found that a DCA algorithm acts as a key function in order to exploit the flexibility of the TD-CDMA/TDD air-interface.

6.3 Limitations and Future work

The results in this research were generated using a series of mathematical models and computer simulations. They are therefore subject to certain limitations in connection with the assumptions supporting the models and simulations used. These limitations are outlined further below:

The interference analyses were based on static system simulations. The author recognises that this model has its weaknesses, for example, with regard to user mobility and real time power

control. The static models, however, provided a good insight into the system with respect to the sensitivity to system functions such as power control and handover. It is further recognised that the system performance of a TD-CDMA/TDD is dependent on a variety of parameters (*e.g.* bit-energy to interference ratio, processing gain, power budgets, cell radii). In particular, the required bit-energy to interference ratio has a significant impact on the maximum system capacity. For this reason it was difficult to generate absolute statements which means that the results are largely scenario specific. For the investigated scenarios, however, clear statements could be made. It was found that BS \leftrightarrow BS interference renders co-siting of BS difficult. However, as this is the most cost-efficient deployment scenario, interference cancellation algorithms or antenna beamforming algorithms may be an interesting field for further study. Furthermore, it was shown by the author that the TDD underlay is an interesting technique to enhance capacity in a dual mode TDD and FDD air interface with harmonised air-interface parameters. Interference issues cause tight constraints with respect to the location of BS's. Once again, techniques to circumvent high interference, including ODMA (opportunity driven multiple access) techniques, will result in relaxing the tight geometrical constraints.

The proposed centralised DCA algorithms made use of the separate measurement of the sum of interference from BS's and the sum of interference from MS's. A method of calculating the individual interference components was proposed. This method requires the interfering cells to be part of the same network. In case of ACI this is not guaranteed since the adjacent carrier might belong to another operator. Therefore, it may be interesting to develop new methods to separately measure the interference contribution from BS's and MS's. Current research at the University of Edinburgh addresses this issue. Moreover, a limitation of this investigation is the underlying assumption of a simple receiver structure. Further research may concentrate on studying the performance of the TS opposing algorithm assuming different types of receiver and coding techniques. In particular, if the impact of own-cell interference is reduced or almost eliminated it is anticipated that the DCA algorithm results in further improvements. An additional point of interest is the question of how the centralised TS opposing algorithm interacts with a decentralised DCA. Furthermore, the process of opposing TS's requires an additional signalling overhead, the extent of which may be interesting to investigate. Although centralised DCA algorithms are envisaged to perform best in low mobility or fixed wireless environments, the effect of various user mobility scenarios and uneven traffic distribution scenarios on the performance of the centralised TS opposing algorithm may represent a way forward to obtaining further knowledge about this technique. In addition, it seems promising to combine the DCA

proposed in [145] with the TS opposing technique.

The decentralised DCA algorithm was designed to ease practical implementation by supporting the interference measurements by a novel TS assignment scheme and idle slot periods. The respective algorithm aimed to minimise interference in the downlink. It became clear that the uplink is the critical path. Therefore, it would be interesting to apply the opposing technique decentrally, but aim at minimising the interference in the uplink. The MS could make use of the knowledge about the path loss and the required transmit power to estimate interference at the BS, or the BS might simply report this to the MS. The MS then has information about interference at the BS and at its own location and can thus use this to exploit the TS opposing technique. Furthermore, it would be interesting to evaluate the system performance for different cell sizes, shapes, number of TS's and deployment scenarios (non-uniformly distributed MS's).

All analyses in this thesis are primarily based on indoor propagation environments. Future research may apply the techniques developed in this thesis to different environments in order to further test these techniques.

It is clear that the flexibility of TDD poses challenges, but these can be exploited constructively in order to enhance the overall system performance. The feasibility of using a hybrid TD-CDMA/TDD air interface in a cellular environment has been demonstrated, emphasising that TDD, in addition, enables other techniques such as, for example, ODMA to co-exist. This technique is currently being investigated as part of another project at the University of Edinburgh.

Appendix A

Derivation of CDMA capacity by Viterbi

The desired signal power at the BS receiver given in (4.1) is:

$$P_u^u = \frac{I_o^u + N}{\frac{pg}{\varepsilon^u} + 1 - M_{FDD}} . \quad (\text{A.1})$$

Furthermore, own-cell interference is defined in (4.6) as follows:

$$I_{own} = P_u^u (M_{FDD} - 1) . \quad (\text{A.2})$$

Equation (A.1) is solved for $(M_{FDD} - 1)$ and modified equivalently by multiplying and dividing by I_{own} which yields:

$$(M_{FDD} - 1) = \frac{pg}{\varepsilon^u} - \frac{\frac{N}{I_{own}} + \frac{I_o^u}{I_{own}}}{P_u^u} I_{own} . \quad (\text{A.3})$$

The term $\frac{I_o^u}{I_{own}}$ equals the definition of f as the ratio of other cell interference to own cell interference in section 4.2.1. Replacing $\frac{I_o^u}{I_{own}}$ by f , substituting (A.2) where appropriate and making re-arrangements (A.3) becomes:

$$(M_{FDD} - 1) = \frac{pg}{\varepsilon^u} \frac{1}{\frac{N}{I_{own}} + f + 1} . \quad (\text{A.4})$$

In the following, the term $\frac{N}{I_{own}}$ in the denominator of (A.4) is eliminated and represented by a constant, c in the numerator:

$$\frac{c}{1 + f} \stackrel{\text{def}}{=} \frac{1}{\frac{N}{I_{own}} + 1 + f} . \quad (\text{A.5})$$

Solving (A.5) for c , using $f = \frac{I_o^u}{I_{own}}$ and carrying out a equivalent modification by adding and subtracting N in the denominator yields:

$$c = \frac{1 + f}{\frac{N}{I_{own}} + 1 + f}, \quad (\text{A.6})$$

$$= \frac{1}{1 + \frac{N}{(1+f)I_{own}}}, \quad (\text{A.7})$$

$$= \frac{1}{1 + \frac{N}{I_{own} + I_o^u + N - N}}. \quad (\text{A.8})$$

Subsequently, the definition of: $\eta = N/I$, where $I = I_{own} + I_o^u + N$, used in (4.7) of section 4.2.1 is substituted into (A.8),

$$c = \frac{1}{1 + \frac{1}{\frac{1}{\eta} - 1}}, \quad (\text{A.9})$$

$$= \frac{\frac{1}{\eta} - 1}{\frac{1}{\eta}}, \quad (\text{A.10})$$

$$= 1 - \eta. \quad (\text{A.11})$$

Finally, (A.11) is substituted into (A.5) and applied to A.4 which becomes:

$$M_{FDD} = \frac{pg (1 - \eta)}{\varepsilon^u (1 + f)} + 1. \quad (\text{A.12})$$

Thus, it holds:

$$M_{FDD} \leq \frac{pg (1 - \eta)}{\varepsilon^u (1 + f)}, \quad (\text{A.13})$$

which shall be demonstrated.

Appendix B

Publications & Patents

B.1 Published papers

- H. Haas and G.J.R. Povey, “Outage Probability of CDMA–TDD Micro Cells in a CDMA–FDD Environment”, Proceedings of the 1998 International Symposium on Personal, Indoor and Mobile Radio Communications (PIMRC 1998), (Boston USA), pp. 94–98, IEEE, September 8–11 1998
- H. Haas and G.J.R. Povey, “Additional Capacity of a CDMA/TDD Micro Cell Utilising the Uplink Frequency Band of a CDMA/FDD Macro Cellular Overlay”, Proceedings of the UMTS Workshop, (Schloss Reisingburg, Ulm, Germany), pp. 151–158, November 26–27 1998
- H. Haas and G.J.R. Povey, “A Capacity Investigation on UTRA-TDD Utilising Underused UTRA-FDD Uplink Resource”, IEE Colloquium on UMTS Terminals and Software Radio, pp. 7/1-7/6, April 26 1999.
- S.M. Heikkinen, H. Haas and G.J.R. Povey, “Investigation of Adjacent Channel Interference on the UTRA-TDD System”, IEE Colloquium on UMTS Terminals and Software Radio, pp. 13/1-13/5, April 26 1999.
- H. Haas, G.J.R. Povey, “A Capacity Investigation on UTRA–TDD Utilising Underused UTRA–FDD Uplink Resources”, Proceedings of the 2000 International Symposium on Personal, Indoor and Mobile Radio Communications (PIMRC 1999), (Osaka, Japan), 5 pages in CD–Rom (A6–4), IEEE, September 12–15 1999 (student paper prize winner)
- H. Haas and G.J.R. Povey, “The Effect of Adjacent Channel Interference on Capacity in a Hybrid TDMA/CDMA–TDD System Using UTRA–TDD Parameters”, Proceedings of the 1999 50th IEEE Vehicular Technology Conference (VTC 1999 Fall), (Amsterdam, The Netherlands), pp. 1086–1090, IEEE, September 19–22 1999
- H. Haas, S. McLaughlin and G.J.R. Povey, “The Effects of Inter–System Interference in UMTS at 1920 MHz”, Proceedings of the IEE International Conference on 3G 2000

Mobile Communication Technologies”, (London, UK), pp. 103–107, IEE, March 27–29 2000

- H. Haas, S. McLaughlin and G.J.R. Povey, “The Effects of Interference Between the TDD and FDD Mode in UMTS at the Boundary of 1920 MHz”, Proceedings of the 6th IEEE Symp. on Spread-Spectrum Tech. & Appli., (New Jersey, (USA)), pp. 486–490, IEEE, September 6–8 2000
- H. Haas, S. McLaughlin and G.J.R. Povey, “A Novel Interference Resolving Algorithm for the TDD TD-CDMA Mode in UMTS”, Proceedings of the 2000 International Symposium on Personal, Indoor and Mobile Radio Communications (PIMRC 2000), (London, UK), pp. 1231–1235, IEEE, September 18–21 2000
- H. Haas S. McLaughlin and G J R Povey, “An Investigation on Capacity versus Guard-Bands in the TDD Mode of UMTS”, Proceedings of the 2000 IEEE 51st Vehicular Technology Conference (VTC 2000 Fall), (Boston USA), 5 pages in CD-Rom, IEEE, September 21–24 2000
- H. Haas and S. McLaughlin, “A Novel Decentralised DCA Concept For a TDD Network Applicable for UMTS”, The IEEE Semiannual Vehicular Technology Conference (VTC 2001 Spring), (Rhodes Island, Greece), May 6–9 2001

B.2 Submissions to advisory bodies

- H. Haas and G.J.R. Povey, “An Investigation of Capacity versus Guard Bands within UTRA-TDD”, Report submitted to UK Third Generation Advisory Group (UKTAG), February 1999
- H. Haas and G.J.R. Povey, “Investigation of Adjacent Channel Interference in a TD-CDMA System”, Report submitted to UK Third Generation Advisory Group (UKTAG), February 1999
- H. Haas and G.J.R. Povey, “An Investigation of Capacity versus Guard Bands within UTRA-TDD”, Report submitted to UK Third Generation Advisory Group (UKTAG), March 1999

B.3 Patents

- H. Haas and G.J.R. Povey, “Apparatus, Method of and System for Improving Capacity in a Communications Network”, International patent application number: PCT/GB99/02223, 25. July 1998
- H. Haas and G.J.R. Povey, “Communications Networks”, UK application number: GB 9930089.9, 20. December 1999 (PCT filing will follow)
- H. Haas and S. McLaughlin, “TS Assignment Scheme with Novel DCA”, UK application number: GB 0017434.2, 14. July 2000

Outage Probability of CDMA-TDD Micro Cells in a CDMA-FDD Environment

H. Haas

G. J. R. Povey

The University of Edinburgh,
Department of Electronics and Electrical Engineering,
Signals & Systems Group
The King's Buildings, Mayfield Road, Edinburgh, EH9 3JL, UK
e-mail: hh@ee.ed.ac.uk

ABSTRACT

We investigated the feasibility of the coexistence of CDMA-TDD micro cells under a CDMA-FDD macro cell network with both sharing the same frequency band. A dynamic channel allocation (DCA) algorithm decides on the basis of mutual interference which FDD band is to use for the micro cell TDD channel. On the assumption of giving the macro cell higher priority we investigated the lower bound probability of total micro cell loss (outage) dependent on the distance between the micro and macro cell BS. We also considered wall loss at the boundary of the micro cell and studied the effect of different propagation conditions on the assumption of equally distributed macro cell subscribers. A mathematical model for outage is developed and the results are compared with simulations. The results reveal a good match between the theoretical approximation and the simulations. This, in turn, indicates that micro cell outage is mainly caused by a single macro cell mobile within a certain area around the micro cell BS. It can be seen that the outage goes up to about 15 % when the micro cell is located at the macro cell boundary. This value exponentially decreases when the micro cell is moved towards the macro cell BS. Walls around micro cells do have a significant influence on outage. It has been shown, that outage converges towards a value determined by the micro cell size.

I INTRODUCTION

In order to cope with the challenges of future personal communication systems (PCS) there is a growing interest in the investigation of intelligent network structures which enable the integration of many sophisticated services [1–3]. New mobile communication standards, such as e.g. “UMTS”, aim to cater for high- and low mobility user populations within an integrated system. The service of pure voice transmission will be complemented by services like data, video, fax, etc. This requirements combined with different environmental conditions point to hierarchical network concepts. However, frequencies which are exclusively allocated to a certain system but remain unused due to low traffic in that specific system represent an inefficient use of common radio resources. DS-SS as a multiple access technique uses the bandwidth more efficiently than TDMA and FDMA systems [4]. These systems are considered to use FDD for serving the duplex channel. Recently, there has been an increased interest in using TDD-SS for

low-mobility users within smaller cells. The combination of TDD and DS-SS has shown to be advantageous in respect to the receiver complexity [5, 6]. However, the benefits of TDD techniques will be reduced in environments with high Doppler shifts, which is shown in [7]. In two investigations [8, 9] these ideas are combined and a hierarchical system with the following properties is proposed:

- the macro cells use DS-SS combined with FDD.
- the micro cells make use of DS-SS and TDD, because they are intended to cover hot-spot areas which are usually located within buildings and, thus, assigned to users of low mobility.
- a DCA algorithm allocates the CDMA-TDD micro cell channel at either the FDD up-link or down-link band, so that least mutual system interference will be generated. It thereby exploits the asymmetry of up- and down-link capacity of a CDMA system.

Figure 1 illustrates this cellular system. The quality of the proposed architecture is derived from the rate of mutual interference. The four instances which can either be a source or a sink of interference are: micro cell mobile (indoor mobile), macro cell mobile (outdoor mobile), micro cell base station (indoor base station) and macro cell base station (outdoor base station). The consequences of BS losses are much worse because many communication links can be affected simultaneously. Combining the four instances it can be found that there are 10 possible link-to-link combinations of mutual interference. Four out of these cannot be directly resolved by the proposed DCA algorithm. They are:

1. Micro Cell BS – Macro Cell MS
2. Micro Cell BS – Macro Cell BS
3. Micro Cell MS – Macro Cell MS
4. Micro Cell MS – Macro Cell BS

In this paper we investigate the outage of case 1., i.e. the influence of a macro cell mobile to a micro cell base station. We, thereby, assume that the DCA algorithm gives the outdoor mobile higher priority and therefore is utilising the FDD up-link for an additional TDD channel. We further assume that a macro cell mobile might not be necessarily switched to the micro cell system because both networks can be run by different operators which do not allow handover, and that the outdoor mobile has no TDD option.

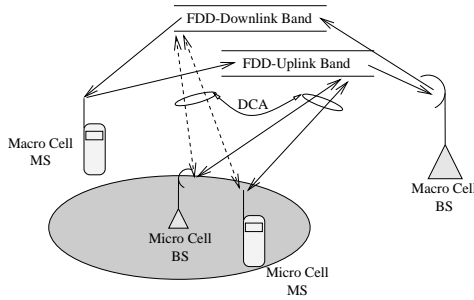


Figure 1: System Overview

II CELL TOPOLOGY ASSUMPTIONS

We consider one macro cell with the BS in the centre. Further we assume that no network planning will be carried out for the micro cells (e.g. the macro- and micro cells might not be run by the same operator). Furthermore the locations of the micro cells are places dictated by increased traffic. So, the distance between the inter network base stations is randomly distributed. Figure 2 gives an overview of the macro and micro cell model.

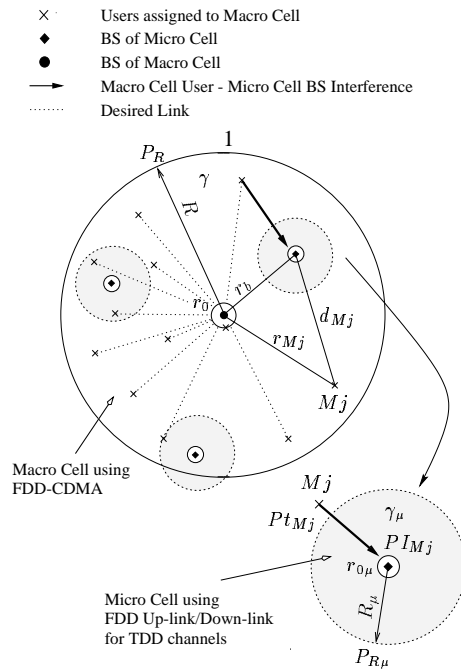


Figure 2: System Topology

For modelling the radio propagation we use a stationary path loss model described by [10, pp. 61–68]. The propagation con-

ditions are determined by two parameters: (a) the path-loss slope γ and (b) a reference power at a certain distance. Furthermore, we assume ideal power control in the up-link. Thus, the transmission power of any mobile in the outdoor environment yields

$$P_{tMj} = P_R \left(\frac{r_{Mj}}{R} \right)^\gamma \quad (1)$$

Where P_R is the transmission power required for a mobile located at radius R from the macro cell centre. R determines the macro cell boundary. r_{Mj} is the distance of mobile M_j from its base station. We normalise every distance to R . γ is the path-loss exponent of the outdoor environment. The micro cell is designated to cover hot-spot areas usually located within buildings. To cater for this circumstance we have introduced a second path-loss slope for the indoor cell in our propagation model. We also consider a specific attenuation at the macro cell boundary due to the walls. Thus, the interference power at the micro cell base station can be written as follows:

$$P_I = \sum_{j=1}^M \begin{cases} P_{tMj} \eta \left(\frac{r_{0\mu}}{d_{Mj}} \right)^{\gamma_\mu} & \text{if } d_{Mj} \leq R_\mu, \\ \frac{P_{tMj}}{\eta} \left(\frac{R_\mu}{d_{Mj}} \right)^\gamma \left(\frac{r_{0\mu}}{R_\mu} \right)^{\gamma_\mu} & \text{otherwise} \end{cases} \quad (2)$$

$r_{0\mu}$ defines a close in area around the micro cell BS in which a mobile is not expected in order to keep the propagation model valid. Thus, signals received at the indoor BS can be related to $r_{0\mu}$. d_{Mj} represents the distance between mobile M_j and the micro cell base station. η is the factor to compensate for wall loss. In order to obtain the lower bound of micro cell outage caused by users assigned to the macro cell system we assume a micro cell mobile at the boundary of its cell. Thus the carrier to interference ratio is given by

$$\left(\frac{C}{I} \right)_{min\mu} = \frac{P_{R\mu} \left(\frac{r_{0\mu}}{R_\mu} \right)^{\gamma_\mu}}{P_I} \quad (3)$$

$P_{R\mu}$ is the power required for a micro cell user at its cell boundary to communicate with the associated base station. R_μ denotes the radius of the micro cell. In order to determine the micro cell outage figures a threshold for $(C/I)_{min\mu}$ has to be determined. A general expression to obtain the lower threshold is given by

$$\frac{C}{I} = \frac{E_b}{N_0} \frac{1}{PG} \quad (4)$$

With a minimum of $E_b/N_0 = 5 \text{ dB}$ (see [4] for example) for error free voice transmission $(C/I)_{min\mu}$ is mainly derived by the applied processing gain. The value $(C/I)_{min\mu}$ will be referred to as *threshold*. In our simulations we assume a processing gain of 128 (21 dB)[11]. Subsequently, this value was increased to 256 to investigate the influence of the processing gain on micro cell outage. We further randomly distributed M mobiles within the macro cell. Totally we generated about 3000 random distributions for each geometrical configuration. From these statistical observations we derived the outage probability $Pr\{(C/I) < \text{threshold}\}$. Since we investigate the micro cell outage dependent on the system geometry and the propagation conditions the total number of subscribers is kept constant, at an upper bound.

III OUTAGE CALCULATION MODEL

To verify the simulation results, we developed a model for a theoretical approximation for the outage. We assume the mobiles to be equally distributed. Hence, the cdf of the user location ξ can simply be expressed by

$$P_r\{\xi < r\} = \frac{r^2}{R^2} \quad (5)$$

Here we neglect the close in area around the base station marked by off r_0 which serves as an area around the outdoor BS where a mobile is not allowed to stay in order to keep the propagation model valid. Because of the assumed independence of the user locations, the probability that *one* mobile stays within an area marked off by r is can be approximated as follows:

$$P_r\{\xi_M < r\} \approx \frac{M}{R^2} r^2 \quad (6)$$

This approximation is only valid for $r \ll R$. M is the number of macro cell subscribers. Since we assume an equal distribution, the relations found by (5) and (6) are valid for any location of a BS. After having defined the *threshold*, the corresponding distance d could be calculated. Where d denotes the minimal separation between macro cell user and the micro cell BS, so that $(C/I)_{min\mu}$ is just kept. Because of the applied propagation model this distance varies dependent on the relative location of the mobile to its base station. However, we can define an upper and lower value of d (Figure 3). Mobiles at the outer region

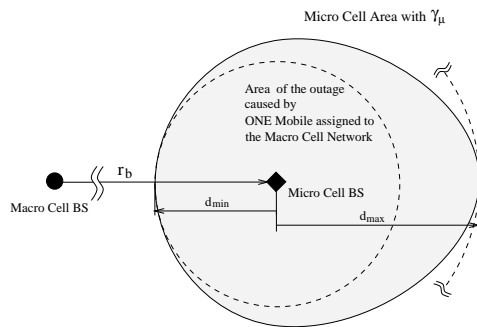


Figure 3: Area of Total Outage

of the cell will have higher transmission power. This results in d_{max} . Whereas, d_{min} is derived from the point closest to the the macro cell base station. We can interpolate an area around the micro cell base station including these two points. This area has the property that only *one* mobile within it will cause 100% loss of the complete micro cell. If we apply the same path-loss exponent for micro- and macro cell which is equal to γ we can calculate d_{min} and d_{max} in closed form by combining (1), (2) (case $d_{Mj} < R_\mu$) and (3), substituting r_{Mj} with $r_b \pm d$ and solving for d which, thus, gives to solutions d_{min} , d_{max}

respectively.

$$d_{min/max} = \frac{r_b}{\left(\frac{R}{R_\mu} \left(\frac{P_{R\mu}}{\eta P_R (C/I)_{min\mu}}\right)^{1/\gamma}\right) \mp 1} \quad (7)$$

In this case we obtain a linear relationship between the distance of the inter network base stations r_b and the resulting $d_{min/max}$. If we substitute r in (6) with $d_{min/max}$ of (7) we get a theoretical upper and lower bound of outage, which results in

$$P_r\{(C/I) < (C/I)_{min\mu}\} = \frac{M r_b^2}{\left(\left(\frac{R}{R_\mu} \left(\frac{P_{R\mu}}{\eta P_R (C/I)_{min\mu}}\right)^{1/\gamma}\right) \mp R\right)^2} \quad (8)$$

In case $\gamma \neq \gamma_\mu$ numerical methods have to be applied. The following equation has to be solved for d to get d_{min} and d_{max} .

$$0 \equiv \eta \times \left(\frac{P_R}{P_{R\mu}}\right) \times (C/I)_{min\mu} \times \left(\frac{R_\mu}{d}\right)^{\gamma_\mu} \times \left(\frac{r_b \pm d}{R}\right)^\gamma - 1 \quad (9)$$

Afterwards we again substitute d_{min} and d_{max} into (6) to obtain the theoretical outage probability.

IV SIMULATION AND RESULTS

The simulations are based upon the parameters listed in Table 1 and 2. The estimated maximal number of users in the macro cell when applying ideal power control is obtained by using [10, pp. 309–312]. All further parameters are related to [8]. By taking a minimum receiver sensitivity of -116 dBm [11, 12] and a total path loss of 142.3 dB [8] at a distance of 1 km we get $P_R \approx 0.4W$. r_0 does not have an impact on outage. However, r_0 must satisfy: $r_0^2 \ll R^2$ so that eq. (5) maintains valid. From (8) and (9) it can be seen, that $r_{0\mu}$ does not have influence on the theoretical outage result, either. The simulations confirm these results. The values of γ and γ_μ are obtained from the investigation undertaken in [13]. In the simulation we first considered different path loss exponents in the micro- and macro cell environments. Figure 4 shows the theoretical and simulated outage results dependent on the distance r_b for a *threshold* of -19 dB. The results shown by Figure 6 are based on a *threshold* of -16 dB. In the following step we increased the indoor path loss slope to match the outdoor exponent in order to simulate a indoor building with several stories. Thus, the probability of line sight for the micro cell mobile to its base station is considerably reduced. Although in reality the attenuation inside a building can be much higher, e.g. with metal shielding inside walls. On the one hand this supports a reduction of micro cell outage because the interfering signal from the macro cell mobile is much more attenuated. On the other hand, since there is a limited power budget for the indoor mobile the useful signal is also received at a lower level. Figure 5 shows the result for a *threshold* of -19 dB, whereas the results given by Figure 7 are based on a *threshold* of -16 dB.

Table 1: Macro Cell Simulation Parameters

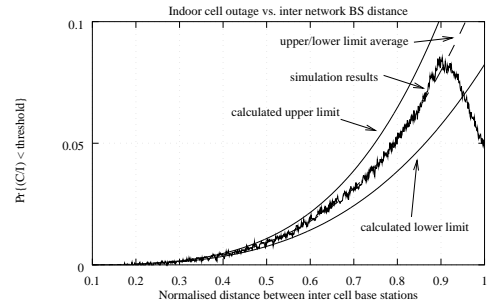
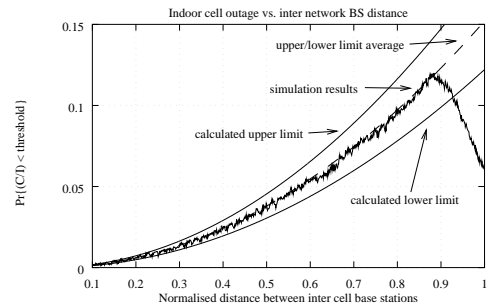
Description	Parameter	Value	Unit
radius	R	1000	m
area of no users	r_0	50	m
reference power	P_R	400	mW
number of subscribers	M	15	

Table 2: Micro Cell Simulation Parameters

Description	Parameter	Value	Unit
radius	R_μ	120	m
area of no users	$r_{0\mu}$	5	m
reference power	$P_{R\mu}$	10	mW

V DISCUSSION

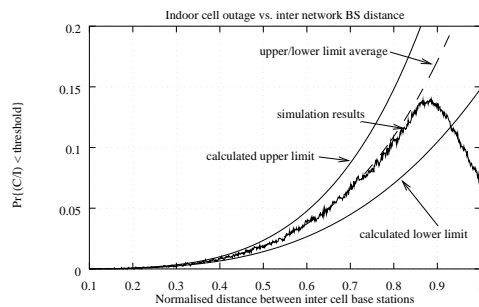
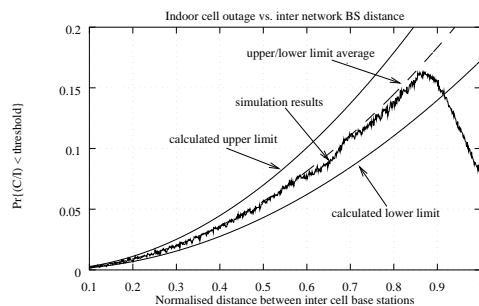
Different propagation conditions have been studied as well as different processing gains. However, it has been found that the parameter with the largest impact on micro cell outage is the distance between micro and macro cell BS, referred to as r_b . The smaller it is the better the outage results. Although, in the latter case the interference from the micro cell system to the macro cell BS will increase. Thus, there is an optimal value for r_b in the sense of mutual interference. In case of locating the indoor BS in a range of about $0.2R < r_b < 0.45R$ the rates of outage do not differ greatly if we either apply a threshold of -16 dB or -19 dB, and they are still below 5%. The assumption of an equal path loss $\gamma = \gamma_\mu = 3.6$ reveals, in total, worse results than in the case of $\gamma = 3.6$ and $\gamma_\mu = 2$. This implies that the effect of the attenuation of the useful signal has a higher impact than the attenuation of the interferer. This could be overcome by giving the micro cell mobile a higher transmission power. However, this, in turn, effects the interference at the macro cell BS caused by the indoor mobile. Since the results are only based on one micro cell mobile it must be taken into account that the probability for micro cell outage will increase if the more realistic case of the existence of several indoor subscribers will be applied. However, some of those mobiles could also be moved by the DCA algorithm to the FDD down-link band. This, on the other hand rises the risk of causing outage to the macro cell mobile. Further it can be stated that the results follow closely the average value between the upper and lower limits given by mathematical approximation of eq. (8) and eq. (9), indicating a close match between them. Although, at the normalised distance of about 0.9 the simulations seem to reveal a decline in outage which is because of the cell-boundary effect. From the close match between theory and simulations it can be concluded, that outage is mainly caused by a single interferer within a distance of d_{max} , d_{min} respectively. This implies that the accumulation of interfering signals from several mobiles located farer away is negligible for severe outage. The walls around a micro cell system also have an influence on outage. Since the theoretical model has served as an accurate approximation the effect of wall shielding can be studied theoretically.

Figure 4: $\gamma = 3.6$, $\gamma_\mu = 2$, $(C/I)_{min\mu} = -19dB$ Figure 5: $\gamma = \gamma_\mu = 3.6$, $(C/I)_{min\mu} = -19dB$

After substituting R_μ into (6) the probability for the event that one macro cell mobile stays within the micro cell coverage is obtained. This immediately can be converted into outage probability which is quasi stationary for a wide range of r_b (see Figure 8). This is because the interfering energy from mobiles outside the building is shielded, whereas a mobile inside has to transmit at an even higher level. This results in a quasi-constant outage probability beginning at certain value of r_b , i.e. from there on the influence of r_b on outage is substantially reduced. Now the most determining factor on outage is the size R_μ of the micro cell. With the parameters given in Table 1 and 2, and an assumed wall loss of 10 dB, this value is 21.6%. Hence, up to an outage range of 21.6% wall shielding will have negative influence on micro cell outage. Above this limit the micro cell will benefit from wall shielding. To make this effect visible, in the simulations we increased P_R to 1 W.

VI CONCLUSIONS

Applying the proposed system architecture macro cell subscribers cause losses of underlayed micro cells, assuming the macro cell system has a higher priority. This outage probability is a lower bound of outage because it was assumed that the conditions of the micro cell system are ideal (only one micro cell user). This lower bound of outage, however, is strongly dependent on the base station separation. Hence, if the FDD band of an overlaid CDMA system is to be used by CDMA micro cell systems utilising TDD techniques at either the up-link or

Figure 6: $\gamma = 3.6$, $\gamma_\mu = 2$, $(C/I)_{min\mu} = -16dB$ Figure 7: $\gamma = \gamma_\mu = 3.6$, $(C/I)_{min\mu} = -16dB$

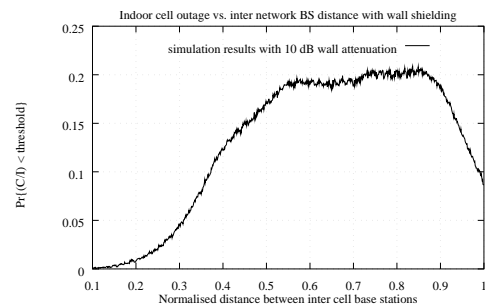
down-link FDD band, the locations of the micro cells have to be defined properly. Otherwise, the lower bound micro cell outage can become intolerably high. This, in turn, raises the need for network planning in respect to the micro cell locations. This constraint restricts the freedom of placing the micro cell anywhere within the macro cell which is inflexible and undesirable. Hence, it can be stated that there are conflicting requirements. If, however, this trade off can be resolved TDD techniques combined with a DCA algorithm represents an excellent method to increase capacity of a CDMA macro cell environment substantially. If the micro cell is used within buildings and the size of the cell is kept small the walls can be used to minimise the outage ratio. However, all these conclusions imply an equal distribution of the subscribers. Furthermore the effects of inter cell interference caused by the micro cell components have not been addressed in this paper.

ACKNOWLEDGEMENTS

The authors gratefully acknowledge the support of these studies by the Faculty of Science and Engineering with the "Colin and Ethel Gordon Scholarship" and the Department of Electronics and Electrical Engineering, both at the University of Edinburgh.

REFERENCES

- [1] W. C. Y. Lee, "Applying the Intelligent Cell Concept to PCS," *IEEE Transactions on Vehicular Technology*, vol. 43, pp. 672–679, August 1994.

Figure 8: $\gamma = 3.6$, $\gamma_\mu = 2$, $(C/I)_{min\mu} = -19dB$, $P_R = 1W$

- [2] I. Chih-Lin, L. J. Greenstein, and R. D. Gitlin, "A Microcell/Macrocell Cellular Architecture for Low- and High-Mobility Wireless Users," *IEEE Journal on Selected Areas in Communication*, vol. 11, pp. 885–890, August 1993.
- [3] K. Takeo, "Uplink Capacity of Macro/Spot-microcellular Systems in Frequency Division CDMA," *IEICE Transactions: Fundamentals*, vol. E80–A, pp. 1218–1225, July 1997.
- [4] K. S. Gilhousen, I. M. Jacobs, R. Padovani, A. J. Viterbi, L. A. Weaver, Jr., and C. E. Wheatly III, "On the capacity of a cellular CDMA system," *IEEE Transactions on Vehicular Technology*, vol. 40, pp. 303–312, May 1991.
- [5] R. Esmailzadeh and E. M. Nakagawa, "Pre-RAKE Diversity Combining for Direct Sequence Spread Spectrum Mobile Communications Systems," *IEICE Transactions: Communications*, vol. E76–B, pp. 1008–1015, August 1993.
- [6] S. E. Elkamy, "Wireless Portable Communications Using PRE-RAKE CDMA/TDD/QPSK Systems with Different Combining Techniques and Imperfect Channel Estimation," in *Proceedings of the PIMRC '97*, vol. 2 of 3, pp. 529–533, IEEE, September 1–4 1997.
- [7] G. J. R. Povey, H. Holma, and A. Toskala, "TDD-CDMA Extension to FDD-CDMA Based Third Generation Cellular System," in *Proceedings of the ICUPC '97*, vol. 2 of 2, pp. 813–817, IEEE, October 12–16 1997.
- [8] M. O. Sunay, Z. C. Honkasalo, A. Hottinen, H. Honkasalo, and L. Ma, "A Dynamic Channel Allocation Based TDD DS CDMA Residential Indoor System," in *Proceedings of the ICUPC '97*, vol. 2 of 2, pp. 228–234, IEEE, October 1997.
- [9] L. Ma, M. O. Sunay, Z. C. Honkasalo, and H. Honkasalo, "A Simulation Bed to Investigate the Feasibility of a TDD DS CDMA Residential Indoor System Underlay," in *Proceedings of the PIMRC '97*, vol. 2 of 3, pp. 286–291, IEEE, September 1997.
- [10] W. C. Y. Lee, *Mobile Communications Design Fundamentals*. John Wiley & Sons, second ed., 1993.
- [11] TIA/EIA/IS-95, *Mobile Station-Base Station Compatibility Standard for Dual-Mode Wideband Spread Spectrum Cellular System*. Telecommunication Industry Association, May 1995.
- [12] R. Padovani, "Reverse Link Performance of IS-95 Based Cellular Systems," *IEEE Personal Communications*, vol. 1, pp. 28–34, 3rd Quarter 1994.
- [13] T. S. Rappaport and L. B. Milstein, "Effect of Radio Propagation Path Loss on DS-CDMA Cellular Frequency Reuse Efficiency for the Reverse Channel," *IEEE Transactions on Vehicular Technology*, vol. 41, pp. 231–242, August 1992.

CAPACITY ANALYSIS OF A TDD UNDERLAY APPLICABLE FOR UMTS

H. Haas, Student Member, IEEE, and G. J. R. Povey

The University of Edinburgh,
Department of Electronics and Electrical Engineering,
Signals & Systems Group
The King's Buildings, Mayfield Road
Edinburgh, EH9 3JL, UK
Phone:+44 (0)131 650 5655, Fax:+44 (0)131 650 6554
Email: hh@ee.ed.ac.uk

Abstract — Asymmetric use of a CDMA-FDD channel results in underused radio spectrum in one of the duplex frequency bands. Due to practical restrictions a dynamic partitioning of the FDD duplex bands is difficult to achieve. However, an asymmetrical channel utilisation is inherent in future multi-media applications supported by, for example, the Universal Mobile Telecommunications System (UMTS). Therefore, we analyse a method which exploits this underused FDD spectrum in a soft manner. The idea is that a CDMA-TDD link is put into the underused CDMA-FDD duplex band. An analytical approach based on a uniform user distribution has been taken to calculate the mutual interference at the base stations of an hierarchical system topology. This consists of a CDMA-TDD pico cell underlaid to a CDMA-FDD macro cell. It is assumed that the pico cell is placed within a building with 10dB wall attenuation. Since this method is ideally applicable for UMTS, we used parameters of the UTRA (UMTS terrestrial radio access) air interfaces (UTRA-FDD and UTRA-TDD) to carry out capacity analysis. It was shown that the TDD underlay can significantly increase the flexibility on the UMTS air-interface and that the greatest advantageous can be gained from a BS separation of about 300m and lognormal shadowing with σ less than 11 dB.

I. INTRODUCTION

Currently the 3rd generation mobile communication system UMTS, which belongs to the IMT-2000 family, is being standardised [1]. Two UTRA interfaces have been chosen: UTRA-FDD and UTRA-TDD. The TDD-mode is useful for low mobility populations and services which require a high channel asymmetry [2, 3]. It is predicted that these asymmetrical services, such as Internet Web-browsing, will be widely used in future mobile communications systems. The channel asymmetry will be mainly in favour of the downlink resulting in underused uplink spectrum when employing the FDD mode. Unused frequency spectrum, however, represents a waste of expensive radio

resources. Taking into account that CDMA is an interference limited system and that the basic frame structures of UTRA-TDD and UTRA-FDD are harmonised, we pursue the idea of exploiting unused UTRA-FDD spectrum by soft-combining both modes. Fig. 1 illustrates the basic

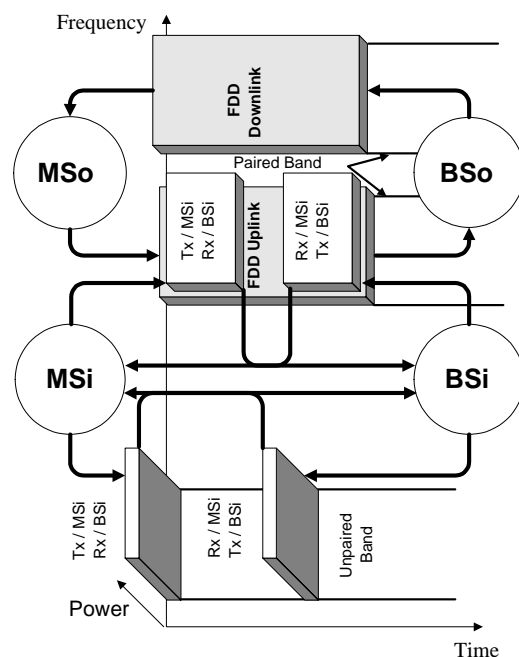


Fig. 1. Principles of the UTRA-TDD underlay. The components of the UTRA-TDD pico cell or indoor cell are followed by the letter 'i' (BSi, MSi respectively) while the UTRA-FDD macro cell or outdoor cell entities are marked with an additional 'o'.

concept of this idea. Additional UTRA-TDD links will be placed into the underused UTRA-FDD uplink band. The fact that many data services have relaxed timing requirements supports the basic concept of the UTRA-TDD

underlay. This method was first proposed in [4].

The UTRA-TDD interface is ideally suitable for pico and micro cell environments. Pico cells are used mainly within buildings and are therefore often shielded by walls. This results in a reduction of interference to an overlaid system. The capacity of a non-hierarchical CDMA-FDD system has been intensively studied [5, 6]. We took a new analytical approach to derive the probability density functions (pdfs) of inter-cell interference¹ of an hierarchical macro/pico cellular CDMA system where the pico or indoor cells utilise unused spectrum of the overlay. Using the generated pdfs and defining an outage threshold, system capacity figures can be calculated. This give evidence about the feasibility of the UTRA-TDD underlay.

In section II, the system model is described and in the subsequent section III simulation results are presented and discussed. Finally, conclusions are drawn in part IV.

II. INTERFERENCE MODEL

In Fig. 2, the hierarchical cell layout is depicted. Both

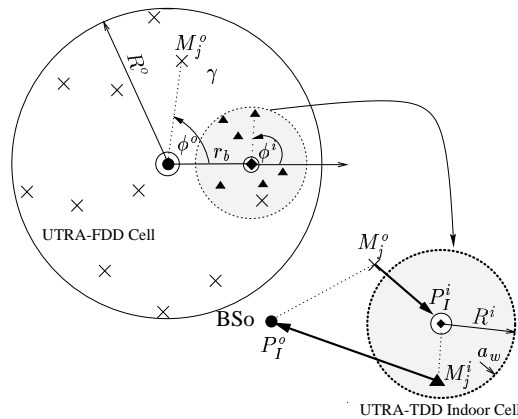


Fig. 2. Cell topology and inter-cell interference definitions.

indoor and outdoor cell mobiles are assumed to be distributed uniformly in space which yields the following pdf:

$$p(r, \phi) = \frac{r}{\pi R^2} \quad (1)$$

where r denotes the distance between the mobile and the BS and R is the cell radius.

The deterministic functions for the inter-cell interference power P_I^i and P_I^o can be derived with the aid of Fig. 2 assuming the mobiles to be ideally power controlled. Using these functions and the pdf found in eqn. (1), a random variable transformation system can be established. In this way it is possible to derive the pdfs of the interference power P_I^i , P_I^o respectively. In the following

¹ inter-cell interference is used to describe the interference between the UTRA-TDD pico cell and the UTRA-FDD macro cell.

all signal powers are in dB. After some calculations the pdfs can be found as:

$$p(P_I^i) = \frac{\beta r_b^2}{\gamma R^{o^2} \sigma \sqrt{2\pi^3}} \int_{-\infty}^{\infty} \int_0^{2\pi} \left(\sum_{n=1}^2 \left| \frac{y_n^2 - 2 y_n \cos(\phi) + 1}{y_n - \cos(\phi)} \right| y_n^{-3} \right) e^{-\frac{\xi^2}{2\sigma^2}} d\phi d\xi \quad (2)$$

with $\beta = \ln(10)/10$, γ the pathloss exponent, r_b the BS separation distance, R^o the macro cell radius and ξ the lognormal shadowing variable. It is assumed that the lognormal shadowing variables on the desired and the interference path have zero mean and equal standard deviation σ . The normalised covariance (correlation coefficient) of both variables is set to 1/2. The auxiliary functions $y_n(\phi, \xi, P_i^i)$ are:

$$y_n(\phi, \xi, P_i^i) = \cos(\phi^o) (-1)^n f_{(\phi, \xi, P_i^i)} \quad n = 1, 2 \quad (3)$$

and

$$f_{(\phi, \xi, P_i^i)} = \begin{cases} \sqrt{\cos(\phi^o)^2 + e^{(-2\beta(P_i^i - \xi - P_u^o - a_w))} - 1} & \text{if MSo in} \\ & \text{pico cell} \\ \sqrt{\cos(\phi^o)^2 + e^{(-2\beta(P_i^i - \xi - P_u^o + a_w))} - 1} & \text{otherwise} \end{cases} \quad (4)$$

Where P_u^i is the signal power coming from the desired user. The angle component of the MSo location is expressed by ϕ^o and a_w describes wall losses at the pico cell boundary. In a similar manner the probability density function of the additional inter-cell interference at the BSo can be denoted.

$$p(P_I^o) = \frac{\beta r_b^2}{\gamma R^{i^2} \sigma \sqrt{2\pi^3}} \int_{-\infty}^{\infty} \int_0^{2\pi} \left(\sum_{n=1}^2 \left| \frac{v_n^2 + 2 v_n \cos(\phi^i) + 1}{v_n + \cos(\phi^i)} \right| v_n^{-3} \right) e^{-\frac{\xi^2}{2\sigma^2}} d\phi^i d\xi \quad (5)$$

with

$$v_n(\phi, \xi, P_i^o) = -\cos(\phi^i) (-1)^n \cdot g_{(\phi^i, \xi, P_i^o)} \quad n = 1, 2 \quad (6)$$

and

$$g_{(\phi^i, \xi, P_i^o)} = \sqrt{\cos(\phi^i)^2 + e^{(-2\beta(P_i^o - \xi - P_u^i + a_w))} - 1} \quad (7)$$

Eqn. (2) and eqn. (5) have been solved numerically. It is straightforward to calculate the first and second moment from the derived pdfs. The moments have been

transformed to the linear scale and the Central Limit Theorem has been applied to extend the pdfs to a multi-user scenario. With the final pdfs and an outage probability $P_{out} = Pr(P_I^i > \hat{P}_I^i)$, \hat{P}_I^i can be calculated and fed into eqn. (8) to obtain the desired capacity figures.

$$C/I^o = \frac{P_u^o}{P_u^o (M^o - 1) + \hat{P}_I^i + \eta} \quad (8)$$

Again, P_u^o is the signal power received from the desired user, \hat{P}_I^i is the total interference coming from the co-existing system, η represents thermal noise and M^o is the number of macro cell mobiles. The same method has been applied to calculate the additional pico cell capacity M^i .

The simulations have been carried out with the parameters listed in Table I. The C/I thresholds and data rate are derived from UMTS system definition found in [7] and [8]:

TABLE I
SIMULATION PARAMETERS

Description	Para – meter	Value	Unit
Radius of macro cell	R^o	1000	m
Radius of micro cell	R^i	50	m
Wall loss	a_w	10	dB
Path loss exponent	γ	3.8	—
Outage threshold	P_{out}	0.05	—
C/I threshold (UTRA-FDD)	C/I^o	-19	dB
C/I threshold (UTRA-TDD)	C/I^i	-8.5	dB
Data rate per user	—	16	kBit/s
Power budget MSo	—	1	W
Power budget MSi	—	10	mW

III. RESULTS AND DISCUSSION

The capacity results are shown for a varying σ of the lognormal shadowing variable. Furthermore, different BS separation scenarios are investigated.

Fig. 3 and 4 show the pdf of the inter-system interference for two different BS separations r_b and a fixed $\sigma = 6$. When comparing both Figures following properties can be derived:

1. $E[P_I^o]$ decreases with an increasing r_b , whereas $VAR[P_I^o]$ does not change significantly.
2. $VAR[P_I^i]$ increases with a greater BS separation r_b , whereas $E[P_I^i]$ does not change significantly.

The capacity results are depicted in Fig. 5 a) – d). Not only can the actual numbers of users be ascertained from Fig. 5, but in addition, it is possible to study the mutual interference effects. With the proposed system underlay the additional pico cell capacity (M^i) basically is a function of the number of macro cell users:

$$M^i = f(M^o) \quad (9)$$

The situation is different for the remaining FDD uplink capacity (M^o) which is determined by the actual number of pico cell mobiles MSi:

$$M^o = f(M^i) \quad (10)$$

Thus, in Fig. 5, the range for eqn. (10) is the ordinate, and the image can be found at the abscissa. The situation is inverse for the additional TDD capacity (eqn. (9)). Hence, the plots in Fig. 5 comprise two *independent* investigations:

1. The solid curves show the remaining capacity in the FDD uplink dependent on the number of MSi's.
2. The dashed curves depict the additional TDD capacity dependent on the number of MSo's.

In both cases the arrows indicate the functional relationship and how to interpret the results. It can be seen that the higher the BS separation the more the basic FDD uplink capacity is preserved. On the other hand, the higher the BS separation the less additional pico cell capacity due to the greater transmission powers of the macro cell mobiles at outer regions. This trade-off leads to an optimum for the BS separation.

The aim is to accommodate as many mobiles as possible within *both* layers (pico and macro cell) instantaneously. There is no real gain in flexibility if there is, for example, additional pico cell capacity but the FDD uplink is blocked. One exception is when there is only downlink capacity required in the FDD cell and the FDD uplink is mainly unused (only a negligible amount of control traffic). Such a scenario is depicted in Fig. 5 a) ($r_b=200m$). It can be seen that with $\sigma = 11$ there is only additional pico cell capacity but any pico cell mobile will on average destroy the FDD uplink capacity due to the close location. This effect is explained more precisely with the aid of Fig. 5 c) and with the following example. Initially 10 macro cell mobiles are assumed which leads to approximately 17 additional links in the pico cell. In turn, 17 pico cell users will accommodate up to about 72 macro cell mobiles. Here the effects of mutual interference become apparent because, on the other hand, 72 macro cell mobiles would generate too much interference even for a single TDD link within the uplink frequency band. Hence, the flexible exchange of radio resources between the FDD and the TDD mode is limited. It is desirable to define a measure for the flexibility of the pico cellular underlay. This can be derived with the aid of Fig. 6. Defining set \mathcal{A} as the operation area of the additional pico cell capacity and \mathcal{B} the same for the FDD uplink capacity. Let $\mathcal{C} = \mathcal{A} \cap \mathcal{B}$ then it can be stated that the flexibility increases with \mathcal{C} . This can be applied to the results in Fig. 5 a) – d). Set \mathcal{C} for $\sigma = 8$ has been highlighted for $r_b=200m$ to $r_b=500m$. It can be seen that the maximum is reached for $r_b=300m$ whereas for $r_b=500m$ it shrinks just to one point. Furthermore, it can be gathered that for small BS separations \mathcal{C} is determined by the reduction of FDD uplink capacity. In contrast for high BS separations only the diminished additional TDD capacity limits \mathcal{C} .

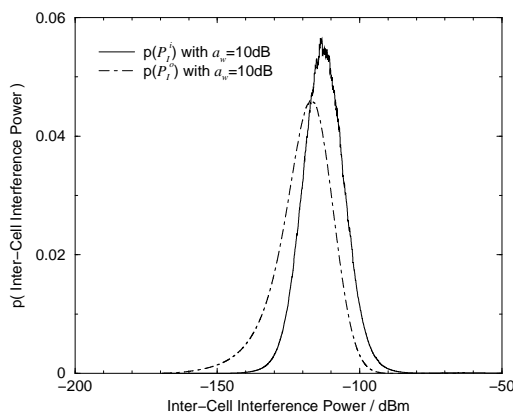


Fig. 3. Probability density function of the inter-cell interference power P_i^o , P_i^i respectively, with $r_b=200m$ and $\sigma=6$.

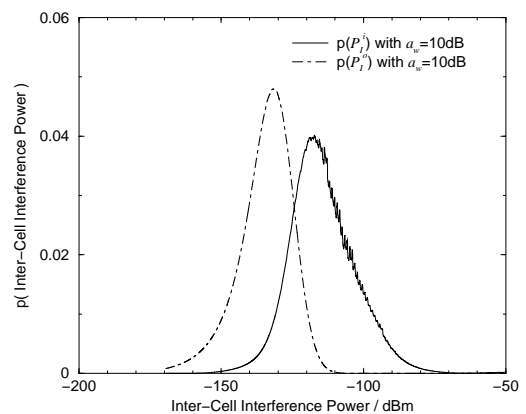


Fig. 4. Probability density function of the inter-cell interference power P_i^o , P_i^i respectively, with $r_b=500m$ and $\sigma=6$.

It is easy to calculate that the theoretical maximum of capacity of one UTRA-TDD channel is 64 (8 users per slot and in total 8 slots per frame) assuming equal data rates, symmetrical services and no multi-user detection. This maximum for the UTRA-FDD uplink is about 81 users with an overall spreading factor (SF) of 256. These figures can be compared with the cumulative maximum in Fig. 5 b) with $\sigma = 8$ which is about 70 users (e.g. 40 pico cell users and 30 macro cell mobiles simultaneously). Thus, there is no absolute increase in spectral efficiency.

It can be found in Fig. 5 that $\sigma = 11$ gives no common capacity, i.e. $C = \emptyset \forall r_b$. Furthermore, lognormal shadowing with $\sigma = 6$ yields optimal results for $r_b=300m$. In this case even the spectral efficiency can be increased because in total more than 81 users can be accommodated within the UTRA-FDD uplink (as an example, with 40 MSo's about 60 MSi's can be served in the FDD uplink resulting in an increased spectral efficiency of about 25%). Moreover, in this case there is significant flexibility for all investigated BS separations (Fig. 5 a) – d)).

IV. CONCLUSIONS

An analytical approach has been adopted to investigate the feasibility of a TDD pico cellular underlay with air interface parameters gathered from the UMTS system. 10dB wall attenuation at the pico cell boundary and a spatially uniform user distribution have been assumed.

It was found that the TDD underlay does not increase the spectral efficiency for a lognormal shadowing of $\sigma > 6$. However, the main gain is the flexible exchange of radio spectrum between the FDD and TDD mode. This becomes important when considering highly asymmetrical data services, which might be dominant in future applications (e.g. Web browsing). With the TDD underlay underused FDD spectrum can be exploited, thus increasing the data throughput by the gained flexibility.

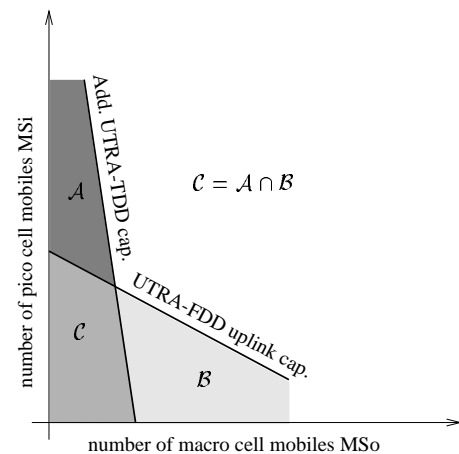


Fig. 6. The area defined by C serves as a measure for the flexibility of the TDD Underlay. Within C FDD uplink radio resources can be exchanged between the macro cell and pico cell.

Hence, with this additional degree of freedom the utilisation of radio spectrum in a dual mode air interface has been significantly improved.

Furthermore, it can be shown that there exists an optimum for the BS separation. This was found to be around 300m. Moreover, the higher the lognormal shadowing the narrower the interval for useful BS separations. In general the flexibility gained by soft-combining UTRA-FDD and UTRA-TDD is dependent on the severity of lognormal shadowing. With $\sigma = 11$ the benefits from TDD underlay are limited because either a single mobile using the UTRA-FDD uplink will inhibit any additional UTRA-TDD capacity or a single additional TDD user will completely occupy the UTRA-FDD uplink. However, even in this case, the option exists to convert FDD uplink radio resource into TDD duplex capacity if, for example, the

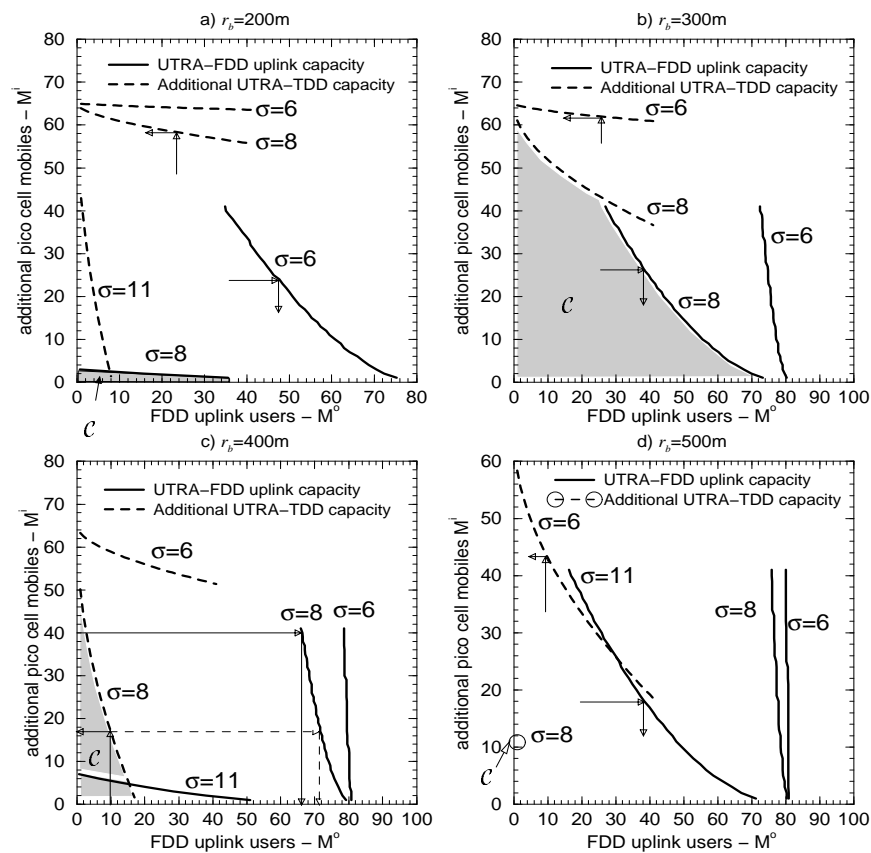


Fig. 5. The additional numbers of mobiles in the pico cell are indicated by dashed lines. Whereas, the capacity reduction in the FDD uplink is shown by the solid lines. Different lognormal shadowing scenarios are depicted in each plot. Moreover the effects of different BS separations are shown in plot a) – d): a) $r_b=200\text{m}$, b) $r_b=300\text{m}$, c) $r_b=400\text{m}$ and d) $r_b=500\text{m}$.

FDD uplink does not carry any data traffic.

With system enhancements such as multi-user detection or antenna sectorisation the constraints to obtain optimal benefits of the TDD underlay might be further relaxed. These enhancements are the subject of further investigation.

ACKNOWLEDGEMENTS

The authors gratefully acknowledge the support of these studies by the *Faculty of Science and Engineering* and the *Department of Electronics and Electrical Engineering* both at the University of Edinburgh.

REFERENCES

- [1] A. Samukic, "UMTS Universal Mobile Telecommunications System: Development of Standards for the Third Generation," *IEEE Transactions on Vehicular Technology*, vol. 47, pp. 1099–1104, November 1998.
- [2] G. J. R. Povey and M. Nakagawa, "A Review of Time Division Duplex-CDMA Techniques," in *Proceedings of the IEEE Fifth In-*

ternational Symposium on Spread Spectrum Techniques and Applications, ISSSTA'98, vol. 2 of 3, (Sun City, South Africa), pp. 630–633, IEEE, September 2–4 1998.

- [3] I. Horikawa, O. Kato, K. Miya, and M. Hayashi, "Performance of Wideband CDMA with TDD Scheme," in *Proceedings of the 1997 Asia Pacific Microwave Conference*, (Hong Kong), pp. 145–148, IEEE, December 2–5 1997.
- [4] M. O. Sunay, Z. C. Honkasalo, A. Hottinen, H. Honkasalo, and L. Ma, "A Dynamic Channel Allocation Based TDD DS CDMA Residential Indoor System," in *Proceedings of the 1997 IEEE 6th International Conference on Universal Personal Communications ICUPC '97*, vol. 2 of 2, pp. 228–234, IEEE, October 1997.
- [5] K. S. Gilhousen, I. M. Jacobs, R. Padovani, A. J. Viterbi, L. A. Weaver, Jr., and C. E. Wheatly III, "On the capacity of a cellular CDMA system," *IEEE Transactions on Vehicular Technology*, vol. 40, pp. 303–312, May 1991.
- [6] G. E. Corazza, G. De Maio, and F. Vatalaro, "CDMA Cellular Systems Performance with Fading, Shadowing, and Imperfect Power Control," *IEEE Transactions on Vehicular Technology*, vol. 47, pp. 450–459, May 1998.
- [7] K. Miya, O. Kato, K. Homma, T. Kitade, and M. Hayashi, "Wideband CDMA Systems in TDD-Mode Operation for IMT-2000," *IEEE Transactions: Communications*, vol. E81–B, pp. 1317–1325, July 1998.
- [8] ETSI, "UTRA TDD, Transport channels and Physical channels description," V0.1.0 1998-09, 1998.

The Effect of Adjacent Channel Interference on Capacity in a Hybrid TDMA/CDMA–TDD System Using UTRA–TDD Parameters

H. Haas, Student Member, IEEE, and G. J. R. Povey

The University of Edinburgh,
Department of Electronics and Electrical Engineering,
Signals & Systems Group
The King's Buildings, Mayfield Road
Edinburgh, EH9 3JL, UK
Phone: +44 (0)131 650 5655, Fax: +44 (0)131 650 6554
Email: hh@ee.ed.ac.uk

Abstract—The subject of this analysis is the effects of adjacent channel interference (ACI) on capacity in a hybrid TDMA/CDMA system using time division duplex (TDD). The parameters of the UTRA (UMTS terrestrial radio access) air interface were used for this investigation. A statistical approach assuming a spatially uniform user distribution was taken to investigate the capacity reduction due to ACI. The probability density function (pdf) of ACI at the base station (BS) of interest was calculated and by defining a certain outage threshold (P_{out}), the interference used to calculate the capacity loss was determined. A pathloss model which accounts for the correlation of lognormal shadowing between useful link and interference link was adopted. The impact of the following parameters were studied: a) BS separation, b) adjacent channel protection (ACP), c) load in the interfering cell and d) frame synchronisation. It was found that there are sub-optimal BS separations due to a trade-off between MS→BS and BS→BS interference. Moreover, it became apparent that an intelligent dynamic channel assignment (DCA) algorithm is required.

I. INTRODUCTION

The Universal Mobile Telecommunications System (UMTS) comprises two air-interfaces which are UTRA–FDD and UTRA–TDD. The UTRA–TDD interface utilises a hybrid multiple access method consisting of a TDMA and CDMA component and the duplex communication channel is achieved in the time domain by means of TDD. The unpaired frequency bands for TDD operation are 1900–1920 MHz and 2010–2025 MHz with the first one being directly adjacent to the UTRA–FDD uplink frequency band. It is likely that the 1900–1920 MHz band will be licensed whereas the 2010–2025 MHz band might be for unlicensed usage. This results in a variety of ACI scenarios. In this paper we restrict the scope of investigation to ACI between UTRA–TDD

carriers and the resulting capacity loss. The effects of ACI in UTRA–TDD differ from those in UTRA–FDD [1, 2] due to the following facts:

- TDD systems are ideally applicable for slow fading channels [3] and, hence, channels with low Doppler spread. Therefore, the TDD mode is predestined for the pico- or micro cell layer.
- Due to the nature of TDD additional mutual interference scenarios exist (MS ↔ MS and BS ↔ BS), the severity of which is dependent on frame synchronisation. In FDD systems these interference scenarios are not significant due to the frequency separation between uplink and downlink. Frame synchronisation between different operators cannot be expected. Thus, MS ↔ MS and BS ↔ BS interference must not be neglected in the analysis of UTRA–TDD.
- The carrier spacing of 5 MHz and the fact that the licensed UTRA–TDD spectrum is likely to be merely 20 MHz have the consequence that in some countries an operator might only obtain *one* UTRA–TDD carrier. The implications are that once ACI reaches a certain threshold services have to be dropped since no other carrier is available for a handover.

Taking into account the properties mentioned above, we studied ACI on the UTRA–TDD air-interface and showed the capacity reduction accompanied. In section II, properties of the UTRA–TDD air-interface and its implications on ACI are given. In section III, the model derived from the previous section is presented. In section IV, results are shown followed by a discussion. Finally, in section V conclusions are given.

II. PROPERTIES OF UTRA–TDD

The air-interface parameters of UTRA–FDD and UTRA–TDD are harmonised. In both cases the

frame duration is 10 ms divided into 16 time slots yielding a slot duration (t_{slot}) of 625 μ s. In the UTRA-TDD case each cell is assigned a set of 16 Walsh codes multiplied by a cell specific PN scrambling sequence. Moreover, each TS can either be used for uplink or downlink transmission which easily enables channel asymmetry. Up to 8 different users can be served by one TS and in case of a single user occupying the whole TS, 9 or even 10 bursts can be accommodated in one TS[4].

In this investigation we used a single cell model since it is likely that UTRA-TDD does not account for a continuous coverage and is rather employed to deal with traffic hot spots. In Fig. 1, a possible UTRA-TDD multi-operator scenario is depicted. The cell locations may overlap in a random man-

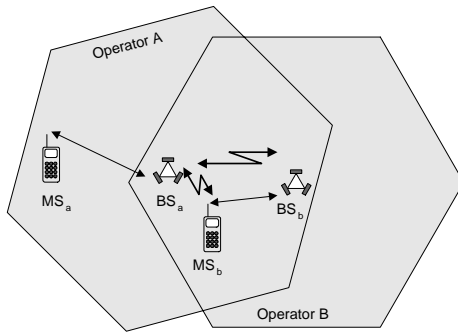


Fig. 1. A possible multi-operator scenario

ner. Hence, as seen from Fig. 1, a mobile station of network B (MSb) might approach a base station of system A (BSa), or vice versa. Taking into account that UTRA-TDD is ideally applicable to micro or pico cells having small antenna heights, the distance between MSb and BSa might become very small.

In Fig. 2, one TS of the scenario shown in Fig. 1 is depicted. The most critical inter-operator interference scenarios (MS \leftrightarrow BS and BS \leftrightarrow BS) are sketched with different shadings. The time slots have an arbitrary time offset (t_{off}) to model incorrect frame synchronisation or different asymmetries. The synchronisation factor is defined as

$$\alpha = t_{off} / t_{slot} \quad (1)$$

The uplink faces interference from the co-existing BS and MS instantaneously. The severity of each type of interference is dependent on frame synchronisation, but the uplink interference has the property that it cannot be resolved completely by manipulating

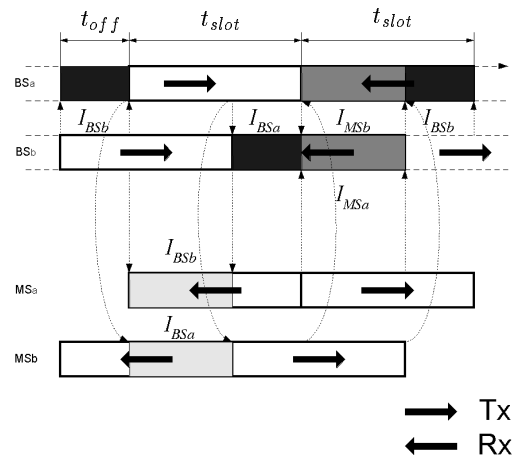


Fig. 2. Interference in a TDD system dependent on frame synchronisation.

frame synchronisation. The synchronisation factor α scales MS \rightarrow BS and BS \rightarrow BS interference as follows: diminishing α reduces the BS \rightarrow BS interference contribution, but causes more MS \rightarrow BS interference to reach the receiver. On the other hand, increasing α permits more BS \rightarrow BS interference and inhibits MS \rightarrow BS interference. Thus, irrespective of what the synchronisation is, the complete uplink TS experiences ACI provided that at least one mobile in the other cell is active. The consequences of this behaviour in respect to BS locations is different. The MS \rightarrow BS interference is highest with the BS located at the other cell boundary. In other words, to minimise the impact of MS \rightarrow BS interference, it is advantageous to co-locate¹ the base stations or to chose synchronisation such that $\alpha=1$. Co-location, on the other hand, results in maximum BS \rightarrow BS interference. In order to circumvent high BS \rightarrow BS interference either the base stations have to be separated as much as possible, which is in direct opposition to the measures taken to reduce MS \rightarrow BS interference, or synchronisation has to be set such that $\alpha=0$. Hence, there is a trade-off with the interesting result that synchronisation can be utilised to compensate for high interference which results from an unfavourable BS separation.

III. INTERFERENCE MODEL

The idea is to get results of capacity reduction in a UTRA-TDD cell resulting from ACI. Other-cell interference (on the same carrier) is ignored in the

¹within this paper, co-location is defined as the state in which the BS separation is less than or equal to 5m.

calculations since it has no significant contribution to the target results.

Thus, we can define the signal-to-noise ratio as follows:

$$E_b/N_0 = \frac{P_u G_P}{P_u (M - 1) + I_{ad} + \eta} \quad (2)$$

where P_u is the power controlled signal conveyed by the desired user, M is the number of users that can be served by one TS, I_{ad} is the adjacent channel interference and η is thermal noise. The processing gain is expressed by G_P . Since we are interested in the capacity reduction due to I_{ad} , eqn. (2) is solved for M and the ratio M / M_0 is calculated where M_0 is the capacity in the cell of interest (COI) without ACI ($I_{ad} = 0$). Hence, the ratio M / M_0 can be written as follows:

$$M / M_0 = 1 - \frac{I_{ad}}{P_u \left(1 + \frac{G_P}{E_b/N_0}\right) - \eta} \quad (3)$$

Since the scope of our investigation is a single time slot, the ratio M / M_0 is interpreted as follows:

- $M / M_0 = 0$: This particular TS_n is completely occupied by the interfering cell. A DCA algorithm might assign TS_{n+1} to the COI. Hence, the total capacity is shared on a time basis yielding a total capacity which is equivalent to that of a single cell. Defining the accumulated capacity of both cells in a non-interfered state as 100%, with $M / M_0 = 0$, the total capacity of the COI is reduced to 50%. However, in this paper the focus is on a single TS, hence we refer to the capacity of a *single* TS implicitly being aware of the implications for the capacity of the whole cell.
- $M / M_0 = 1$: This particular TS of the COI suffers no capacity reduction from ACI. Hence, according to the previous definition the total, accumulated capacity is now 100%. However, this is just an asymptotic upper bound.

From Fig. 2, one can see that ACI at the BS has two sources:

$$I_{ad} = I_{BS} + I_{MS} \quad (4)$$

where I_{BS} represents the BS→BS interference and I_{MS} defines the MS→BS interference. Downlink power control can only be applied for the whole TS i.e. the downlink power is determined by the mobile which experiences the highest pathloss [5].

The path loss is modelled according to the COST-231 indoor model with no wall or floor losses.

$$a = 37 + \gamma \cdot 10 \cdot \log(\max\{d, d_{\min}\}) + \xi \text{ [dB]} \quad (5)$$

where γ is the path loss exponent and d the distance between transmitter and receiver. The distance d is lower-bounded by an exclusion zone defined by d_{\min} . Lognormal shadowing is modelled by ξ with the standard deviation σ and zero mean.

To account for the correlation between desired path and interfering path it is necessary to introduce a relation between the BS separation distances and the correlation coefficient of the lognormal shadowing variables on each path. Let $\hat{\xi}$ be the lognormal shadowing variable on the desired link and ξ the same on the interference link, then the conditional probability assuming a certain correlation coefficient r can be denoted as:

$$p(\xi | \hat{\xi}) = \frac{1}{\sigma \sqrt{2\pi(1-r)}} \exp\left(-\frac{(\xi - r \cdot \hat{\xi})^2}{2\sigma^2(1-r^2)}\right) \quad (6)$$

In eqn. (6) it is implied that on both links the standard deviation σ is the same. Furthermore, we assume the following relation between r and the BS separation distance d :

$$r = \begin{cases} 1 - \frac{d}{R} & \text{if } d \leq R, \\ 0 & \text{otherwise} \end{cases} \quad (7)$$

where R is the cell radius.

Monte Carlo simulations are carried out assuming a spatially uniform user distribution to obtain the probability density function (pdf) of I_{ad} at the BS of the COI. A constant bit rate, which was set to 16 kbit/s, is assumed for each mobile. The cell radius R was set to be 100 m and the standard deviation of lognormal shadowing was 10 dB. Given a certain outage threshold, which is $P_{out} = Pr(\mathbf{I}_{ad} > I_{ad})$, I_{ad} can be derived and fed into eqn (3) to get the relative capacity reduction.

IV. RESULTS AND DISCUSSION

From Fig. 3, it can be seen that the BS→BS interference (dashed curves) decreases monotonically as the BS separation increases, whereas the MS→MS interference (solid curves) has a maximum when the COI is placed at the cell boundary of the interfering cell. The reasons for this are twofold: firstly, the power control mechanism in CDMA to cope with the near-far effect results in high transmission powers of the mobiles at the cell boundary and low transmission powers close to the BS, and secondly the high correlation of lognormal shadowing for close BS separations results in reduced ACI. The latter effect can be

explained by the fact that, the higher the correlation between interference path and the useful path the less the interference power varies. Furthermore, it can be seen from Fig. 3 that the better the synchronisation ($\alpha \approx 0$) the less BS \rightarrow BS and the more MS \rightarrow BS interference. With the parameters assumed here, co-

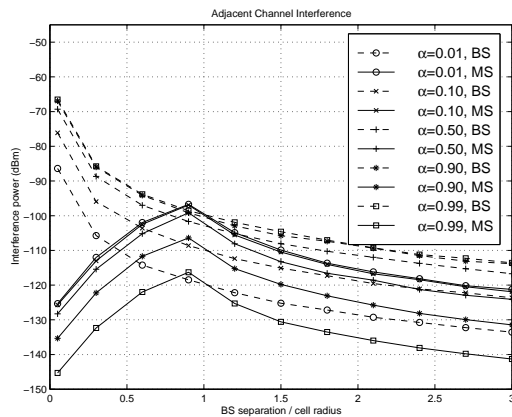


Fig. 3. Adjacent channel interference at the BS with ACP=30 dB, $M=8$ and $P_{out}=5\%$.

location of base stations using adjacent carriers results in a significant capacity loss (Figures 4 and 5). This is because, despite almost perfect synchronisation ($\alpha \approx 0$), the BS \rightarrow BS interference in case of co-location is quite severe (about -90 dBm). Comparing

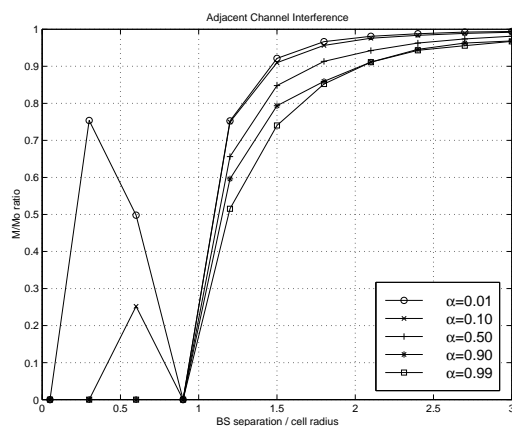


Fig. 4. Remaining capacity — M / M_0 with ACP=30 dB, $M=8$ and $P_{out}=5\%$.

Fig. 4 with Fig. 5 it can be inferred that by increasing the ACP from 30 dB to 35 dB the capacity drop can be reduced considerably, especially when locating the COI within the area of the interfering cell. With a synchronisation of $\alpha = 0.1$ and a BS separation of 60 m, for example, the remaining capacity

increases from about 25 % to 75 %. Furthermore, in Fig. 4 the capacity for $\alpha=0.01$ and $\alpha=0.1$ increases significantly when moving the COI out of the centre of the interfering cell before it drops again in a BS separation range between 30 m and 90 m. With BS separations higher than the cell radius (> 100 m) the capacity constantly increases since no continuous coverage was assumed. Hence, sub-optimal BS locations can be found inside the cell employing the adjacent carrier. This effect can be explained with the aid of Fig. 3. From eqn. (4) it can be seen that ACI is composed of I_{MS} and I_{BS} . The trade-off that I_{MS} has its maximum at the cell boundary whereas I_{BS} is highest for co-location and the fact that I_{MS} does not increase in the same way as I_{BS} decreases results in the discovered sub-optimal BS locations. In addition, to this effect can be attributed that in Fig. 5 for a BS separation of 90 m the capacity for inverse synchronisation (BSa is transmitting whereas BSb is receiving — $\alpha = 0.99$) is better (70 %) than for $\alpha=0.01$ (52 %). Again, it is worth noting that the graphs in Figures 4 – 6 only show the remaining capacity due to ACI; other cell interference on the same carrier is omitted. The results in Figures 4 and 5 are from a worst case scenario since the interfering TS is at its maximal load. Therefore, in Fig. 6, the load has been

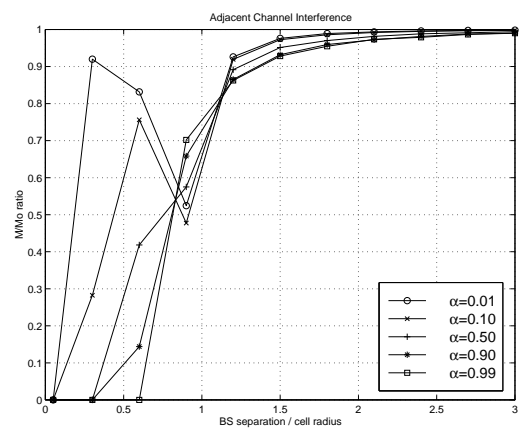


Fig. 5. Remaining capacity — M / M_0 with ACP=35 dB, $M=8$ and $P_{out}=5\%$.

reduced to a single user. The most significant result here is that co-location is still accompanied by a considerable reduction of capacity. Qualitatively, the same behaviour can be ascertained as in Fig. 4. The results improve significantly; assuming, for example, a BS separation of 90 m and $\alpha=0.01$ the capacity increases from 0 % up to about 78 %. All the results are gained by a static analysis not considering any

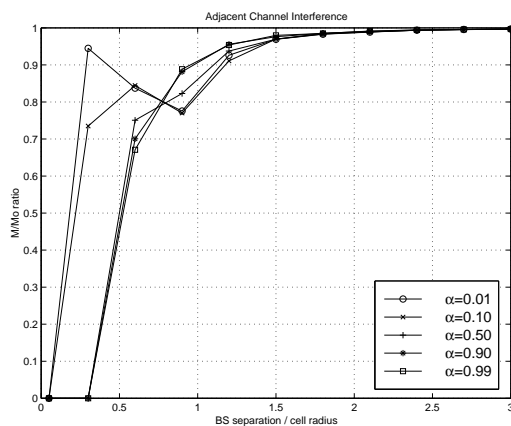


Fig. 6. Remaining capacity — M / M_0 with $ACP=30$ dB, $M=1$ and $P_{out}=5\%$.

DCA algorithm. However, the potential of such an DCA algorithm is of general interest since the results shown are rather poor. Therefore, we modelled the utilisation of a DCA algorithm by increasing the outage threshold P_{out} to 50 % implicitly assuming that the increased probability of high interference can be resolved by intelligent radio resource management. The results are given in Fig. 7. The results in Fig.

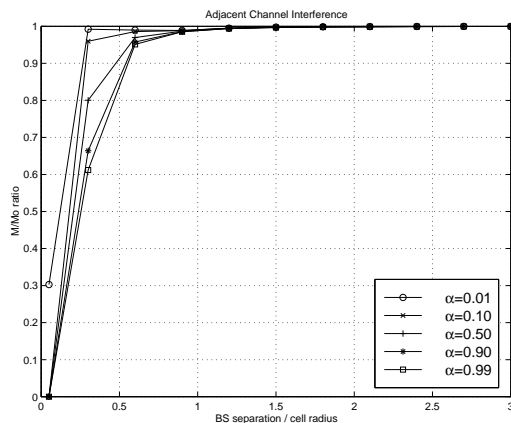


Fig. 7. Remaining capacity — M / M_0 with $ACP=30$ dB, $M=8$ and $P_{out}=50\%$.

7 have to be compared with those in Fig. 4. It can be seen that the improvement in capacity is significant. With a BS separation of 30 m and perfect synchronisation ($\alpha = 0.01$) the remaining capacity is almost 100 % compared to 75 % in the previous case. Since the underlying assumption is that outage for the given TS is 50%, on average, every second uniformly distributed mobile requires the DCA to rearrange users between time slots. It remains unclear

whether a DCA algorithm is capable of dealing with this situation so that the overall performance does not deteriorate.

It can be shown that the results gained by the single-cell model do not differ significantly compared to those obtained by a multiple-cell scenario. The reasons for this are that, on the one hand, in a single-cell scenario there is a greater probability of high power interference due to lognormal shadowing and not having the possibility to hand over to the adjacent cell. On the other hand the interference from surrounding cells is neglected. Both effects counter each other.

V. CONCLUSIONS

From the set of scenarios investigated it is apparent that an intelligent DCA algorithm has to be employed to enable co-location of cells using adjacent carriers unless a significant drop of capacity can be tolerated. Furthermore, a DCA algorithm can exploit the fact that perfect synchronisation does not always yield the highest capacity and that sub-optimal BS separations exist. Further investigation will concentrate on exploiting these findings to develop an appropriate DCA algorithm.

ACKNOWLEDGEMENTS

The authors gratefully acknowledge the support of these studies by the *Faculty of Science and Engineering* and the *Department of Electronics and Electrical Engineering* at the University of Edinburgh.

REFERENCES

- [1] J. Plechinger, T. Kella, F. M. Berens, P. Jung, and K. Schneider, "Interference in cellular joint detection code division multiple access (JD-CDMA) mobile radio systems," in *Proceedings of the 1998 48th IEEE Vehicular Technology Conference*, vol. 3 of 3, (Ottawa, Canada), pp. 1864–1867, IEEE, May 18–21 1998.
- [2] ETSI SMG2 UMTS L1 Expert Group#3, "Adjacent Channel Interference in UTRA system, revision 1." Tdoc SMG2 UMTS-L1 100/98, May 1998.
- [3] G. J. R. Povey, "Capacity of a cellular time division duplex CDMA system," *IEE Proceedings: Communications*, vol. 141, pp. 351–356, October 1994.
- [4] ETSI, "UTRA TDD, Transport channels and Physical channels description." V0.1.0 1998-09, 1998.
- [5] K. Miya, O. Kato, K. Homma, T. Kitade, and M. Hayashi, "Wideband CDMA Systems in TDD-Mode Operation for IMT-2000," *IEICE Transactions: Communications*, vol. E81-B, pp. 1317–1325, July 1998.

The Effects of Interference Between the TDD and FDD Mode in UMTS at the Boundary of 1920 MHz

H. Haas and S. McLaughlin
 Department of Electronics and Electrical Engineering,
 The University of Edinburgh
 The King's Buildings, Mayfield Rd.
 Edinburgh, EH9 3JL, UK
 Ph: +44 (0)131 650 5659, Fax: +44 (0)131 650 6554
 email: hh@ee.ed.ac.uk

G. J. R. Povey
 Elektrotit (UK) Ltd.,
 Edinburgh Technology Transfer Centre
 Mayfield Road, Edinburgh EH9 3JL,
 Scotland UK

Abstract— The Universal Mobile Telecommunications System (UMTS) is composed of an FDD and TDD mode. The spectrum allocation is in such a way that both modes have an adjacent carrier at 1920 MHz. The implications thereof with respect to system capacity are investigated in this paper. In this context the separation distance of the TDD and FDD base station (BS) and frame synchronisation are varied. It is shown that the most detrimental effects for the FDD interface are for small BS separations. In contrast, the optimum with respect to TDD capacity is found for the co-location of both base stations. This yields a trade-off for the optimal BS locations. Moreover, an adjacent channel protection factor of 30 dB in an interference limited system such as CDMA is shown to be too low unless a significant capacity loss is acceptable.

I. INTRODUCTION

In Europe, the third generation mobile telecommunication standard UMTS comprises two air interfaces. One of these interfaces utilises CDMA combined with frequency division duplex (FDD). The other uses CDMA/TDMA and time division duplex (TDD) to achieve two way communication. The TDD mode is referred to as UTRA-TDD with UTRA standing for *UMTS terrestrial radio access*. Likewise, the FDD mode is referred to as UTRA-FDD. The spectrum allocation for UTRA-TDD is split into two bands: 1900–1920 MHz and 2010–2015 MHz. The UTRA-FDD uplink frequency band is between 1920–1980 MHz and the UTRA-FDD downlink uses the frequency band in the range of 2110–2170 MHz[1]. In this frequency plan UTRA-TDD and the uplink of UTRA-FDD have a common boundary at 1920 MHz. This situation has several implications on adjacent channel interference (ACI¹).

In a previous paper [2] the statistics of the minimum coupling loss (MCL) between UTRA-TDD and UTRA-FDD were investigated without showing the effects on system capacity.

In general, the main problem is that, due to the different duplex methods, both systems suffer differently from ACI. In the FDD system only the uplink is affected, i.e. only the BS of the FDD system is subject to ACI from UTRA-TDD entities. In turn, the FDD mobiles contribute to ACI at the UTRA-TDD interface. Since in a TDD system, uplink and downlink are on the same carrier frequency both directions are affected by interference from FDD mobiles. This scenario is depicted in Fig. 1.

In section II, a general equation for the relative capacity reduction due to ACI is developed, followed by the description of the propagation

¹Usually ACI is defined as interference from an adjacent carrier of the same radio interface. However, throughout this paper ACI is defined as interference between UTRA-TDD and UTRA-FDD at the boundary of 1920 MHz.

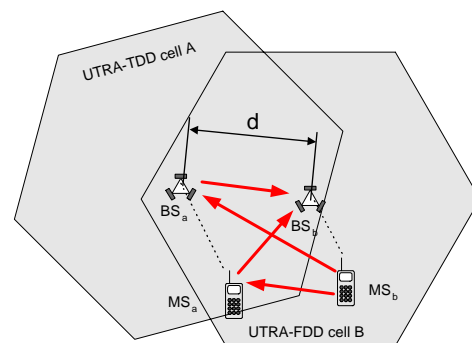


Fig. 1: Principles of inter-system interference in UMTS. Operator A is assumed to utilise the UTRA-TDD carrier below 1920 MHz and operator B uses the FDD uplink carrier next to 1920 MHz. Since each cell is assumed to belong to a different operator the cells may overlap in a random manner.

model in section III. In section IV, the results of the capacity analysis for the UTRA-FDD system are presented while in section V the impact of ACI on capacity in the UTRA-TDD system is investigated. Finally, conclusions are drawn in section VI.

II. CAPACITY DEFINITIONS

The capacity calculation used here is based on the methodology as defined in [3,4]. In these papers cell capacity in the presence of other-cell interference² is analysed. The characteristic of ACI is different from other-cell interference. As demonstrated in [5] this is because in a CDMA system, the assignment of users based on the minimum path loss rather than on the minimum distance has a severe impact on capacity. As a consequence, handover, soft-handover in particular, can decrease high other-cell interference. All these methods are of limited use in the presence of ACI since the adjacent channel might belong to a different operator. This becomes particularly important when only a limited number of carriers are available, as in W-CDMA (Wideband CDMA).

Ideal power control in the uplink is assumed. With this assumption

²Interference from cells using the same carrier. Usually a reuse distance of 1 is assumed.

E_b/I_0 can be denoted using the same model as in [3],

$$E_b/I_0 = \frac{P_u pg}{P_u(M-1) + I_{ad} + N} \quad (1)$$

where P_u is the received, power-controlled signal power from the desired user, M is the number of users that can be served, I_{ad} is ACI power, N is thermal noise and pg is the processing gain. Since in this paper the focus is on the capacity reduction due to I_{ad} , equation (1) may be rearranged and the ratio M/M_0 calculated, where M_0 is the capacity derived from (1) with no adjacent channel interference ($I_{ad} = 0$),

$$M_0 = \frac{pg}{E_b/I_0} - \frac{N}{P_u} + 1 \quad (2)$$

Thus, the ratio M/M_0 , which can be interpreted as the relative remaining cell capacity, denoted as follows:

$$M/M_0 = 1 - \frac{I_{ad}}{P_u \left(1 + \frac{pg}{E_b/I_0}\right) - N} \quad (3)$$

From (3), it can be seen that the capacity reduction term is directly proportional to I_{ad} . Moreover, it can be shown that the useful signal becomes:

$$P_u = \frac{N E_b/I_0 I_{mar}}{pg} \quad (4)$$

with I_{mar} representing an interference margin to account for an increased noise floor due to own-cell interference. I_{mar} can be calculated as follows:

$$I_{mar} = \frac{1}{1 - \frac{(M-1)E_b/I_0}{pg}} \quad (5)$$

Since the denominator in (5) must be positive and greater than zero, an upper bound for the cell load can be determined which yields M_{max} ,

$$M_{max} = \frac{pg}{E_b/I_0} + 1 \quad (6)$$

Moreover, in this paper the relative capacity load is expressed by:

$$\mu = \frac{M}{M_{max}} \quad (7)$$

By substituting (4) and (5) into (3) and using (7) the relative capacity M/M_0 can be written as:

$$M/M_0 = 1 - \frac{I_{ad}}{N} \left(\frac{1}{\mu} - 1\right) \quad (8)$$

Equation (8) highlights an interesting property. It is that the sensitivity to ACI decreases with the cell load because the useful signal P_u is lowest for only one own-cell user and increases in a non-linear fashion with the number of users, i.e. for M_{max} users P_u tends to infinity (equation (5)). However, the conclusion is not that a large population in the own-cell diminishes the impacts of ACI. This is because the TDD and FDD mode are mutually coupled by ACI. This means an increase of the number of own-cell users results in a greater ACI term, I_{ad} , in the co-existing, independent mode. Therefore, the victim cell has to increase its useful signal power to compensate for an augmented ACI contribution. This, in turn, results in an increased ACI in the system which originally has increased the number of users.

The aim of this paper is to calculate I_{ad} with the cell load not exceeding a certain threshold set by the admission control of the radio resource management.

Tab. 1: Simulation parameters

Parameter	Value
Logn. standard deviation, σ	10 dB
ACIR	30 dB
Noise figure (receiver)	5
Minimum distance, d_{min}	5 m
Path loss exponent, γ	3.0

ACI is caused by transmitter and receiver imperfections. The final adjacent channel protection factor taking into account transmitter and receiver imperfections is defined as *Adjacent Channel Interference Power Ratio* ACIR [6]. Throughout this paper this definition will be used.

III. PROPAGATION MODEL

The path loss model used here is based on the COST-231 static propagation models [7]. The same path loss model is applied for the TDD mode and the FDD mode as well as for the interference between both modes. In particular, the indoor office test environment assuming no floor or wall losses is used. This results in:

$$a = 37 + \gamma 10 \log(\max\{d, d_{min}\}) + \xi \text{ [dB]} \quad (9)$$

where γ is the path loss exponent and d is the distance between transmitter and receiver. The distance d is lower bound by an exclusion zone defined by d_{min} . The effects of shadowing are modelled by a lognormal random variable, ξ , with the standard deviation σ and zero mean.

If the UTRA-TDD BS (BS_{TDD}) and the UTRA-FDD BS (BS_{FDD}) are co-sited and both mobiles (MS_{FDD} and MS_{TDD}) are in close proximity, the desired signal and the interfering signal experience similar propagation conditions. Therefore, the signals cannot be assumed to be uncorrelated. To account for the correlation between the main path and the interfering path it is necessary to introduce a functional relationship between the BS separation distances and the correlation coefficient of the lognormal shadowing variables on each path [8]. Let ξ_d be the lognormal random variable on the desired link and ξ_I that on the interference link, then the conditional probability assuming a correlation coefficient r can be modelled as:

$$p(\xi_I | \xi_d) = \frac{1}{\sigma \sqrt{2\pi(1-r)}} \exp\left(-\frac{(\xi_I - r\xi_d)^2}{2\sigma^2(1-r^2)}\right) \quad (10)$$

In (10) it is implied that the standard deviation σ is the same on both links. Furthermore, we assume the following relationship between r and the BS separation distance d

$$r = \begin{cases} 1 - \frac{d}{R} & \text{if } d \leq R, \\ 0 & \text{otherwise,} \end{cases} \quad (11)$$

where R is the cell radius. This model is applied for interference calculation at the BS_{TDD} and BS_{FDD} . For the interference calculation the parameters listed in Tab. 1 are used. In the subsequent sections the interference scenarios are described.

IV. INTERFERENCE: UTRA-TDD TO UTRA-FDD

A Interference Model

In the first instance the UTRA-TDD mode may primarily be used for locations with tensed traffic ('hot-spots'). Therefore, a single TDD

Tab. 2: UTRA-TDD simulation parameters

Parameter	Value
Radius	100m
Maximum MS Tx power	4 dBm
Maximum BS Tx power	10 dBm
Minimum E_b/I_0 at the MS	2.0 dB
Minimum E_b/I_0 at the BS	2.0 dB
Bitrate	16 kbps

cell is considered. In this analysis a symmetric services in the UTRA-TDD mode is assumed. The UTRA-TDD interface is designed in such a way that up to 8 individual mobiles can be served by one TS. Only a simple downlink power control mechanism is applied: the code power is determined by the mobile experiencing the greatest path loss. The same code power is then applied to each user. This ensures that the E_b/I_0 threshold is maintained for all users as shown in the following:

Let the downlink code power, P_{code} , be determined by that user for which the maximum path loss, a_{max} , applies so that the required bit energy to interference ratio, $(E_b/I_0)_{req}$, is maintained which results in:

$$(E_b/I_0)_{req} = \frac{P_{code} P_G}{(M-1) P_{code} + a_{max} (I_{ad} + N)}, \quad (12)$$

and it follows that:

$$E_b/I_0 > (E_b/I_0)_{req} \quad \forall a < a_{max}. \quad (13)$$

The interference scenario of UTRA-TDD interfering with UTRA-FDD is depicted in Fig. 2. The illustration shows that ACI at the

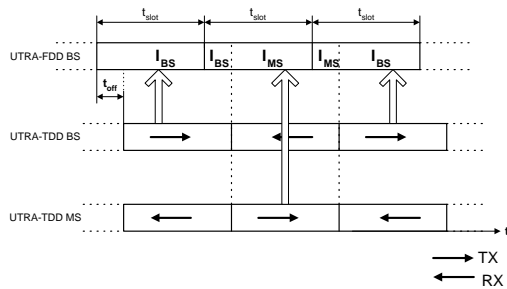


Fig. 2: Interference at the BS of the UTRA-FDD system

BS_{FDD} is not constant for each TS, but is dependent on the frame offset (t_{off}). Let the transmission power of the TDD entities be constant over one TS period and with $\alpha = t_{off} / t_{slot}$ being the frame offset relative to one slot duration (t_{slot}), the maximal interference at the BS_{FDD} becomes:

$$\hat{I}_{ad} = \max \{ ((1-\alpha)I_{BS} + \alpha I_{MS}), (\alpha I_{BS} + (1-\alpha)I_{MS}) \}, \quad (14)$$

where I_{BS} represents the $BS_{TDD} \rightarrow BS_{FDD}$ interference and I_{MS} defines the $MS_{TDD} \rightarrow BS_{FDD}$ interference as shown in Fig. 2. Simulations were carried out using the parameters as shown in Tab. 2. A spatial uniform user distribution, uniform in x and y, was assumed to obtain the probability density function (pdf) of I_{ad} at the BS of the cell of interest (COI). Given a certain outage threshold, which is

$P_{out} = Pr(\hat{I}_{ad} > I_{ad}), I_{ad}$ can be derived and fed into (8) to get the relative remaining capacity.

B Results

In Fig. 3, the interference power at the BS_{FDD} caused by UTRA-TDD entities is shown. Since only the uplink of the FDD cell is affected by ACI from the TDD mode the actual FDD cell radius does not have an impact on the results. Therefore, the BS separation, on the x-axis, is normalised to the TDD cell radius. As expected, the relative frame offset of $\alpha = 0.5$ improves the results by about 3 dB. As can be seen from (14), the results with α and $1-\alpha$ are equal by symmetry.

Fig. 3 demonstrates that the interference decreases with an increasing BS separation. However, the interference power is almost constant for a relative BS separation in the range of 0.5 to 1.0. The reason for this is that I_{ad} is the sum of I_{MS} , which increases with a greater BS separation until the cell boundary of the UTRA-TDD cell is reached, and I_{BS} , which decreases monotonically.

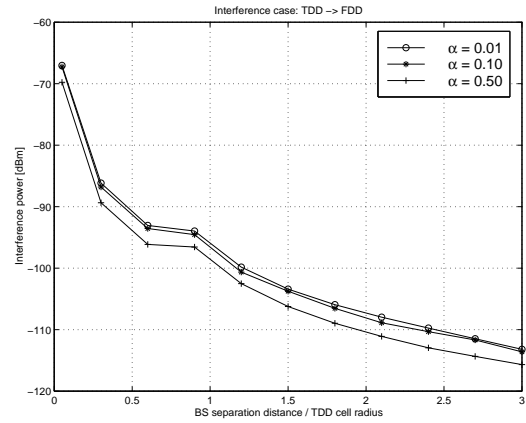


Fig. 3: Interference at the BS_{FDD} caused by UTRA-TDD entities which use the adjacent UTRA-TDD carrier with $M = 8$ users, $ACIR = 30$ dB and $P_{out} = 5\%$.

Fig. 4 shows the relative capacity in the UTRA-FDD cell as a consequence of ACI from the adjacent TDD interface. It can be found that the capacity reduction in the FDD cell changes drastically for BS_{FDD} locations close to the TDD cell boundary. Locating the BS_{FDD} inside the TDD cell causes a significant capacity loss whereas locating the BS_{FDD} outside the TDD cell results in a considerable increase of the relative FDD capacity. This means that the FDD system cannot be operated without largely stealing capacity from the TDD system within a relative BS separation range of 0 to 1.0.

The UTRA-TDD system inherently generates a bursty type of interference. Therefore, as seen from Fig. 2, the interference profile over one UTRA-FDD frame is not constant. Given that the interference maximum calculated according to (14) does not apply over the entire frame, the results are for the worst case. Moreover, a symmetrical speech service with fully loaded TDD time slots is assumed. Since the symbols of the UTRA-FDD user are spread over one frame, forward error correction (FEC) coding and interleaving may be capable

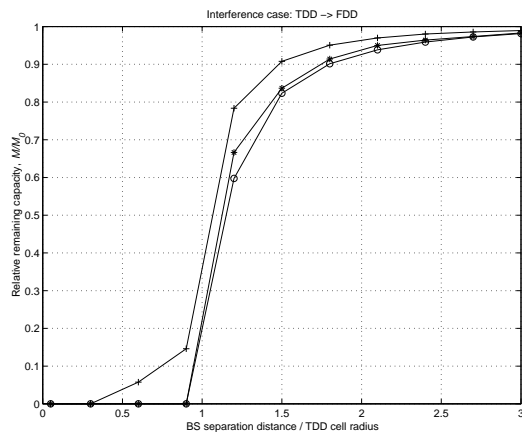


Fig. 4: Capacity in the UTRA-FDD cell relative to capacity in a non-interfered state — M/M_0 with $ACIR = 30$ dB, $M = 8$ users, $\mu = 0.75$ and $P_{out} = 5\%$.

Tab. 3: UTRA-FDD simulation parameters

Parameter	Value
Radius	2000 m
Max MS Tx power	24 dBm
Max BS Tx power	30 dBm
Minimum E_b/I_0 at the MS	7.9 dB
Minimum E_b/I_0 at the BS	5.6 dB
Bitrate	15 kbps
Users per frame	70

of compensating for the bursty UTRA-TDD interference. Therefore, the results have to be considered as a worst case scenario.

V. INTERFERENCE: UTRA-FDD TO UTRA-TDD BS

A Interference Model

The parameters for UTRA-FDD (Tab. 3) are taken from ETSI (European Telecommunications Standards Institute) simulations of Vehicular A, 120km/h and speech service [9].

UTRA-FDD mobiles are assumed to transmit continuously. Ideal handover in the FDD system is assumed. A frame offset as outlined in Fig. 2 does not have any impact. The UTRA-FDD system is assumed to account for full spatial coverage. In contrast, the TDD mode is likely to be used for 'hot spots' in pico cellular environments. Therefore, the cell topology according to Fig. 5 is applied.

B Results

Fig. 6 shows the interference at the BS_{TDD} . Due to the underlying cell topology it is apparent that the results are symmetrical to a BS separation which equals the FDD cell radius (2000 m).

The interference has a maximum when placing the BS_{TDD} at the cell boundary of the FDD cell since the interferer (UTRA-FDD mobile) transmits high powers when located at the cell boundary.

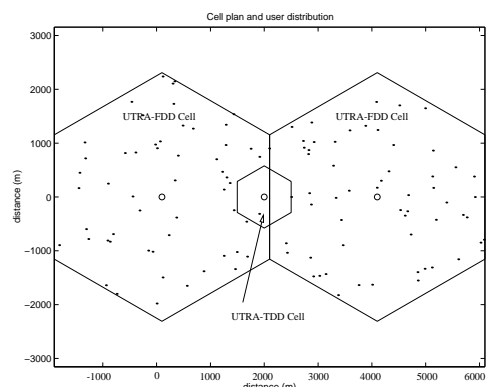


Fig. 5: Cell topology applied for calculation of UTRA-FDD to UTRA-TDD interference.

The gradient of the interference as a function of the BS separation distance in Fig. 6 is significantly greater for a BS separation range between 5 m – 500 m (about 2.0 dB/100m) than for the range between 1500 m – 2000 m (about 0.17 dB/100m). However, the absolute interference level for small BS separations is about 20 dB below the thermal noise floor. Therefore, the greater sensitivity of interference to small BS separations will not greatly affect capacity. On the other hand, the interference level approaches the thermal noise level for BS_{TDD} locations at the cell boundary and since the spatial sensitivity of interference is low for these locations a great percentage of the area within the FDD cell may cause considerable capacity reductions in the TDD cell if the BS_{TDD} is located within these areas.

Fig. 7 shows the relative capacity results in the TDD cell. When the BS_{FDD} and BS_{TDD} are co-sited, the interference at the BS_{TDD} is minimal since the interfering signal from the MS_{FDD} arrives in a power controlled manner. Therefore, co-location of the BS_{TDD} and BS_{FDD} results in the least capacity reduction with respect to the TDD mode. This is contrary to the results from the TDD → FDD interference investigation. For the scenario investigated the maximum capacity reduction in the TDD cell is about 22 % for a BS_{TDD} location at the FDD cell boundary. The capacity reduction in the TDD cell is less severe than in FDD cell. One explanation for this is that the FDD mobiles can choose between two serving BS which results in significantly less interference than if only one serving BS would exist. This was demonstrated by Viterbi in [13]. However, since the UTRA-FDD mobiles transmit continuously, all 15 time slots of the UTRA-TDD interface are affected. This is an important difference from the case of ACI between carriers of the UTRA-TDD interface where a dynamic channel allocation (DCA) algorithm can be employed to resolve severe interference scenarios [10, 11].

VI. CONCLUSIONS

- On the one hand, it has been shown that in order to minimise interference of the UTRA-TDD carrier from the UTRA-FDD uplink carrier, it is advantageous to co-locate BS_{FDD} and BS_{TDD} . On the other hand, in order to minimise the interference at the UTRA-FDD carrier caused by the UTRA-TDD mode, it is necessary to separate the base stations as far as possible. Clearly, these conclusions yield a trade-off for the

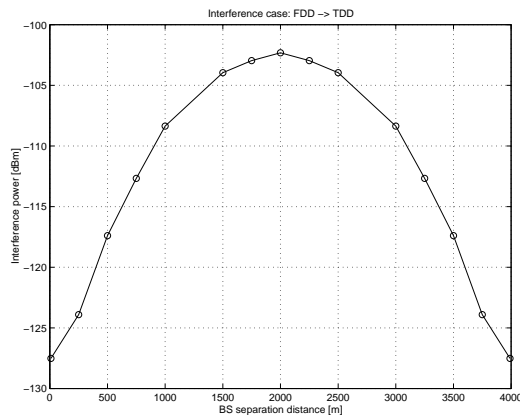


Fig. 6: Interference at the BS_{TDD} caused by mobiles using the adjacent UTRA-FDD uplink carrier with $M = 70$ users, $ACIR = 30$ dB and $P_{out} = 5\%$.

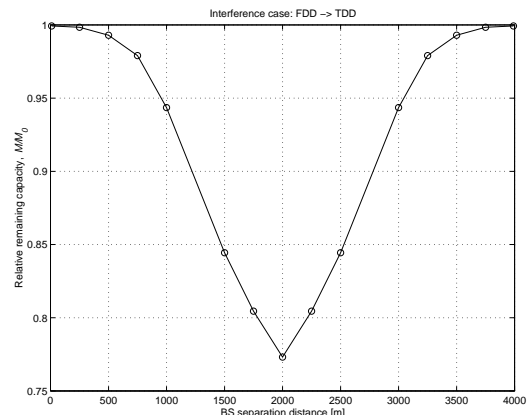


Fig. 7: Capacity in the UTRA-TDD cell relative to capacity in a non-interfered state — M/M_0 with $ACIR = 30$ dB, $M = 70$ users, $\mu = 0.75$ and $P_{out} = 5\%$.

optimal BS locations. Co-location with the assumed $ACIR$ is not feasible and the BS_{FDD} is ideally located outside the TDD cell unless the $ACIR$ is increased significantly.

- An adjacent channel protection factor of 30 dB results in a significant capacity reduction in both modes, i.e. both interfaces have to share capacity. This is of special importance if both carriers belong to different operators. Therefore, it is recommended that the $ACIR$ is increased in this particular case.
- It has been shown that the effect of the bursty interference from the UTRA-TDD carrier to the UTRA-FDD uplink is more significant since the receiver sensitivity at the UTRA-FDD BS is greater. However, due to continuous transmission in UTRA-FDD, baseband methods such as forward error correction coding (FECC) might be able to compensate for the bursty interference from the TDD interface. This is an area of further investigation.

The capacity reductions may be compensated by dynamic transmit power adjustments on the expense of cell coverage. This mechanism was studied in an extended paper [12] where also non-ideal power control was assumed.

ACKNOWLEDGMENTS

The authors gratefully acknowledge the support of this study by NOKIA, the EPSRC and The Royal Society.

REFERENCES

- [1] K. Miya, O. Kato, K. Homma, T. Kitade and M. Hayashi, "Wideband CDMA Systems in TDD-Mode Operation for IMT-2000," *IEICE Transactions: Communications*, vol. E81-B, pp. 1317-1325, July 1998.
- [2] P. Seidenberg, M. Peter Althoff, Egon Schulz and G. Herbst, "Statistics of the Minimum Coupling Loss in UMTS/IMT-2000 Reference Scenario," in *Proceedings of VTC 1999 - Fall*, vol. 2, (Amsterdam, The Netherlands), pp. 963-967, September 19-22 1999.
- [3] K. S. Gilhousen, I. M. Jacobs, R. Padovani, A. J. Viterbi, L. A. Weaver Jr. and C. E. Wheatly III, "On the capacity of a cellular CDMA system," *IEEE Trans. on Vehicular Tech.*, vol. 40, pp. 303-312, May 1991.

- [4] Y. Ishikawa and S. Onoe, "Method for evaluating W-CDMA system capacity considering adjacent channel interference," *Electronics Letters*, vol. 35, pp. 968-969, June 1999.
- [5] T. Chebaro and P. Godlewski, "About the CDMA Capacity Derivation," *Proceedings of the International Symposium on Signals, Systems and Electronics*, (Paris, France), pp. 36-39, September 1-4 1992.
- [6] 3rd Generation Partnership Project (3GPP), Technical Specification Group (TSG), Radio Access Network (RAN), Working Group 4 (WG4), "Evaluation of up- and downlink adjacent channel performance," *TSGR4#2(99)048*, February 1999.
- [7] ETSI 30.03, V3.2.0 (1998-04), "Universal Mobile Telecommunications System (UMTS); Selection procedures for the choice of radio transmission technologies of the UMTS," *TR 101 112*, 1998.
- [8] M. Gudmundson, "Correlation Model for Shadow Fading in Mobile Systems," *Electronics Letters*, vol. 27, pp. 2145-2146, November 1991.
- [9] ETSI, "The ETSI UMTS Terrestrial Radio Access (UTRA) ITU-R RTT Candidate Submission," ITU, January 1998.
- [10] H. Haas and G. J. R. Povey, "The Effect of Adjacent Channel Interference on Capacity in a Hybrid TDMA/CDMA-TDD System Using UTRA-TDD Parameters," in *Proceedings of VTC 1999 - Fall*, vol. 2, (Amsterdam, The Netherlands), pp. 1086-1090, September 19-22 1999.
- [11] H. Holma, G. J. R. Povey and A. Toskala, "Evaluation of Interference Between Uplink and Downlink in UTRA/TDD," in *Proceedings of VTC 1999 - Fall*, vol. 2, (Amsterdam, The Netherlands), pp. 2616-2620, September 19-22 1999.
- [12] H. Haas, S. McLaughlin and G. J. R. Povey, "Capacity-Coverage Analysis of the TDD and FDD Mode in UMTS at 1920 MHz," submitted to: *IEE Proceedings - Communication*, May 2000.
- [13] A. J. Viterbi and A. M. Viterbi, "Other-Cell Interference in Cellular Power-Controlled CDMA," *IEEE Trans. on Communications*, vol. 42, no. 2/3/4, pp. 1501-1504, February/March/April 1994.

A Novel Interference Resolving Algorithm for the TDD TD-CDMA Mode in UMTS

H. Haas, S. McLaughlin and G. J. R. Povey[†]
 Department of Electronics and Electrical Engineering,
 The University of Edinburgh,
 The King's Buildings, Mayfield Road
 Edinburgh, EH9 3JL, UK
 Phone:+44 (0)131 650 5655, Fax:+44 (0)131 650 6554
 Emails: hh@ee.ed.ac.uk, sml@ee.ed.ac.uk

ABSTRACT — When comparing UTRA-TDD with UTRA-FDD it can be found that in the UTRA-TDD mode additional interference scenarios exist. Mobile stations (MS's) can interfere with each other and so can base stations (BS's). Since the source and sink of this type of interference are the same we call it *same-entity* interference. It is shown by a novel interference resolving algorithm that *same-entity* interference can be constructively exploited to enable asynchronous overlaps in a UTRA-TDD network. Asynchronous overlaps exist when any cell A is transmitting while the neighbour cell B is receiving. It was found that in a network where an asynchronous overlap exists the algorithm proposed reduces outage from 14 % to 6 %. In contrast, the outage of an ideally synchronised network was found to be 3.5 %. In this 'ideal' network asynchronous overlaps are disallowed resulting in a significant drawback. This is that the flexibility of a TDD system to easily adopt different channel asymmetries is significantly limited.

I. INTRODUCTION

The air interface of UMTS is composed of two types of access modes. Firstly, the FDD mode in combination with W-CDMA is employed in the paired spectrum (2 x 60 MHz). Secondly, in the unpaired radio frequency bands (20 MHz and 15 MHz) the TDD mode and a hybrid form of TDMA and CDMA are used. The latter is referred to as UTRA-TDD where UTRA is UMTS Terrestrial Radio Access. The FDD mode is referred to as UTRA-FDD.

Previous capacity analyses have concentrated on FDD systems [1–5]. The analysis carried out in this paper will focus on the UTRA-TDD mode and its TDD inherent features. In this context, when comparing UTRA-TDD with UTRA-FDD two main differences can be ascertained:

1. The TDMA component in UTRA-TDD results in an additional orthogonality due to the separation in time and thus provides an additional degree of freedom with respect to allocating a radio resource unit. This requires special radio resource management algorithms [6].

[†]Elektrobit (UK) Ltd, Edinburgh Technology Transfer Centre, Mayfield Road, Edinburgh EH9 3JL, Scotland UK

2. Due to the nature of the TDD method additional interference scenarios exist [7]. In an FDD system primarily $MS \leftrightarrow BS$ interference exists which we call *other-entity* interference. In addition to that, in a TDD system $MS \leftrightarrow MS$ and $BS \leftrightarrow BS$ interference exist since uplink and downlink are on the same carrier frequency. Since source and sink of interference are the same we categorise this type of interference as *same-entity* interference. This means that a TDD system in principle is subject to more interference mechanisms than an FDD system. In order to demonstrate this, Fig. 1 shows a possible interference scenario in UTRA-TDD.

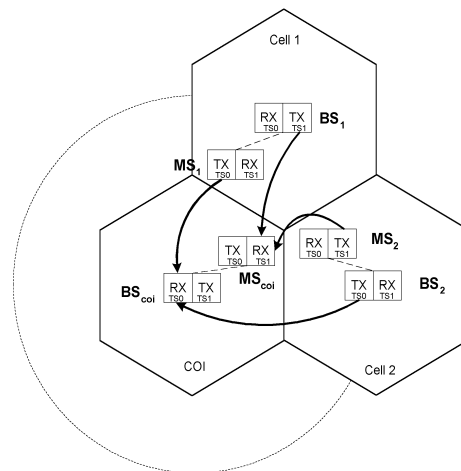


Fig. 1. A cell arrangement with each cell using two successive time slots where the first begins at the same time in each cell is shown. The direction of transmission is arranged so that the cell of interest (COI) and cell 1 receive in TS0 and transmit in TS1. In contrast, the BS of cell 2 first transmits and then receives resulting in an asynchronous overlap in TS0 and TS1 with respect to the COI and cell 1.

Since a TDD system is exposed to more interference scenarios than an FDD system, and CDMA is an interference limited technique, the performance of UTRA-TDD can be significantly poorer compared to an equivalent FDD system. Therefore, it is suggested that the TDD network is synchronised such that all time slots (TS's) are aligned

and that neighbouring cells need to adopt the same *rate of asymmetry*¹. This means that at any arbitrary time, t , the direction of transmission of two neighbouring cells must be the same. In contrast, we define the state in which one cell transmits while the other receives as an *asynchronous cell overlap*. Being aware that one advantage of TDD is to enable different rates of asymmetry, since this can be managed in the time domain, a requirement to avoid *asynchronous overlaps* is clearly a significant limitation.

However, the TDMA inherent property stated in 1., i.e. that an additional dimension of orthogonality exists, can be utilised to overcome the problems of additional interference stated in 2.. In this paper a novel method is proposed called the *opposing algorithm* [8]. This exploits the fact that interference in TDD is composed of *same-entropy* interference and *other-entropy* interference, where the magnitude of each varies depending on the current scenario [7].

The remainder of this paper is organised as follows: In section II, the motivation for the *opposing algorithm* is derived from an analytical consideration of the TDD inherent properties. Subsequently, in section III the *opposing algorithm* and the simulation model are presented. The results are given in section IV which are followed by conclusions in section V.

II. MOTIVATION

In previous papers [1, 4] the capacity (number of users) for a CDMA system using FDD was approximated as,

$$M_{FDD} = \frac{pg(1-\eta)}{E_b/I_0(1+f)}, \quad (1)$$

where pg is the processing gain, $\eta = N_0/I_0$ with N_0 the thermal noise density and I_0 the total maximum allowable interference density, E_b the bit energy and f the ratio of other-cell interference to own-cell interference at the cell of interest (COI). It is assumed that joint detection in UTRA-TDD is applied [9] which means that own-cell interference in the baseband is reduced. The utilisation of joint detection in the baseband is modelled by assuming a reduction in the required carrier-to-interference (C/I) ratio.

In the assumptions leading to eqn. (1) only the mobiles of the adjacent cells contribute to the other-cell interference in the uplink since it is an FDD system. The model described in Fig. 1 is adopted here. A factor α is introduced to account for the different interference scenarios shown in Fig. 1. Thus, interference at the BS from the first tier with k adjacent cells can be written as

$$I_{other} = \sum_{i=1}^k [(1-\alpha_i) I_{MS_i} + \alpha_i I_{BS_i}] \quad \alpha_i \in \{0, 1\} \quad (2)$$

¹Since the symmetric use of a channel can be considered as a special case of an asymmetrical usage of a communication channel we use the term *rate of asymmetry* to indicate that a duplex channel can carry different loads in uplink and downlink.

where I_{MS_i} is *other-entropy* interference at the BS_i , I_{BS_i} *same-entropy* interference at the BS_i and α_i is defined as

$$\alpha_i = \begin{cases} 1 & \text{if opposed TX/RX direction,} \\ 0 & \text{otherwise.} \end{cases} \quad (3)$$

Substituting eqn. (2) into eqn. (1) yields,

$$M_{TDD} = \frac{pg(1-\eta)}{E_b/I_0 [1 + \sum_{i=1}^k (f_i + \zeta_i)]}, \quad (4)$$

with

$$\zeta_i = \alpha_i (g_i - f_i), \quad (5)$$

where g_i is the ratio of other-cell interference conveyed by the BS number i to own-cell interference in the cell of interest (COI). Similarly, f_i is the ratio of the total MS interference of cell i to own-cell interference in the COI. The quantity f_i is related to f for an FDD system. Eqn. (4) shows an interesting property of a TDD system. It says that the capacity of a CDMA/TDD system can, in principle, be higher than in an equivalent FDD system if the RX/TX direction of two neighbouring cells are cleverly chosen. If, for example, g_i is smaller than f_i and α_i is chosen such that the time slots overlap asynchronously (hence $\alpha_i = 1$) the total other-cell interference is smaller than f_i and thus smaller than in a similar FDD system.

To demonstrate this, let

$$\alpha_i = \begin{cases} 1 & \text{if } g_i < f_i. \\ 0 & \text{otherwise.} \end{cases} \quad (6)$$

In words, whenever the BS interference contribution from adjacent cell i is smaller than the total MS interference power from cell i , the algorithm opposes the respective time slot, i.e. the direction of transmission between two cells in the same time slot is always in the opposite direction. Thus, ζ_i in eqn. (4) becomes:

$$\zeta_i = \begin{cases} 0 & \text{if } g_i \geq f_i, \\ g_i - f_i & \text{if } g_i < f_i. \end{cases} \quad (7)$$

As a consequence, and quite important to note, it holds that

$$\sum_{i=1}^k \zeta_i \leq 0 \quad \forall \text{ scenarios.} \quad (8)$$

This means, the capacity in a particular CDMA/TDD cell can even be greater than or equal to the capacity of an equivalent CDMA/FDD cell. Thereby *asynchronous cell overlaps* are exploited constructively. The implications of these findings are counter intuitive as one would expect neighbouring cells in a TDD system adopting a different rate of asymmetry to cause a significant capacity loss. However, it is clear that if each cell in a multi-cell environment is using the strategy proposed, conflicting situations may arise. Therefore, a simulation model has been developed to assist in the analysis. This model will be described in the subsequent section.

III. SYSTEM MODEL AND OPPOSING ALGORITHM

A. System Model

The system consists of four cells placed on a square grid as depicted in Fig. 2. Each cell has $k=8$ neighbouring cells (due to the application of a wrap around technique) in order to overcome cell boundary effects. The square grid has been chosen since the mobiles are assigned to a BS based on the minimum path loss, in addition to a handover margin, rather than based on the cell-membership. Thus, the actual cell layout does not greatly affect the results. After a predefined number of users have been distributed

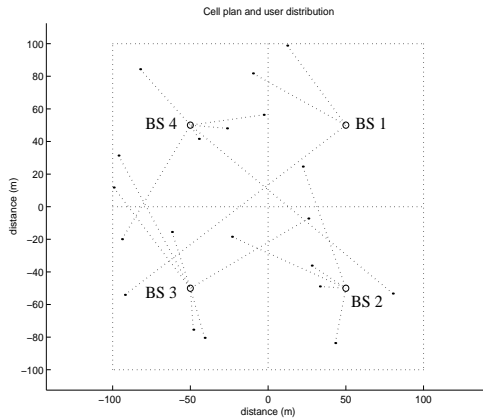


Fig. 2. The user distribution and user assignment based on the minimum path loss is shown for a random scenario. A wrap around technique is applied to prevent cell boundary effects.

randomly and uniformly in space the power control loops in the up- and downlink are initiated. In Fig. 3, a power control snapshot of a mobile, which was randomly chosen, is shown. It can be seen that the transmission power rapidly increases, which leads to the conclusion that the total noise floor in the system is high due to mutual interference effects in a CDMA system. However, a high noise floor means that some mobiles will not achieve the target C/I ratio at the BS and so will experience outage. Removing extreme interferers in turn results in a reduction of the noise floor until the TX power converges to a stable level as can be seen in Fig. 3.

The distribution of a predefined number of mobiles was repeated n times with $n = 10,000$ and the number of mobiles which experience outage in each Monte Carlo run was stored. This enables one to calculate the probability density function (pdf) of outage from which the expected value of outage can be extracted.

B. Opposing Algorithm

In the model above dynamic power control is considered. If the noise floor can be minimised the capacity is optimised automatically. If a TDD system is synchronised in principle two scenarios of interference exist. Firstly, consider the BS of the COI and any neighbouring BS to

transmit and receive at the same time, then only *other- entity* interference exist. The implication for the uplink, for example, is that only the mobiles of the neighbouring cell contribute to interference. Secondly, the BS of the COI transmits while the neighbouring cell is receiving. In this case only *same- entity* interference exists. Hence, the only interferer in the uplink is the BS of the neighbouring cell. Therefore, as described in section II, an algorithm can be developed which minimises interference by either applying opposed or synchronised transmission. This leads to the following algorithm which is operated within the radio network controller (RNC):

BEGIN

Determine the required TX power of user i , P_i , in time slot j of cell k

if $P_i > P_{\max}$

for $l = 1 : \max(\text{Neighbouring_Cells})$

for $n = 1 : \max(\text{TS_in_Use})$ with $j \in \text{TS_in_Use}$

if $\text{TS}_n^l == \text{RX time slot}$

determine interference from mobiles:

$$I_n^l = \frac{I_{\text{thermal}}^l + I_{\text{other}}^l}{1/(C/I_{\min}) - \text{number of mobiles in TS}_n^l + 1} \times \text{number of users in TS}_n^l \times W$$

else

determine interference from BS:

$$I_n^l = \frac{\text{Transmitted carrier power in TS}_n^l}{\text{pathloss}(BS^l, BS^k)}$$

end if

if $\left[\begin{array}{l} (I_n^l < I_j^l) \ \& \\ (\text{direction}(\text{TS}_n^l) \neq \text{direction}(\text{TS}_j^l)) \end{array} \right]$
exchange TS n for TS j in cell l

end if

end for

end for

else

assign channel

end if

END

The algorithm starts when the mobile is requested to transmit with higher power than the maximum permitted, i.e. the state where outage would occur. The algorithm steps in assuming that at least two time slots are occupied by the communication link processed ($\text{TS_in_Use} \geq 2$). It monitors the interference in **all TS's** n of **all** neighbouring cells. Two cases can then be distinguished:

1. If TS n in cell l is used for RX the interference from this particular neighbouring TS is caused exclusively from its mobiles due to the assumption of ideal synchronisation. Since the interference seen at the TS j of cell k

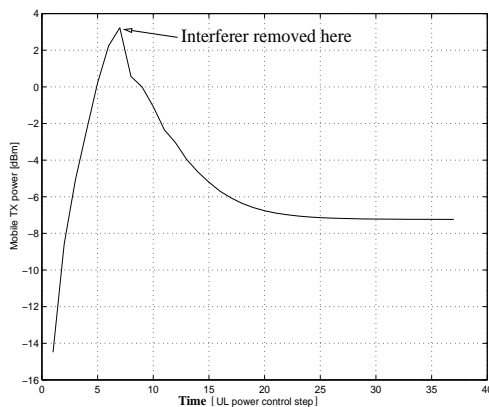


Fig. 3. Dynamic uplink power control: The transmission power of the mobile is successively adjusted.

(the cell and TS inspected by the algorithm) is composed by different sources in a multi-cell environment the exact interference contributed by the mobiles in the observed cell l is not known *a priori* in a real system. However, this interference can be estimated and an upper bound can be calculated. Since the mobiles are assigned on the basis of the minimum path loss, with an inaccuracy modelled by the handover margin, the interference from these mobiles cannot significantly exceed the power level to which these mobiles are controlled by their BS, of cell l , multiplied with the total number of mobiles in cell l . The power level to which a mobile is controlled can easily be reported to a RNC. The same holds for the number of mobiles served. In the estimation process a weight factor W is introduced which nominally is less than 1.

2. If TS n is a TX TS the interference contribution from cell l results only from the BS. The TX power at the BS is known and can be reported to the RNC.

It is examined whether there exists one TS n in the neighbouring cell l which would cause less interference than the current TS j . If this is true **and** TS n is used for RX while TS j was used for TX, or vice versa, then the neighbouring cell interchanges TS n with TS j . This results in *opposing* time slots with respect to the COI. This algorithm is carried out for each mobile, but would only be executed if the TX power exceeds the maximum.

IV. RESULTS AND DISCUSSION

The scenario depicted in Fig. 4 has been applied to investigate the outage experienced by the mobiles. Cell 1 employs a rate of asymmetry which is 3:1, i.e. the traffic in the uplink is 3 times higher than in the downlink. The simulation parameters are given in Table I. Thus, the bit rate in the uplink is 48 kbps compared to 16 kbps in the downlink. In all other cells (cell 2 – cell 4) a symmetric service is assumed with 16 kbps in the uplink as well as in the downlink. This scenario inevitably results in asynchronous cell overlaps. It is assumed that the admission control does not allow more than 8 users to share one TS.

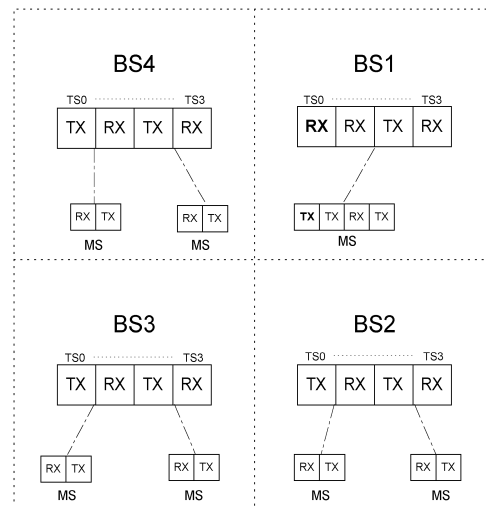


Fig. 4. A scenario with asynchronous cell overlaps.

TABLE I
SIMULATION PARAMETERS

Parameter	Value
Cell radius	50 m
channel bit rate	16 kbps
Chip rate	3.84 Mcps
Standard deviation of lognormal shadowing	10 dB
Receiver noise figure	5
Max. MS TX power	4 dBm
Max. BS TX power	10 dBm
Minimum required E_b/I_0	2.0 dB
Path loss	indoor test environment [10]
Handover margin, γ	2 dB
Estimation weight, W	1.0

This means that in each of the cells 2 – 4 16 mobiles can be accommodated. In contrast, cell 1 is able to serve 8 users. Therefore, the total network can accommodate 56 users under the assumptions made. The offered load to the network is varied and the outage calculated. The results are compared with the case where no asynchronous cell overlaps exist, i.e. where TS0 of cell 1 is also used for TX instead of RX.

Finally, the results are shown in Fig. 5. The curve marked with '+' shows the results for the case in which the opposing scheme is not used. In contrast, the results with the opposing algorithm applied is marked with a circle. A significant improvement can be observed. With the offered load of 21 mobiles, for example, the outage without the opposing algorithm is about 14 % compared to 6 % when the proposed algorithm is applied, i.e the relative outage is reduced by more than 50 %. For comparison, the curve marked with the squares represents the result for the

'ideal' case in which no asynchronous overlaps exist. It can be seen that the results of the opposing algorithm are close to the results obtained by an ideally synchronised network while different asymmetries in the network are applied. Hence, the algorithm allows to exploit channel asymmetry in TDD without resulting in significant capacity reductions. The advantages resulting from the proposed algorithm decrease as the load in the network is increased. This behaviour is typical for dynamic channel algorithms [11].

The slope of outage as a function of the number of active users decreases with a loading between 30 and 40 mobiles. This behaviour can be attributed to the user allocation algorithm. The strategy for cell 2 – cell 4 is such that at first TS0, TS1 respectively, are 'filled'. The overflow is directed to TS 3 and TS 4. This overflow occurs with an offered load in the range between 30 and 40 users. At the beginning of this new allocation process outage will not significantly increase which causes the slope of outage to decrease locally before it rises again.

The algorithm has been applied to the uplink. Therefore, situations may arise in which mobile stations interfere with each other. However, in [12] it has been demonstrated that MS \leftrightarrow MS interference is less of an issue than, for example, BS \leftrightarrow BS interference. Due to the TDMA component in UTRA–TDD severe MS \leftrightarrow MS interference can be resolved by an overlaid DCA algorithm.

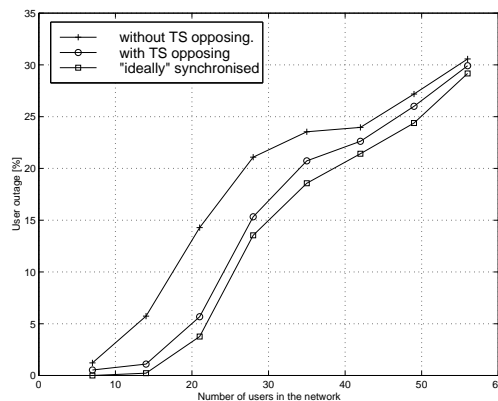


Fig. 5. Outage results.

V. CONCLUSIONS

An interference resolving algorithm for UTRA–TDD has been presented. This novel algorithm enables asynchronous cell overlaps to exist without resulting in a significant capacity drop. On the contrary, it has been demonstrated that the asynchronous overlaps can be exploited constructively resulting in similar performance to the case in which all cells transmit and receive at the same time. Hence, with the proposed algorithm the advantages of the TDD technique can be exploited whilst the disadvantages (i.e. capacity reduction) are significantly reduced.

The highest gain of the proposed algorithm is for cell loads between 30 % and 60 %.

ACKNOWLEDGEMENTS

The authors gratefully acknowledge the support of this study by Nokia Networks OY, the EPSRC and The Royal Society. In addition, the authors are grateful to Harri Posti (Nokia Networks), Kalle Passoja (Nokia Networks) and Kari Rikkinen (Nokia Mobile Phones) for many fruitful discussions.

REFERENCES

- [1] K S Gilhousen, I M Jacobs, R Padovani, A J Viterbi, L. A. Weaver, Jr., and C. E. Wheatly III, "On the capacity of a cellular CDMA system," *IEEE Transactions on Vehicular Technology*, vol. 40, no. 2, pp. 303–312, May 1991.
- [2] Y Ishikawa and S Onoe, "Method for evaluating W-CDMA system capacity considering adjacent channel interference," *Electronics Letters*, vol. 35, no. 12, pp. 968–969, June 1999.
- [3] Giovanni Emanuele Corazza, Giovanni De Maio, and Francesco Vatalaro, "CDMA Cellular Systems Performance with Fading, Shadowing, and Imperfect Power Control," *IEEE Transactions on Vehicular Technology*, vol. 47, no. 2, pp. 450–459, May 1998.
- [4] Audrey M Viterbi and Andrew J Viterbi, "Erlang Capacity of a Power Controlled CDMA System," *IEEE Journal on Selected Areas in Communication*, vol. 11, no. 6, pp. 892–900, August 1993.
- [5] Sungmoon M Shin, Cheol-Hye Cho, and Dan Keun Sung, "Interference –Based Channel Assignment for DS–CDMA Cellular Systems," *IEEE Transactions on Vehicular Technology*, vol. 48, no. 1, pp. 233–239, January 1999.
- [6] C Mihalescu, X Lagrange, and Ph Godlewski, "Dynamic Resource Allocation For Packet Transmission in TDD TD–CDMA Systems," in *Proceedings of the 1999 IEEE Vehicular Technology Conference*, Houston, Texas, USA, May 16–19 1999, IEEE, pp. 1737–1741.
- [7] Harald Haas and Gordon J R Povey, "The Effect of Adjacent Channel Interference on Capacity in a Hybrid TDMA/CDMA–TDD System Using UTRA–TDD Parameters," in *Proceedings of the 1999 50th IEEE Vehicular Technology Conference*, Amsterdam, The Netherlands, September 19–22 1999, IEEE, vol. 2, pp. 1086–1090.
- [8] Harald Haas and Gordon J R Povey, "Communications networks," UK Patent Application by NOKIA: 9930089.9, 20th December 1999.
- [9] Lauro Ortigoza-Guerrero and A H Aghvami, "Capacity Assessment For UTRA," in *Proceedings of the 1999 IEEE Vehicular Technology Conference*, Houston, Texas, USA, May 16–19 1999, IEEE, pp. 1653–1657.
- [10] 3rd Generation Partnership Project (3GPP), Technical Specification Group (TSG), Radio Access Network (RAN), Working Group 4 (WG4), "Evaluation of up– and downlink adjacent channel performance," TSGR4#2(99) 048, February 1999.
- [11] Sanjiv Nanda and David J Goodmann, *Third Generation Wireless Information Networks*, chapter Dynamic Resource Acquisition: Distributed Carrier Allocation for TDMA Cellular Systems, pp. 99–124, Kluwer Academic Publishers, 1992.
- [12] Harri Holma, Gordon J R Povey, and Antti Toskala, "Evaluation of Interference Between Uplink and Downlink in UTRA/TDD," in *Proceedings of the 1999 50th IEEE Vehicular Technology Conference*, Amsterdam, The Netherlands, September 19–22 1999, IEEE, vol. 5, pp. 2616–2620.

An Investigation on Capacity versus Guard-Bands in the TDD Mode of UMTS

H. Haas, S. McLaughlin and G. J. R. Povey*

Department of Electronics and Electrical Engineering,
The University of Edinburgh,
The King's Buildings, Mayfield Road
Edinburgh, EH9 3JL, UK
Phone:+44 (0)131 650 5655, Fax:+44 (0)131 650 6554
E-mail: hh@ee.ed.ac.uk

Abstract

The UMTS terrestrial radio access (UTRA) is composed of a frequency division duplex (UTRA-FDD) mode and a time division duplex (UTRA-TDD) mode. In UTRA-TDD the uplink and downlink are on the same carrier frequency. This creates additional interference scenarios, to be precise: MS \leftrightarrow MS and BS \leftrightarrow BS interference. Since power leakage between adjacent carriers cannot be avoided this inherent property of TDD has an impact on adjacent channel interference (ACI) and thus on cell capacity. The power leakage results from transmitter mask imperfections and non-ideal receiver filters. From interference power measurements using a 7th and a 9th order butterworth receiver filter the relationship between carrier spacing and adjacent channel interference power ratio (ACIR) is established. This relationship is used to find the best carrier spacing in UTRA-TDD considering several cell deployment scenarios. It is found that the ACIR must be greater than 30 dB, but the capacity gains from an ACIR greater than 40 dB converge rapidly.

1. Introduction

The interference mechanisms in an FDD system are that mobile stations (MS's) cause interference at the neighbouring base stations (BS's), and the BS's, in turn, interfere with the MS's at the adjacent cells. When considering the UTRA-TDD system the complexity in terms of interference is increased since both the uplink and downlink are time multiplexed on the same carrier frequency. If the frames and TS's of two cells are not synchronised additional interference scenarios occur [7]. The MS's can interfere with each other as can the BS's. The misalignment of two frames

is modelled by a time offset (t_{off}), which is normalised to the slot duration (t_{slot}) resulting in a synchronisation factor,

$$\alpha = \frac{t_{off}}{t_{slot}} \text{ with } 0 \leq \alpha \leq 1. \quad (1)$$

Due to a frame misalignment two BS's, BS_a and BS_b interfere with each other. In the same way as there is BS_a \leftrightarrow BS_b interference, the associated MS's, MS_a and MS_b, will interfere with each other. These mechanisms are valid for ACI, too, as there is power leakage from the transmitter to the receiver on the adjacent carrier. This power leakage is a consequence of transmit and receive filter imperfections. In the case of ACI, a transmitter and a victim receiver may be in close proximity since two cells using adjacent carriers might not be coordinated as they could belong to different operators.

Taking these mechanisms into account, ACI in UTRA-TDD is calculated assuming certain adjacent channel interference power ratios (ACIR). In the following section 2 the problem is formulated and also an equation on the capacity reduction due to ACI is given. This is followed in section 3 by a description of the simulation platform. In section 4 the results are presented and with measurements of ACIR versus carrier spacing obtained from a 7th and 9th order butterworth receiver filter, conclusions on the best carrier spacing are drawn in section 5.

2. Problem statement

In a TDD system adjacent channel interference, I_{ad} , at an arbitrary location specified by its x and y coordinates, may be denoted as:

$$I_{ad}(x, y) = \frac{1}{ACIR} \sum_{j=1}^K \sum_{i=1}^{M_j} \underbrace{\alpha_j \frac{P_{c_{i,j}}^u}{a_i(x, y)}}_{I_{MS}} + (1 - \alpha_j) \underbrace{\frac{P_{c_j}^d}{a_j(x, y)}}_{I_{BS}}, \quad (2)$$

*now with: Elektrobit (UK) Ltd., Edinburgh Technology Transfer Centre Mayfield Road, Edinburgh EH9 3JL, Scotland UK

where K is the number of neighbouring cells taken into consideration, M_j the total number of active users in the neighbouring cell j and $a_i(x, y)$ the path loss between the interfering user i and the location of interest (x, y) . Similarly, $a_j(x, y)$ is the path loss between the location of interest and the BS of cell j , $P_{c_{i,j}}^u$ the transmitted carrier power of user i in cell j and $P_{c_j}^d$ the total carrier power transmitted by BS j .

The ACIR is determined by two factors: a) one related to the transmitter filter and referred to as: *Adjacent Channel Leakage Power Ratio (ACLR)* b) one related to the receiver filter and defined as *Adjacent Channel Selectivity (ACS)*. The relationship between ACIR, ACLR and ACS was investigated in [1] and found to be:

$$ACIR = \frac{1}{\frac{1}{ACLR} + \frac{1}{ACS}} \quad (3)$$

From (2) it can be seen that interference at any location is composed of interference from MS's (I_{MS}) and BS's (I_{BS}), the severity of which depends on frame synchronisation.

The transmitted powers $P_{c_{i,j}}^u$ and $P_{c_j}^d$ are random variables which are determined by several factors, the most important of which are the location of MS's, the path loss, the severity of lognormal shadowing, the handover algorithm, the power control algorithm and the receiver architecture. Additionally, the path losses between the interferer and victim receiver, $a_i(x, y)$ and $a_j(x, y)$, are random variables, too. Moreover, in the case of ACI the sink of interference and the desired receiver may be in close proximity so that the path loss on the desired link and interference link cannot be assumed to be uncorrelated. Frame synchronisation between different operators may also vary randomly, i.e. $0 \leq \alpha_j \leq 1$. Due to its complexity the ACI power as described in (2) is calculated using Monte Carlo techniques with the simulation platform described in the subsequent section 3.

Once ACI power is known, the impact it causes on capacity can be assessed by considering the uplink direction. For this purpose an equation is developed [5] to calculate the relative remaining capacity as a consequence of other-cell interference. In this paper other-cell interference is confined to ACI. Co-channel interference is not considered here.

Ideal power control in the uplink is assumed. With this assumption the same model as in [4] can be used resulting in,

$$E_b/I_0 = \frac{P_u pg}{P_u(M-1) + I_{ad} + N} \quad (4)$$

where P_u is the received, power-controlled signal power from the desired user, M the number of users which are served by one time slot (TS), N is thermal noise and pg is the processing gain. Since in this paper the focus is on the capacity reduction due to I_{ad} , equation (4) may be rearranged and the ratio M/M_0 calculated, where M_0 is the

number of users derived from (4) with no adjacent channel interference ($I_{ad} = 0$),

$$M_0 = \frac{pg}{E_b/I_0} - \frac{N}{P_u} + 1 \quad (5)$$

Thus, the relative remaining capacity, M/M_0 , is:

$$M/M_0 = 1 - \frac{I_{ad}}{P_u \left(1 + \frac{pg}{E_b/I_0}\right) - N} \quad (6)$$

From (6), it can be seen that the capacity reduction term is directly proportional to I_{ad} . Moreover, it can be shown that the useful signal becomes:

$$P_u = \frac{NE_b/I_0 I_{mar}}{pg} \quad (7)$$

with I_{mar} representing an interference margin to account for an increased noise floor due to own-cell interference. I_{mar} can be calculated as follows:

$$I_{mar} = \frac{1}{1 - \frac{(M-1)E_b/I_0}{pg}} \quad (8)$$

Since the denominator in (8) must be positive and greater than zero, an upper bound for the cell load can be determined which yields M_{max} ,

$$M_{max} = \frac{pg}{E_b/I_0} + 1 \quad (9)$$

Moreover, in this paper the relative capacity load is expressed by:

$$\mu = \frac{M}{M_{max}} \quad (10)$$

μ is limited by the admission control of the radio resource management layer. By substituting (7) and (8) into (6) and using (10), M/M_0 can be written as:

$$M/M_0 = 1 - \frac{I_{ad}}{N} \left(\frac{1}{\mu} - 1 \right) \quad (11)$$

Equation (11) highlights an interesting property. It is that the sensitivity to ACI decreases with the cell load because the useful signal P_u is lowest for only one own-cell user and increases in a non-linear fashion with the number of users, i.e. for M_{max} users P_u tends to infinity (equation (8)). However, the conclusion is not that many own-cell users diminish the impact of ACI. This is because two cells are mutually coupled by ACI power. This means, increasing the number of own-cell users will result in a greater ACI term, I_{ad} , at the close-by cell employing the adjacent carrier. Therefore, the victim cell may have to increase its useful signal power to compensate for an augmented ACI contribution. This, in turn, results in increased ACI, I_{ad} , in the system which originally had increased the number of users.

3. Simulation platform

The cell structure as depicted in Figure 1 is used to carry out simulations in order to calculate I_{ad} at the BS of the COI. The location of the COI is varied along the x -axis

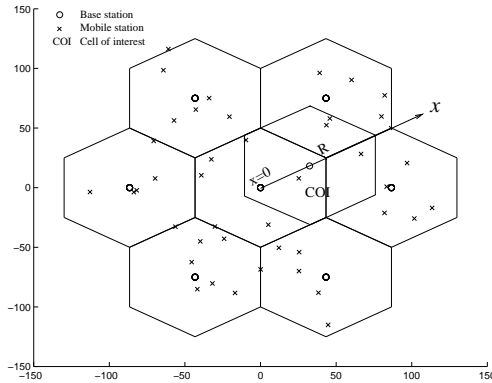


Figure 1: Cell topology used to calculate interference at the BS of the COI.

within the range: $5 \text{ m} \leq x \leq R$. It is anticipated that the MS interference is greatest at the cell corner which is the reason why the x -axis is placed as depicted in Figure 1.

User distribution ACI is calculated at the BS of the COI for different user populations in an interfering network of 7 cells. In these cells users are distributed uniformly in space. Chebaro [2] and later Viterbi [9] have shown that allocating a mobile to the closest BS rather than to the BS that results in the smallest signal attenuation can create up to 4–20 times higher interference in a CDMA system. Note, that these results were obtained for an FDD system in which only the MS's contribute to interference at the BS. However, an ideal handover technique would be required if a mobile was always to be connected to that BS for which the path loss is minimal. Therefore a *handover margin* is introduced to model handover imperfections.

Propagation model The path loss model for indoor office test environment according to [3] is used,

$$a = 37 + 30 \log_{10}(d) + 18.3 n^{[(n+2)(n+1)-0.46]} + \xi \text{ [dB]}, \quad (12)$$

where d is the transmitter–receiver separation in metres, n is the number of floors in the path and ξ is the lognormal variable modelling shadow fading.

In the analyses of cellular networks it is usually assumed that lognormal shadowing on the propagation path is uncorrelated for different propagation paths. However measurements have shown that shadowing on the desired link and on the interference link can be highly correlated. In the interference analysis conducted in this research a model used by Klingenbrunn [8] is adopted. In that paper it is reported that the correlation coefficient is primarily dependent on the relative distance of the receivers to the transmitter and the angle-of-arrival difference. The correlation coefficient is computed as follows:

Firstly, the relative difference between desired path, d_1 , and interference path, d_2 , is calculated,

$$A = \left| 10 \log_{10} \left(\frac{d_1}{d_2} \right) \right| \text{ [dB]}. \quad (13)$$

A threshold, X , is introduced which determines the point at which the distance dependency of the correlation coefficient reaches its minimum,

$$f(X, A) = \begin{cases} 1 - \frac{A}{X} & \text{if } A \leq X, \\ 0 & \text{otherwise.} \end{cases} \quad (14)$$

and finally, the correlation coefficient is defined as:

$$\rho(\varphi, A) = \begin{cases} f(X, A) \left(0.6 - \frac{|\varphi|}{150} \right) + 0.4 & \text{if } |\varphi| \leq 60, \\ 0 & \text{otherwise,} \end{cases} \quad (15)$$

where φ is the angle-of-arrival difference. Note, the minimum correlation coefficient is non-zero so as to account for local scattering around the receiver. The threshold X is in the range of 6–20 dB.

Power control A C/I -based power control algorithm is used in the uplink and downlink direction.

4. Results and Discussion

The parameters given in Table 1 are used to carry out system simulations. Using (2) the cumulative density function (cdf) of I_{ad} , $Pr(I_{ad} < \mathbf{I}_{ad})$, is calculated. Using this cdf, I_{ad} is then calculated assuming a certain tolerable outage, P_{out} : $I_{ad} = Pr^{-1}(1 - P_{out})$.

I_{ad} as a function of the BS location, x , with α as a parameter is depicted in Figure 2. As expected, if the BS of the interfering system and the victim BS are located in close proximity, with synchronous transmission and reception, i.e. small values for α are applied, this results in the least ACI power. As the victim BS is shifted along the x -axis the situation changes since the interference from the MS's becomes more dominant. Therefore, as x increases it is more advantageous to oppose transmission and reception direction, i.e. let α be close to 1. This discovery

Table 1: Simulation parameters

Parameter	Value
Cell radius, R	50 m
Information bit rate	16 kbit/s
Chip rate	3.84 Mchip/s
Shadowing	10 dB
Receiver noise figure	5
Max. MS TX power	15 dBm
Max. BS TX power	24 dBm
E_b/I_0	3.5 dB
Handover margin	5 dB
Correlation threshold, X	6 dB
Tolerable outage, P_{out}	5 %
Number of floors, n	2
Relative cell load, μ	0.75

has been exploited in a novel DCA algorithm for a hybrid TDMA/CDMA-TDD system [6]. It is interesting to note that from a distance of 25 m onwards, which is half the cell radius, values of α greater than 0.5 result in better performance. This point at which: $I_{ad}|\alpha>0.5 < I_{ad}|\alpha\leq 0.5$ is only slightly below 25 m for an increased cell load of 6 users. This is interesting to note since irrespective of the synchronisation with the co-existing network and the load in the interfering cells (provided that they are equally loaded), the interference for a BS location at about half the cell radius is almost constant.

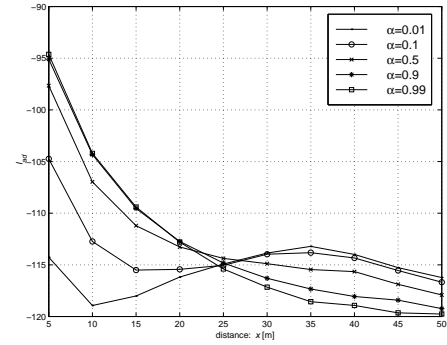
In the following it is assumed that the system using an adjacent carrier can adjust the frame offset to the co-existing network so as to minimise I_{ad} . The ACI power then becomes:

$$I_{ad}(x) = \min_{0 \leq \alpha \leq 1} [I_{ad}(x, \alpha)] . \quad (16)$$

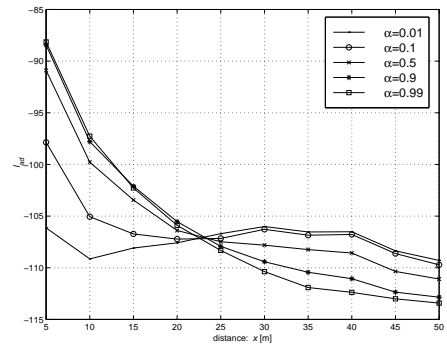
The ACI power as calculated in (16) is used to derive the remaining capacity in the COI using (11). The results are shown in Figure 3. It can be seen that, if the interfering cells are populated with 6 users the capacity reduction with $ACIR = 25$ dB is significantly high. For a BS location at $x=20$ m, for example, the remaining capacity at the adjacent carrier is only about 4 %. In contrast, for 4 interfering users per cell the remaining capacity increases considerably to about 83 %. Note, that this is with a tolerable outage of 5 %.

The capacity reduction is very sensitive for $ACIR$ values between 25 dB and 40 dB. The gain by an $ACIR$ greater than 40 dB is only marginal and probably over-compensated by the increasing costs for the realisation of appropriate transmitter and receiver filters.

The effect that I_{ad} does not vary greatly with different values for α between 22 m and 25 m (see Figure 2) results in



(a) 4 interfering users per cell

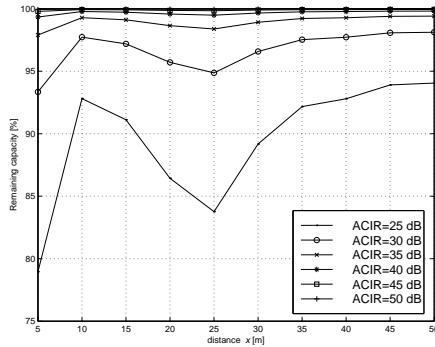


(b) 6 interfering users per cell

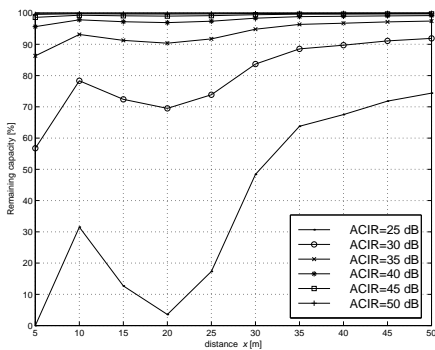
 Figure 2: Adjacent channel interference power with $ACIR$ set to 35 dB.

the local minimum at these locations which becomes clear from (16).

As it is intended in this paper to find the best carrier spacing it is necessary to make certain assumptions on the transmitter and receiver filters. To assist in this, measurement data provided by Nokia was used. A 7th and 9th order butterworth filter at the BS of the COI was considered. The associated ACS values were 34.5 dB, and 40.0 dB respectively. The ACLR in the first case was assumed to be 30 dB whereas in the second case an ACLR of 35 dB was considered. The results are summarised in Table 2. From the results in Figure 3(b) it can clearly be stated that $ACIR$ should not be below 30 dB, otherwise the capacity reduction would be too high. Mapping these results to those in Table 2 it can be found that the carrier spacing should be above 5.0 MHz for the 7th order butterworth filter at the BS receiver



(a) 4 interfering users per cell



(b) 6 interfering users per cell

Figure 3: Remaining capacity as a consequence of adjacent channel interference power.

and not below 4.8 MHz for the 9th order butterworth filter.

5. Conclusions

The ACIR between adjacent carriers in the TDD mode of UMTS must be greater than 30 dB unless a significant capacity reduction is tolerable. The gain in capacity for ACIR values above 40 dB is only marginal. These results are used to find the best carrier spacing for a practical realisation of a receiver and transmitter filter. For the given data it is recommended that the carrier spacing is kept equal to or greater than 4.8 MHz in the TDD mode of UMTS.

Table 2: ACIR for two different types of receiver and transmitter filters and with the carrier spacing as a parameter.

Channel spacing [MHz]	ACIR [dB] (ACS=34.5 dB, ACLR = 30 dB)	ACIR [dB] (ACS=40.0 dB, ACLR=35.4 dB)
5.0	28.9	33.7
4.8	27.0	31.4
4.6	24.1	27.4
4.4	20.6	22.4
4.2	17.0	17.7
4.0	14.0	14.0

Acknowledgments

The authors gratefully acknowledge the support of this study by NOKIA, the EPSRC and The Royal Society.

References

- [1] 3rd Generation Partnership Project (3GPP), Technical Specification Group (TSG), Radio Access Network (RAN), Working Group 4 (WG4). Evaluation of up- and downlink adjacent channel performance. TSGR4#2(99) 048, February 1999.
- [2] T. Chebaro and P. Godlewski. About the CDMA Capacity Derivation. In *Proceedings of the International Symposium on Signals, Systems and Electronics*, pages 36–39, Paris, France, September 1–4 1992.
- [3] ETSI 30.03, V3.2.0 (1998-04). Universal Mobile Telecommunications System (UMTS); Selection procedures for the choice of radio transmission technologies of the UMTS. TR 101 112, 1998.
- [4] K. S. Gilhousen, I. M. Jacobs, R. Padovani, A. J. Viterbi, L. A. Weaver, Jr., and C. E. Wheatly III. On the capacity of a cellular CDMA system. *IEEE Transactions on Vehicular Technology*, 40(2):303–312, May 1991.
- [5] H. Haas, S. McLaughlin, and G. J. R. Povey. The Effects of Interference Between the TDD and FDD Mode in UMTS at the Boundary of 1920 MHz. In *Proceedings of the 6th IEEE Symp. on Spread-Spectrum Tech. & Appl.*, New Jersey, (USA), September 6–8, 2000.
- [6] H. Haas and G. J. R. Povey. Communications networks. UK Patent Application by NOKIA: 9930089.9, 20th December 1999.
- [7] H. Haas and G. J. R. Povey. The Effect of Adjacent Channel Interference on Capacity in a Hybrid TDMA/CDMA-TDD System Using UTRA-TDD Parameters. In *Proceedings of the VTC-Fall*, volume 2, pages 1086–1090, Amsterdam, The Netherlands, September 19–22 1999. IEEE.
- [8] T. Klingbrunn and P. Mogensen. Modelling Cross-Correlated Shadowing in Network Simulations. In *Proceedings of the VTC-Fall*, pages 1407–1411, Amsterdam, The Netherlands, September 19–22 1999. IEEE.
- [9] A. J. Viterbi and A. M. Viterbi. Other-Cell Interference in Cellular Power-Controlled CDMA. *IEEE Transactions on Communications*, 42(2/3/4):1501–1504, February 1994.

References

- [1] B. Eylert, "The Extended UMTS Vision," in *Proceedings of the UMTS 2000 Conference*, (Barcelona, Spain), p. 12, October 11–13 2000. published at: <http://www.umts-forum.org>.
- [2] W. Dangelmaier, D. Förster, V. Horsthemke, and S. Kress, "Penetration and Outlook of Telework in Europe — An Internet Snapshot," in *Proceedings of the 32nd Hawaii International Conference on System Sciences*, (Mauri, Hawaii, USA), p. 16, IEEE, January 5–8 2000.
- [3] GSM Europe, "History of GSM." <http://www.gsmworld.com>, October 2000.
- [4] J. F. Huber, "Consequences of UMTS Entering the Internet World," in *Proceedings of the UMTS 2000 Conference*, (Barcelona, Spain), p. 24, UMTS Forum, October 11–13 2000. published at: <http://www.umts-forum.org>.
- [5] W. Mohr, "Investigation of the UMTS Radio Interface in the ACTS FRAMES Project," in *Proceedings UMTS workshop*, vol. 1 of 1, (Schloss Reisingen near Ulm, Germany), pp. 33–64, IEEE ComSoc Germany, University of Ulm, November 26–27 1998.
- [6] H. Holma and A. Toskala, *WCDMA for UMTS*. John Wiley, 2000.
- [7] Y. Yamao, H. Suda, N. Umeda, and N. Nakajima, "Radio Access Network Design Concept for the Forth Generation Mobile Communication System," in *Proceedings of the 2000 IEEE 51st Vehicular Technology Conference*, (Tokyo, Japan), pp. 2285–2289, IEEE, May 15–18 2000.
- [8] T. Sidenbladh, "Current status of 3G licensing," in *Proceedings of the UMTS 2000 Conference*, (Barcelona, Spain), p. 15, UMTS Forum, October 11–13 2000. published at: <http://www.umts-forum.org>.
- [9] H. Luediger and S. Zeisberg, "User and Business Perspectives on an Open Mobile Access Standard," *IEEE Communications Magazine*, pp. 160–163, September 2000.
- [10] A. Viterbi, *Principles of Spread Spectrum Communication*. Addison–Wesley, 1995.
- [11] T. S. Rappaport, *Wireless communications*. Prentice Hall, 1996.
- [12] ETSI SMG2, "The ETSI UMTS Terrestrial Radio Access (UTRA) ITU–R RTT Candidate Submission," January 1998.
- [13] M. O. Sunay, Z. C. Honkasalo, A. Hottinen, H. Honkasalo, and L. Ma, "A Dynamic Channel Allocation Based TDD DS CDMA Residential Indoor System," in *Proceedings of the 1997 IEEE 6th International Conference on Universal Personal Communications ICUPC '97*, vol. 2 of 2, pp. 228–234, IEEE, October 1997.

-
- [14] H. Haas and G. J. R. Povey, "Apparatus, Method of and System for Improving Capacity in a Communications Network." International Patent Application Number: PCT/GB99/02223, 25 July 1998.
- [15] H. Haas and G. J. R. Povey, "Outage Probability of CDMA-TDD Micro Cells in a CDMA-FDD Environment," in *Proceedings of the 1998 International Symposium on Personal, Indoor and Mobile Radio Communications PIMRC 98*, vol. 1 of 3, pp. 94–98, IEEE, September 8–11 1998.
- [16] H. Haas and G. J. R. Povey, "A Capacity Investigation on UTRA–TDD Utilising Underused UTRA–FDD Uplink Resources," in *Proceedings of the 10th International Symposium on Personal, Indoor and Mobile Radio Communications PIMRC '99*, (Osaka, Japan), pp. A6–4, IEEE, September 12–15 1999.
- [17] H. Haas and G. J. R. Povey, "Additional Capacity of a CDMA/TDD Micro Cell Utilising the Uplink Frequency Band of a CDMA/FDD Macro Cellular Overlay," in *Proceedings UMTS Workshop*, vol. 1 of 1, (Schloss Reisingen near Ulm, Germany), pp. 151–158, November 26–27 1998.
- [18] H. Haas, S. McLaughlin, and G. J. R. Povey, "The Effects of Interference Between the TDD and FDD Mode in UMTS at the Boundary of 1920 MHz," in *Proceedings of the 6th IEEE Symp. on Spread–Spectrum Tech. & Appl.*, (New Jersey, (USA)), pp. 486–490, September 6–8 2000.
- [19] H. Haas, S. McLaughlin, and G. J. R. Povey, "The Effects of Inter–System Interference in UMTS at 1920 MHz," in *Proceedings of the IEE International Conference on 3G 2000 Mobile Communication Technologies*, (London, UK), pp. 103–107, IEE, March 27–29 2000 2000.
- [20] T. Chebaro and P. Godlewski, "About the CDMA Capacity Derivation," in *Proceedings of the International Symposium on Signals, Systems and Electronics*, (Paris, France), pp. 36–39, September 1–4 1992.
- [21] G. E. Corazza, G. De Maio, and F. Vatalaro, "CDMA Cellular Systems Performance with Fading, Shadowing, and Imperfect Power Control," *IEEE Transactions on Vehicular Technology*, vol. 47, pp. 450–459, May 1998.
- [22] J. S. Wu, J. K. Chung, and M. T. Sze, "Analysis of uplink and downlink capacities for two–tier cellular system," *IEE Proceedings – Communication*, vol. 144, pp. 405–411, December 1997.
- [23] V. V. Veeravalli and A. Sendonaris, "The Coverage–Capacity Tradeoff in Cellular CDMA Systems," *IEEE Transactions on Vehicular Technology*, vol. 48, pp. 1443–1450, September 1999.
- [24] K. Takeo, S. Sato, and A. Ogawa, "Optimum Cell Boundary for Uplink and Downlink in CDMA Systems," *IEICE Transactions : Communications*, vol. E83-B, pp. 865–868, April 2000.
- [25] K. S. Gilhousen, I. M. Jacobs, R. Padovani, A. J. Viterbi, L. A. Weaver, Jr., and C. E. Wheatly III, "On the capacity of a cellular CDMA system," *IEEE Transactions on Vehicular Technology*, vol. 40, pp. 303–312, May 1991.

-
- [26] A. M. Viterbi and A. J. Viterbi, "Erlang Capacity of a Power Controlled CDMA System," *IEEE Journal on Selected Areas in Communication*, vol. 11, pp. 892–900, August 1993.
- [27] A. J. Viterbi and A. M. Viterbi, "Other-Cell Interference in Cellular Power-Controlled CDMA," *IEEE Transactions on Communications*, vol. 42, pp. 1501–1504, February 1994.
- [28] C. E. Shannon, "A Mathematical Theory of Communication," *Bell System Technical Journal*, vol. 27, pp. 379–423 and 623–656, July and October 1948.
- [29] T. Ojanperä, P. A. Ranta, S. Hämäläinen, and A. Lappeteläinen, "Analysis of CDMA and TDMA for 3rd Generation Mobile Radio Systems," in *Proceedings of the 1997 47th IEEE Vehicular Technology Conference*, vol. 2 of 3, (Phoenix, Arizona, USA), pp. 840–844, IEEE, May 4–7 1997.
- [30] K. Pehkonen, H. Holma, I. Keskitalo, E. Nikula, and T. Westman, "A Performance Analysis of TDMA and CDMA Based Air Interface Solutions for UMTS High Bit Rates Services," in *Proceedings of the 1997 International Symposium on Communications PIMRC 97*, vol. 1 of 3, (Helsinki, Finland), pp. 22–26, IEEE, September 1–4 1997.
- [31] A. Klein, R. Pirhonen, J. Sköld, and R. Suoranta, "FRAMES Multiple Access Mode 1 – Wideband TDMA with and without Spreading," in *Proceedings of the 1997 International Symposium on Mobile Radio Communications PIMRC 97*, (Helsinki, Finland), pp. 37–41, IEEE, September 1–4 1997.
- [32] R. Esmailzadeh, M. Nakagawa, and E. A. Sourour, "Time-Division Duplex CDMA Communications," *IEEE Communications Magazine*, vol. 4, pp. 51–56, April 1997.
- [33] I. Horikawa, O. Kato, K. Miya, and M. Hayashi, "Performance of Wideband CDMA with TDD Scheme," in *Proceedings of the 1997 Asia Pacific Microwave Conference*, (Hong Kong), pp. 145–148, IEEE, December 2–5 1997.
- [34] W. H. W. Tuttlebee, "Cordless Personal Communications," *IEEE Communications Magazine*, vol. 30, pp. 42–53, December 1992.
- [35] M. Zeng, A. Annamalai, and V. K. Bhargava, "Recent Advances in Cellular Wireless Communications," *IEEE Communications Magazine*, vol. 37, pp. 128–138, September 1999.
- [36] H. Li, G. Malmgren, and M. Pauli, "Performance Comparison of the Radio Link Protocols of IEEE802.11a and HIPERLAN/2," in *Proceedings of the Vehicular Technology Conference*, (Boston, USA), pp. 7p. in CD-Rom, paper 4.3.3.2, IEEE, September 21–24 2000.
- [37] S. Garg, M. Kalia, and R. Shorey, "MAC Scheduling Policies for Power Optimization in Bluetooth: A Master Drive TDD Wireless System," in *Proceedings of the 2000 IEEE 51st Vehicular Technology Conference*, (Tokyo, Japan), pp. 196–200, IEEE, May 15–18 2000.
- [38] T. Ojanperä and R. Prasad, "An Overview of Air Interface Multiple Access for IMT-2000/UMTS," *IEEE Communications Magazine*, vol. 36, pp. 82–95, September 1998.

- [39] K. Miya, O. Kato, K. Homma, T. Kitade, and M. Hayashi, "Wideband CDMA Systems in TDD-Mode Operation for IMT-2000," *IEICE Transactions : Communications*, vol. E81-B, pp. 1317-1325, July 1998.
- [40] M. Haardt, A. Klein, R. Koehn, S. Oestreich, M. Purat, V. Sommer, and T. Ulrich, "The TD-CDMA Based UTRA TDD Mode," *IEEE Journal on Selected Areas in Communication*, vol. 18, pp. 1375-1385, August 2000.
- [41] A. Samukic, "UMTS Universal Mobile Telecommunications System: Development of Standards for the Third Generation," *IEEE Transactions on Vehicular Technology*, vol. 47, pp. 1099-1104, November 1998.
- [42] G. J. R. Povey, H. Holma, and A. Toskala, "TDD-CDMA Extension to FDD-CDMA Based Third Generation Cellular System," in *Proceedings of the 1997 IEEE 6th International Conference on Universal Personal Communications ICUPC '97*, vol. 2 of 2, pp. 813-817, IEEE, October 12-16 1997.
- [43] T. Harrold and A. Nix, "Capacity Enhancement Using Intelligent Relaying for Future Personal Communication Systems," in *Proceedings of the Vehicular Technology Conference*, (Boston, USA), pp. 6p. in CD-Rom, paper 4.3.1.1, IEEE, September 21-24 2000.
- [44] A. Michail and A. Ephremides, "Energy Efficient Routing for Connection-Oriented Traffic in Ad-hoc Wireless Networks," in *Proceedings of the International Symposium on Personal, Indoor and Mobile Radio Communications PIMRC 2000*, vol. 2 of 2, (London, UK), pp. 762-766, IEEE, September 18-21 2000.
- [45] P. Jung, P. W. Baier, and A. Steil, "Advantages of CDMA and Spread Spectrum Techniques over FDMA and TDMA in Cellular Mobile Applications," *IEEE Transactions on Vehicular Technology*, vol. 42, pp. 357-364, August 1993.
- [46] R. Prasad and A. Kegel, "Improved Assessment of Interference Limits in Cellular Radio Performance," *IEEE Transactions on Vehicular Technology*, vol. 40, pp. 412-419, May 1991.
- [47] W. C. Y. Lee, "Spectrum efficiency in cellular," *IEEE Transactions on Vehicular Technology*, vol. 38, pp. 69-75, May 1989.
- [48] W. C. Y. Lee, *Mobile Communications Engineering*. McGraw-Hill, 1997.
- [49] V. M. Jovanović and J. Gazzola, "Capacity of Present Narrowband Cellular Systems: Interference-Limited or Blocking-Limited?," *IEEE Personal Communications*, vol. 4, pp. 42-51, December 1997.
- [50] B. H. Walke, *Mobile Radio Networks*. John Wiley & Sons, Ltd, 1999.
- [51] A. J. Paulraj and C. B. Papadias, "Space-Time Processing for Wireless Communications," *IEEE Signal Processing Magazine*, vol. 14, pp. 49-83, November 1997.
- [52] A. J. Paulraj and B. C. Ng, "Space-Time Modems for Wireless Personal Communications," *IEEE Personal Communications*, vol. 1, pp. 36-48, February 1998.

- [53] U. Vornefeld, C. Walke, and B. Walke, "SDMA Techniques for Wireless ATM," *IEEE Communications Magazine*, vol. 37, pp. 52–57, November 1999.
- [54] J. S. Thompson, P. M. Grant, and B. Mulgrew, "Smart Antenna Arrays for CDMA Systems," *IEEE Personal Communications*, vol. 3, pp. 16–25, October 1996.
- [55] J. H. Winters, "Smart Antennas for Wireless Systems," *IEEE Personal Communications*, vol. 1, pp. 23–27, February 1998.
- [56] G. R. Cooper and C. D. McGillem, *Modern Communications and Spread Spectrum*. McGraw–Hill, 1986.
- [57] J. K. Omura and P. T. Yang, "Spread Spectrum S–CDMA For Personal Communication Services," in *MILCOM'92*, (San Diego, USA), pp. 269–273, IEEE, October 11–14 1992.
- [58] R. L. Pickholtz, L. B. Milstein, and D. L. Schilling, "Spread Spectrum for Mobile Communications," *IEEE Transactions on Vehicular Technology*, vol. 40, pp. 313–322, May 1991.
- [59] C. Kchao and G. L. Stüber, "Analysis of a Direct–Sequence Spread–Spectrum Cellular Radio System," *IEEE Transactions on Communications*, vol. 41, pp. 1507–1516, October 1993.
- [60] A M J Goiser, *Handbuch der Spread–Spectrum Technik*. Springer, 1998.
- [61] TIA/EIA/IS–95, *Mobile Station–Base Station Compatibility Standard for Dual–Mode Wideband Spread Spectrum Cellular System*. Telecommunication Industry Association, May 1995.
- [62] G. R. Cooper and R. W. Nettleton, "A Spread–Spectrum Technique for High–Capacity Mobile Communications," *IEEE Transactions on Vehicular Technology*, vol. VT–27, pp. 264–275, November 1978.
- [63] A. Baier and W. Koch, "Potential of CDMA for 3rd generation mobile radio," in *Proceedings of the Mobile Radio Conference*, (Nice, France), pp. 282–290, November 1991.
- [64] D. L. Schilling, "Spread spectrum for commercial communications," in *IEEE Communications Magazine*, pp. 66–79, April 1991.
- [65] S. Verdu, *Multiuser Detection*. Cambridge University Press, 1998.
- [66] F. Adachi, M. Sawahashi, and K. Okawa, "Tree–structured Generation of Orthogonal Spreading Codes with Different Lengths for Forward Link in DS–CDMA Mobile," *Electronics Letters*, vol. 33, no. 1, pp. 27–28, 1997.
- [67] H. Sari, F. Vanhaverbeke, and M. Moeneclaey, "Extending the Capacity of Multiple Access Channels," *IEEE Communications Magazine*, vol. 38, pp. 74–82, January 2000.
- [68] H. Sari, F. Vanhaverbeke, and M. Moeneclaey, "Channel Overloading in Multiuser and Single–User Communication," in *Proceedings of the International Symposium on Personal, Indoor and Mobile Radio Communications PIMRC 2000*, (London, UK), pp. 1106–1111, IEEE, September 18–21 2000.

- [69] J. C. Liberti, Jr. and T. S. Rappaport, "Analytical Results for Capacity Improvements in CDMA," *IEEE Transactions on Vehicular Technology*, vol. 43, pp. 680–690, August 1994.
- [70] W. M. Tam and F. C. M. Lau, "Capacity Analysis of a CDMA Cellular System with Power Control Schemes," in *Proceedings of the 1997 IEEE 6th International Conference on Universal Personal Communications ICUPC '97*, vol. 2 of 2, (San Diego, USA), pp. 608–612, IEEE, October 12–16 1997.
- [71] B. Hashem and E. Sousa, "On the Capacity of a Cellular DS/CDMA System Under Slow Multipath Fading and Fixed Step Power Control," in *Proceedings of the 1997 IEEE 6th International Conference on Universal Personal Communications ICUPC '97*, vol. 2 of 2, (San Diego, USA), pp. 352–355, IEEE, October 12–16 1997.
- [72] C.-S. Kim, W.-Y. Kim, and O.-S. Park, "On the Capacity of W-CDMA System with Different Bandwidths in a Realistic Mobile Channel," in *Proceedings of the 1997 IEEE 6th International Conference on Universal Personal Communications ICUPC '97*, vol. 2 of 2, (San Diego, USA), pp. 613–617, IEEE, October 12–16 1997.
- [73] H Jeon and S Kwon and C Kang, "Reverse Link Capacity Analysis of a DS-CDMA Cellular System with Mixed Rate Traffic," *IEICE Transactions : Communications*, vol. E81-B, pp. 1280–1282, June 1998.
- [74] A. J. Viterbi, "Wireless Digital Communication: A View Based on Three Lessons Learned," *IEEE Communications Magazine*, vol. 29, pp. 33–36, September 1991.
- [75] J. G. Proakis and M. Salehi, *Communication System Engineering*. Prentice Hall, 1994.
- [76] A. J. Viterbi, A. M. Viterbi, K. S. Gilhousen, and E. Zehavi, "Soft Handoff Extends CDMA Cell Coverage and Increases Reverse Link Capacity," *IEEE Journal on Selected Areas in Communication*, vol. 12, pp. 1281–1287, October 1994.
- [77] D. Wong and T. J. Lim, "Soft Handoffs in CDMA Mobile Systems," *IEEE Personal Communications*, pp. 6–17, December 1997.
- [78] T. Chebaro and P. Godlewski, "Average External Interference in Cellular CDMA Systems," *IEEE Transactions on Communications*, vol. 44, pp. 23–25, January 1996.
- [79] A. Jalali and P. Mermelstein, "Effects of Diversity, Power Control, and Bandwidth on the Capacity of Microcellular CDMA Systems," *IEEE Journal on Selected Areas in Communication*, vol. 12, pp. 952–961, June 1994.
- [80] R. Prasad, M. G. Jansen, and A. Kegel, "Capacity Analysis of a Cellular Direct Sequence Code Division Multiple Access System with Imperfect Power Control," *IEICE Transactions : Communications*, vol. E76-B, pp. 894–905, August 1993.
- [81] W. Mohr and M. Kottkamp, "Downlink Performance of IS-95 DS-CDMA under Multipath Propagation Conditions," in *Proceedings of the 1996 4th International Symposium on Spread Spectrum Techniques and Applications, ISSSTA'96*, (Mainz, Germany), pp. 1063–1067, IEEE, September 22–25 1996.

- [82] F. Kikuchi, H. Suda, and F. Adachi, "Effect of Fast Transmit Power Control on Forward Link Capacity of DS-CDMA Cellular Mobile Radio," *IEICE Transactions : Communications*, vol. E83-B, pp. 47-55, January 2000.
- [83] E. Kudoh, "On the Capacity of DS/CDMA Cellular Mobile Radios under Imperfect Transmitter Power Control," *IEICE Transactions : Communications*, vol. E76-B, pp. 886-893, August 1993.
- [84] S. Verdu, "Wireless Bandwidth in the Making," *IEEE Communications Magazine*, pp. 53-58, July 2000.
- [85] S. Moshavi, "Multi-User Detection for DS-CDMA Communications," *IEEE Communications Magazine*, pp. 124-136, October 1996.
- [86] C. H. W. Hassell-Sweatman, B. Mulgrew, J. S. Thompson, and P. M. Grant, "Multi-user detection for CDMA antenna array receivers using spatial equivalence classes," *IEE Proceedings - Communication*, vol. 147, pp. 105-113, April 2000.
- [87] S. Hämmäläinen, H. Holma, and A. Toskala, "Capacity Evaluation of a Cellular CDMA Uplink With Multiuser Detection," in *Proceedings of the 1996 4th International Symposium on Spread Spectrum Techniques and Applications, ISSSTA'96*, vol. 1, (Mainz, Germany), pp. 339-343, IEEE, September 22-25 1996.
- [88] A. Klein, G. K. Kaleh, and P. W. Baier, "Zero Forcing and Minimum Mean-Square-Error Equalization for Multiuser Detection in Code-Division Multiple-Access Channels," *IEEE Transactions on Vehicular Technology*, vol. 45, pp. 276-287, May 1995.
- [89] P. Jung and J. Blanz, "Joint Detection with Coherent Receiver Antenna Diversity in CDMA Mobile Radio Systems," *IEEE Transactions on Vehicular Technology*, vol. 44, pp. 76-88, February 1995.
- [90] A. J. Viterbi, "Performance Limits of Error-Correcting Coding in Multi-Cellular CDMA Systems With and Without Interference Cancellation," in *Code Division Multiple Access Communications* (S. G. Glisic and P. A. Leppänen, eds.), pp. 47-52, Kluwer Academic Publishers, 1995.
- [91] S. Hämmäläinen, A. Toskala, and M. Laukkanen, "Analysis of CDMA Downlink Capacity Enhancements," in *Proceedings of the 1997 International Symposium on Communications PIMRC 97*, vol. 1 of 3, (Helsinki, Finland), pp. 241-245, IEEE, September 1-4 1997.
- [92] G. L. Stüber and L.-B. Yiin, "Downlink Outage Predictions for Cellular Radio Systems," *IEEE Transactions on Vehicular Technology*, vol. 40, pp. 521-531, August 1991.
- [93] K. Miya, M. Watanabe, M. Hayashi, T. Kitade, O. Kato, and K. Homma, "CDMA/TDD Cellular Systems for 3rd Generation Mobile Communication," in *Proceedings of the 1997 47th IEEE Vehicular Technology Conference*, (Phoenix, Arizona, USA), pp. 820-824, IEEE, May 4-7 1997.
- [94] T. Ojanpera and R. Prasad, *Wideband CDMA for Third Generation Mobile Communications*. Artech House Publishers, 1998.

- [95] S. E. Elkamy, "Wireless Portable Communications Using PRE-RAKE CDMA/TDD/QPSK Systems with Different Combining Techniques and Imperfect Channel Estimation," in *Proceedings of the 1997 International Symposium on PIMRC 97*, vol. 2 of 3, (Helsinki, Finland), pp. 529–533, IEEE, September 1–4 1997.
- [96] R. Esmailzadeh and E. M. Nakagawa, "Pre-RAKE Diversity Combining for Direct Sequence Spread Spectrum Mobile Communications Systems," *IEICE Transactions : Communications*, vol. E76–B, pp. 1008–1015, August 1993.
- [97] R. Esmailzadeh, E. Sourour, and M. Nakagawa, "Pre-RAKE diversity combining in time division duplex CDMA mobile communications," in *Proceedings of the 1995 6th IEEE International Symposium on Personal, Indoor and Mobile Radio Communications PIMRC'95*, vol. 2 of 3, (Toronto, Canada), pp. 431–435, IEEE, September 27–29 1995.
- [98] T. A. Kadous, E. E. Sourour, and S. E. Elkamy, "Comparison Between Various Diversity Techniques of the PRE-RAKE Combining System in TDD/CDMA," in *Proceedings of the 1997 47th IEEE Vehicular Technology Conference*, vol. 3 of 3, (Phoenix, Arizona, USA), pp. 2210–2214, IEEE, May 4–7 1997.
- [99] R. L.-U. Choi, K. B. Lataief, and R. D. Murch, "CDMA pre-RAKE diversity system with base station transmit diversity," in *Proceedings of the 2000 IEEE 51st Vehicular Technology Conference*, vol. 2, (Tokyo, Japan), pp. 951–955, IEEE, May 15–18 2000.
- [100] W. C. Jakes, ed., *Microwave Mobile Communications*. IEEE Press, 1974.
- [101] M. Hayashi, k Miya, O. Kato, and K. Homma, "CDMA/TDD Cellular System Utilizing a Base-Station-Based Diversity Scheme," in *Proceedings of the 1995 IEEE 45th Vehicular Technology Conference*, vol. 2 of 2, (Chicago, USA), pp. 799–803, IEEE, July 25–28 1995.
- [102] B. Steiner, "Performance Aspects of Transmit antenna diversity (TxAD) techniques for UTRA-TDD," in *Proceedings of the 2000 IEEE 51st Vehicular Technology Conference*, vol. 2, (Tokyo, Japan), pp. 1165–1169, IEEE, May 15–18 2000.
- [103] Z. Yongsheng and L. Daoben, "Power Control based on Adaptive Prediction in the CDMA/TDD system," in *Proceedings of the 1997 IEEE 6th International Conference on Universal Personal Communications ICUPC '97*, (San Diego, USA), pp. 790–794, IEEE, October 12–16 1997.
- [104] Y. Sanada, K. Seki, Q. Wang, S. Kato, M. Nakagawa, and V. K. Bhargava, "A Transmission Power Control Technique on a TDD-CDMA/TDMA System for Wireless Multimedia Networks," *IEICE Transactions : Communications*, vol. E78–B, pp. 1095–1103, August 1995.
- [105] R. Esmailzadeh and E. M. Nakagawa, "Time Division Duplex Method of Transmission of Direct Sequence Spread Spectrum Signals for Power Control Implementation," *IEICE Transactions : Communications*, vol. E76–B, pp. 1030–1038, August 1993.
- [106] G. J. R. Povey, "Capacity of a cellular time division duplex CDMA system," *IEE Proceedings: Communications*, vol. 141, pp. 351–356, October 1994.

-
- [107] W. S. Jeon and D. G. Jeong, "Comparison of Time Slot Allocation Strategies for CDMA/TDD Systems," *IEEE Journal on Selected Areas in Communication*, vol. 18, pp. 1271–1278, July 2000.
- [108] P. Chaudhury, W. Mohr, and S. Onoe, "The 3GPP Proposal for IMT-2000," *IEEE Communications Magazine*, vol. 37, pp. 72–81, December 1999.
- [109] H. Holma, G. J. R. Povey, and A. Toskala, "Evaluation of Interference Between Uplink and Downlink in UTRA/TDD," in *Proceedings of the 1999 50th IEEE Vehicular Technology Conference*, vol. 5, (Amsterdam, The Netherlands), pp. 2616–2620, IEEE, September 19–22 1999.
- [110] J. B. Punt, D. Sparreboom, F. Brouwer, and R. Prasad, "Mathematical Analysis of Dynamic Channel Selection in Indoor Mobile Wireless Communication Systems," *IEEE Transactions on Vehicular Technology*, vol. 47, pp. 1302–1313, November 1998.
- [111] L. Chen, S. Yoshida, H. Murata, and S. Hirose, "A Dynamic Timeslot Assignment Algorithm for Asymmetric Traffic in Multimedia TDMA/TDD Mobile Radio," *IEICE Transactions : Fundamentals*, vol. E81–A, pp. 1358–1365, July 1998.
- [112] C. Mihailescu, X. Lagrange, and P. Godlewski, "Dynamic Resource Allocation For Packet Transmission in TDD TD-CDMA Systems," in *Proceedings of the 1999 IEEE Vehicular Technology Conference*, (Houston, Texas, USA), pp. 1737–1741, IEEE, May 16–19 1999.
- [113] W. C. Y. Lee, "Applying the Intelligent Cell Concept to PCS," *IEEE Transactions on Vehicular Technology*, vol. 43, pp. 672–679, August 1994.
- [114] I. Chih-Lin, L. J. Greenstein, and R. D. Gitlin, "A Microcell/Macrocell Cellular Architecture for Low- and High-Mobility Wireless Users," *IEEE Journal on Selected Areas in Communication*, vol. 11, pp. 885–890, August 1993.
- [115] L. Ma, M. O. Sunay, Z. C. Honkasalo, and H. Honkasalo, "A Simulation Bed to Investigate the Feasibility of a TDD DS CDMA Residential Indoor System Underlay," in *Proceedings of the 1997 International Symposium on Personal, Indoor and Mobile Radio Communications PIMRC 97*, vol. 2 of 3, pp. 286–291, IEEE, September 1997.
- [116] K. Takeo, "Improvement of Coverage Probability by Subband Scheme in CDMA Macro-micro Cellular System," in *Proceedings of the 1996 7th IEEE International Symposium on Personal, Indoor and Mobile Radio Communications PIMRC'96*, vol. 1 of 3, (Taipei, Taiwan), pp. 93–97, IEEE, October 15–18 1996.
- [117] W. Wong and E. S. Sousa, "Feasibility Study of TDD- and FDD-CDMA Frequency Sharing Cellular Networks," in *Proceedings of the International Conference on Communications ICC'99*, (Vancouver, Canada), pp. 531–535, IEEE, June 6–10 1999.
- [118] W. Wong and E. S. Sousa, "Frequency Selection Strategies for Hybrid TDD/FDD-CDMA Cellular Networks," in *Proceedings of the International Conference on Universal Personal Communications ICUPC '98*, (Florence, Italy), pp. 1152–1156, IEEE, October 5–9 1998.

-
- [119] 3rd Generation Partnership Project (3GPP), Technical Specification Group (TSG), Radio Access Network (RAN), Working Group 4 (WG4), “UTRA (UE); Radio Transmission and Reception.” 3GPP TS 25.102 V3.4.0 (2000–10), October 2000.
- [120] 3rd Generation Partnership Project (3GPP), Technical Specification Group (TSG), Radio Access Network (RAN), Working Group 4 (WG4), “Physical channels and mapping of transport channels onto physical channels (TDD).” 3GPP TS 25.221 V3.1.1 (1999-12), December 1999.
- [121] L. Ortigoza-Guerrero and A. H. Aghvami, “Capacity Assessment For UTRA,” in *Proceedings of the 1999 IEEE Vehicular Technology Conference*, (Houston, Texas, USA), pp. 1653–1657, IEEE, May 16–19 1999.
- [122] L. Ahlin and J. Zander, *Principles of Wireless Communications*. Studentlitteratur, 1998.
- [123] D. C. Cox and D. O. Reudink, *Microwave Mobile Communications*, ch. layout and control of high-capacity systems. IEEE Press, 1974.
- [124] D. Everitt and D. Manfield, “Performance Analysis of Cellular Mobile Communication Systems with Dynamic Channel Assignment,” *IEEE Journal on Selected Areas in Communication*, vol. 7, pp. 1172–1179, October 1989.
- [125] R. Beck and H. Panzer, “Strategies for Handover and Dynamic Channel Allocation in Micro-Cellular Mobile Systems,” in *Proceedings of the 1989 IEEE Vehicular Technology Conference*, vol. 1, (San Francisco, USA), pp. 178–185, IEEE, May 1–3 1989.
- [126] D. Kunz, “Transitions from DCA to FCA Behavior in a Self-Organizing Cellular Radio Network,” *IEEE Transactions on Vehicular Technology*, vol. 48, pp. 1850–1861, November 1999.
- [127] P. T. Tan, C. B. Soh, E. Gunawan, and B. H. Soong, “Dynamic Flow Model for Borrowing Channel Assignment Scheme in Cellular Mobile System,” *Wireless Personal Communications*, vol. 6, pp. 249–264, March 1998.
- [128] S. Nanda and D. J. Goodmann, *Third Generation Wireless Information Networks*, ch. Dynamic Resource Acquisition: Distributed Carrier Allocation for TDMA Cellular Systems, pp. 99–124. Kluwer Academic Publishers, 1992.
- [129] T.-P. Chu and S. S. Rappaport, “Overlapping coverage and channel rearrangement in microcellular communication systems,” *IEE Proceedings – Communication*, vol. 142, pp. 323–332, October 1995.
- [130] K. A. West and G. L. Stüber, “An Aggressive Dynamic Channel Assignment Strategy for a Microcellular Environment,” *IEEE Transactions on Vehicular Technology*, vol. 43, pp. 1027–1038, November 1994.
- [131] K.-R. Lo, C.-J. Chang, C. Chang, and C. B. Shung, “A Combined Channel Assignment Strategy in a Hierarchical Cellular Systems,” in *Proceedings of the 1997 IEEE 6th International Conference on Universal Personal Communications ICUPC '97*, (San Diego, USA), pp. 651–655, IEEE, October 12–16 1997.

-
- [132] L. Jorgueski, J. B. Punt, and D. Sparreboom, "A Comparison of Dynamic Channel Allocation Algorithms," in *Proceedings of the FRAMES Workshop 1999*, (Delft University of Technology, Delft, (Netherlands)), pp. 131–136, January 18–19, 1999.
- [133] L. J. Cimini, G. J. Foschini, C.-L. I, and Z. Miljanic, "Call Blocking Performance of Distributed Algorithms for Dynamic Channel Allocation," *IEEE Transactions on Communications*, vol. 42, pp. 2600–2607, August 1994.
- [134] L. J. Cimini, G. J. Foschini, and C.-L. I, "Call Blocking Performance of Distributed Algorithms for Dynamic Channel Allocation in Microcells," in *Proceedings of the International Conference on Communications ICC'92*, (Chicago, IL, USA), pp. 1327–1332, IEEE, June 14–17 1992.
- [135] S. K. Das, S. K. Sen, and R. Jayaram, "A Distributed Load Balancing Algorithm for the Hot Cell Problem in Cellular Mobile Networks," in *Proceedings of the 1997 6th IEEE International Symposium on High Performance Distributed Computing*, pp. 254–263, IEEE, August 5–8 1997.
- [136] R. Prakash, N. Shivaratri, and M. Singhal, "Distributed Dynamic Fault-Tolerant Channel Allocation for Cellular Networks," *IEEE Transactions on Vehicular Technology*, vol. 48, pp. 1874–1888, November 1999.
- [137] Z. Haas, J. H. Winters, and D. S. Johnson, "Simulation Results of the Capacity of Cellular Systems," *IEEE Transactions on Vehicular Technology*, vol. 46, pp. 805–817, November 1997.
- [138] K. L. Yeung and T.-S. P. Yum, "Cell Group Decoupling Analysis of a Dynamic Channel Assignment Strategy in Linear Microcellular Radio Systems," *IEEE Transactions on Communications*, vol. 43, pp. 1289–1292, February–April 1995.
- [139] S. K. Das, S. K. Sen, and R. Jayaram, "A dynamic load balancing strategy for channel assignment using selective borrowing in cellular mobile environment," *Wireless Networks*, vol. 3, pp. 333–347, October 1997.
- [140] K.-N. Chang, J.-T. Kim, C.-S. Yim, and S. Kim, "An Efficient Borrowing Channel Assignment Scheme for Cellular Mobile Systems," *IEEE Transactions on Vehicular Technology*, vol. 47, pp. 602–608, May 1998.
- [141] L. Ortigoza-Guerrero and D. Lara-Rodriguez, "Dynamic channel assignment strategy for mobile cellular networks based on compact patterns with maximised channel borrowing," *Electronics Letters*, vol. 32, pp. 1342–1343, July 1996.
- [142] J. Zander and M. Frodigh, "Capacity Allocation and Channel Assignment in Cellular Radio Systems Using Reuse Partitioning," *Electronics Letters*, vol. 28, pp. 438–440, February 1992.
- [143] D. Lucatti, A. Pattavina, and V. Trecordi, "Bounds and Performance of Reuse Partitioning in Cellular Networks," *International Journal of Wireless Information Networks*, vol. 4, no. 2, pp. 125–134, 1997.

-
- [144] S. M. Shin, C.-H. Cho, and D. K. Sung, "Interference-Based Channel Assignment for DS-CDMA Cellular Systems," *IEEE Transactions on Vehicular Technology*, vol. 48, pp. 233–239, January 1999.
- [145] Y. Argyropoulos, S. Jordan, and S. P. R. Kumar, "Dynamic Channel Allocation in Interference-Limited Cellular Systems with Uneven Traffic Distribution," *IEEE Transactions on Vehicular Technology*, vol. 48, pp. 224–232, January 1999.
- [146] A. Lozano and D. C. Cox, "Integrated Dynamic Channel Assignment and Power Control in TDMA Mobile Wireless Communication Systems," *IEEE Journal on Selected Areas in Communication*, vol. 17, pp. 2031–2040, November 1999.
- [147] T. Klingenbrunn and P. Mogensen, "Modelling Cross-Correlated Shadowing in Network Simulations," in *Proceedings of the 1999 50th IEEE Vehicular Technology Conference*, (Amsterdam, The Netherlands), pp. 1407–1411, IEEE, September 19–22 1999.
- [148] 3rd Generation Partnership Project (3GPP), Technical Specification Group (TSG), Radio Access Network (RAN), Working Group 4 (WG4), "Evaluation of up- and downlink adjacent channel performance." TSGR4#2(99) 048, February 1999.
- [149] ETSI 30.03, V3.2.0 (1998-04), "Universal Mobile Telecommunications System (UMTS); Selection procedures for the choice of radio transmission technologies of the UMTS." TR 101 112, 1998.
- [150] A. Papoulis, *Probability, Random Variables, and Stochastic Processes*. McGraw-Hill, 1991.
- [151] M. Gudmundson, "Correlation Model for Shadow Fading in Mobile Systems," *Electronics Letters*, vol. 27, pp. 2145–2146, November 1991.
- [152] H. Haas and G. J. R. Povey, "Communications networks." UK Patent Application Number: GB 9930089.9, 20th December 1999.
- [153] H. Haas and S. McLaughlin, "TS Assignment Scheme with Novel DCA." UK Patent Application Number: GB 0017434.2, 14th July 2000.
- [154] H. Haas, S. McLaughlin, and G. J. R. Povey, "Capacity-Coverage Analysis of the TDD and FDD Mode in UMTS at 1920 MHz," *submitted to: IEE Proceedings : Communications*, May 2000.
- [155] W. C. Y. Lee, "Overview of cellular CDMA," *IEEE Transactions on Vehicular Technology*, vol. 40, no. 2, pp. 291–302, 1991.
- [156] P. Seidenberg, M. P. Althoff, E. Schulz, and G. Herbster, "Statistics of the Minimum Coupling Loss in UMTS/IMT-2000 Reference Scenario," in *Proceedings of the 1999 50th IEEE Vehicular Technology Conference*, vol. 2, (Amsterdam, The Netherlands), pp. 963–967, IEEE, September 19–22 1999.
- [157] A. A. Abu-Dayya and N. C. Beaulieu, "Outage Probabilities of Cellular Mobile Radio Systems with Multiple Nakagami Interferers," *IEEE Transactions on Vehicular Technology*, vol. 40, pp. 757–768, November 1991.

- [158] 3rd Generation Partnership Project (3GPP), Technical Specification Group (TSG), Radio Access Network (RAN), Working Group 4 (WG4), “Physical layer — Measurements (TDD).” 3GPP TS 25.225 V3.1.0 (1999-12), December 1999.
- [159] S. C. Schwartz and Y. S. Yeh, “On the Distribution Function and Moments of Power Sums With Log–Normal Components,” *The Bell System Technical Journal*, vol. 61, pp. 1441–1462, September 1982.
- [160] L. R. Schaeffer, “Matrix Algebra.” <http://www.aps.uoguelph.ca/~lrs/Animalz/lesson1>, March 1999.
- [161] G. H. Golub and C. F. van Loan, *Matrix Computations*. The John Hopkins University Press, 1996.
- [162] R. J. Wilson, *Introduction to Graph Theory*. Longman Scientific & Technical, 1987.
- [163] 3rd Generation Partnership Project (3GPP), Technical Specification Group (TSG), Radio Access Network (RAN), Working Group 4 (WG4), “Radio Resource Management Strategies.” 3GPP TS 25.922 V3.0.0 (2000–01), January 2000.
- [164] W. C. Y. Lee, *Mobile Communications Design Fundamentals*. John Wiley & Sons, second ed., 1993.